R. G. Donnelly
R. E. Cohen

Enhancement of the Stability of Common Polymeric Materials Against Undersea Degradation

MIT Sea Grant
College Program

Massachusetts
Institute of Technology
Cambridge
Massachusetts 02139

MITSG 81-14
October 1981

ENHANCEMENT OF THE STABILITY OF COMMON POLYMERIC MATERIALS AGAINST UNDERSEA DEGRADATION

by

R.G. Donnelly

R.E. Cohen

Sea Grant College Program

Massachusetts Institute of Technology

Cambridge, Massachusetts 02139

Report No. 81-14
Index No. 81-314-C8
October, 1981

ACKNOWLEDGEMENTS

This report describes the results of research done as a part of the MIT Sea Grant College Program with financial support from the Office of Sea Grant in the National Oceanic and Atmospheric Administration, U.S Department of Commerce, through grant number 04-6-158-44081; project number R/T-5, and from Gorman Rupp Industries and the Massachusetts Institute of Technology, and with technical assistance by Cryovac Division, W.R. Grace Company. The U.S. Government is authorized to produce and distribute reprints for governmental purposes, notwithstanding any copyright notation that may appear within.

AUTHORS AND CONTRIBUTORS

R.G. Donnelly, Associate Professor of Chemical Engineering
R.E. Cohen, Associate Professor of Chemical Engineering

Research Assistants
R.W. Baird
M.J. Garry

Other Contributors
B.S. Albom
D. Morrow

MIT SEA GRANT REPORTS

The Sea Grant Marine Resources Information Center maintains an inventory of all technical and advisory publications. We invite orders and inquiries to:

MIT Sea Grant Program
Marine Resources Information Center
77 Massachusetts Avenue
Building E38-302
Cambridge, Massachusetts 02139

ABSTRACT

Several common polymeric materials, including low-density polyethylene, polypropylene, polymethylmethacrylate and polystyrene, were subjected to small amplitude cyclic flexure in a simulated marine environment, and changes in crystallinity and molecular weight were monitored by various means, including dilute solution viscosimetry, melt viscosimetry, stress-strain measurement, and wide-angle X-ray diffraction. Low-density polyethylene was further subjected to cyclic flexure in other environments in order to compare degradation rates therein to that in marine water. The polyethylene resin tested was treated by a variety of surface-modification techniques including surfactant absorption, radiofrequency glow-discharge exposure in air, post-treatment with diacid or triisocyanate to form a cross-polymerized coating, and surface irradiation with partially-shielded 500 keV electrons. Modified polyethylene surfaces were characterized quantitatively and semi-quantitatively by tensiometry of treat solution and by examination of the surface under ATR IR and ESCA spectroscopy. Electron dosage was monitored by gel content and cellophane dosimetry. Treated polyethylene samples were then subjected to small amplitude cyclic flexure in simulated marine water, and wide-angle X-ray diffraction results indicated that each treatment method studied caused retardation of degradation; however, the relative effectiveness of the various techniques varied greatly.

TABLE OF CONTENTS

		Page
I.	INTRODUCTION	1
	A. Overview on Degradation	1
	B. Alternative Surface-Modification Methods Studied Previously	2
II.	EXPERIMENTAL	8
	A. Surfactant Absorption Experiments on Polyethylene Powder	8
	B. Surface Modification of Polyethylene Sheet by Various Techniques	14
	1. Surfactant Absorption	14
	2. DM100 Posttreats	16
	3. Adipic Acid Posttreats	18
	4. Plasma-Treated Strip	19
	5. Electron Irradiation	21
	C. Accelerated Testing of Polymer Strip by Cyclic Flexure	26
	1. Vertical Flexor	26
	2. Horizontal Flexor	29
	D. Characterization of Modified Polyethylene Surfaces	31
	E. Monitoring of Polymer Degradation	34
	1. Solution Viscosity	34
	2. Stress-Strain Measurements	34
	3. Melt Viscosity	34
	4. X-ray Diffraction	38
III.	RESULTS	41
	A. Baseline Degradation Studies	41
	1. Initial Flexure Testing of Polyethylene and Polymethylmethacrylate	41
	2. Additional Flexure Experiments on Polyethylene	48
	3. Melt Viscosity Studies on Polyethylene, Polypropylene, and Polystyrene	65
	a. Polyethylene	65
	b. Polypropylene	66
	c. Polystyrene	70
	B. Surfactant Absorption on Polyethylene Powder	76

Page

C. Characterization of Modified Polyethylene Surfaces 101
1. ATR IR 101
2. Transmission IR 106
3. ESCA 107
4. High-Resolution ESCA 120
5. Contact Angle 124
D. Flexure Performance of Surface-Modified Polyethylene Samples. 128
1. Polyethylene and Surfactant 128
2. DM100 Posttreats 133
3. Plasma Treatment 136
4. Adipic Acid Posttreats 137
5. Irradiated Strip 137
6. Summary of Flex-Performance Results 142

IV. DISCUSSION 144
A. General Consideration of Degradation 145
B. Melt-Viscosity Studies 150
1. Polyethylene 150
2. Polypropylene 150
3. Polystyrene 151
C. Possible Polyethylene Degradation Modes 152
D. Effects of Surface Modification on Polyethylene Degradation . 155
1. The Polyethylene Surface 155
2. Surfactant Absorption on Polyethylene 156
3. DM100 Posttreats 157
4. Plasma Treatment 158
5. Plasma and DM100 159
6. Adipic Acid Posttreats 160
7. Electron Irradiation 161

Page

V. POSSIBLE EXTENSIONS OF WORK 163

APPENDIX I: Structural Configuration of LDE, DM100, and Adipic Acid . . 165

APPENDIX II: Physical Property Data for LDE, DM100, and Adipic Acid . . 166

APPENDIX III: Preliminary Calculations for Expected Surfactant Absorption by P.E. 169

APPENDIX IV: LDE Tensiometric Calibration Curve: Surface Tension Versus Concentration 171

APPENDIX V: Basis for Establishing Posttreat Solution Concentration Tested on PE Strip 172a

APPENDIX VI: Dilute Solution Viscosity Measurements - Theory and Data . 174

APPENDIX VII: A. Preliminary PE Flexure Runs in Air and Sea Water at 60 rpm 182

B. Instron Stress-Strain Measurements 183

APPENDIX VIII: Deconvolution of Wide-Angle X-Ray Diffractograms: Two Algorithms Used in This Work 188

APPENDIX IX: Study of Effect of Flexure Frequency on Degradation of PMMA 192

APPENDIX X: Data for Melt-Viscosity Studies on PE, PP, and PS . . . 195

APPENDIX XI: Calculation of Surfactant Absorption Rate if Mass-Transfer Limited 200

APPENDIX XII: Data from LDE Absorption Experiments on PE Powder . . . 202

LITERATURE CITATIONS 203

LIST OF FIGURES

		Page
Figure 1	LDE Adsoption onto PE Followed by Cross-Polymerization with DM100 or AA	5
Figure 2	a) LDE Powder Adsorption Apparatus	15
	b) LDE Strip Adsorption Apparatus	15
Figure 3	Plasma Treatment Apparatus	20
Figure 4	a) 500-keV Electron-Beam Irradiation Apparatus .	22
	b) Electron Radiation Dose vs. Sample Depth for Various Electron Energies	22
Figure 5	a) Cellophane Stack Dosimetry of 2.0 MR Surface-Irradiated PE Sheet	24
	b) Typical Gel-Dose Curve for Low-Density PE .	24
Figure 6	a) Flex Tank Apparatus General Layout	27
	b) Geometry of Sample-Holder and Plunger . . .	27
Figure 7	Vertical Flexor Apparatus	30
Figure 8	Plate and Cone Geometry and Equations	36
Figure 9	PMMA Degradation due to Flexure in Air at 60 c.p.m., Monitored by Molecular Weight	43
Figure 10	PMMA Degradation due to Flexure in Synthetic Seawater at 30 c.p.m., Monitored by Molecular Weight	44
Figure 11	PE Degradation due to Flexure in Air at 60 c.p.m., Monitored by Percent Crystallinity .	46
Figure 12	PE Degradation due to Flexure in Synthetic Seawater at 60 c.p.m., Monitored by Percent Crystallinity	47
Figure 13	PE Degradation due to Flexure in Synthetic Seawater at 60 c.p.m., Monitored by Young's Modulus	49
Figure 14	PE Degradation due to Flexure in Synthetic Seawater at 60 c.p.m., Monitored by Yield Stress	50

		Page
Figure 15	Crystallinity vs. Log Cycles Flex for Blank PE Flexed at 70 rpm in Various Environments	53
Figure 16	Crystallinity vs. Log Cycles Flex for Blank PE Flexed in Various Environments at 400 rpm	54
Figure 17	Crystallinity vs. Anneal Time in Distilled Water for Bank PE at 87°C and 92°C	57
Figure 18	Crystallinity vs. Log Cycles Flex at 400 rpm for PE Annealed up to 72 hr at 87°C and 92°C in Distilled Water	58
Figure 19	Low Density Polyethylene Crystallinity vs Flexure	59
Figure 20	Low Density Polyethylene Rheometrics Sepctrometer Results	60
Figure 21	Error Correlation for Fig. 20	61
Figure 22	Low Density Polyethylene Rheometrics Spectrometer Results	62
Figure 23	Error Correlation for Fig. 22	63
Figure 24	Polypropylene Crystallinity vs Flexure	64
Figure 25	Polypropylene Rheometrics Spectrometer Results	67
Figure 26	Error Correlation for Fig. 25	68
Figure 27	Outline of Polystyrene X-ray Scan	69
Figure 28	Polystyrene Rheometrics Spectrometer Results	72
Figure 29	Error Correlation for Fig. 28	73
Figure 30	Polystyrene Rheometrics Spectrometer Results	74
Figure 31	Error Correlation for Fig. 30	75
Figure 32	Adsorption Data for Experiments at 92°C	81
Figure 33	Adsorption Data for Initial Concentrations of 4×10^{-5} M	84
Figure 34	Adsorption Data for Initial Concentration of 8×10^{-5} M	85

		Page
Figure 35	Adsorption Data for Initial Concentrations of 8×10^{-5} M	86
Figure 36	Moles of Surfactant Adsorbed at 87°C as a Function of Time	87
Figure 37	Moles of Surfactant Adsorbed at 92°C as a Function of Time	88
Figure 38	Adsorption Isotherms for LDE on PE at 82°C, 87°C, 90°C, and 92°C	89
Figure 39	Sticking Coefficient vs Adsorption at 82°C . . .	94
Figure 40	Determination of Heat of Adsorption from C_{eq} at Constant Coverage	95
Figure 41	LDE Concentration vs. Time for Adsorption on PE at 90°C	99
Figure 42	Moles LDE Adsorbed vs. Time for PE Powder at 90°C .	99
Figure 43	a) through c) Plots of kS vs. Specific Molar Adsorption for LDE on PE at 87°C, 90°C and 92°C	100
Figure 44	a) and b) Representative ATR IR Spectrograms (Carbonyl Region) for Various Surface Modification Methods	102
Figure 44	c) ATR IR Spectrograms of the Carbonyl Region for PE + Plasma (2 cm^3/min atm) for Various Exposure Times	103
	d) ATR IR Spectrograms of the Carbonyl Region for PE + Plasma (25 cm^3/min atm) for Various Exposure Times	104
Figure 45	Transmission IR Spectrograms of the Carbonyl Region for Polymers of LDE and DM100, Formulated with Various Stoichiometric Ratios of OH:NCO	108
Figure 46	Morphology of LDE + DM100 Polymers of Various Composition	110
Figure 47	a) ESCA N/C Ratios vs. Log Posttreat Time for PE + DM100 and PE + LDE + DM100, at 4.44×10^{-5}M DM100	116
	b) ESCA N/C Ratios vs. Log Posttreat Time for PE + DM100 and PE + LED + DM100, at 4.44×10^{-3}M DM100	116

Page

Figure 47 c) ESCA N/C Ratios vs. Log Posttreat Concentration for 2-min Posttreats in DM100 of PE + LDE. . 117
d) ESCA N/C Ratios vs. Log Posttreat Concentration for 24-hr Posttreats in DM100 of PE + LDE. . 117

Figure 48 a) ESCA N/C Ratio vs. Log Posttreat Time in 4.44×10^{-5}M DM100 for PE Pretreated 6 min in 2 cm^3/min atm Plasma. 118
b) N/C Ratio vs. Log Posttreat Time for Plasma-Pretreated PE in 4.44×10^{-3}M DM100. 118

Figure 49 ESCA N/C Ratio vs. Log Time of Exposure to Air Plasma at Various Flowrates for Blank PE. 119

Figure 50 a) NSCA N/O Ratios vs. Log Posttreat Time for PE + LDE in AA. 121
b) N/O Ratios vs. Log Posttreat Time for PE + 6-min-Plasma Exposure in 6.67×10^{-5}M AA 121

Figure 51 a) ESCA O/C Ratio vs. Log Posttreat Time for PE + 6-min Plasma Exposure in DM100. 122
b) O/C Ratios vs. Log Posttreat Time for PE + LDE in AA. 122a
c) O/C Ratios vs. Log Posttreat Time for PE + 6-min Plasma Exposure in 6.67×10^{-5}M AA 122a

Figure 52 ESCA O/C Ratios vs. Log Exposure Time in Air Plasma at Various Flowrates for Blank PE. 123

Figure 53 a) Crystallinity vs. Log Cycles Flex for PE and PE + LDE at 70 rpm. 130
b) Crystallinity vs. Log Cycles Flex for PE and PE + LDE at 400 rpm 130

Figure 54 a) Crystallinity vs. Log Cycles Flex for PE + LED and PE + LDE + DM100 at 70 rpm. . . . 131
b) Crystallinity vs. Log Cycles Flex for PE + LDE, PE + DM100, and PE + LDE + DM100 at 400 rpm. 131

Figure 55 a) Crystallinity vs. Log Cycles Flex for PE + Plasma (2 cm^3/min atm) for Various Exposure Times 135
b) Crystallinity vs. Log Cycles Flex for PE + Plasma + DM100 135

Figure 56 Crystallinity vs. Log Cycles Flex for PE + LDE + AA PE + Plasma + AA. 140

Figure 57 a) Crystallinity vs. Log Cycles Flex for Isotropically Irradiated PE Blank at Various Dosages. . 141

Page

Figure 57 b) Crystallinity vs. Log Cycles Flex at 70 rpm for PE Surface-Irradiated with 500 keV Electrons. 141

Figure 58 Log Lifetime-Enhancement Factors for the Surface Modification Methods Studied. 142

Figure 59 Mechanochemical Degradation 146

Figure 60 Submicrocrack Propagation 146

Figure 61 Crystallinity Effect on Modulus and Yield Strength for Polypropylene. 147

Figure 62 Flex Life Dependence on Crystallinity and Molecular Weight. 147

Figure 63 Peterlin Model for Semicrystalline Degradation 149

LIST OF TABLES

		Page
Table 1	Characterization of the Garry PE Resin by Various Methods	45
Table 2	X-Ray Diffraction Data for Blank PE Flexed at 70 rpm in Various Environments	51
Table 3	X-Ray Data for Blank PE Flexed at 400 rpm in Various Environments	52
Table 4	X-Ray Data for Blank PE Annealed at 87°C and 92°C	55
Table 5	X-Ray Data for Blank PE Annealed at 87°C and 92°C, then Flexed for 6.33 Log Cycles	56
Table 6	Adsorption Data for 9.44×10^{-6} M Surfactant Solution at 92°C	79
Table 7	Adsorption Data for 4.22×10^{-5} M Surfactant Solution at 93°C	80
Table 8	Adsorption Data for 8.32×10^{-5} M Surfactant Solution at 92°C	80
Table 9	Adsorption Data for 3.89×10^{-5} M Surfactant Solution at 82°C	82
Table 10	Adsorption Data for 4.22×10^{-5} M Surfactant Solution at 87°C	82
Table 11	Adsorption Data for 8.32×10^{-5} M Surfactant Solution at 82°C	83
Table 12	Adsorption Data for 7.94×10^{-5} M Surfactant Solution at 87°C	83
Table 13	Adsorption Rates at 82°C for Surfactant Concentration of 3.89×10^{-5} M	90
Table 14	Adsorption Rates at 82°C for Surfactant Concentration of 8.32×10^{-5} M	90
Table 15	Adsorption Rates at 87°C for Surfactant Concentration of 4.22×10^{-5} M	91
Table 16	Adsorption Rates at 87°C for Surfactant Concentration of 7.94×10^{-5} M	91
Table 17	Adsorption Rates at 87°C for Surfactant Concentration of 7.94×10^{-5} M	92

Page

Table 18 Adsorption Rates at 92°C for Surfactant Concentration of 4.12×10^{-6} M 92

Table 19 Adsorption Rates at 92°C for Surfactant Concentration of 8.32×10^{-5} M 93

Table 20 Tensiometric Data and Calculated Quantities of Interest for LDE Absorption Runs Done at 90°C 96

Table 21 ESCA Atomic Ratio Surface Data for All Strip Samples Tested 111

Table 22 High - Resolution ESCA Photoelection Peak Energy Assignments (and Probable Chemical Identification of C1s, O1s and N1s in Various Modified PE Surfaces) 126

Table 23 Data from Contact-Angle Determinations of Selected Surface Types 127

Table 24 X-Ray Data for PE Reflexed 75 hr at 90°C in LDE and Flexed for Various Log Cycles 129

Table 25 X-Ray Data for PE+LDE+DM100 Strip and PE+DM100 Strip . . . 132

Table 26 X-Ray Data for PE +plasma and PE+plasma+DM100 Samples Flexed at 400 rpm 134

Table 27 X-Ray Data for PE+LDE+AA and PE+plasma+AA at Various AA Concentration. Flexed at 400 rpm 138

Table 28 X-Ray Data for Blank PE Irradiated Isotropically or on the Surface with 500 keV Electrons and Flexed at 70 rpm 139

INTRODUCTION

One of the classic problems of materials engineering has been that of corrosion or degradation of mechanical performance through adverse chemical interaction with the environment. A broad range of remedies has been applied over the years to this problem, including the development of special impermeable coatings and bulk substitution by new materials with superior intrinsic resistance to the corrosive agents in question. In recent years, various polymeric and composite materials have been quite successfully employed to combat performance loss due to corrosion.

There are limits however, even to this approach, for even such relatively inert polymers as polyethylene suffer significant degradation, with consequent failure of performance, when subjected to vigorous mechanical working in an active chemical environment. An important case of such an environment is saline water, which readily attacks aluminum and steel, and rapidly tarnishes brass. Marine water also attacks, albeit more slowly, many important polymeric resins such as polystyrene(PS), polypropylene (PP), polymethyl methacrylate (PMMA) and polyethylene (PE). In the last decade, several workers (Jacobs, 1968; Hamner, 1966; Demchik, Mandell, McGarry, 1973) have conducted studies on the degradation of several resins in marine environment.

In the usage adopted here, "corrosion" is defined as chemical reaction (e.g., oxidation) of elemental metal, with consequent deviation of performance from design specifications. "Degradation" implies a breakdown of chemical structure; for polymeric materials, such breakdown usually results in a loss of molecular weight or undesirable change in some other property, e.g., crystallinity.

The aim of this research was twofold: (a) to establish baseline degradation behavior in seawater and in other environments for several major resin classes (PE, PP, PS and PMMA were studied); and (b) to evaluate several classes

of surface modification techniques as inhibitors of seawater-promoted polymer degradation.

Alternative surface-modification methods studied previously.

The variety and ingenuity of the various surface-modifications that have been tried on polymers are almost endless. The primary motivation for this broad exploration lies in the fact that alteration of the physical properties of a relatively thin surface region leaves the vast majority of the total bulk of the sample unaltered. In this way, the bulk phase and surface layer can be optimized for different, often mutually exclusive operating parameters. The more important procedures already well-characterized include CASING (crosslinking by activated species of inert gas), radiation grafting, surface fluorination, and surfactant adsorption followed by cross-polymerizing posttreat. Newer methods explored in this work include partially-shielded high-voltage electron-beam bombardment and glow-discharge plasma exposure followed by cross-polymerization posttreat.

CASING has been extensively studied by Schonhorn and Hansen; they used a variety of working gases, including helium, argon, neon, hydrogen and nitrogen. These species were excited usually in a radio frequency glow discharge or "cold-plasma" environment, and allowed to come in contact with a polymer surface. A thin crosslinked skin would then be formed for those polymers possessing a weak (low-molecular-weight or unbranched) surface region. CASING was not found to be effective on polymers (e.g., elastomers) already having a strong surface region (Schonhorn and Hansen, 1967). The beauty of this technique lies in the formation of a highly crosslinked surface region without materially changing either bulk properties or such surface properties as wettability and surface conductivity.

A different process involves exposure of a polymer substrate to an elemental fluorine stream (Lagow and Margrave, 1974). Depth of surface modification is controllable by adjusting the exposure time, and the extent of fluorination of

the treat region is essentially complete. Thus, one obtains a teflon-like region on the surface of polyethylene. Lagow and Margrave studied a variety of additive-free resins including amides, nitriles, aromatics, phenolics and branched hydrocarbons, as well as PE. In each case hydrogen or hydroxyl was replaced with fluorine; nitriles and carbonyl groups were found to be untouched, while aromatic rings were fully saturated.

Use of a helium-fluorine "cold plasma" to achieve formation of a teflon-like coating on polyethylene is currently being studied by Anand et al., at MIT. Infrared (ATR) and ESCA analyses clearly show formation of a C-F bond in high abundance using a 5% F_2, 95% H_e ($^v/_v$) plasma stream at around 10 cc/min and 0.1 mm Hg.

Radiation grafting consists of exposing a substrate to ionizing radiation e.g., X-rays, electrons, gamma rays, alpha particles, ultra-violet, etc., while passing a stream over it which consists of monomeric or polymeric species posessing desired chemical moieties. Depth of treat is largely a function of dosage depth and the swelling power of the grafting stream in the substrate polymer. Stream component molecules or fragments are actually "grafted" onto the backbone (usually carbon skeleton) of the substrate (Ceresa, 1965). Both radiation grafting and fluorination bridge the gap between strictly surface-modification and actual bulk alteration, since both have highly controllable treat depths.

A newer treatment method was explored by Ericsson and Lagergren (1971) and pursued further by Lagergren, Olsson and Swedenborg (1974). The object was to render polymeric biomaterials non-thrombogenic, and the 1971 work developed a process in which a cationic surfactant was adsorbed onto the substrate, thus providing binding sites for heparin. Heparin (a non-thrombogenic agent) was allowed to bind onto the cationic surfactant sites and was then crosslinked or cross-polymerized to retard desorption in the blood environment.

The initial adsorption step was found by these workers to be a function of substrate polarity and additive content. Also, the strength of the sorption is

a function of hydrocarbon chain length. An optimization between fast tail diffusion into substrate bulk (short chain length) and low desorption rates (long chain length) was found to be at about 16-18 carbon atoms. Best substrates for such adsorption were found to be additive-free and nonpolar. Semicrystalline polymers such as PE also were found to be suitable. This method proved very encouraging for biomaterial application; thrombogenic activity of treated shunts in fresh blood was decreased by a factor of 50 to 100, as monitored by time required to become clotted over.

The present research extended the Lagergren-Olsson-Swdenborg surfactant-adsorption concept to the problem of protecting the polymer substrate from the fluid medium, the opposite case from that of the previous work. The idea was to expose the polymer surface (low-density PE in the present work) to a dilute solution of molecules which would probably physisorb onto the PE surface (see Fig. 1a), and at elevated temperature, undergo diffusion of the long aliphatic "tail" into the PE surface zone. Subsequent cooling of the PE + LDE surface to room temperature would sterically anchor the LDE molecules against desorption, and the polar "head" moiety would protrude into the polar aqueous phase above the PE surface.

The second step in this modification process would be cross-polymerization with polyacid (to obtain polyester) or with polyisocyanate (to obtain polyurethane), as shown in Fig. 1b. The polyurethane should be more stable against hydrolysis than polyester, but polyisocyanates are more difficult to handle (e.g. they cannot be used in an aqueous system). The cross-polymerization agents shown in Fig. 1b are representative, and were also the actual ones used in this work.

Two other relatively novel surface-modification methods were also studied, namely partially-shielded high-voltage electron beam bombardment and radiofrequency plasma exposure in air followed by cross-polymerization posttreat with diacid and triisocyanate. Much exploratory work has been done on the bulk irradiation of various substances, including PE, with high-voltage electrons.

Figure 1.a)

LDE adsorption onto PE

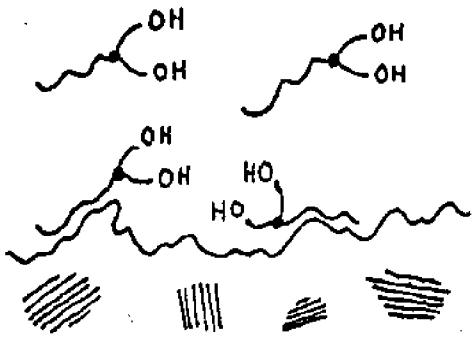

1. Physisorption

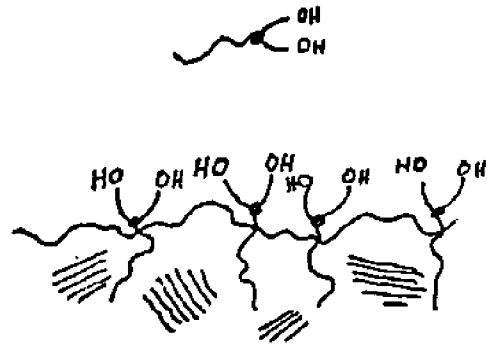

2. Tail diffusion into bulk at elevated temeprature; sterically anchored at room temperature.

Figure 1.b)

Cross-Polymerization step

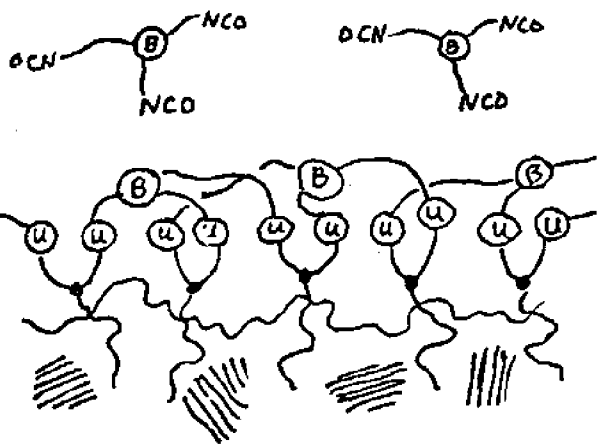

1. DM100 Triisocyanate
   U = Urethane linkage
   ʊ = Biuret Core of DM100

   2-dimensional network

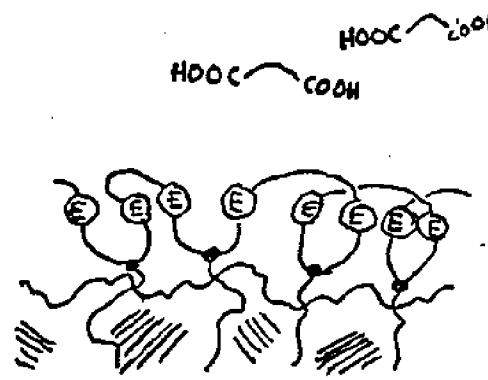

2. Adipic Acid
   E = Ester linkage

   linear system

Figure 1. LDE adsorption onto PE follwed by cross-polymerization with DM100 or AA.

Good reviews on the topic are Harmer and Ballantine (1971) and V.L. Lanza's chapter in the anthology Crystalline Olefin Polymers (1964); both discuss electron-beam irradiation as well as treatment with other forms of ionizing radiation.

The area of plasma treatment is newer; work most relevant to the present study is covered in Hollahan (1969) and in a patent by Baird et al (Pat. No. 3,870,610; 1975). Schonhorn, Ryan and Hansen's work (1969) concerned CASING rather than chemical modification, although they used an O_2 glow discharge. Battell Memorial Institute carried out in 1970-71 a study of scaled-up plasma-treatment processes on polyolefins and other substrates in air and in selected gases, and at a range of pressures down to 10^{-4} torr. The present study was limited to air at 1.0 torr.

The present study extended the bulk high-voltage electron-beam irradiation to a surface technique by partially shielding the polyethylene from the electron beam, thereby achieving a half-thickness (at which radiation dose is 50% the surface value) of less than 100 micrometers. The result is similar to that obtained by the CASING process, namely a highly crosslinked surface shell around an unaltered bulk region. Plasma treatment work first optimized the oxidation and nitrification level of the surface (as monitored by ATR-IR and ESCA) and then subjected the plasma-treated surface to a diacid and a triisocyanate to form a cross-polymerized surface skin akin to that obtained by radiation by grafting (but avoiding the expense and hazard of high-energy radiation).

To recapitulate, the present surface-modification work concerned itself with the objective of demonstrating the effectiveness of several novel surface-treatment methods for retarding seawater-promoted degradation of polyethylene. Among those methods tested were (a) LDE adsorption followed by formation of urethane or ester cross-polymerized surface networks; (b) exposure to radio-frequency cold-plasma in air followed by the posttreat used in (a) above; and (c) irradiation of a surface skin by partially-shielded 500 keV electrons. Each

method was found to be effective in retarding degradation, for different reasons.

EXPERIMENTAL

Surfactant adsorption experiments on polyethylene powder.

In adapting the method of surface treatment developed by Lagergren and Ericsson (1971) to the conditions imposed by this research, the major problems to be solved included the choice of surfactant, the selection of an appropriate method to detect successful adsorption of surfactant, and determination of the appropriate reaction to be performed on the adsorbed surfactant.

The adsorption studies focused on low density polyethylene as the polymeric substrate and water as the solvent. To maximize adsorption the hydrophobic tail of the surfactant should be "polyethylene-like" i.e. consist of methylene groups; in this way the polymer would "see" no difference between surfactant tails and polymeric chains. The tail must have sufficient length to firmly anchor the surfactant in the polymer; a tail which is too short would have too great a mobility to hold the surfactant in place, whereas one which is too long requires excessive heating for adequate diffusion. The "ideal" length was thought to be (Lagergren and Ericsson, 1971) 12-16 methylene groups.

To achieve an effective coating for the polymer, the hydrophilic head of the surfactant is required to remain on the polymer surface available for further reaction. A head which is polar would associate with the water, a polar solvent, rather than the methylene groups of the polyethylene, thus remaining on the polymer surface.

The achievement of a continuous skin for the polyethylene depends on a reaction of the surfactant head with a monomer or prepolymer. Using a bifunctional surfactant head would allow chain propagation along the polymer surface with a bifunctional monomer as reagent. Alternatively, the use of a monofunctional surfactant would require reaction with a prepolymer, later undergoing polymerization, to result in a skin coating. Finally, the surfactant must be water soluble.

Lauric diethanolamide ($C_{11}H_{23}CON(C_3H_4OH)_2$) was chosen mainly due to its availability. The commercial product used was NINOL AA-62 EXTRA, obtained from Stepan Chemical Company. The properties of lauric diethanolamide are given in Appendix I.

The methods to detect surfactant adsorption included quantitative as well as qualitative determinations. Qualitative methods involved staining the surfactant-treated polyethylene surface for the surfactant. The slightly basic amide group in lauric diethanolamide could be detected with a water soluble acid dye. Specifically, "Woodstain Scarlet" from E.I. duPont de Nemours and "Pylam Rose Pink" from Pylam Products were used as stains. Untreated polyethylene had no affinity for either stain and thus remained uncolored. The staining procedures would show that some surfactant was tightly anchored in the polymer even after vigorous washing.

The quantification of surfactant adsorption was accomplished by monitoring the surfactant concentration in the remaining solution. Preliminary calculations (Appendix III) showed that 6.352×10^{-8} moles of surfactant could be expected to be adsorbed by one gram of polyethylene powder. Therefore any quantitative determination of concentration would have to be extremely precise and sensitive. The method of monitoring the surfactant concentration in the remaining solution provides an upper bound to the surfactant adsorbed as a portion of lauric diethanolamide removed from solution could be associated with the polymer surface and not strongly adsorbed.

Surface tension measurements of the solution provided the link to solution concentration; a surfactant significantly lowers the surface tension of water, even when present in very low concentrations. The surface tension determinations were sensitive to the amount of surfactant present as well as to the small changes in concentration occurring upon adsorption.

Interpretation of the surface tension data required establishment of

a calibration curve relating the surface tension to log concentration of surfactant (Appendix IV). Solutions of the surfactant in water were made up to known concentrations in the range from 1 x 10^{-3}M to 1 x 10^{-6}M and the corresponding surface tension measurements were made at room temperature (22°C ± .5°C) using a du Nuoy ring tensiometer.

Powder samples to be used in the dasorption runs were prepared by grinding 5 mm x 5 mm chips at liquid nitrogen temperature and sieving out the fine fraction of largest dimension ≤ 200 microns. The fines thus obtained were washed with methylene chloride and acetone to remove organic contamination, and floated on distilled water to remove heavy insoluble particles, e.g. from the grinder. Surface area was determined by the BET method, which makes use of the BET Equation:

$$\frac{P}{V(P_o-P)} = \frac{1}{V_m C} + \left(\frac{C-1}{V_m C}\right)\left(\frac{P}{P_o}\right)$$

where V=STP gas volume (krypton) adsorbed on powder, P=pressure on sample when V cm^3 or krypton has been adsorbed, P_o=vapor pressure at sample temperature, V_m=volume of a monomolecular krypton layer on sample, and C=a constant dependent on the heat of adsorption of krypton on sample. Use of a sufficiently large sample enabled the specific surface area to be determined to about ± 1%. The value found was roughly twice that predicted from a smooth-sphere model of the mean diameter noted by microscopic inspection; hence about half of the area is thought to be accounted for by pores and cracks on the particle surfaces.

In the LDE adsorption experiments, a 5.00g sample of powder was charged to a reflux apparatus containing 300 ml of LDE solution of the concentration being tested. The refluxer was immersed in a large (~10ℓ) water bath kept at the reaction temperature. Adsorption runs were performed at 82°C 87°C, 90°C and 92°C. Ten-milliliter solution samples were extracted from the refluxer at various times of interest, and the surface tension at ambient temperature was measured on a

Cenco-DuNuoy 70535 ring tensiometer using a platinum ring of precisely known circumference. The 10ml samples were then re-charged to the refluxer. The refluxer was vigorously stirred to maintain a high degree of mixedness of the powder and solution phases, but allowed to settle completely before samples taken for tensiometry. The adsorption runs were terminated after 70 to 75 hrs, to insure that equilibrium had been achieved at the powder surface.

To evaluate the importance of desorption from the PE, treated powder samples were immersed in distilled H_2O for up to 14 days. No LDE was detected in the water by either tensiometry or staining with Pylam Rose Pink dye, suggesting an upper limit of 9×10^{-10} mol/hr for desorption as 20°C (i.e. negligible).

Raw surface-tension data were converted to LDE concentration data by use of the calibration curve in Appendix IV. In the initial adsorption studies, done in the absence of ESCA facilities, it was found that the most sensitive monitor of LED uptake was solution phase surface-tension increase; this restricts the LDE concentration to values at or below critical micelle density (3.55×10^{-4}M) and above about 3.35×10^{-6}M. The linearity of the surface tension vs. log concentration curve affords easy conversion of tensiometry data to concentrations. From the concentration difference obtained and knowledge of total moles of LDE initially present, total LDE uptake is found. Plotting moles of LDE adsorbed against reflux time, and determining the slope of this curve at given times, gives adsorption-rate data vs time. The general rate equation governing LDE adsorption can be represented by

$$\frac{dn_s}{dt} = kSC$$

where n_s=moles LDE adsorbed per unit area, C=LDE solution concentration, k is the concentration-independent rate constant and S is a quantity known as the sticking coefficient.

This last value is invoked for the following reason. Due to the molecular

nature of LDE and of LDPE (low-density polyethylene) the adsorption mechanism appears to consist of relatively rapid physisorption of the aliphatic LDE tails onto the PE surface, followed by a much slower thermally-promoted diffusion of these tails several molecular layers into the PE bulk, leaving only the hydrophilic diol-amide moieties at the surface. This two-step process is best represented by a precursor model, where the fraction of LDE collisions with the PE surface resulting in prolonged (i.e. inelastic) contact is included in a value known as the sticking coefficient, S. The sticking coefficient is related to T and the coverage n_s by

$$S = k' \exp(-E/RT)\, f(n_s)$$

where k´=constant, E is the activation energy and n_s is related to n_s by

$$n_s = \frac{n_s \bar{A}_s}{m_{PE} A_{PE}}$$

where $\bar{A}_s$=molar "packing area" of LDE, A_{PE} = the surface area per gram of PE, and m_{PE} = 5.000 g.

One can obtain ns from the relation

$$n_s = \frac{V_{soln}}{m_{PE} A_{PE}} (C_o - C)$$

where C_o-initial solution concentration; dividing $\frac{dn_s}{dt}$ by C gives the kS product. Plotting this last quantity against n_s yields curves whose shape reveal the sort of adsorption mechanism involved.

Other interesting properties can also be found if the adsorption is allowed to proceed to equilibrium. The isosteric heat of adsorption Q can be obtained from equilibrium LDE concentration Ceq by

$$\left(\frac{\partial \ln Ceq}{\partial (1/T)}\right)_{coverage} = \frac{Q}{R}$$

in the fashion of an ordinary chemical reaction. This expression can be derived from Kipling's (1965) similar formula involving the activity, a, of adsorbate LDE in solution. For dilute ideal solutions, ln Ceq approaches ln a, and Kipling's formula reduces to the above form. Ceq at constant coverage is obtained from a plot of Ceq vs n_s, which yields the adsorption isotherm.

Surface modification of polyethylene sheet by various techniques.

Several major surface-treatment processes were studied in this work: (a), LDE adsorption from aqueous solution; (b), LDE adsorption followed by posttreatment either with a dilute toluene solution of DM100 (a triisocyanate) or with a dilute aqueous solution of adipic acid (AA); (c) irradiation with 500 keV electrons either on a surface skin or isotropically through the sample bulk; (d), exposure to a radiofrequency glow discharge ("plasma") at 1.0torr (135 Pa) in air and (e) plasma exposure followed by posttreatment either with DM100 or AA, in dilute toluene or aqueous solution respectively. DM100 is a biuret trimer condensation product derived from hexamethylene diisocyanate and water; ti is essentially an aliphatic tri-isocyanate containing a biuret moiety and is marketed by Mobay Chemical Co. under the name Desmodur N-100. Appendix I contains chemical formulas for LDE, DM100 and AA; Appendix II details relevant physical properties.

In order to adsorb LDE onto PE sheet, the LDE solution must be refluxed at an elevated temperature near 90°C. The powder adsorption studies suggested that in order to assure complete LDE tail diffusion and equilibrium adsorption conditions at the surface, the solution should be refluxed for about 70 hours at 90 to 92°C, at an LDE concentration of 8.32×10^{-5}M. As in the powder-adsorption apparatus described above (see also fig. 2a), a 10-liter hot-water bath was required to maintain constant, isothermal conditions. Fig. 2b shows the strip-adsorption apparatus design. Strips of the test PE were cut to the 1" x 3" size (2.54 cm x 7.62 cm) accepted by the vertical flex tank, discussed later. A coolant-water (~10°C) stream was run through a 400 ml reflux condenser at about 200-250 ml/min. The strips were encased in a special nickel-mesh holder, to prevent flotation, in a charge of about 850 ml LDE solution, in a reaction kettle with 4-hole top. Ports were provided for condenser, stir shaft, thermometer, and the fourth port was unused. As in the powder apparatus, glass wool insulated the walls of the temperature bath. At 90°C, evaporation of bath fluid was a serious problem, and it was effec-

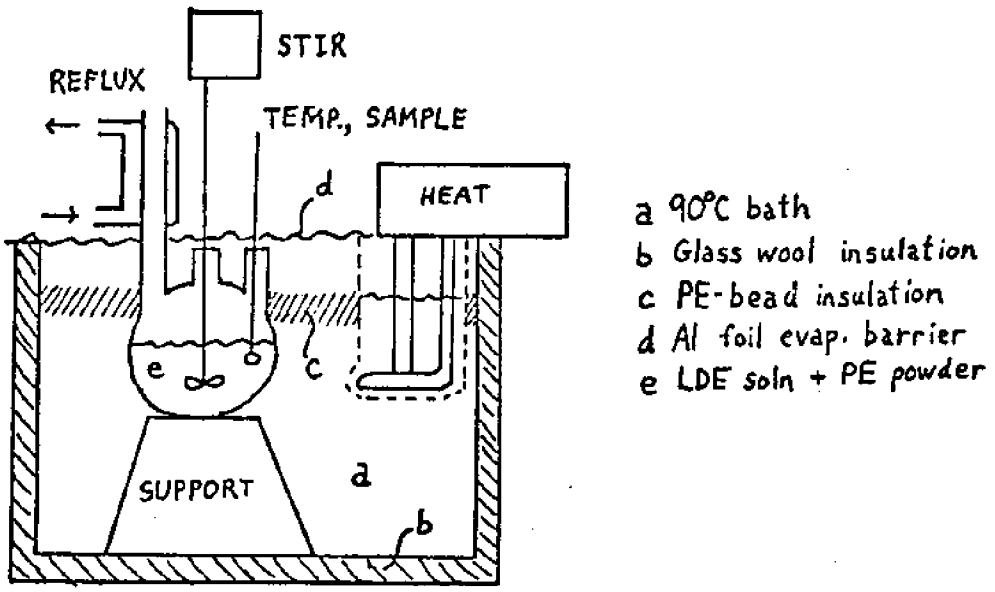

Figure 2. a) LPE Powder Adsorption Apparatus

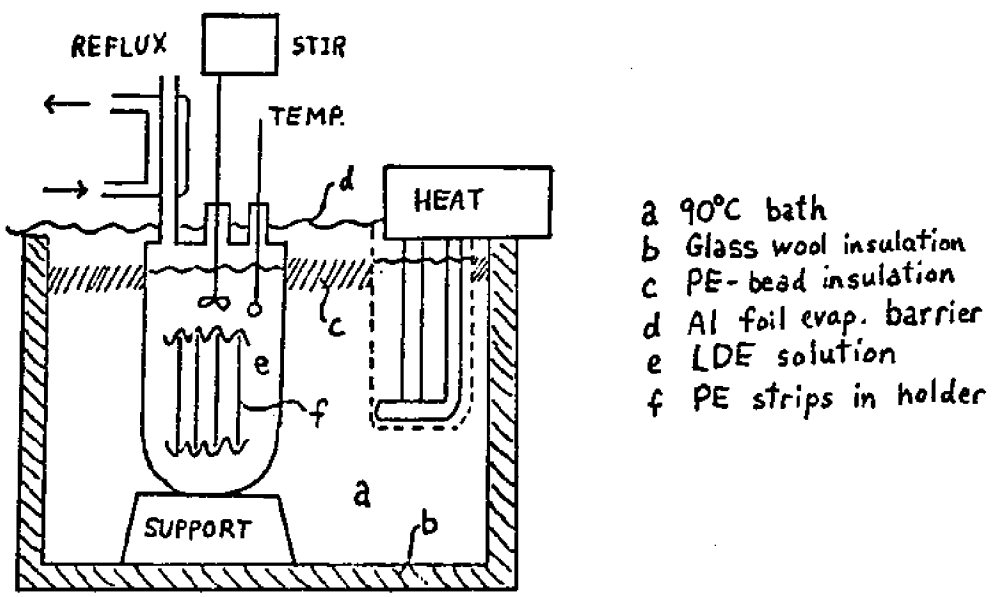

Figure 2. b) LDE Strip Adsorption Apparatus

tively solved by use of a 3 cm layer of PE pellets at the bath surface and a tightly wrapped aluminum-foil hood over the bath, through which only the immersion heater and reaction kettle protruded. Using a thermostatically-controlled immersion heater, temperature was controlled to within ±0.5°C, as monitored in the LDE solution.

It was found that the pre-cut PE strips tended to suffer about 1-2% linear shrinkage; this can be regarded as a practical drawback to this process if dimensional stability is important. The LDE-treated strip usually showed little difference in visual appearance from untreated strip, other than a very slight creamy or bluish cast, and a noticeable warp.

DM100 Posttreats: The second step in the surfactant adsorption-cross polymerization process involved exposure to dilute dry toluene solutions of DM100 triisocyanate at ambient temperature for times ranging from 2 min. to 24 hrs. The chemistry involved can be summarized by the equation $3nR(OH)_2 + 2nR'(NCO)_3 \longrightarrow (R'NHCOOR)n$. Three concentrations were used, all based on the estimated molar LDE uptake of a standard 1" x 3" PE strip with a unimolecular LDE skin; Appendix V outlines the procedure used to determine that each strip adsorbs 2.78×10^{-8} mole of LDE. Therefore, a perfectly stoichiometric reaction between all adsorbed LDE and DM100 from the surrounding solution would involve 1.85×10^{-8} mole DM100 or 8.87×10^{-6} g. This is to say that a unimolecularly coated PE strip exposed to a charge of solvent containing 8.87×10^{-6} g of DM100 should consume all of the polyisocyanate, if the addition reaction proceeded to completion. Adding in an arbitrary factor of 1.2 to provide a small surplus of isocyanate (in the event that untrapped moisture in the solvent had destroyed some of the water-sensitive DM100 molecules), a concentration unit, hereafter known as "R", was defined to describe the DM100 solutions used on LDE-treated strip and on all other PE strips. Thus, a total of 1.06×10^{-5} g DM100, dissolved in a solvent charge of 500 ml, yields a concentration of $1R=4.44 \times 10^{-7}M$. (The standard solvent charge per 1" x 3" strip was 50 ml.) Three concentration levels were used, namely

1R, 100R and 10,000R (i.e., 4.44×10^{-7}M, 4.44×10^{-5}M, and 4.44×10^{-3}M). These three concentration levels will be referred to as "L", "H", and "V", respectively.

The choice of solvent for DM100 became a tradeoff between low water affinity and low PE swelling ability. Toxicity was also considered as a secondary factor. The solvent also had to be non-reactive to isocyanate; any hydrocarbon was suitable in this regard. Toluene was finally chosen, since it swells PE less than benzene, and is less volatile than either benzene or hexane, and relatively non-toxic. Acetone also is chemically compatible, but reagent-grade acetone has roughly ten times the moisture content. Even the 300 ppm H_2O content of the toluene reagent used was enough to destroy the "H" solution of 4.44×10^{-5}M DM100, so it was passed through a 20-cm column of 4Å Linde sodium aluminosilicate sieves at about 1 to 5 ml/min. ESCA analysis of strip exposed to thusly dried DM100 solutions showed activity at the "L" concentration, hence the sieves apparently were successful in bringing the H_2O level down under 0.1 ppm.

The choice of DM100 was based on its largely aliphatic chemical structure, its trifunctionality and its commercial availability from Mobay Chemical. As mentioned above, it is a condensation product of 3 moles hexamethylene diisocyanate and 1 mole water, and is expected to be sterically more flexible than an aromatic diisocyanate such as MDI, or methylene di-p-phenyl diisocyanate. This flexibility is probably due to the flexible hexamethylene chains linking the biuret and urethane junctions, and comprising the backbone of the elastomer network. The trifunctionality of DM100 offers an opportunity to form a two-dimensional cross-polymerized network over the PE surface, while a difunctional isocyanate would only form a series of linear poly-urethane chains with insignificant degree of branching. The presence of an extensive two-dimensional molecular network would seem an important part of an effective barrier to salt-ion diffusion across the PE surface.

To react the LDE-treated strip, DM100 was prepared by successive dilutions in dry toluene at the "L", "H", and "V" concentrations defined above. One-half

strip was immersed at ambient temperature in 25 ml of solution for each of a range of times from 2 min. through 24 hrs. under gentle stirring. All reaction beakers were tightly sealed against atmospheric moisture. A similar series of such beakers were run at each of the three concentrations. In addition, a set of control strips which had not been LDE-treated were immersed in the identical manner in the dry toluene solutions of "L", "H", and "V" concentrations.

After DM100 reaction, each sample was quenched in running distilled H_2O for about 30 sec., to destroy unreacted isocyanate still on the strip surface. Full-length strips were prepared only at the 100-min. and 24-hr. times. The half-strips i.e., 1" x 1.5") were analyzed by ATR-IR and ESCA. Selected samples had contact-angle determinations done on them. Strips were then placed under rough vacuum for a minimum period of 3-5 days continuous pumping (mechanical), even then there were toluene outgassing problems during ESCA analysis. The pump was isolated from the samples by a 10-12 cm column of molecular sieve as a safeguard against back-diffusion of oil.

AA Posttreats: LDE-treated strip was also reacted with adipic acid (AA) in order to compare the performance of a polyester coating to the polyurethane coating just described. The reaction can be summarized as: $nR(OH)_2 + nR'(COOH)_2 \longrightarrow (R'COOR)n + 2n\ H_2O$. Conditions were nearly identical, except that AA was dissolved in distilled water, which is easier to work with and poses negligible swelling problems. Again, 50 ml of solution was used per strip; and the same total equivalent weights of AA per strip were used as in the DM100 experiments, or 3.34×10^{-8} mole AA per 1" x 3" strip, or 1.17×10^{-8} mole AA per 1" x 1.5" half-strip. The actual concentrations obtained at the "L", "H", and "V" levels, then, were 6.67×10^{-7}M, 6.67×10^{-5}M and 6.67×10^{-3}M, respectively. Again, a duplicate series of untreated controls were also exposed to each concentration. Reaction times again ran from 2 min. to 24 hrs. Reacted samples were rinsed for about 30 sec. in distilled running water. Almost all strips run were the "half" size, and all were

examined by ATR-IR. Selected LDE + AA strips also were observed by ESCA. Full-size strips were prepared at 24 hours only, for flexure testing.

Plasma-treated strip: The above posttreat procedures for DM100 and AA were repeated for strip samples exposed to a radiofrequency glow-discharge plasma. The plasma was standardized at 1.0 torr (~135 Pa) of air, with a flowrate of 2.0 cm^3/min atm (i.e. measured at P = 1 atm). Power delivered to the plasma region was kept at 50W, for a power density estimated to be in the 3-4mW/cm^3 range. For an initial study, blank PE strips were plasma-exposed for times ranging from 0.1 sec to 200 min. For times longer than about 20 min, power levels higher than the 50W used tended to overheat (and melt) the samples. The other parameters were suggested by the work of Hall, Westerdahl et. al. (1969). The 6-min. samples were chosen for posttreatment with DM100 and AA. Other samples were run at a high (25 cm^3/min atm) flow rate.

The plasma reactor used was a commercial model, the LFE Corporations's PFS/PDE/PDS 501 with an operating chamber about 22 cm diameter by 37 cm long. At 1.0 torr the inductively generated 13.56 MHz discharge fills isotropically the entire chamber; the samples were supported so that both sides received equal exposure. After about two min., samples became noticeably frosty in appearance, probably due to etching effects. Frosting is excessive beyond about 20 min. The discharge itself is a diffuse pinkish luminous region of static appearance when operating normally. About 8 full strips were reacted at one time; this allowed for wide spacing between strips to insure free flow of plasma gases between them. Gas was injected to the chamber by four rows of inlet ports spaced equidistant from each other around the circumference. A single exit port opposite the access hatch was connected to the pump. Figure 3 shows the layout of the LFE reactor as used in this work. Plasma treatment was found to alter the PE almost to the extent of LDE treatment, and in far shorter reaction time.

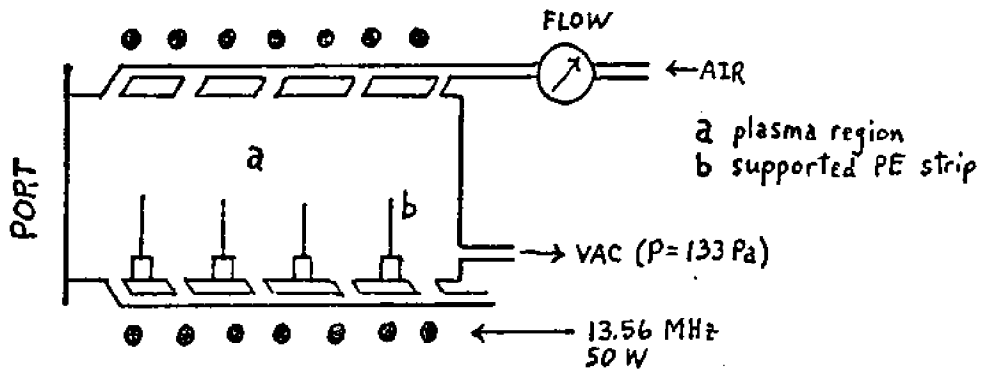

SIDE VIEW

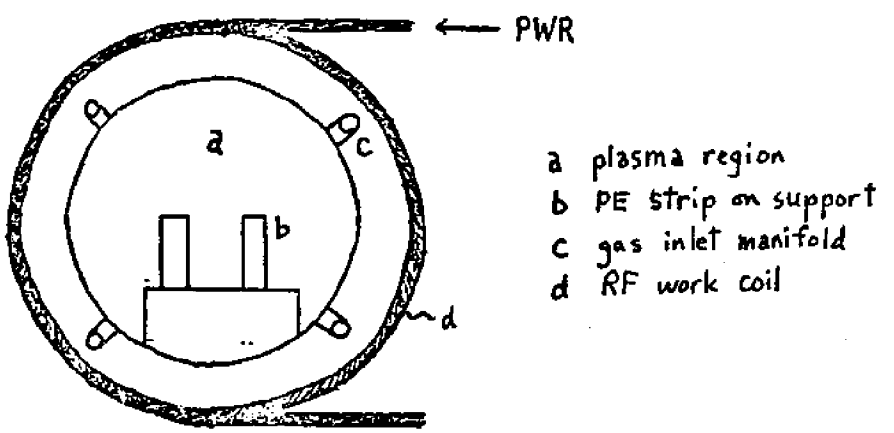

END VIEW

Figure 3. Plasma Treatment Apparatus

Electron irradiation: A radically different approach from the above methods was irradiation of the surface by shielded 500-keV electrons. Sheets of test PE were mounted on a special conveyor which passed under a 500 kV electron accelerator at the Cryovac Division, E. R. Grace & Co, Duncan, SC pilot plant. The beam from this accelerator is about 4 cm wide and 60 cm long; the sample passed perpendicular to the long dimension and to the beam axis. Conveyor speed was 25 cm/sec, for a dwell time in the beam of about 10 sec. Dosage received by the sample is linear in both beam current and residence time (hence, number of passes under beam); dosages as low as 0.1 megarad (1.0 MR = 10J/g or 10kJ/kg) were possible with this system. Dosage levels of 2.0 MR, 0.6 MR and 0.1 MR were administered to three large samples of test polyethylene; for the 2.0 MR sample the beam current was 4 ma and the sample was exposed for 8 passes or roughly 80 sec. For the 0.6 MR sample, the same current was used. and exposure time cut to about 20 sec. The low-dose sample was exposed for about 10 sec. at 1ma beam current. Fig 4a shows the electron-beam irradiation layout.

Two independent methods of monitoring dose were used. Cryovac has developed a special blue-dyed cellophane which bleaches when exposed to radiation in a well-characterized way. The cellophane is prepared in 25 μm film, and this enables one to stack layers of this film to any multiple of 25 μm thickness. Dosage is monitored by determining the decrease of absorbance at the characteristic wavelength of the dye chromophore. Using a stack of this cellophane, one can plot electron-beam dose vs. depth in the stack, to a resolution of 25 μm. In this way, experiments with varying thicknesses of aluminum foil shielding showed that 500 μm (0.5 mm) of foil blocked out all of the dose curve from the cellophane except a tail region, where the dose was seen to drop to half its cellophane-surface value at a depth of 75 μm into the plastic (see Fig. 4b). This was the desired dose profile, since the overall thickness of the polyethylene sheet was 1.58 mm or 1580 μm. With this shielding in place, the exposure times and beam currents mentioned above gave the desired surface dosages of 2.0 MR, 0.6 MR and 0.1 MR.

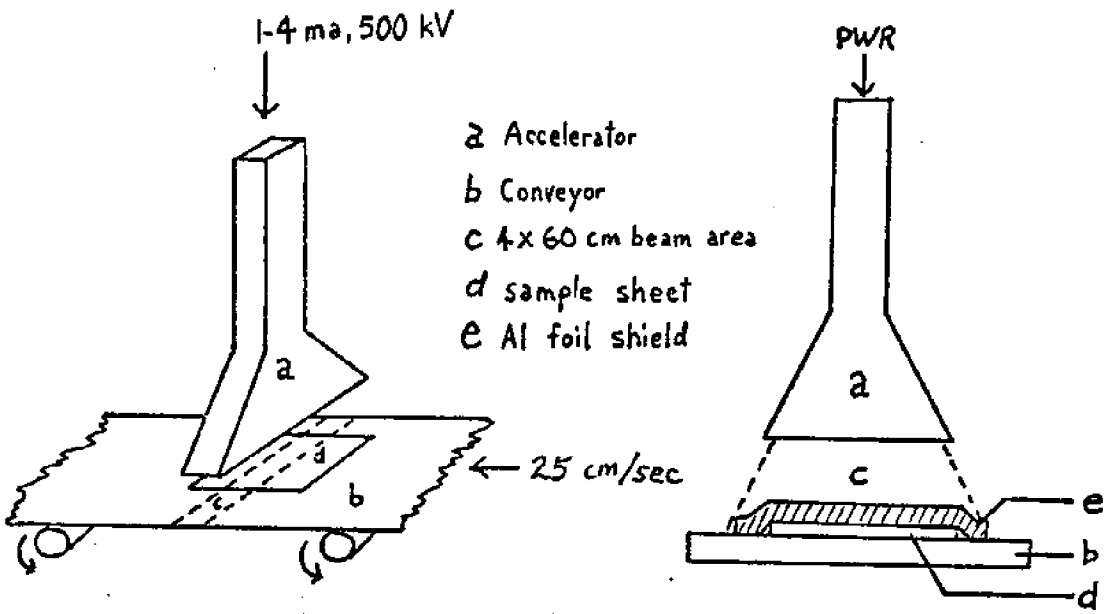

Figure 4. a) 500 keV Electron-Beam Irradiation Apparatus (Cryovac)

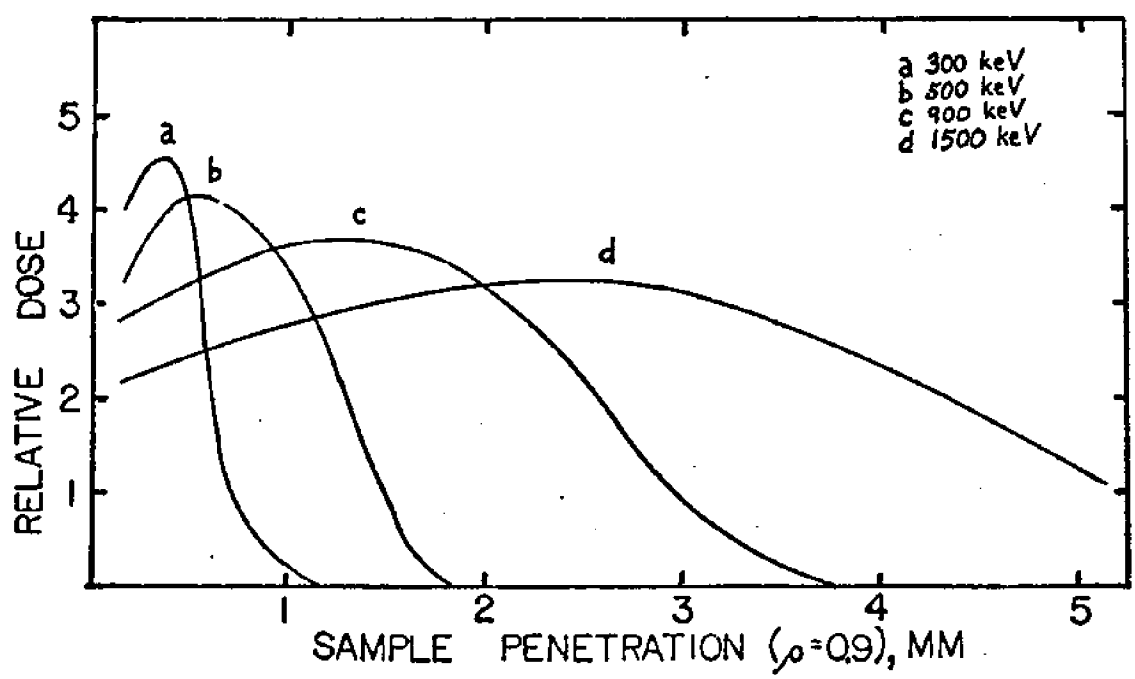

Figure 4. b) Electron Radiation Dose vs. Sample Depth for Various Energies (Trump et al., 1940).

To obtain some idea of the extent of crosslinking that these measured dosages actually generated in the test PE, gel-content measurements were done on samples actually removed from various positions in the PE sheet's bulk. Chip samples thus taken were refluxed in toluene for 24 hrs. and the non-dissolved residue was vacuum dried under gentle heat for 48 hours. Totally un-dosed PE would show zero gel content; totally crosslinked PE would show near 100% gel. The actual maximum gel possible at infinite dose tends to be less than 100%; usually near 75% for LDPE resins similar to the test PE resin. For the 2.0 MR sample, surface scrapings (sampling perhaps 100-150 μm of surface region) showed 1.0% gel; similar samples from the center of the sheet were un-gelled. These figures are consistent with the cellophane-stack data (see Figs. 5a and 5b). Since the detection limit for reasonably small samples (i.e. 0.5g) is about 0.5% gel, the 0.6 MR sample was just at this limit, and the 0.1 MR sample well below it. The gel-dose curve in Fig. 5b is insensitive to doses below about 0.7 MR. It was thus necessary to invoke the linearity of the dose vs exposure time and dose vs beam current relationships to infer from the 2.0 MR sample data the probable dose profiles found at lower exposure times than 80 sec. The cellophane dosimeter also unfortunately becomes inaccurate below about 1 MR; it was designed for industrial applications which lie in higher dosage regimes.

The choice of beam voltage was strongly dictated by available industrial installations; Cryovac exclusively uses accelerators at or above 500 keV. The ideal voltage is actually closer to around 150 keV, as seen in Fig 4b; the lower voltage tends to yield a sharper dose-depth distribution. Below 150 keV, air resistance severely degrades beam output at the sample surface for air pathlength generally in use (5-10 cm). However, the desired depth profile for this work was found to be well within the capacity of the Cryovac 500 keV machine, rendering this question largely moot.

Finally, bulk-irradiated strip was also tested; this work actually preceded

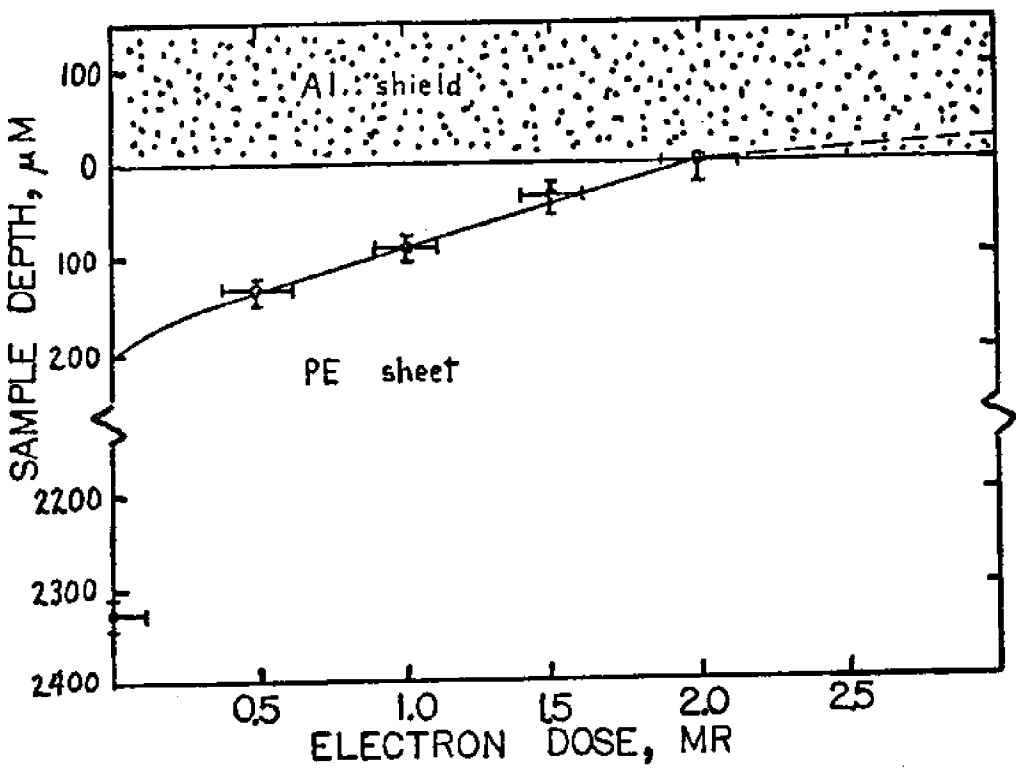

Figure 5. a) Cellophane Stack Dosimetry of 2.0 MR Surface-Irradiated PE Sheet (done at Cryovac).

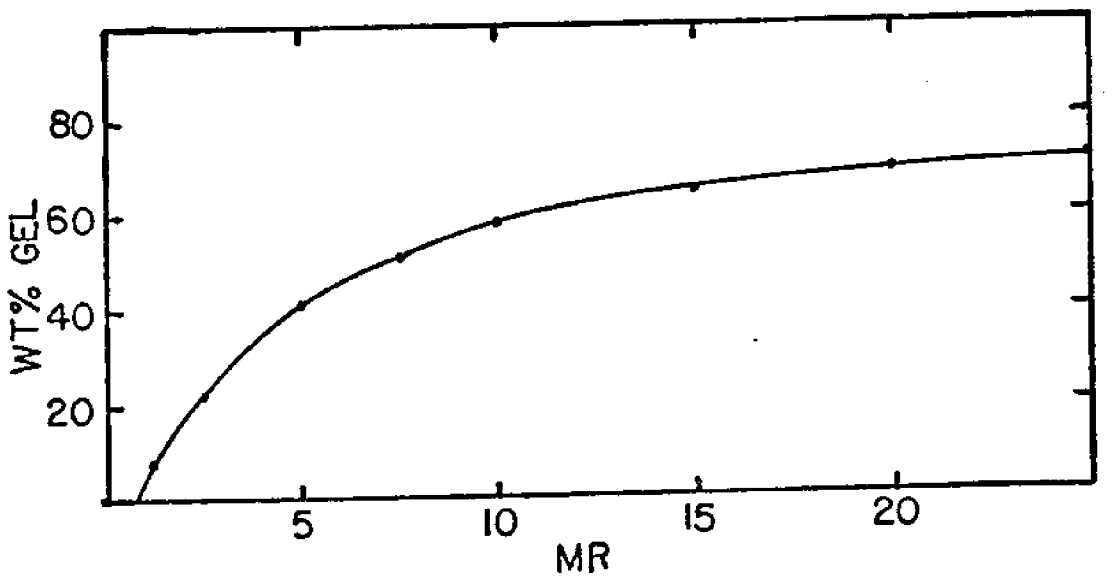

Figure 5. b) Typical Gel-Dose Curve for Low-Density PE (ρ = 0.921 g/cm^3). (Pike, 1975).

the more involved surface-irradiation work as a pilot experiment. Dosages of 11.5 MR, 5.9 MR and 2.9 MR were utilized. Polyethylene dosimeters were used in this work; here the 930 cm^{-1} transvinylene IR band was quantitatively monitored for radiation-induced increase in intensity. Again, gel contents were determined and found to be consistent with the dosimeter data.

Accelerated testing of polymer strip by cyclic flexure.

Since in a typical marine environment, polymer samples would most likely be subjected to a repetitive loading due to wave action, the dominant failure mode is thought to be fatigue failure. This defined as "a reduction [by degradation] of the ability of a [of a polymer] to withstand cyclic or repeated stresses." (Perry and Chilton, p. 23). In accordance with this reasoning, two cyclic flexure systems were designed and built for this work, referred to hence forth as the vertical apparatus and the horizontal apparatus.

The vertical cyclic flexure apparatus designed by Garry was used as a way to telescope a typical degradation time regime (~years) to a more manageable range (~days). As seen in Fig. 6a, torque from an adjustable-speed gearhead motor system (a fluid drive was used for 400 rpm work) was converted to reciprocal plunging action by a simple crank and lever arrangement with a solidly anchored fulcrum. The plunging action was conveyed to the test strips by an eight fold plunger bar, which was carefully aligned to insure uniform amplitude across the entire row of eight sample positions. Each 1" x 3" (2.54 cm x 7.62 cm) strip was firmly bolted into a special brass holder (fig. 6b) by the two short sides, and the plunger pushed down on a 2.5 cm x 2.5 cm region at the strip's center. The plunger geometry was intended to distribute the load reasonably broadly over the entire flexed portion of the strip. Plunger amplitude when fully loaded with eight strips was 1.0 mm with the original Garry 60 rpm motor system, and slightly less (0.6 mm) with the 400 rpm configuration. The difference was largely due to design limitation imposed by the much more demanding high-speed load regime. While PE was flexed primarily at 60, 70 and 400 rpm, most work on PP, PS and PMMA was done at 30 rpm.

The vertical apparatus used a 15-liter lucite tank sealed with silicone rubber. For paralled baseline runs featuring salt water, distilled water and air environments simultaneously, lucite partitions were installed as shown in Fig. 6a. The

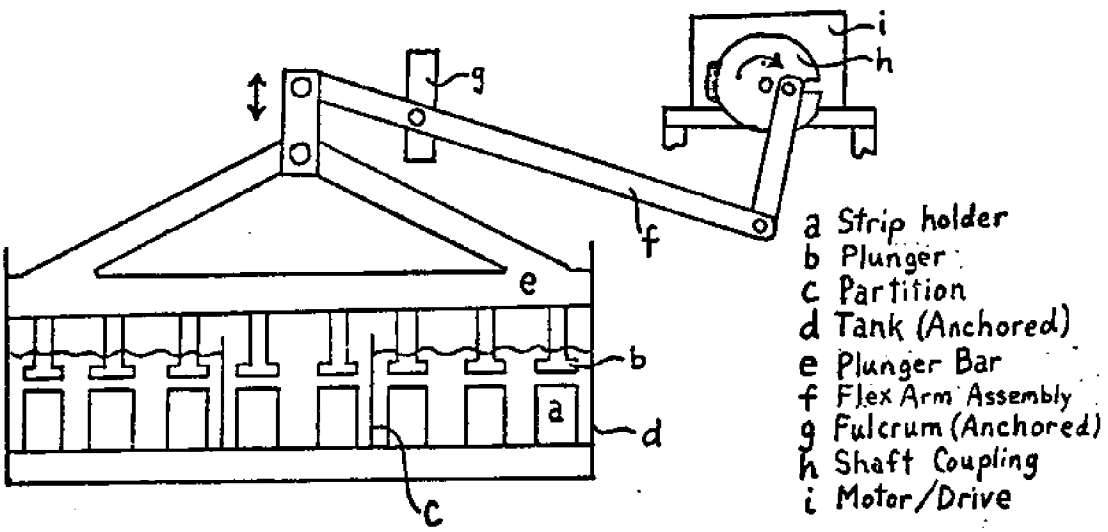

Figure 6. a) Flex Tank Apparatus General Layout

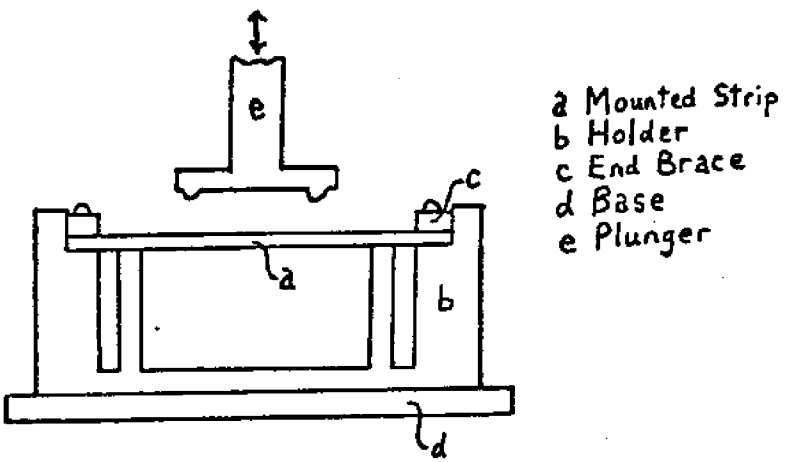

Figure 6. b) Geometry of Sample Holder and Plunger

tank was filled with about 7 to 7.5 liters of synthetic seawater (Aquarium Systems, Inc.'s "Instant Ocean" salt formula was used as directed by the manufacturer). The entire tank and moter/flex arm assembly were braced to vertical supports extending from floor to ceiling to eliminate plunger-induced slippage or "walking".

The original vertical apparatus was designed to be run at about 70 rpm or less, that is, 70 cycles flex/min or less. This meant that flex-duration regimes out to about $10^{6.1}$ or $10^{6.2}$ cycles were conveniently accessible. However, it became clear that much interesting flex behavior occurs beyond 6.1 or 6.2 log cycles flex, so a higher-speed apparatus was constructed which used a larger motor and and a Vickers fluid transmission infinitely variable over a speed range of 1800 rpm backwards to 1800 rpm forward (with respect to the motor). The use of high flex cycling rates meant that flywheel effects and centrifugal tensions were to become excessive at the crank end of the flex arm; as a result the entire shaft, disk and crank assembly was cemented together as an intergral unit after experience showed that this measure was necessary. Even with these precautions, it was found that flex-cycling rates higher than about 400 rpm required delicate balancing of the entire flex-arm system, and it was feared that the bearings, already worn out by continuous duty at 60-70 rpm, would fail altogether. Even so, at 400 rpm the conveniently available flex regime extends out to as far as 7.0 log cycles flex. To reach 8 log cycles would require 174 days vs. 17.4 days at 7 log cycles. Higher cycling rates would have been the only practical answer — e.g. to 1800 rpm (and even then it would require 39 days to reach 8 log cycles). Thus it was concluded that the point of diminishing returns in this respect was reached at about 400 rpm.

The Vickers transmission proved to be remarkably stable, when adjusted by strobe to 400 rpm ±0.3%, the drift in speed after 24 hrs never exceeded 1.5%. The plunger was capable of being leveled to ±0.1 to 0.2 mm across its length; when loaded fully with strips the actual leveling difference was evened out to less

than 0.1 mm by the elastic rebound of the strips themselves. Assuming a roughly linear relationship between flex amplitude and degradation extent for a given number of flex cycles (for small amplitudes), this implies an error of around 10% or less in the total amount of, say, crystallinity loss measured. This fortunately was smaller than the size of most retardation effects observed.

The horizontal flex apparatus (Figure 7) consisted of a standard bottle shaking apparatus outfitted so that it will accept a 2.5 gallon lucite tank filled with sea water. Inside, on the bottom of the tank is a clamp for samples. The samples can be of varying width and thickness but must all be approximately 12 inches long so that they extend out of the top of the tank. Above the tank and shaker is a fixed apparatus to hold the ends of the samples. When in operation, the ends of the samples are affixed to the moving bottom of the sea water tank and to the stationary clamps above the tank, thereby achieving a gentle, repetitive flexing of the samples. The frequency of the shaker was set at approximately 60 rpm for all tests. To inhibit evaporation, the tank was also fitted with a clear plastic top which did not interfere with the protruding samples. Finally, the tank was also fitted with baffles to retard splashing and to promote moderate circulation of the solution.

For all flex runs, the solution was constantly monitored to insure that a specific gravity of 1.020 and a temperature of 20°C was maintained. Evaporation occurring during the experiments was compensated for by the addition of distilled water in such amounts as were required to keep the specific gravity constant.

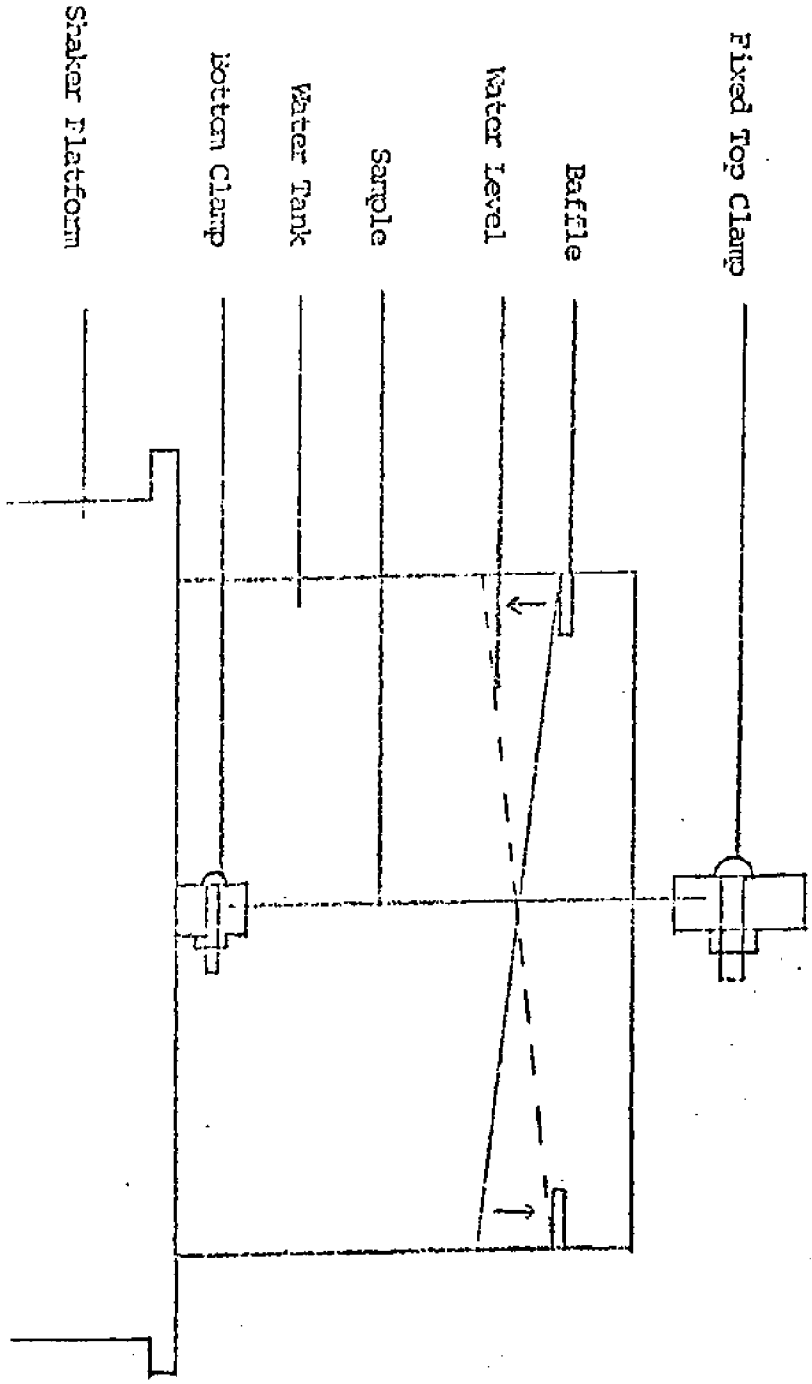

Figure 7: Horizontal Flexer Apparatus

Characterization of modified polymer surfaces. Characterization of the modified surface layer poses especially difficult problems owing to its extreme thinness, probably less than 100nm. Bulk analytical methods such as transmission IR, NMR, visible/UV or X-ray diffraction tend to generate a signal whose surface-region component is swamped out by the vastly larger bulk component. Related techniques to the above which preferentially sample a surface layer of the sample are ATR-IR, ESR, ESCA (X-ray photelectron spectroscopy) and X-ray fluoresence. As mentioned above, ATR-IR and ESCA were both extensively employed in the effort to characterize the results of the various surface-modification methods studied in this work. The sampling depth of ATR-IR, as discussed in N.J. Harrick's book (1973) is of the order of the illuminating wavelength, i.e. several microns. This is probably at least two orders of magnitude deeper than the LDE layer, for example; nevertheless, significant carbonyl signal does appear at 1720cm^{-1}, which is absent in blank polyethylene samples. However, the cross-polymerized DM100 or AA region must be thinner, as it appears only marginally (as a shoulder near 1620cm^{-1} for DM100, and a noticeable enlargement of the 1720^{-1} peak for AA). The characteristic sampling depth for ESCA signals is a function of the penetrating power of the soft X-rays used to excite the sample, and of the ejected inner-shell electrons which are electronically dispersed and counted in the detector. The value falls in the 10nm range, which is comparable to the expected depth of the LDE layer. Significant signals do show up here; the N/O, O/C ratios are all noticeably different for posttreated LDE samples and LDE-only strips (the 1s peak was used in all cases.)

All the above discussion, however, is based on the cavalier assumption of the existence of a sharp, smooth PE boundary. Such is not the case. In reality, there is a density gradient which varies from near zero (i.e. atmosphere) to 0.918 (the density of the test PE resin) in some small fraction of a micron. The gradient effect is result of surface porosity and on a much smaller scale, the amor-

phous molecular nature of the surface.

On a larger scale (i.e., microns), the surface of the Garry resin is scoured with fine milling grooves, and still larger random scratches, pits and other deformitie show up in the 10 to 100μm size range. All of these irregularities degrade the specularity of reflected light, hence degrading ATR signal. ESCA is less affected by this problem as it does not depend on optical reflection of the incident radiation.

While ATR-IR is principally useful in qualitatively characterizing the chemical moieties present in the surface region, ESCA sheds light on elemental abundances for atoms possessing inner shells (e.g., C,N,O), and some degree of chemical information is obtainable from examination at high resolution of element-peak shifts. Hence the two methods are somewhat complementary. In this research the principal advantage of ATR-IR over ESCA was the ease of obtaining spectrograms. ESCA requires a high (10^{-8} torr or 10^{-6}Pa) vacuum, necessitating elaborate procedure and posing a significant sample-processing bottleneck, since about two full days are absorbed in the complete operation, from loading to reloading of specimen chamber, for only about a dozen samples. At least 4 or 5 times that number could be processed in fast-scan mode on IR, using the available micro-ATR module and a Perkin-Elmer grating instrument, in those two days.

Given the circumstances of the modified surface layers encountered in this research, it was found that ATR-IR was best used to qualitatively characterize broad classes of surfaces: e.g., all the PE + LDE surfaces, all the PE + DM100 samples, and all the PE + plasma exposure surfaces. Each of the major categories, including the above ones and PE + AA, PE + LDE + DM100, PE + LDE + AA, PE + plasma + DM100, and PE + plasma + AA, were all discernible from one another, if only barely in several cases. To obtain such information as concentration effects and time dependence of reaction extent, ESCA was used to monitor the O/C, N/C and N/O ratios. The N/C ratio was found to show the greatest sensitivity to class of surface and to the more detailed rate and concentration phenomena. Rough conclusions as to

kinetics thus seem possible if these reactions are carried out a variety of temperatures so as to obtain information about thermal behavior.

Mention should be made of error sources and their importance. ESCA elemental abundances are calculated from peak-area ratios on the same sample location at the same machine settings; the detector has a built-in error, conservatively estimated at 10% to 20% but typically found to be closer to 5% or even less. Added to this is the problem of determining baselines, which can be a small error source (~1%) for large, noise-free signals, but major (~50% or more) for faint, broad peaks (such as N 1s, which was important to this work). The peaks are usually photocopied onto standard Xerox paper stock, which is reasonably (to 1%) uniform in thickness and density. They are then cut out and weighed to the nearest 10^{-4}g. Weighing errors are again small for large cutout masses (<<1%) but significant (up to 10%) for the tiny slivers which usually resulted for nitrogen traces. For chemical-shift determination, resolution in the fast-scan mode suitable for elemental-ratio work was too low (about 0.6% of the pass energy was found to be typical for the instrument used). The pass energy (analogous to slit width in IR work) was usually set at 200 eV, hence the resolution was ~1.2eV, which is slightly less than most shifts. Reducing the pass energy also reduces this figure, and also reduces the input to the detector. The compromise was made at 25eV, for a resolution of about 0.15eV, which was adequate for rough chemical shift assignments in all of the samples examined under high resolution.

Monitoring of polymer degradation. Actual degradation of the resins studied, and the retardation effects on polyethylene degradation of the surface treatments studied, was assessed by several means. Destructive-testing methods included yield-stress measurements on an Instron stress apparatus, dilute-solution viscosity determination of molecular weight (for soluble resins), and melt-viscosity determination. The non-destructive method used was crystallinity determination (for semicrystalline resins) by wide-angle X-ray diffraction.

Each resin studied required the use of different properties as degradation monitors. For PMMA, dilute-solution viscosity was used; for PP and PS, melt viscosity was employed. X-ray diffraction and yield-stress were useful monitors for PE.

Solution Viscosity. In the case of polymethylmethacrylate, an amorphous polymer, the parameter to monitor degradation was molecular weight since dilute solution viscosity measurements easily lend themselves to use with PMMA. Samples of PMMA were taken from the center portion of the flexed specimen and dissolved in chloroform to concentrations of approximately 0.2 grams/deciliter. Dilutions of 0.1 g/dL, 0.05 g/dL, and 0.025 g/dL were then made and the respective viscosities measured at 25.00°C ± 0.05PC using a 100 cm^3 Ostwald viscometer. Upon obtaining the intrinsic viscosity, [n], the molecular weight was calculated for each sample. Appendix VI details the theory and includes the data obtained.

Stress-Strain: For polyethylene, stress-strain measurements were made on the flexed samples, as detailed in Appendix VII. Instron experiments were done on 1 1/2" x 5/16" x 1/16" polyethylene samples. The crosshead speed was 2 inches per minute and measurements were made until the yield point was reached. The yield stress was found to be an effective monitor on the stability of polyethylene.

Melt Viscosity: The melt viscosities which were used as direct indicators of molecular weight were obtained on the Mechanical Spectrometer manufactured by Rheometrics, Inc., available in the Polymer Rheology Laboratory of the Chemical

Engineering Department. Throughout the current work, the 25 mm cone and plate geometry was used with the environmental chamber.

Viscosity tests were run on low density polyethylene at 150°C which is well above its experimentally-determined melt peak near 107°C. This insures that the polymer is completely amorphous during testing so that all variations in viscosity from sample to sample result from molecular weight variations. The tests on polypropylene were conducted at 180°C, 190°C and 200°C compard to its experimentally determined melt temperature of 160°C. The polystyrene tests were a bit more difficult because the test sample was an adulterated (i.e., not pure polystyrene) high impact version. At 200°C the samples were obviously melts and the experiments yielded reasonable viscosities. At lower temperatures, the melt was also obvious, but the higher viscosities introduced greater instabilities to the melt and measurements were not possible at the upper range of shear rates.

Each of the polymer groups was subjected to a number of tests. First, base line curves of identical, untreated samples were taken to insure the reproducibility of known results. For polystyrene, an untreated blank was run before or after each of the altered samples to insure valid comparisons. This was because of difficulties in the operation of the mechanical spectrometer at the time of these runs. Samples were tested that were subjected to a wide range of treatment conditions. The most extreme cases were tested first to determine if any detectable change was made at these conditions before going on to the milder conditions.

The experimental geometry and associated rheological equations for viscosity measurements are shown in Figure 8. Only the shear viscosity data were required in this work although the measurements necessary to calculate the first normal stress difference were also made and may be examined at a later date. The melt viscosity can be calculated directly from the data according to the equation:

$$\eta = \frac{3M\beta}{2\pi R^3 \omega} = 9.6 \frac{M}{\omega}$$

Figure 8: Plate and Cone Geometry and Equations
(From: Rheometrics Operation Manual)

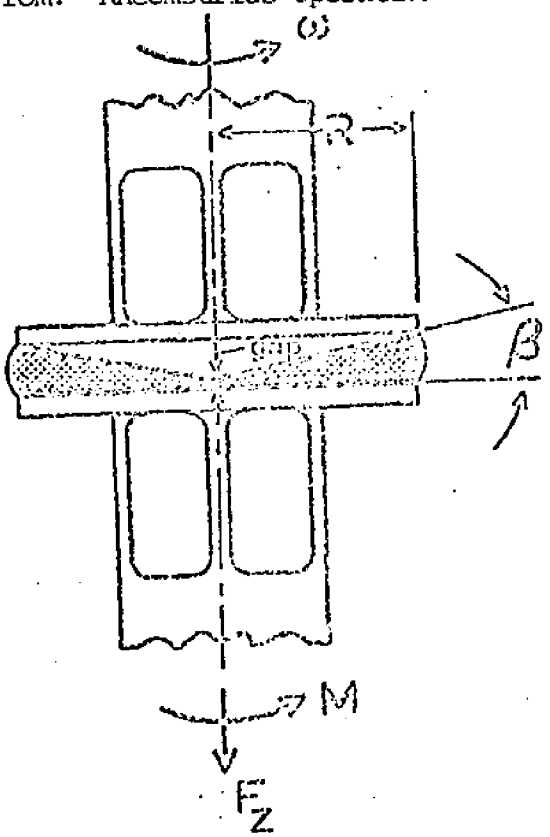

Steady Flow

$$\dot{\gamma} = \omega/\beta$$ shear rate

$$T_{12} = \frac{3M}{2\pi R^3}$$ shear stress

$$\eta = \frac{T_{12}}{\dot{\gamma}} = \frac{3M\beta}{2\pi R^3 \omega}$$ shear viscosity

$$T_{11} - T_{22} = \frac{2F_z}{\pi R^2}$$ first normal stress difference

where:

M = Measured Torque [gm/cm] ω = Input Angular Velocity [Rad/sec]

β = .04 Rad R = 12.5 cm η = Viscosity [Poise]

The chart below shows some sample calculations:

ω [Rad/Sec]	M [Gm/Cm]	η [Poise]
.001	7	6.84×10^5
.0016	10	6.11×10^5
.0025	15	3.75×10^5

Upon completing this data reduction, the log melt viscosity is plotted against the log angular velocity. This is the format used for all melt-viscosity plots appearing later.

Some additional reduction of this data was considered necessary to determine the statistical significance of differences in the measurements. The following ratio as a measure of the statistical significance was used:

$$\frac{\eta_{FLEX} - \eta_{BLANK}}{\sqrt{s.d._{FLEX}^2 - s.d._{BLANK}^2}}$$

The numerator is simply the difference between the viscosity at a given shear rate of a treated sample and a standard sample. The denominator is one standard deviation (s.d.) for the data involved at this shear rate. This s.d. can be calculated in a number of ways depending on the data available. Optimally, the square root of the sum of the squares of the s.d.'s for both the flexed and the blank samples is the composite s.d. Unfortunately, since only one run is made for a degraded sample, degraded s.d.'s are not directly obtainable. This problem was tackled in the following two ways.

The easiest way was to assume that the s.d. for the treated sample was the same as that for the blank. The composite then becomes:

$$s.d._{comp} = \sqrt{2}\ s.d._{blank}$$

This seems like a valid assumption since all measurements are made in roughly the same range and should therefore be subject to similar experimental error.

A second approach that was used for some samples was to estimate the s.d. for the flexed samples based on observed oscillations and other instabilities during the measurement process for each data point. In this case, the composite s.d. becomes:

$$s.d._{comp} = \sqrt{s.d._{EST}^2 + s.d._{BLANK}^2}$$

This is admittedly a slightly more subjective method than the first but in those cases where both forms were applied, the s.d. values came out reasonably close together.

The ratio of the actual deviation to the s.d. reveals how close to the 68% confidence limit the data has come. Each of the viscosity graphs in the next section is accompanied by a plot of the above defined ratio against the log shear rate. Theoretically, for large sample sizes, 68% of the data should fall between 1 and -1 on the error correlation graphs in the next section. 95% should fall between approximately 2 and -2. The main assumption in the above analysis is that the data is subject to a normally distributed error scatter.

All samples of polyethlene and polypropylene were measured for crystallinity before viscosity tests were made since the melt viscosity is a destructive test. An unflexed sample of polystyrene was also tested to insure that it was in fact amorphous.

X-Ray Diffraction: The best monitor of degradation for semicrystalline resins

was found to be the quantitative determination, by wide-angle X-ray diffraction, of the bulk crystallinity of polymer strip (PE or PP) subjected to the desired test conditions. The initial step was to determine the crystallinity X_c of the test PE and PP resins by several independent methods, including wide-angle diffraction. First, the densities of several samples were accurately determined by settling in a density-gradient column with resolution of about 0.0001 g/cm^3. From this the specific volume V was obtained, and from there it was only a matter of applying the formula of Helmuth and Wunderlich (1965):

$$1 - X_c = \frac{V_a - V}{V_a - V_c}$$

where V_a = 1.172 cm^3/g and V_c = 1.001 cm^3/g are the extrapolated amorphous and crystalline specific volumes for PE according to these workers..

A second method involves determining ΔH_c (the enthalpy of crystallization) from differential scanning calorimetry (DSC) data obtained for the Garry resin. Mandelkern, Gopalan and Jackson (1967) found that

$$X_c = 1.49\ \Delta H_c$$

for polyethylenes: the value for ΔH_c is obtained from the area of the "melting" peak from the DSC trace referred to a known standard melt curve (In was used in this work). Values for X_c found by DSC usually are several percent low due to contamination of sample by exposure to oxidizing environment (the test PE resin had considerable surface oxidation, and the DSC X_c values were about 10% low).

Wide-angle X-ray diffractograms show a number of sharp crystalline diffraction maxima and several broader maxima due to amorphous regions. Reasonably consistent data for PE can be obtained by use of the amorphous hump between $2\theta = 30°$ and $2\theta = 12°$, and the 110 and 200 crystalline bands which appear in this region. Appendix VIII discusses the actual deconvolution and peak-area-ratio computation algorithms used. As mentioned earlier with regard to processing of ESCA data, a

prime error source is definition of baselines. Fortunately, this can be kept low (<1% of peak area) due to large signal to noise ratios usually achieved on the diffractogram. Errors from planimeter tracing are insignificant; the error is primarily due to the accuracy of the readout scale itself.

RESULTS

Baseline Degradation Studies. Extensive investigations into the baseline degradation behavior of PE, PP, PMMA, and PS were done prior to the surface-modification experiments on PE. Crystallinity and melt viscosity were monitored vs. cycles of flexure for PE and PP; molecular weight vs. cycles flex was determined for PMMA, and melt viscosity vs. shear rate studied for PE, PP and PS. In addition, yield stress and crystallinity change with flexure were correlated for PE. The effect of flex environment on crystallinity loss was also studied for PE.

The PE and PP resins used in this work were in addition subjected to a series of tests, the results of which are contained in Table 1, in order to characterize them more completely.

The initial flexure experiments were conducted in air and in seawater on PMMA and PE. Through viscosity measurements it was possible to monitor the molecular weight of a polymethylemethacrylate sample as a function of flexure cycles (Appendix IX). For PMMA flexed in air at 60 cpm, as shown in Figure 9, the molecular weight steadily decreases with an increasing number of flexure cycles. The plot of molecular weight in gram per gram-mole as a function of log cycles indicates no appreciable degradation occurs up to 1000 cycles (17 minutes). During the course of 10^6 cycles (11.5 days) the molecular weight decreases from the blank value of 1,520,000 to 1,050,000 representing a 30% change.

Similarly, Figure 10 is a graph of molecular weight versus log flexure cycles for polymethylmethacrylate flexed in synthetic seawater at 30 c.p.m. The same characteristics are present in this plot although the molecular weight decreased from 1,520,000 to 1,065,000 after 10^6 flexures (23 days). There is some incongruity in the PMMA data because of a frequency change from the flexures in aire (60 c.p.m.) to those in seawater (30 c.p.m.). Further details are provided in Appendix IX.

An additional finding in the experiments involving polymethylmethacrylate flexure in synthetic seawater indicated that degradation was decelerated when samples experienced significantly lengthy rest periods from flexure. For instance a sample which was flexed for 25 hours, removed from the flexure apparatus for 10 hours and then flexed for 10 hours showed less degradation than expected. From figure 8 the molecular weight after 6.3×10^4 cycles (35 hours) should be 1,293,000 whereas for a sample experiencing the above history the molecular weight was 1,471,000, close to that for 10 hours flexure.

Experiments with low density polyethylene were performed in air as well as synthetic seawater (figures 11 and 12, respectively). Figure 9 shows the per cent crystallinity of the polyethylene as a function of log cycles for flexures in air at 60 c.p.m. The initial crystallinity of about 52% was unchanged after 100,000 cycles (1.2 days); however, after 800,000 cycles (9.2 days) the crystallinity has decreased to 44.5%. For identical tests performed in a sea environment at 60 c.p.m., Fig. 12 shows the crystallinity decreasing from 52% to 41% after 1.5×10^6 cycles (17 days). Raw data for crystallinity studies of polyethylene are presented in Appendix VII.

As a further confirmation that degradation of polyethylene was in fact occurring, stress-strain tests were made on the flexed samples. The relative Young's modulus (ratio of modulus of flexed sample to that of the unflexed) is plotted as a function of log cycles in figure 13 for polyethylene flexed in synthetic seawater. The relative modulus decreases from 1 at zero flexures to 0.86 after 1.1×10^6 flexures (13 days). A similar behavior is seen in Figure 14 in which the relative yield stress (ratio of yield stress of flexed samples to yield stress of unflexed) is plotted against log cycles. The relative yield stress decreases from 1 at zero flexures to 0.87 after 1.1×10^6 cycles (13 days). The stress-strain data can be found in Appendix VII.

Thus, in view of the results presented concerning flexure experiments, it is clear that over the range of flexures studied the parameters investigated are

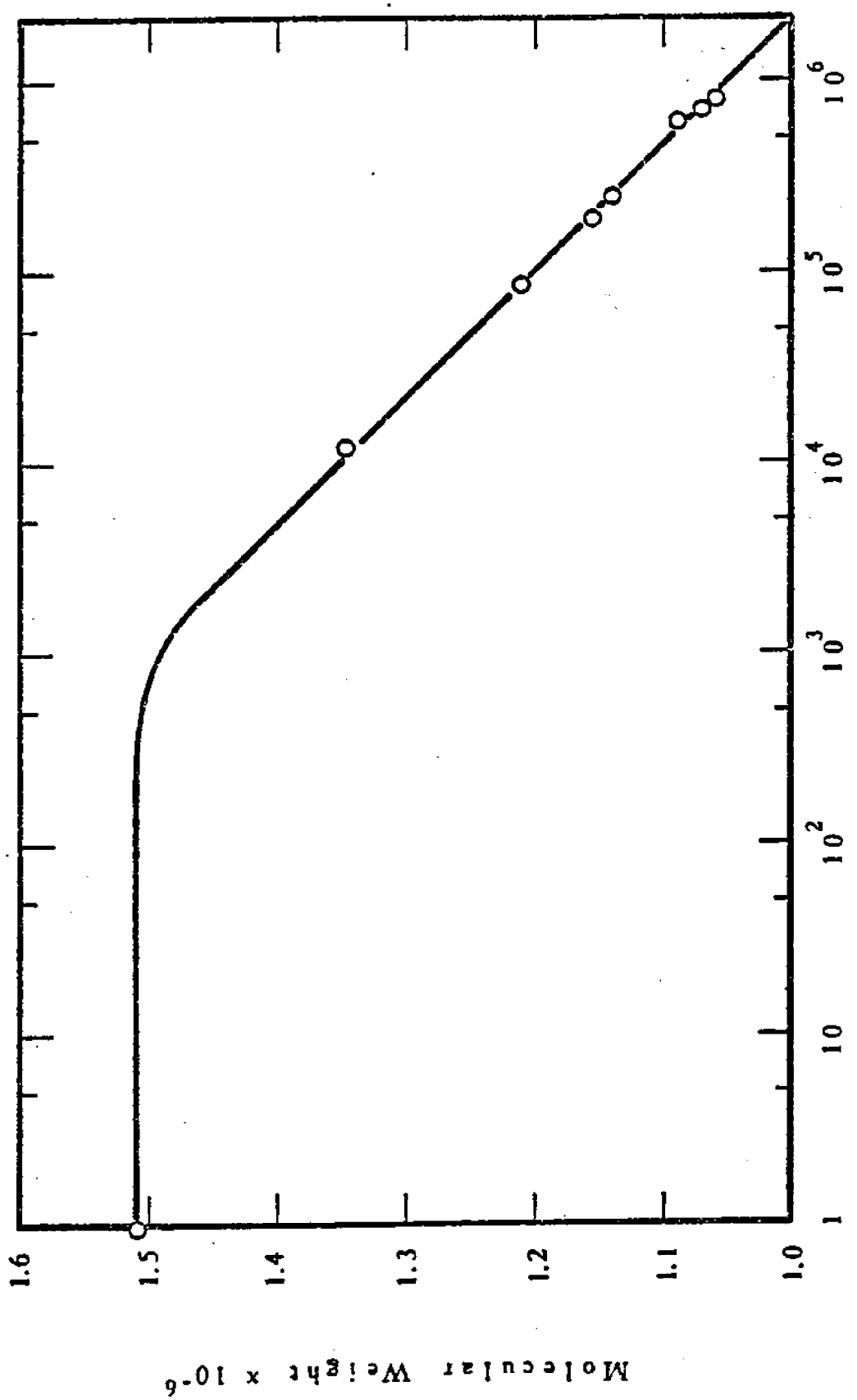

Figure 9: PMMA Degradation due to Flexure in Air at 60 c.p.m., Monitored by Molecular Weight

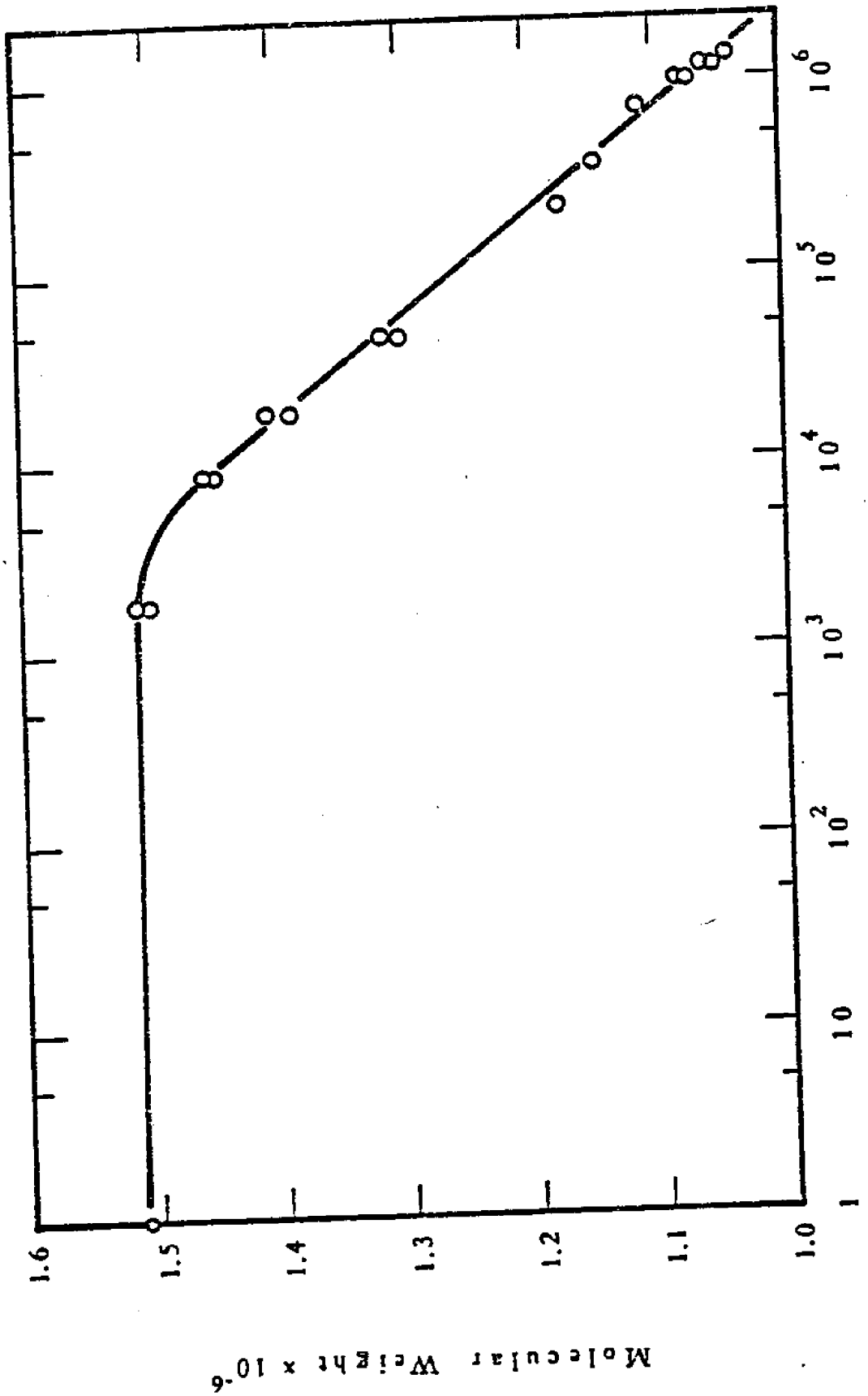

Figure 10: PMMA Degradation due to Flexure in Synthetic Seawater at 30 c.p.m. Monitored by Molecular Weight

Table 1. Characterization of the PE and PP Resins by Various Methods

	PE	PP
Density (gradient column method)	0.9182 g/cm^3	0.905g/cm^3
Volume	1.089 cm^3/g	1.105g/c
X_c, crystalline fraction (volumetric)	0.486	-
X_c (wide-angle X-ray diffractometry)	0.51 to 0.52	0.50 to 0.52
X_c (differential scanning calorimetry)	0.418 to 0.428	-
ΔH_f of crystallites (DSC)	119 ± 1.5 kJ/kg	83.1±1.5kJ/kg
Melt Index	1.8	0.57
Sheet Thickness	1.58 mm	1.67mm
Yield Stress (Garry, Instron method)	8.460 ± 0.070 MPa	-
Young's Modulus (Garry, Instrom method)	63.4 ± 3 MPa	-
DSC Peaks: 1st Melt	107°C	160°C
Recrystallization	90°C	106°C
2nd Melt	108°C	160°C
Shoulders: 1st Melt	53°, 96°C	144°C
Recrystallization	53°C	none
2nd Melt	none	none

PE Transmission IR Absorbances: CH_2 stretch at 2910 cm^{-1}, 2860 cm^{-1}
CH_2 bend at 1470 cm^{-1}, 1380 cm^{-1}
CH_2 rock at 730 cm^{-1}, 720 cm^{-1}
CH_3 bend at 1310 cm^{-1}
Oxidation: CO at 1720 cm^{-1}, OH ~ 3600 cm^{-1}

PE ATR IR Absorbances: Same as transmission plus H_2O spikes in the 1800 cm^{-1} to 1350 cm^{-1} region.

PE ESCA Atomic Ratios on Surface: O/C = 0.135; N/C = 0.0014; N/O = 0.0077

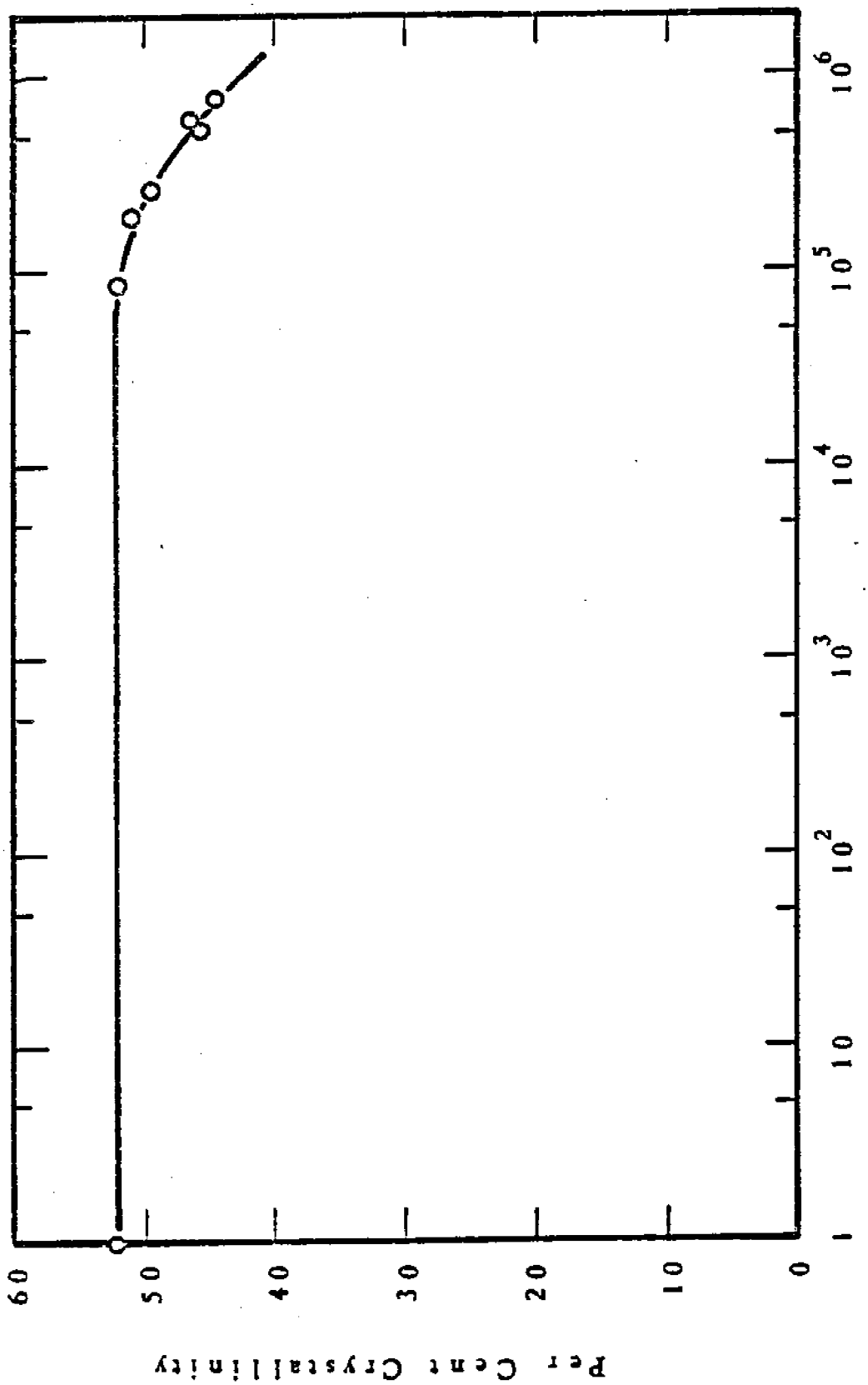

Figure 11: PE Degradation due to Flexure in Air at 60 c.p.m., Monitored by Percent Crystallinity

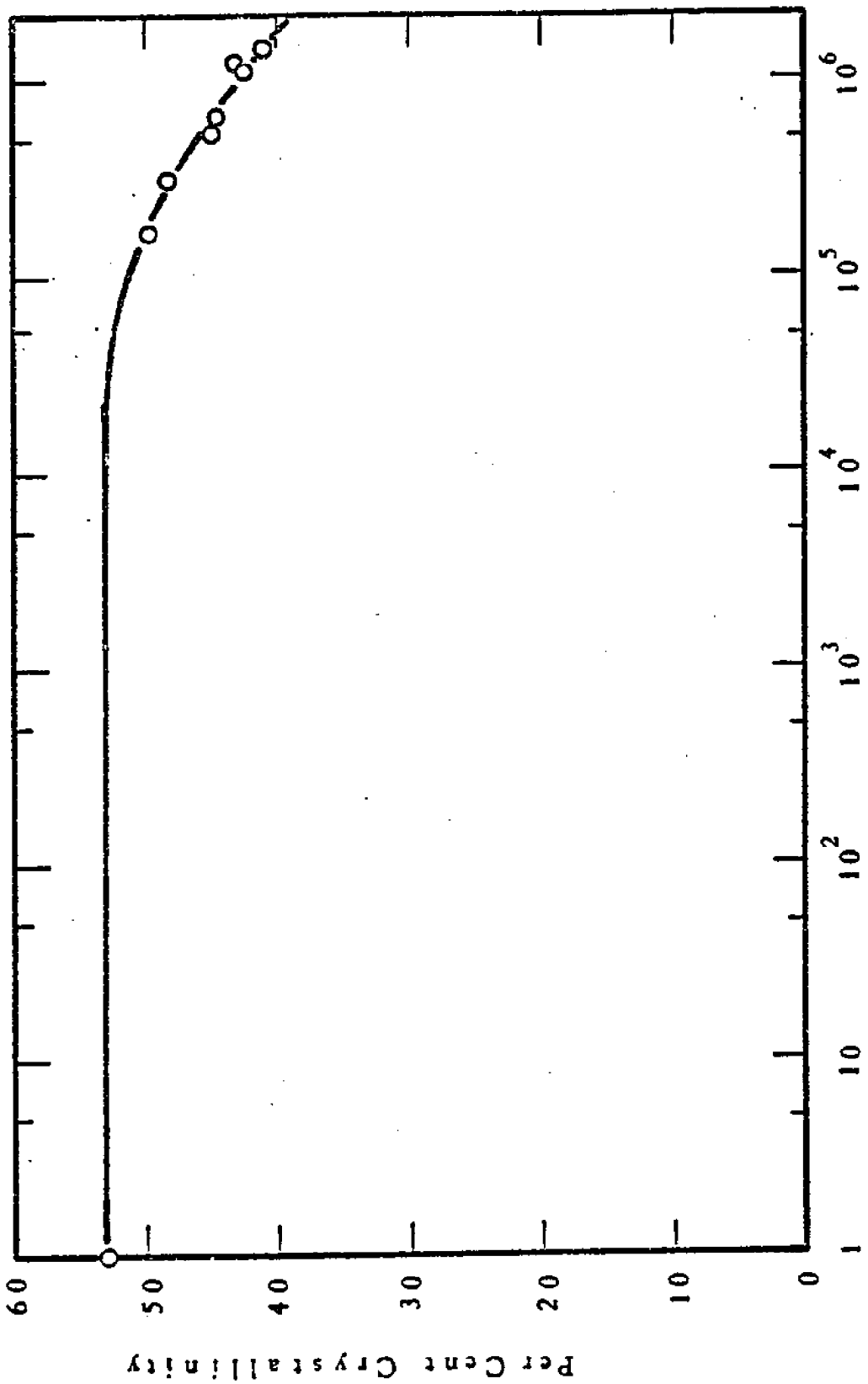

Figure 12: PE Degradation due to Flexure in Synthetic Seawater at 60 c.p.m., Monitored by Percent Crystallinity

approximately linearly related to the log of flexure cycles. Furthermore, 1.5 to 2.5 hours of flexure time at 60 rpm must elapse before appreciable degradation occurs.

Additional flexure experiments on polyethylene served to extend these early findings. To better understand the effects due to the flex environment, a three-way run featuring seawater, distilled water and air was done, both with the Garry 70 rpm (Fig. 15) motor and the newer 400 rpm. rig (Fig 16). In each case it was found that while actual onset of degradation occurred roughly at the same time (within about half a log cycle of flex), the degradation rates were actually different in each environment. Degradation rates were fastest in seawater in both cases, and noticeably slower for fresh water. The air environment showed still slower degradation. Because of the irreducible magnitude of data scatter (in part due to inherent polymeric inhomogeneities), it is risky to make more than qualitative statements about the magnitude of the degradation-rate differences involved; such analysis awaits more precise (or more numerous and hence statistically treatable) data. No basic change was noted between 70 and 400 rpm other than the important observation that onset of degradation occurs near 3.0 to 3.5 log cycles flex at 400 rpm, but did not occur until 4.5 to 5.0 log cycles flex at 70 rpm. This significant finding may shed light on the mechanical contribution to the degradation process. Tables 2 and 3 give the crystallinity and log-cycle data as well as flex time in hours.

Since LDE-treated strip is brought close to the softening point for extended periods, crystallinity was monitored as a function of dwell time at 87°C and 92°C. In figure 17 the crystallinity of annealed strip is plotted against dwell time in distilled water at 87°C and 92°C. Crystallinity was found to be unchanging throughout.

In addition, strips annealed for various periods at 87°C and 92°C were flexed for 6.33 log cycles at 400 rpm. Figure 18 shows the effect of annealing for various periods at 87°C and 92°C on degradation rate, relative to unannealed resin. Cry-

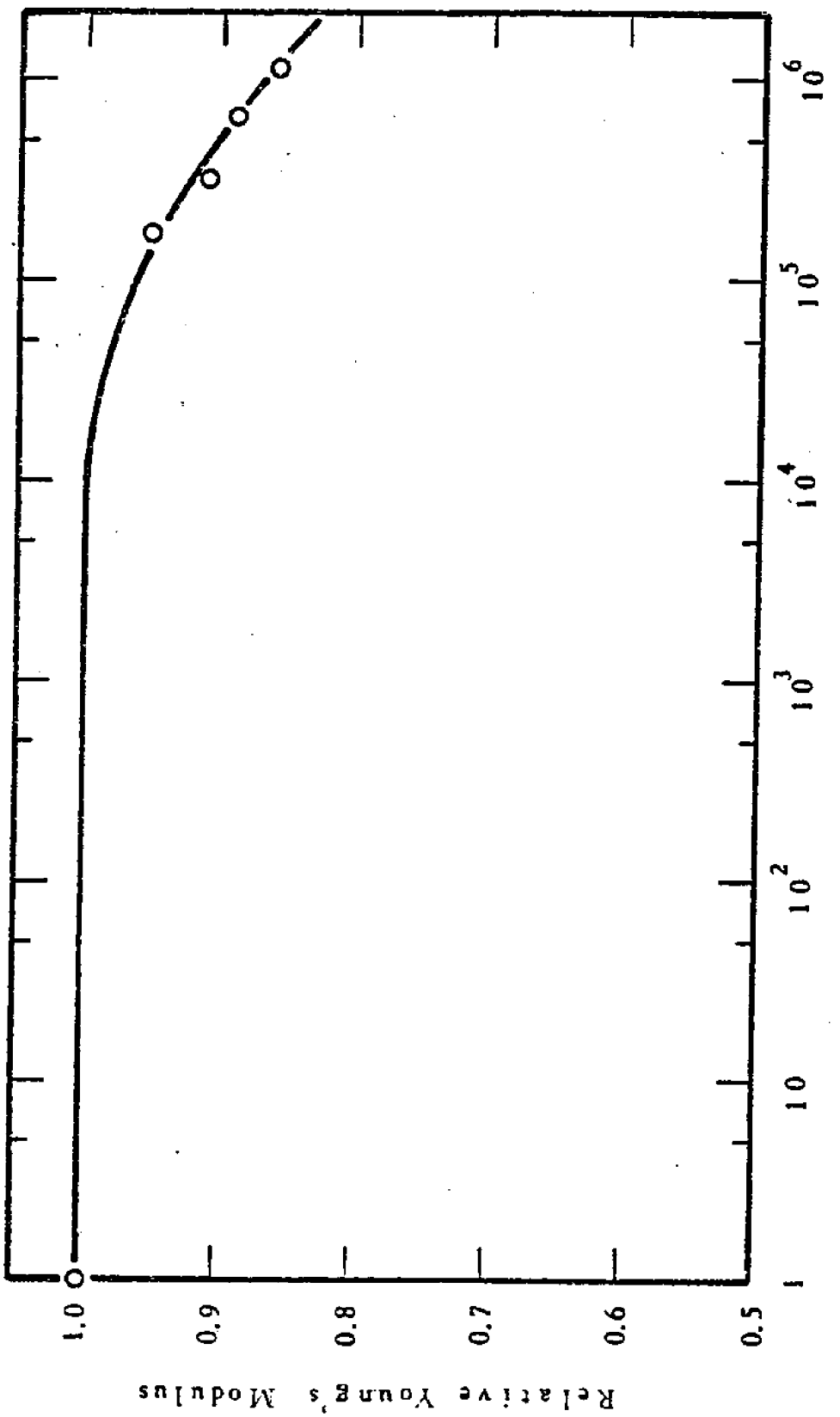

Figure 13 : PE Degradation due to Flexure in Synthetic Seawater at 60 c.p.m. Monitored by Young's Modulus

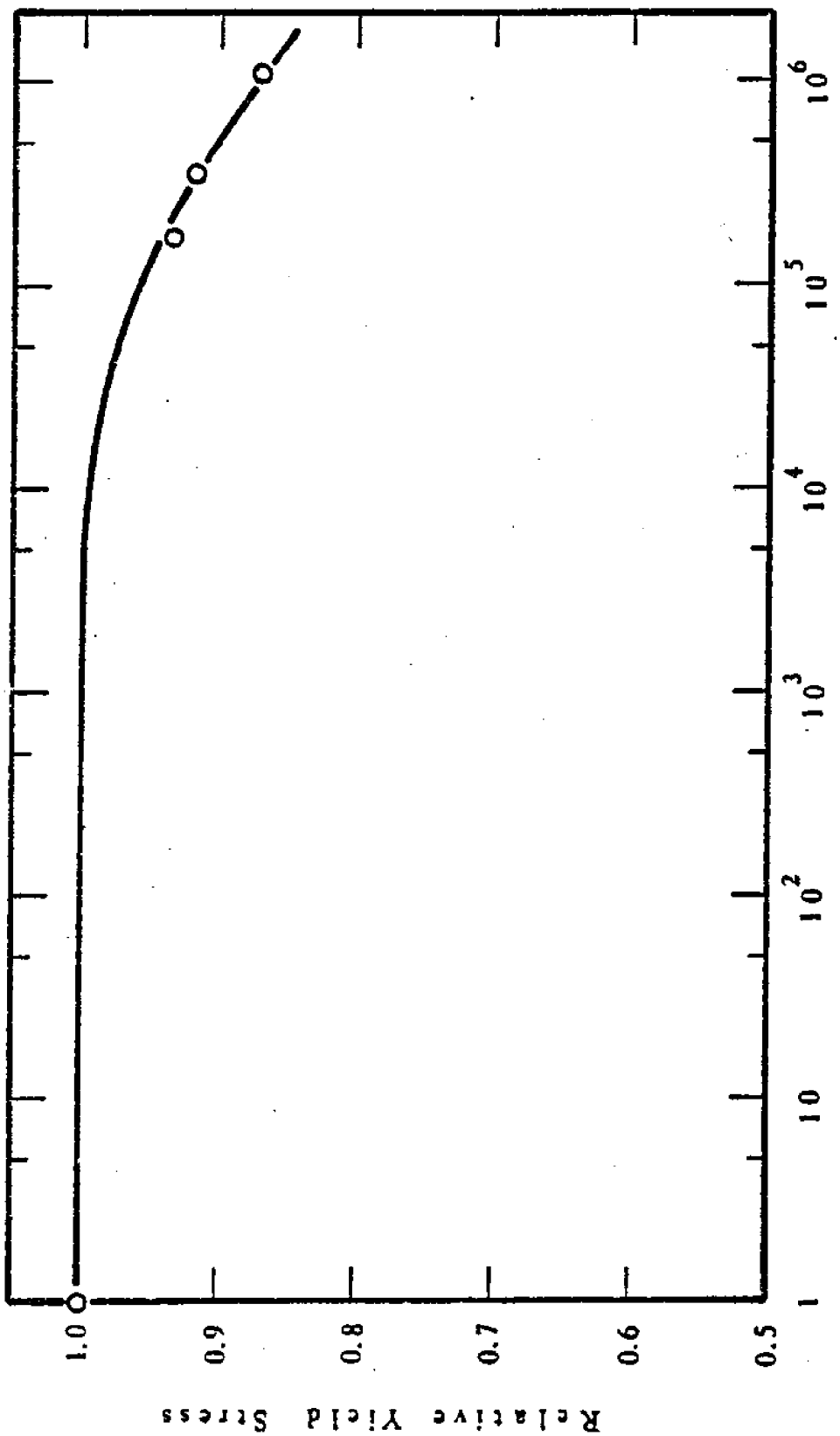

Figure 14: PE Degradation due to Flexure in Synthetic Seawater at 60 c.p.m., Monitored by Yield Stress

Table 2. X-Ray Diffraction Data for Blank PE Flexed at 70 rpm in Various Environments

No.	Log Cycles	$X_c(100)$	Environment
D-1	Standard	52.0	-
2	4.06	51.8	Seawater
3	4.50	51.2	"
4	5.07	50.9	"
5	5.29	48.7	"
6	5.71	46.4	"
7	6.15	44.2	"
8	4.06	51.9	Distilled Water
9	4.50	51.3	"
10	5.07	51.2	"
11	5.29	49.9	"
12	5.71	47.7	"
13	6.15	45.8	"
14	4.06	52.6	Air
15	4.84	51.5	"
16	5.51	49.7	"
17	6.15	47.0	"

Table 3. X-Ray Data for Blank PE Flexed at 400 rpm in Various Environments

No.	Log Cycles	$X_c(100)$	No.	Log Cycles	$X_c(100)$
E-1	Standard #1 }	51.0	E-20	Standard #2	50.7
2	Standard #2 }		21S	6.06	47.3
3S	4.20	50.8	22S	"	46.7
4S	"	49.9	23S	"	46.5
5S	"	49.8	24A	"	48.0
6A	"	49.6	25A	"	47.8
7A	"	49.5	26D	"	47.4
8D	"	49.6	27D	"	47.5
9D	"	49.6	28D	"	47.6
10D	"	49.9	29	Standard #1	50.4
11S	5.23	49.9	30	Standard #2	51.1
12S	"	49.3	31S	6.94	44.9
13S	"	48.6	32S	"	45.9
14A	"	49.6	33S	"	45.0
15A	"	49.3	34A	"	47.2
16D	"	49.0	35A	"	47.1
17D	"	49.8	36D	"	46.5
18D	"	48.6	37D	"	45.5
19	Standard #1	51.0	38D	"	45.8

S = Seawater; A = Air; D = Distilled Water

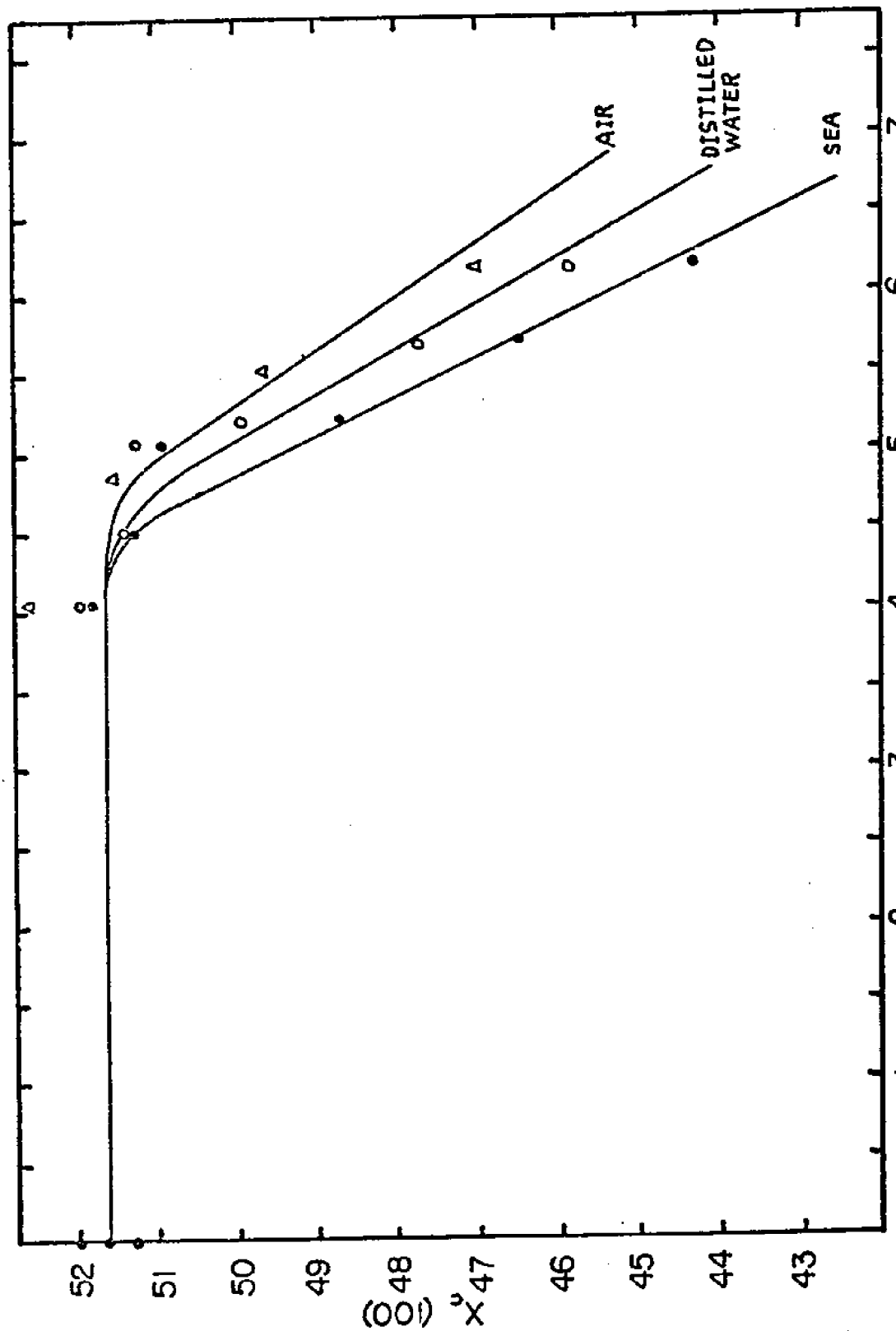

Figure 15: Crystallinity vs. Log Cycles Flex for Blank PE at 70 rpm in Various Environments.

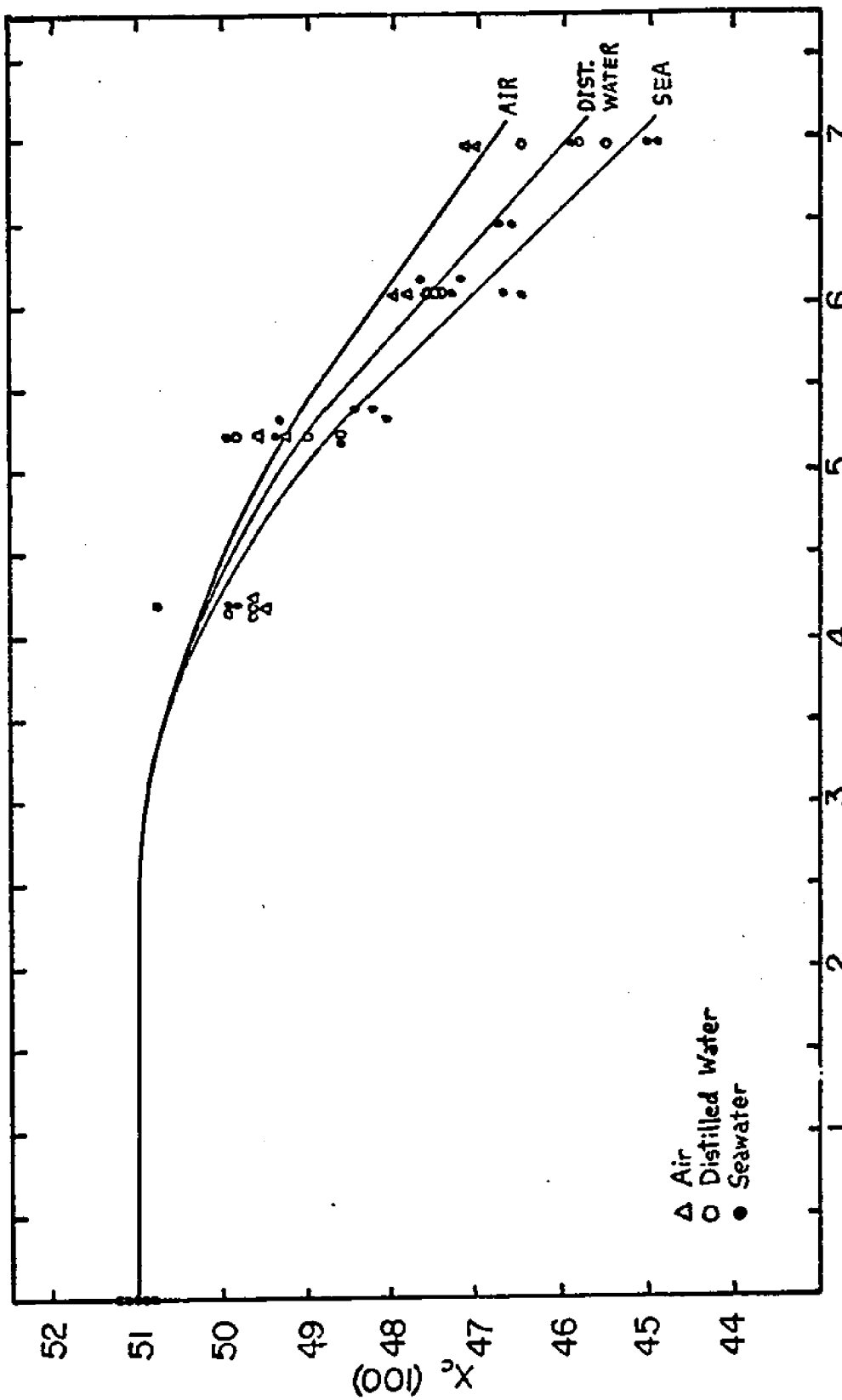

Figure 16: Crystallinity vs. Log Cycles Flex for Blank PE Flexed in Various Environments at 400 rpm.

Table 4. Data for Blank PE Annealed at 87°C and 92°C.

No.	Anneal Time	$X_c(100)$	T=87°C
A-1	Standard	52.0	
2	2.8 hr.	50.9	
3	9.5	51.3	
4	22.25	51.2	
5	30.5	52.2	
6	36.7	50.6	
7	46.8	50.9	
8	58.7	50.7	
9	73.1	50.7	
B-1	Standard	52.8	T=92°C
2	1.5 hr.	50.7	
3	4.5	51.2	
4	14.8	51.0	
5	25.2	47.9	
6	43.2	48.1	
7	53.8	48.8	
8	72.3	51.2	

Run B suffered from noise-promoted data scatter.

Table 5. X-Ray Data for Blank PE Annealed at 87° and 92°C, then Flexed at 400 rpm for 6.33 log cycles.

No.	Anneal Time	$X_c(100)$	Temp.
1,	Standard #1	50.8	-
2	" #2	50.7	-
3	" #3	51.5	-
4	Untreated Blank #1	49.1	-
5	" " #2	48.6	-
6	2.8 hr	49.5	87°C
7	22.25	48.6	"
8	58.7	48.2	"
9	4.5	48.6	92°C
10	25.2	49.2	"
11	72.3	48.7	"

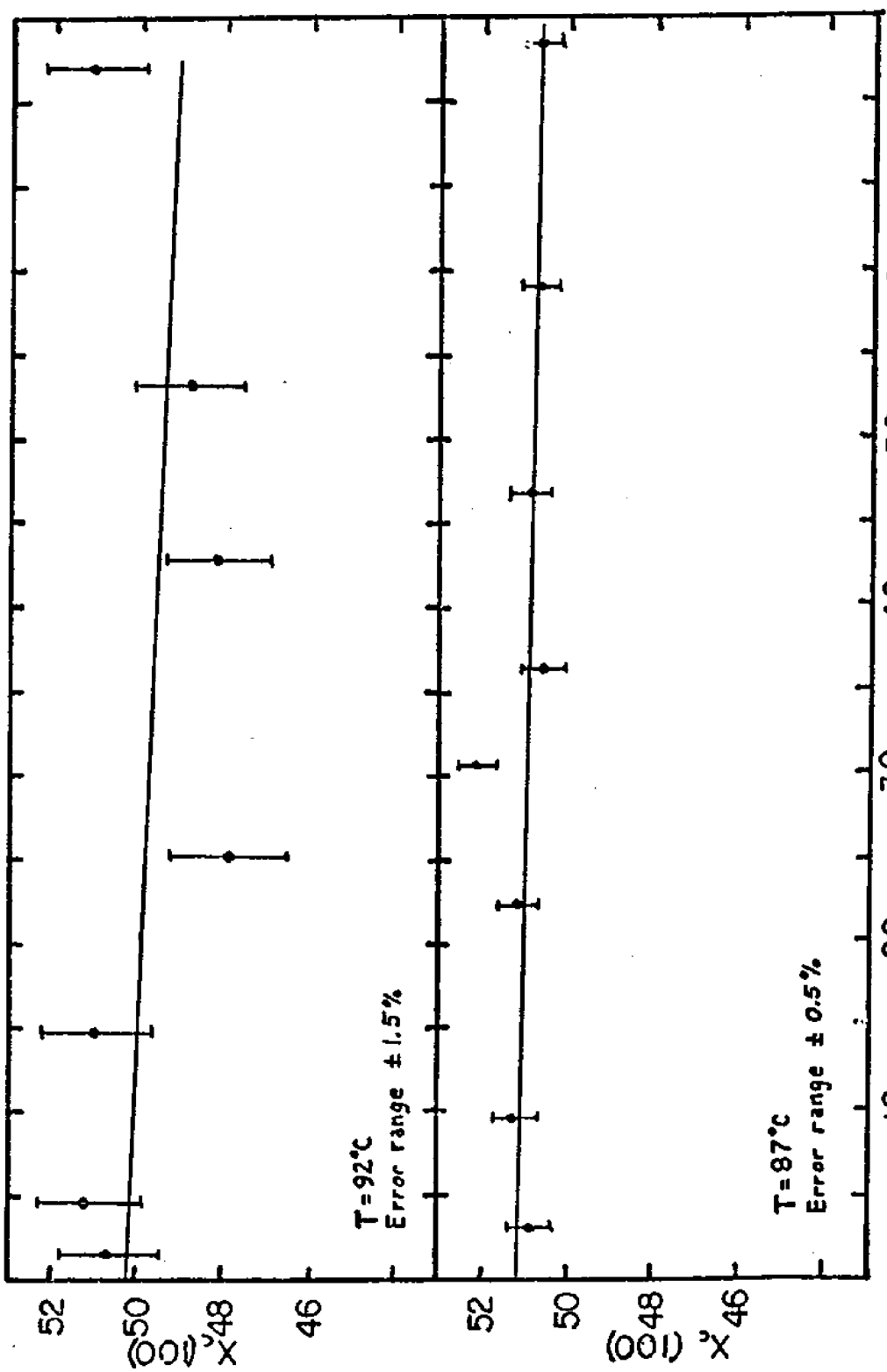

Figure 17: Crystallinity vs. Anneal Time in Distilled H_2O for Blank PE at 87° and 92°C.

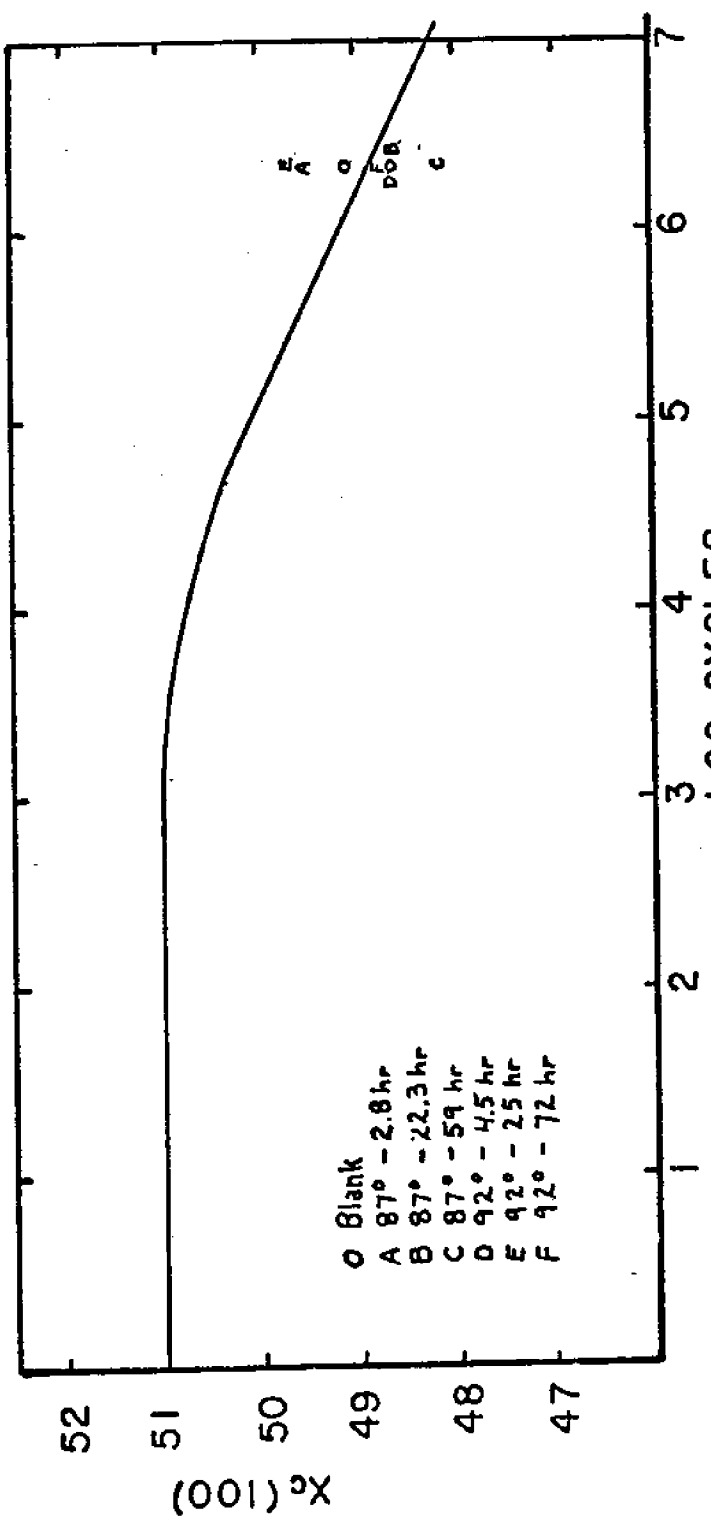

Figure 18: Crystallinity vs. Log Cycles Flex at 400 rpm for PE Annealed up to 72 hr at 87° and 92°C in Distilled H_2O.

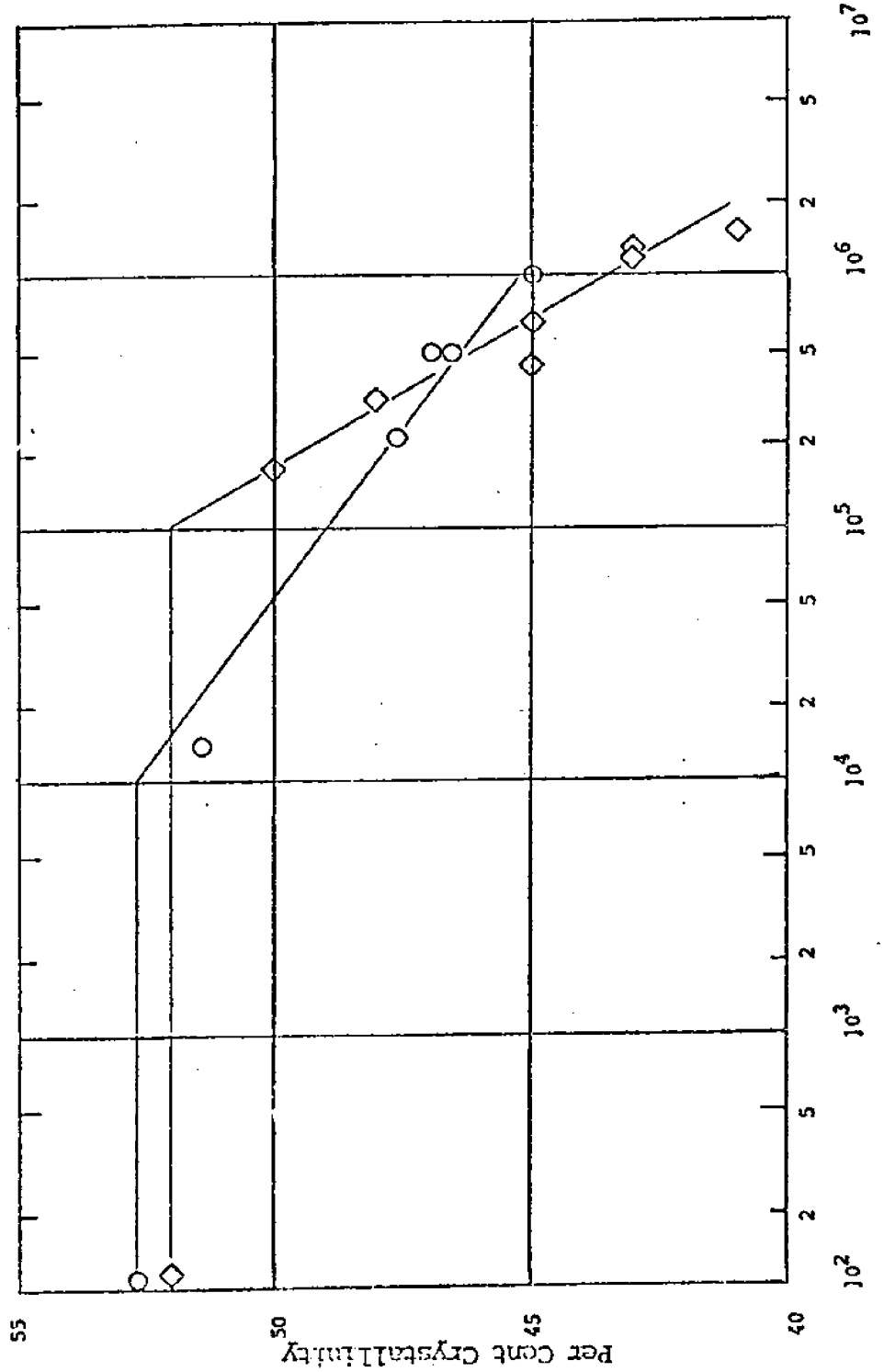

Fig. 19: Low Density Polyethylene Crystallinity vs Flexure
○ - Flexure Data From Initial Studies on PE
◇ - Flexure Data From Repeat PE Run.

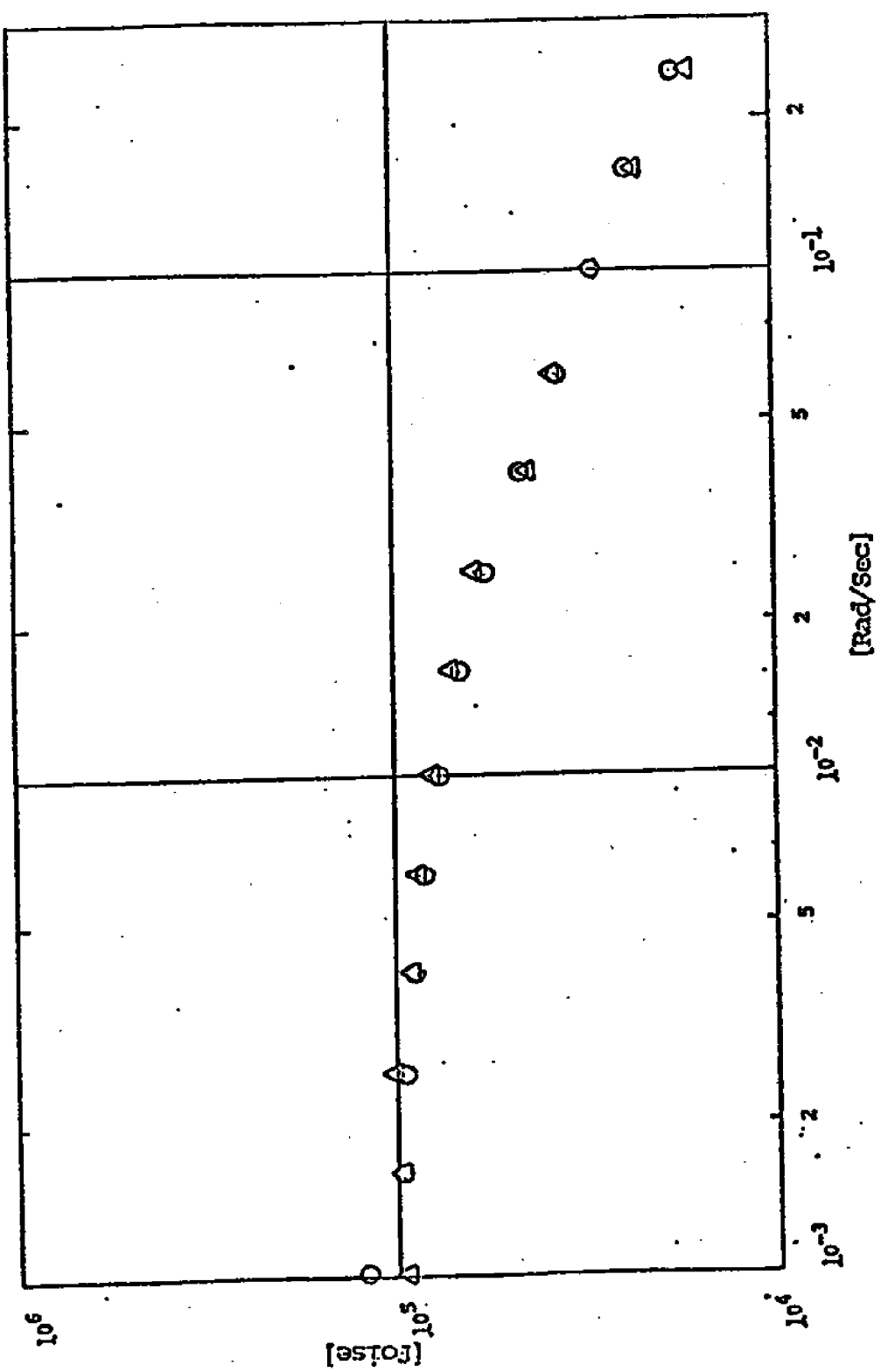

Fig. 20: Low Density Polyethylene Rheometrics Spectrometer Results
25 mm Plate and Cone, Temperature = 150°C
○ - Unflexed Sample
△ - Sample Flexed 1.00×10^6 Cycles

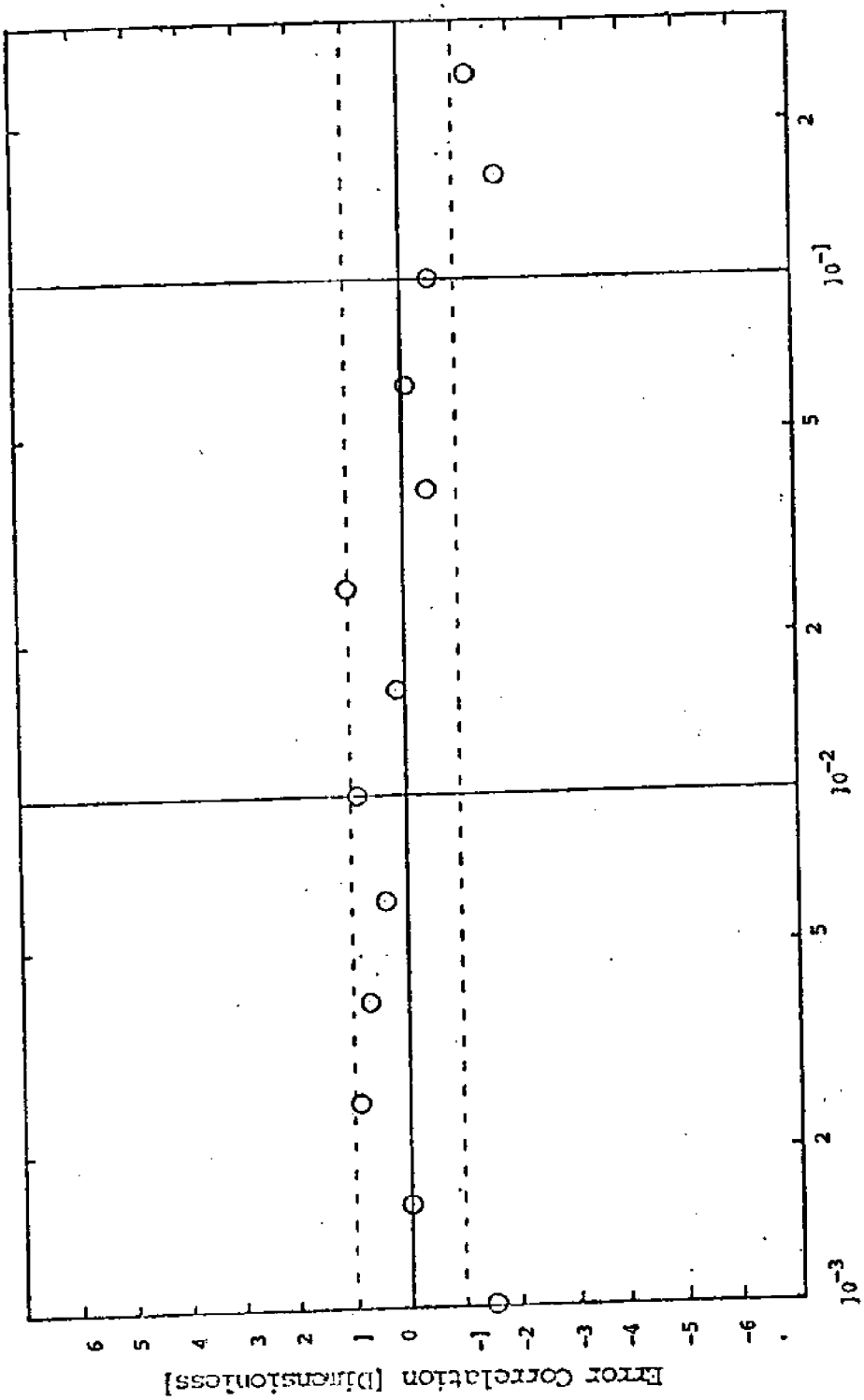

Fig. 21: Low Density Polyethylene Error Correlation for Fig. 20

$$O = \frac{\eta_{OBS} - \eta_{BASE}}{\sqrt{\Omega}\ \sigma_{EST}}$$

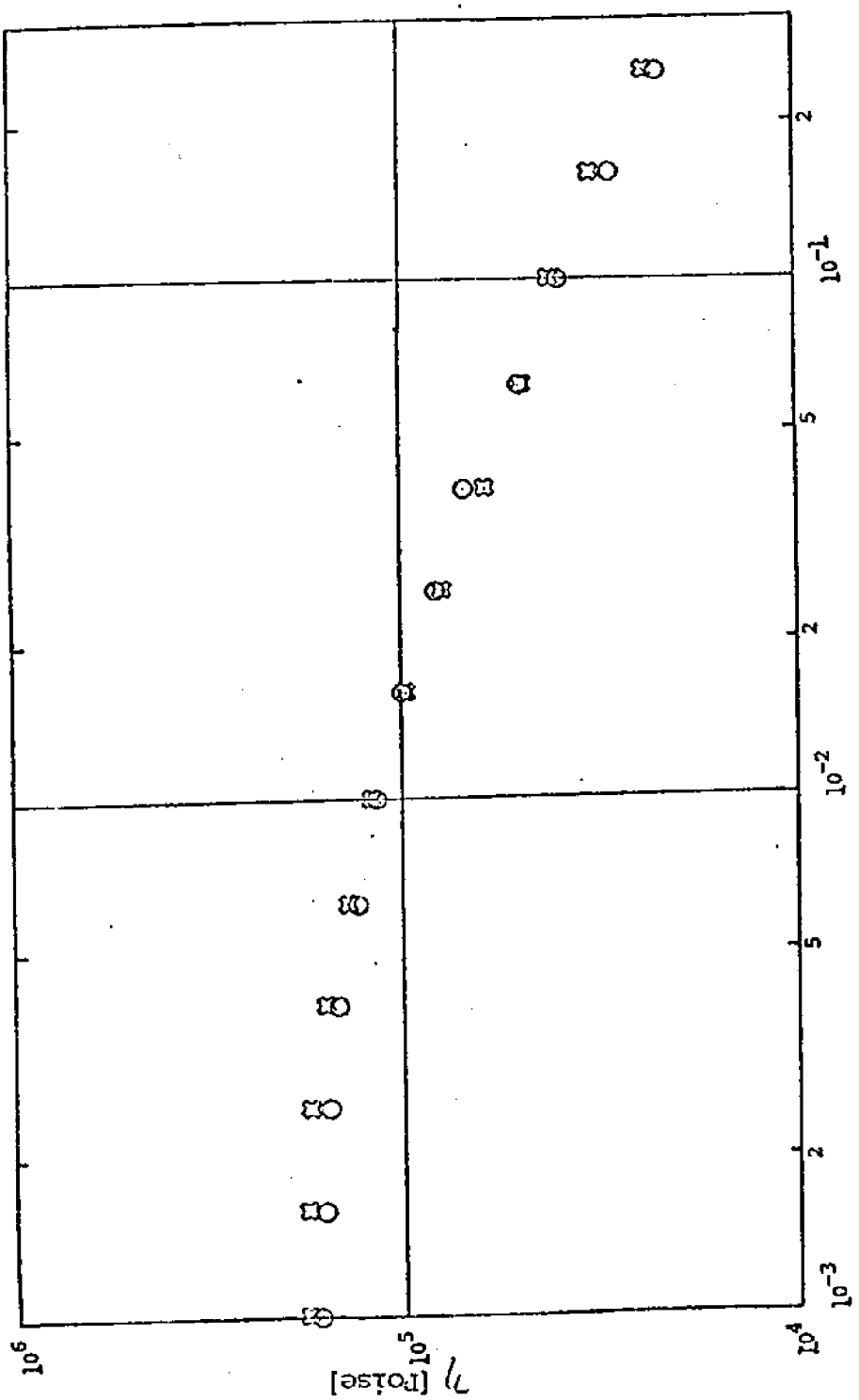

Fig. 22: Low Density Polyethylene Rheometrics Spectrometer Results
25 mm Plate and Cone, Temperature = 150°C
○ - Average of Three Unflexed Samples
⊠ - Sample Flexed 6.31×10^4 Cycles

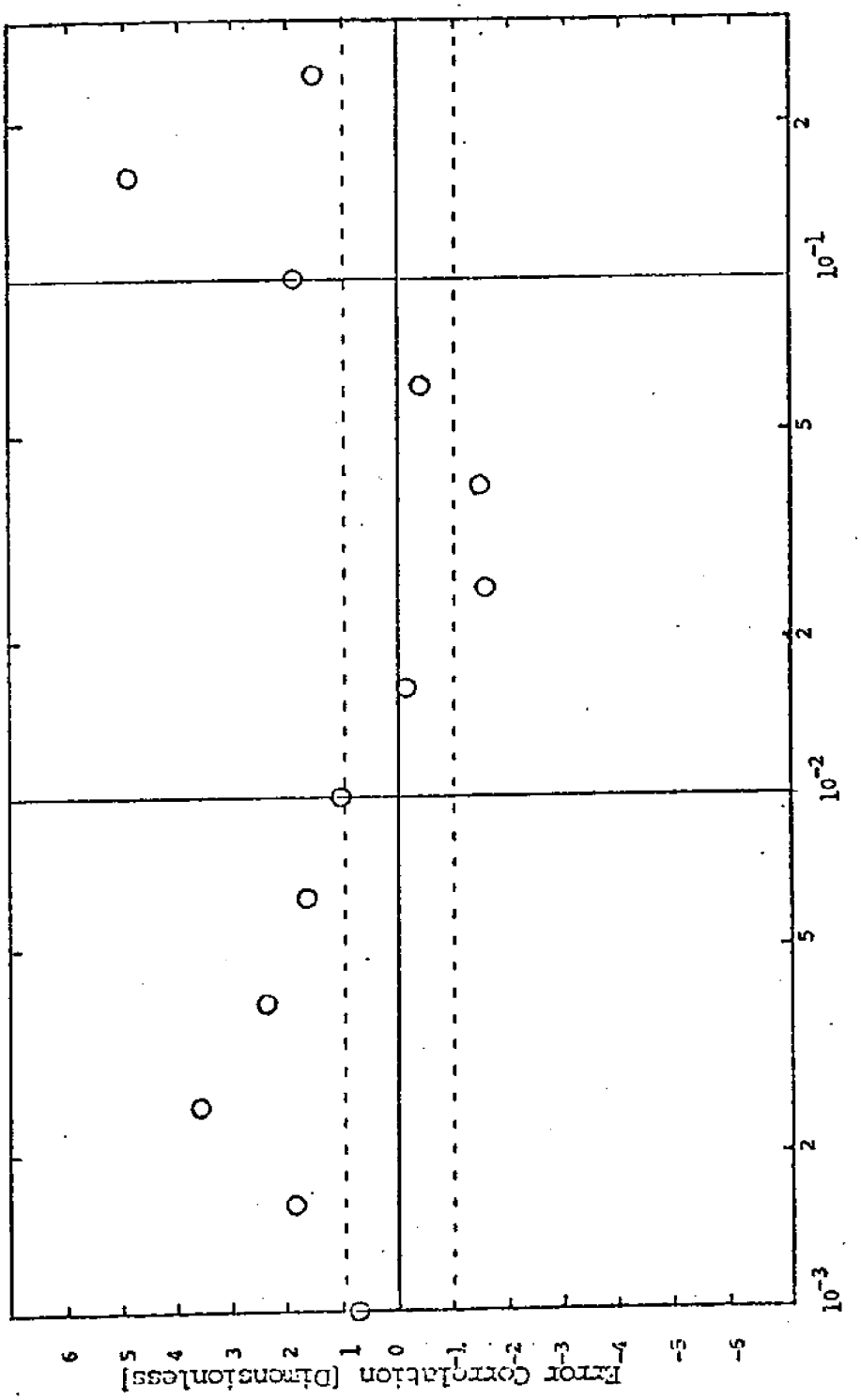

Fig. 23: Low Density Polyethylene Error Correlation for Fig. 22.

$$\bigcirc = \frac{\eta_{DEG} - \eta_{AVG}}{\sqrt{2}\ \sigma_{AVG}}$$

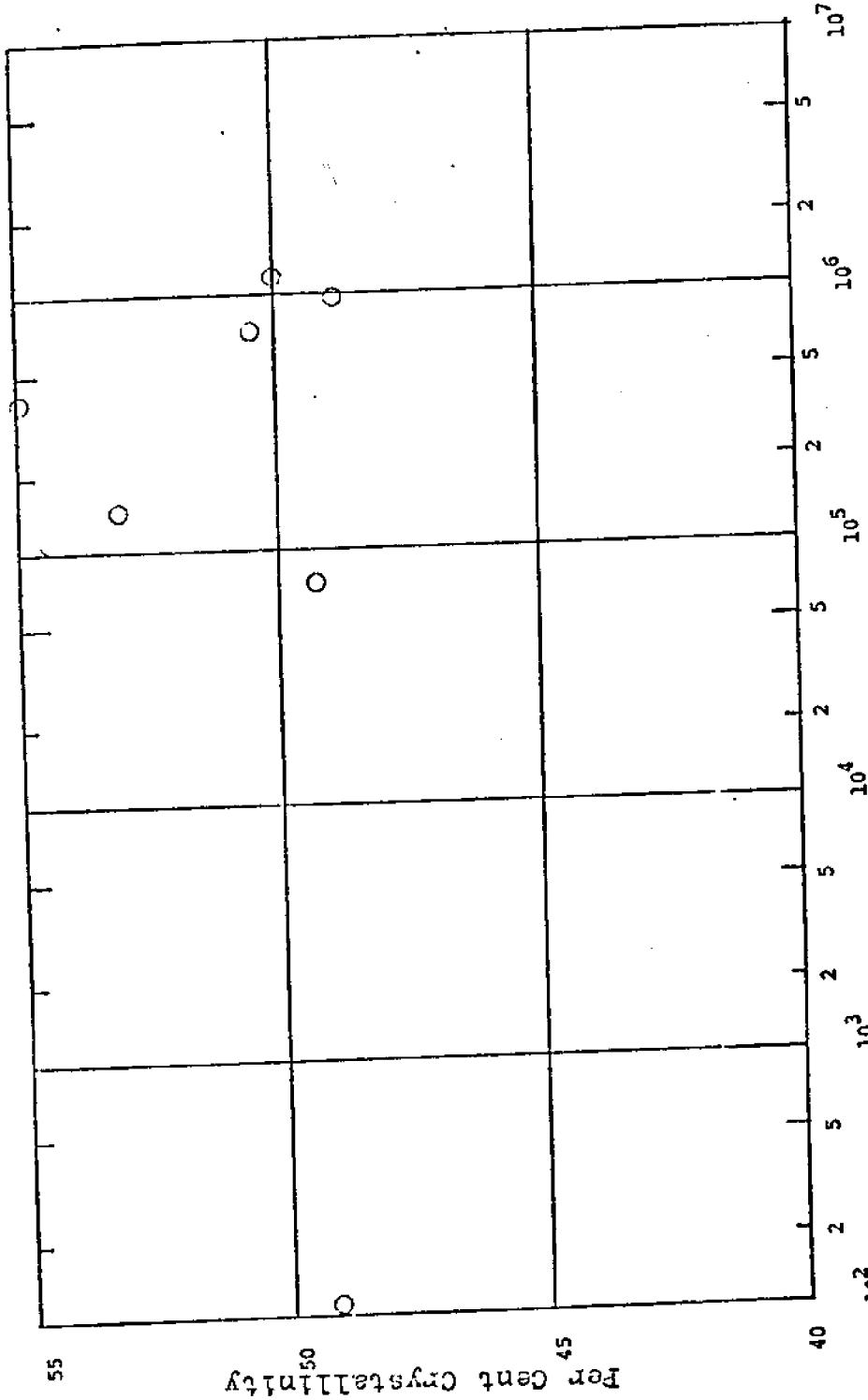

Fig. 24: Polypropylene Crystallinity vs Flexure

O - Flexure Data From Current Work

Stallinity is plotted against log cycles flex. The shallowness of the baseline degradation slope, relative to the slope observed for the seawater curves in Figure 16, is an artifact due to fatigue in the shaft coupling between motor and flex arm assembly (which was solid steel). This fatigue degraded flex amplitude output to the plunger, and hence decreased the total flexure working received by the strips. Tables 4 and 5 were used to generate Figures 17 and 18 respectively. Again, within limits of scatter, no effect on degradation rate relative to unannealed PE was discernible. This tends to rule out the theory that any surface smoothing due to annealing over the temperature range studied retards the degradation process.

Melt Viscosity studies on PE, PP and PS. The melt viscosity vs. shear rate behavior was studied for both unflexed and flexed samples of each resin. Crystallinity vs. log cycles flex was also studied for polypropylene.

PE: Two sets of data for the melt viscosity tests have been analyzed and are presented here. Fig. 20 shows the data for one of the samples used in obtaining crystallinity data for Fig. 19. Fig. 22 is the second sample plotted and is representative of the data generally obtained for all polyethylene samples. The accompanying error correlations are given in Figs. 21 and 23. Data for Figs. 19, 23, 22, 24, 25, 28 and 30 are contained in Appendix X.

Fig. 20 shows results of tests on the sample corresponding to the final data point in Fig. 19 with crystallinity of 45% after 1.00×10^6 flexure cycles. This sample was used because it was assumed that it was subjected to the greatest degree of degradation as indicated by the crystallinity data. The unflexed sample in Fig. 20 corresponds to the first data point from the crystallinity test with 52.8% crystallinity after 0 (zero) flexures. These data indicate the pseudoplastic behavior of polyethylene specifically and of polymers in general. There is a good deal of overlap and as can be seen in Fig. 21, in most instances, differences between flexed samples and unflexed samples can be explained entirely by experimental

error. That is, the error correlation points lie within or very close to the standard deviation region described earlier. Therefore, there is no significant change in the melt viscosity between samples tested in this set of data.

Fig. 22 gives data for low density polyethylene sample that was flexed 6.31 x 10^4 times and the unflexed data are the average of three separate runs with fresh samples. Overlap of the data is again prevalent. The accompanying error correlation, Fig. 23 shows that some of the differences between the unflexed and the flexed samples are outside the assumed area of experimental error, but also that there is no consistent positive or negative direction of these differences. There is, however, an apparent cyclical dependence of the melt viscosity deviation on the shear rate.

In general, the cyclic variation exhibited in Figs 22 and 23 was not reproduced in other tests. There were, however, a number of cases in which the difference variations ranged well outside of the assumed region of experimental error. Since there was no overall correlation in the direction of these differences among the samples tested, it seems reasonable that there are other error terms which have not been included in the present analysis. Another explanation may be that the standard deviations used were the result of an average of only 3 or 4 values. This small sample size could have easily been biased to one extreme or the other of the actual error range. In general, it seems that low density polyethylene does not exhibit any change in the melt viscosity resulting from flexure in sea water.

PP: Polypropylene samples flexed in sea water using the vertical flexor provided the data for this section. The crystallinity data are plotted on Fig. 24. As can be seen, the scattering of the data is much more severe than in the case of polyethylene. As a result, it is impossible to draw any conclusions about trends in crystallinity with respect to flexure. The possible reasons for this scatter are many. One of the drawbacks to this technique of measurement is the "by eye" fitting of a base line curve to the x-ray scans. It was felt that this is probably the major source of error here.

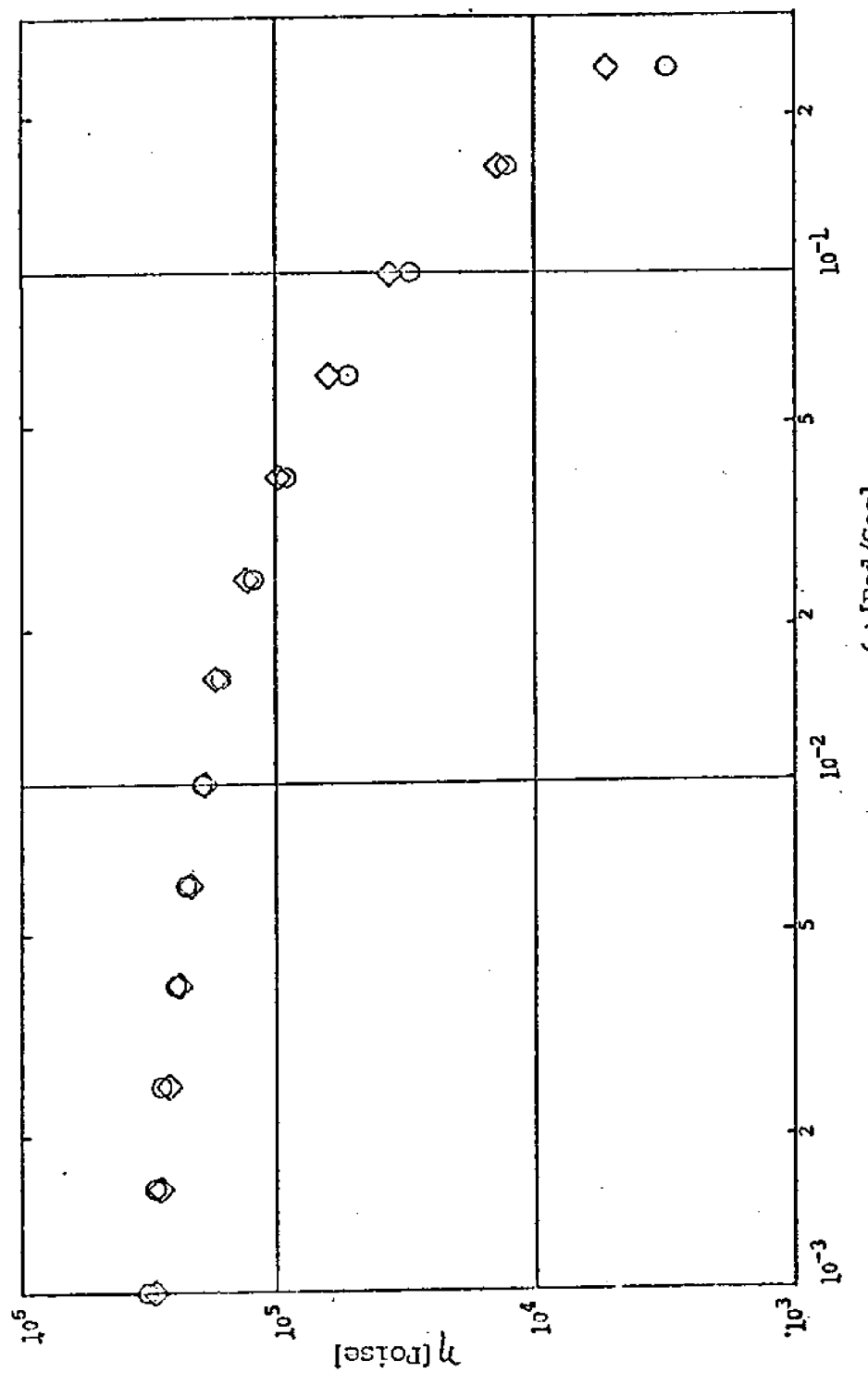

Fig. 25: Polypropylene Rheometrics Spectrometer Results
25 mm Plate and Cone, Temperature = 180°C
○ - Average of Two Unflexed Samples
◇ - Sample Flexed 8.50×10^5 Cycles

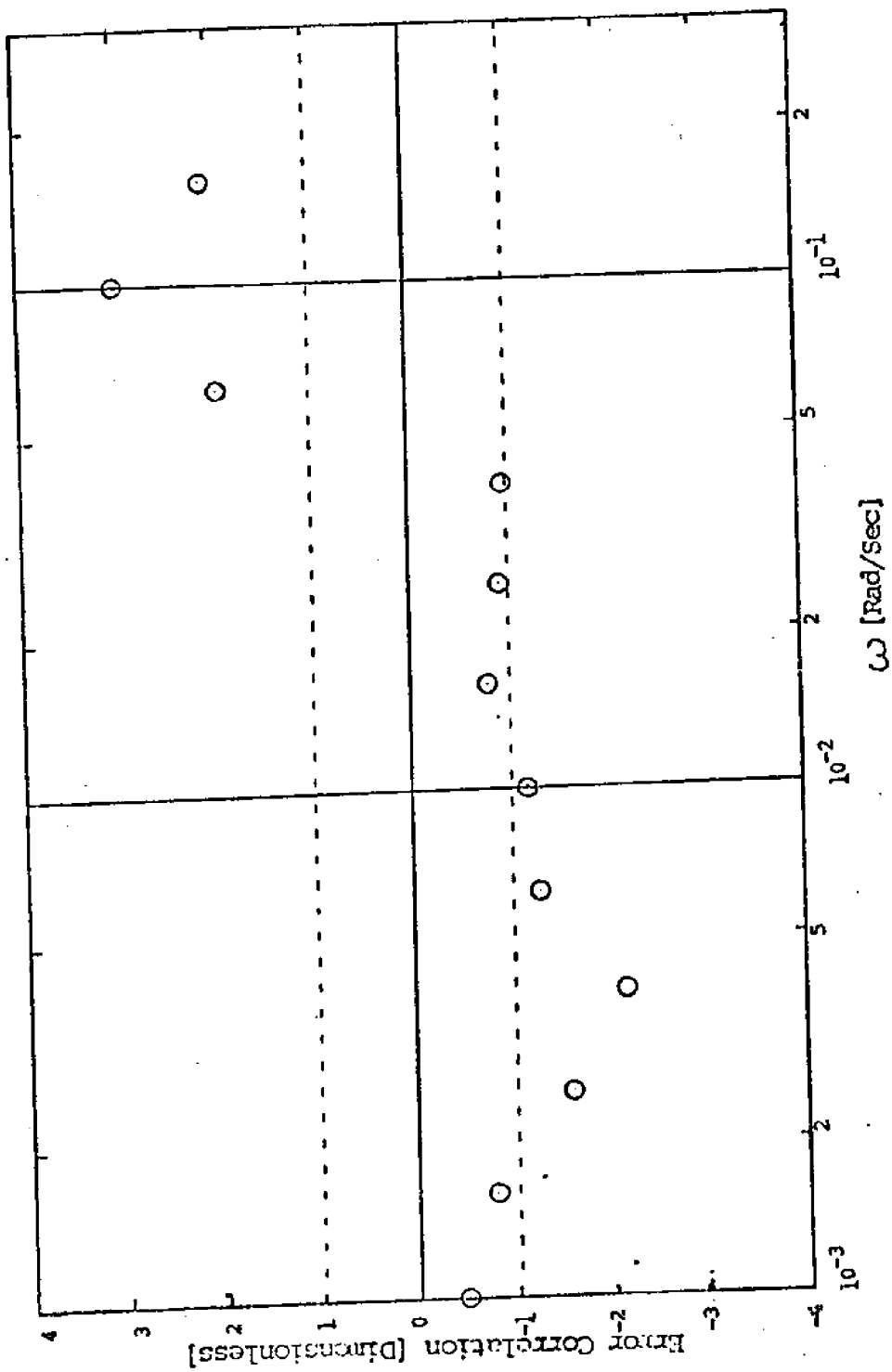

Fig. 26: Polypropylene Error Correlation for Fig. 25

$$\bigcirc = \frac{\eta_{DEC} - \eta_{AVG}}{\sqrt{\sigma^2_{DEC} + \sigma^2_{AVG}}}$$

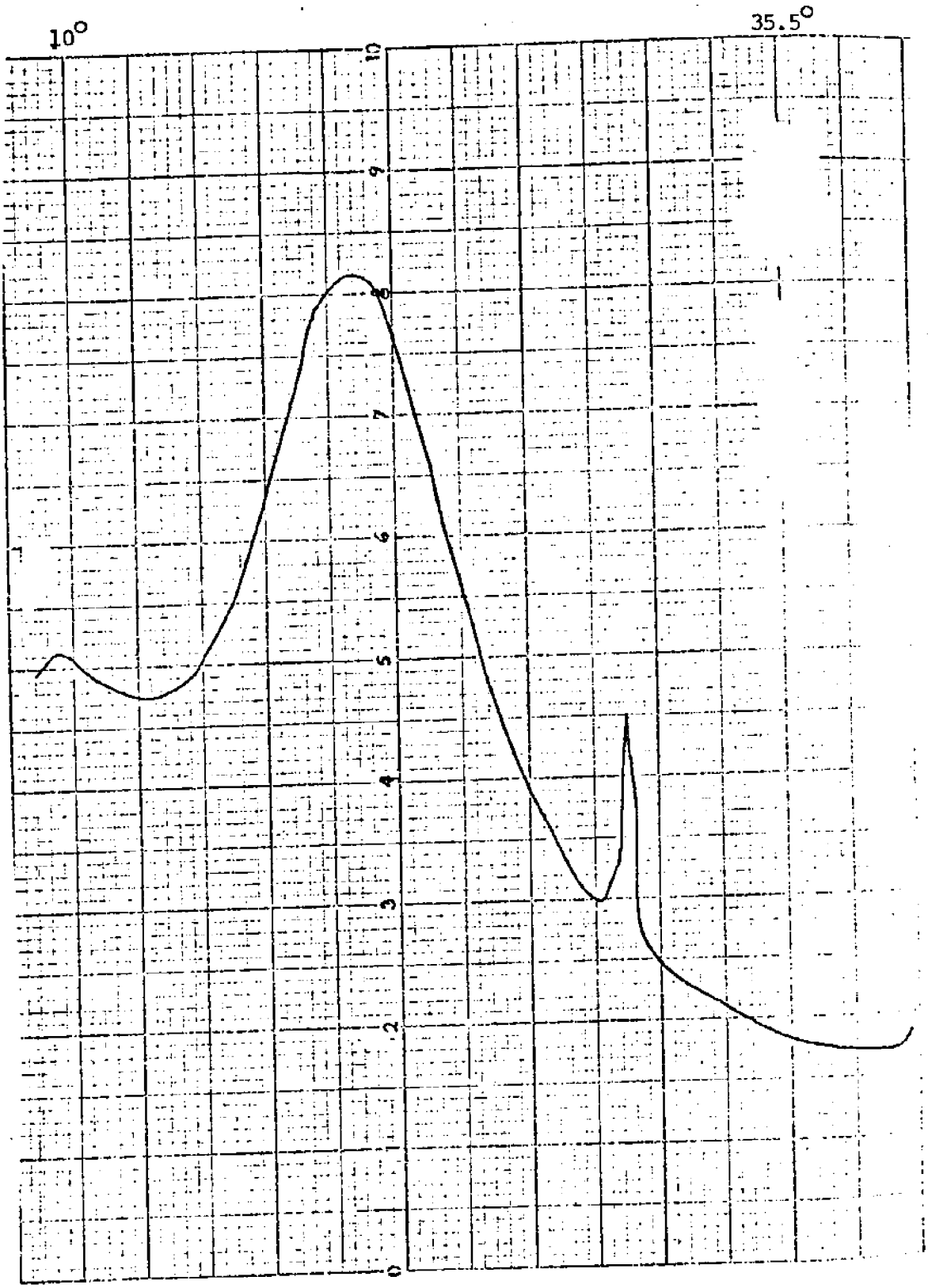

Fig. 27: Outline of Polystyrene X-ray Scan.

Figure 25 shows melt viscosity vs. shear rate at 180°C for polypropylene. The degraded sample was flexed 8.50×10^5 cycles and is the same sample as was used for the final data point of the crystallinity tests. The blank datum was provided by an average of two unflexed polypropylene samples. Once again, as with polyethylene, there was a lot of data overlap between the degraded and the fresh samples. This is also indicated in the error correlation, Fig. 26, where many of the changes in the data points could be accounted for by experimental error. There is some data scatter outside of the estimated error region, forming again an apparent cyclical dependence of melt viscosity deviation on shear rate. Again a possible explanation is the incomplete definition of error region and not any real change in the polymer melt viscosity. In this case, polypropylene does not exhibit any statistically significant changes in viscosity resulting from the flexure treatment.

PS: The polystyrene used was atactic which means that it was totally amorphous with no crystalline regions. This is shown in Fig. 27 which is a direct reproduction of the wide angle X-ray scan of an unflexed sample. Note the single broad peak and the absence of individual spikes in the scan which normally denote the presence of crystalline regions. There is one small glitch in the scan which shows up as a small spike at around 26.5 degrees. Since it does not correspond to any of the normally observed peaks, it is assumed that this is coming from one of the other materials added to the polystyrene and not an indication of crystallinity.

Two sets of viscosity data are analyzed and shown for polystyrene degradation. Samples subjected to 5.46×10^5 and 8.86×10^5 cycles are compared to unflexed samples at two different melt temperatures. In this case, the horizontal flexor provided the samples.

Fig. 28 compares the sample flexed at 8.86×10^5 cycles with an unflexed sample at a mechanical spectrometer test temperature of 200°C. The separation between the two curves is striking when compared to the overlap encountered in

polyethylene and polypropylene. The error correlation, Fig. 29, supports the hypothesis that the two samples are indeed different. In all cases, the difference in the data points is well beyond the range of experimental error. In addition, there is a consistent trend in the correlation curve with all the data for the degraded sample falling below the unflexed case. As the shear rate increases, the statistical significance of this difference increases greatly. This polystyrene sample has apparently undergone significant molecular weight change resulting from cyclic flexure. The melt viscosity decreases with respect to flexure.

Fig. 30 is a similar comparison of polystyrene flexed 5.46×10^5 cycles, tested in the mechanical spectrometer at 190°C. The unflexed case is an average of the results for two unflexed samples run at the same mechanical spectrometer temperature. The viscosities are expectedly higher than those in Fig. 28, owing to the lower temperature. The difference between the two sets of data is again visually obvious. The error correlation, Fig. 31, shows that the data differences fall well outside the range of experimental error. The trend is also the same as the previous case with the statistical significance becoming greater with increasing shear rate.

In general, these two cases indicate that the decrease of melt viscosity with the increase of cyclic flexure is a non-random, reproducible effect.

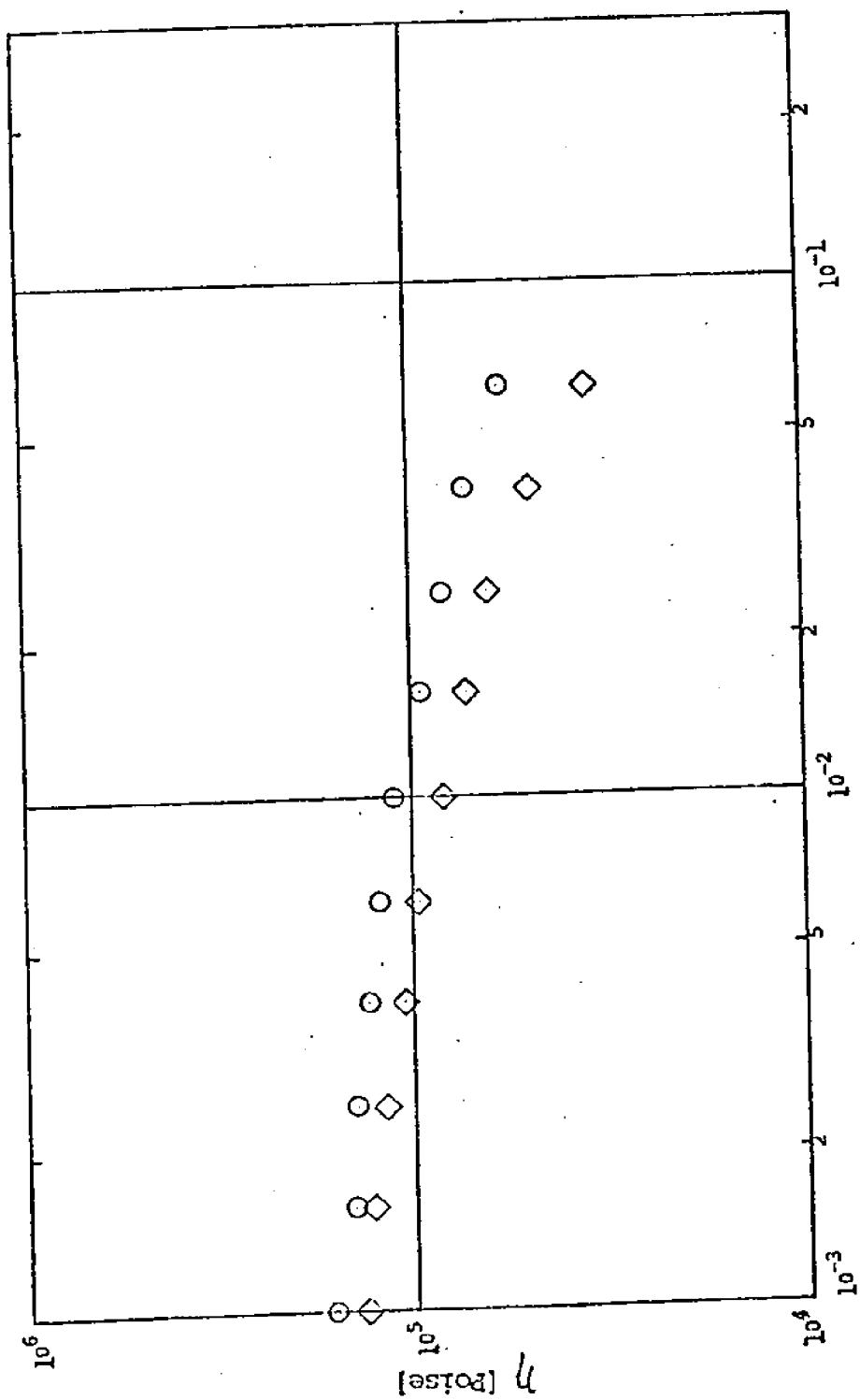

Fig. 28: Polystyrene Rheometrics Spectrometer Results
25 mm Plate and Cone, Temperature = 200°C
○ - Unflexed Sample
◇ - Sample Flexed 8.86 x 10^5 Cycles

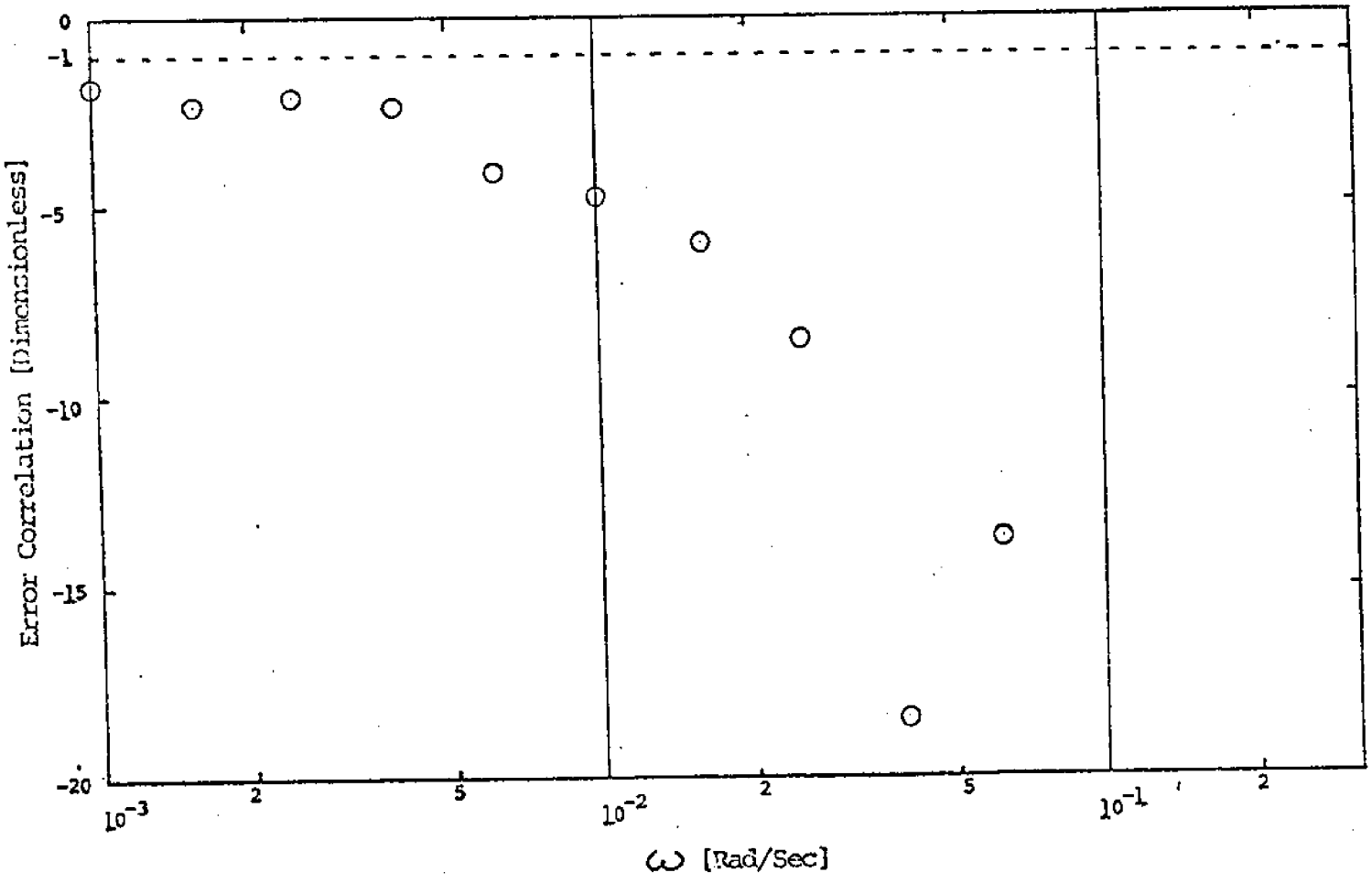

Fig. 29: Polystyrene Error Correlation for Graph 10

$$\bigcirc = \frac{\eta_{DEG} - \eta_{BASE}}{\sqrt{\sigma^2_{DEG} + \sigma^2_{BASE}}}$$

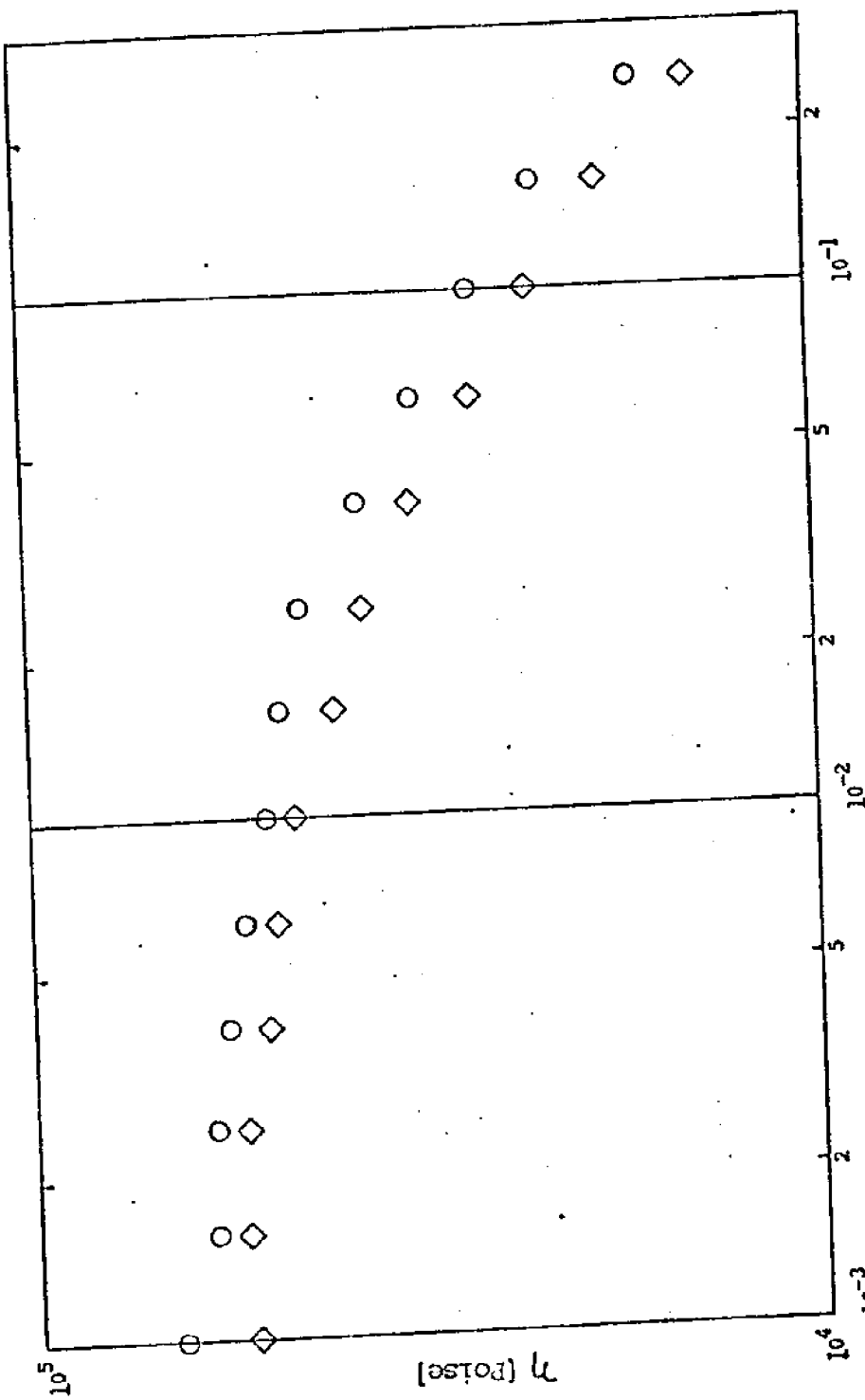

Fig. 30: Polystyrene Rheometrics Spectrometer Results
25 mm Plate and Cone, Temperature = 190°C
○ - Averaged Unflexed Samples
◇ - Sample Flexed 5.46×10^5 Cycles

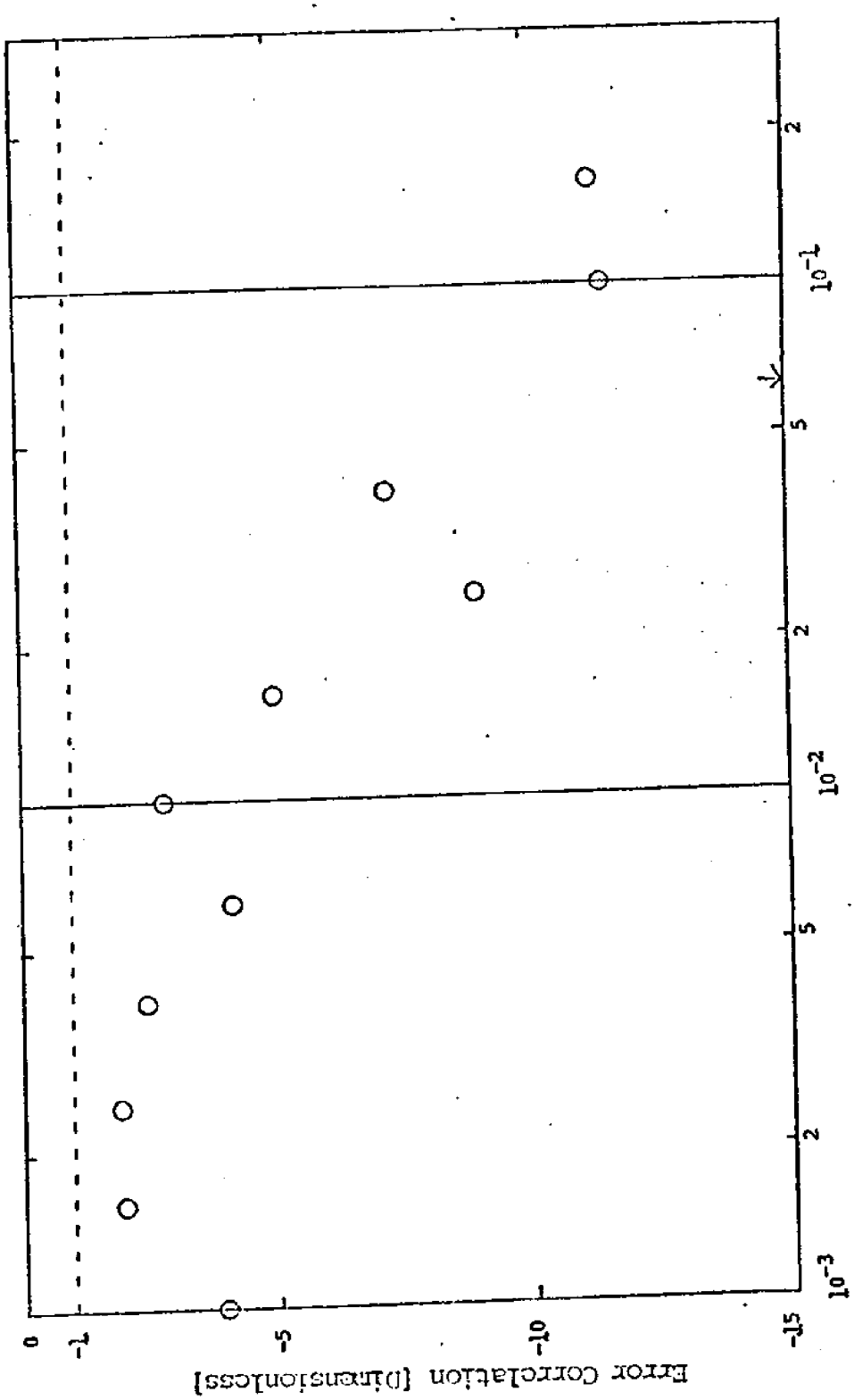

Fig. 31: Polystyrene Error Correlation for Fig. 30.

$$\bigcirc = \frac{\eta_{DEG} - \eta_{AVG}}{\sqrt{2}\,\sigma_{AVG}}$$

Surfactant adsorption on PE powder. Tensiometric data were obtained at 82°, 87°, 90° and 92°C, as outlined earlier. The experiments done at 90°C were intended to clear up certain discontinuities in the adsorption behavior between 87° and 92°C. The effects of hydrolysis of LDE were found to be negligible, since no surface-tension change was noted in samples of 9.44×10^{-6} M LDE after 35 hr at 92°C. Desorption of LDE into distilled water at 20°C was found to be less than 9×10^{-10} mol/hr (less than 5% desorbed from a typical powder sample after 14 days). Leaching in ethanol failed to remove all LDE, since ethanol-treated powder still stained strongly with Pylam Rose Pink and Woodstain Scarlet. Additionally, PE and LDE strip was found to wet much more readily than blank PE.

Initial adsorption runs were done at 92°, 87° and 82°C, for several LDE concentrations at each temperature. At 92°C, experiments were done at three initial surfactant concentrations, 9.44×10^{-6} M, 4.22×10^{-5} M, and 8.32×10^{-5} M. Samples were taken as a function of time giving the results contained in Tables 6,7, and 8.

These data are shown in Figure 32 as a plot of concentration in moles per liter as a function of time in hours. Several trends should be noted on the graph: 1) The total amount adsorbed at steady state increases with increasing surfactant concentration. 2) An accelerated adsorption is evident at higher initial concentrations. 3) Attainment of steady state adsorption occurs at longer times for higher initial surfactant concentrations in the bulk solution.

Modifications in the experimental procedure were made to determine whether an instantaneous adsorption of the surfactant by the polymer occurred at times of five minutes or less. For several tests no change in solution concentration was observed upon the addition of polymer; therefore the possibility of an initially accelerated adsorption was discounted.

In addition to accumulating data at a single temperature for several initial solution concentrations, results were obtained for fixed initial con-

centrations at various temperatures. For solution concentrations of about 4×10^{-5} M and 8×10^{-5} M experiments were done at 82°C, 87°C and 92°C; results are contained in Tables 9, 10, 11 and 12.

Figures 33 and 34 show the adsorption data at several temperatures for solution concentrations of 4×10^{-5} M and 8×10^{-5} M, respectively. The figures plot concentration in moles per liter as a function of time in hours. Several features of the curves are noteworthy: 1) The amount of surfactant adsorbed at a steady state is greater at higher temperatures. 2) The final solution concentration is lower for higher temperatures. 3) The time interval required for attainment of adsorption equilibrium is longer with higher temperatures.

Some crude studies of desorption were made; these included the qualitative observations concerning the staining and wetting properties of polyethylene as well as quantitative efforts to detect lauric diethanolamide in washing of the treated polymer. When treated polyethylene was allowed to stand in water at 20-22°C for times up to 2 weeks, no detectable desorption was found with surface tension measurements. However that merely implies that lauric diethanolamide was present at concentrations less than 3×10^{-6} M (see Appendix IV). The amount of desorption required to result in a solution concentration of 3×10^{-6} M would represent 3 to 6% of the total adsorbed moles for experiments conducted at 92°C and 8 to 15% of the adsorbed moles for studies done at 82°C.

Additional quantities derived from these initial runs included specific molar adsorption n_s and kS, the sticking-coefficient product, both of which were discussed earlier. In addition, the "parking area" per molecule was calculated for a monolayer model of the LDE region. Figures 35, 36, and 37 show the n_s vs. time data for 82°C, 87°C and 92°C respectively. The extent of sorption at equilibrium was found to be strongly concentration dependent, and adsorption rates were seen to increase monotonically with both concentration and reflux temperature. The adsorption rate is far from the mass-transfer limit (Appendix XI), thus the observed behavior reflects real changes at the PE surface. The surface of the test low-

density PE is thought (Schonhorn, 1977) to be entirely amorphous, as indicated by the fact that the critical surface tension of wetting is independent of resin formulation for a fairly broad selection of resin samples of different bulk crystallinities. Hence, parking-area data suggest adsorbate coverage levels near 100%.

Adsorption isotherms were obtained from plots on $\underline{n_s}$, total moles adsorbed vs. equilibrium concentration C_{eq}, as shown in Fig. 38. Over the regime studied, the isotherms did not level off with increasing C_{eq}, indicating multilayer formation. Plots of n_s vs. kS (Figs. 39 and 43; Tables 13 through 19) showed a discontinuity between 87° and 92°C, indicating a change of dominant adsorption mechanism in this range (which contains the DSC recrystallization peak at 90°C).

Plotting in C_{eq} vs. 1/T, and determining the slope of this curve (Fig 40) at a given temperature, gives the quantity $\frac{Q}{R}$, where Q is the isosteric heat of adsorption. Values of Q thus calculated ranged from 12.6 kJ/mole at 82°C to 49.0 kJ/mole at 92°C; this is consistent with a two-step precursor mechanism featuring surface physisorption followed by tail diffusion into the PE, as shown by Adamson (1967).

TABLE 6

Adsorption Data for 9.44×10^{-6} M surfactant solution at 92°C

Time (hrs)	C(moles/liter)	moles adsorbed	area/molecule ($\AA^2$)
0	9.44×10^{-6}		
5.0	9.18×10^{-6}	1.29×10^{-8}	3793
10.0	8.13×10^{-6}	6.56×10^{-8}	745
15.0	7.50×10^{-6}	9.71×10^{-8}	503
24.3	5.96×10^{-6}	1.48×10^{-7}	331
30.0	5.96×10^{-6}	1.48×10^{-7}	331
35.0	5.96×10^{-6}	1.48×10^{-7}	331

TABLE 7

Adsorption data for 4.22×10^{-5} M surfactant solution at 92°C

Time (hrs)	C(moles/liter)	moles adsorbed	area/molecule ($\AA^2$)
0	4.22×10^{-5}		
3.0	3.76×10^{-5}	4.43×10^{-7}	110
5.0	3.16×10^{-5}	1.10×10^{-6}	44
10.0	3.06×10^{-5}	1.20×10^{-6}	41
22.0	2.40×10^{-5}	1.77×10^{-6}	28
31.8	1.93×10^{-5}	2.12×10^{-6}	23
48.5	1.41×10^{-5}	2.44×10^{-6}	20
59.0	1.12×10^{-5}	2.58×10^{-6}	17
72.0	1.30×10^{-5}		

TABLE 8

Adsorption data for 8.32×10^{-5} M surfactant solution at 92°C

Time (hrs)	C(moles/liter)	moles adsorbed	area/molecule ($\AA^2$)
0	8.32×10^{-5}		
1.5	7.08×10^{-5}	6.21×10^{-7}	79
3.0	6.31×10^{-5}	1.01×10^{-6}	49
5.0	5.96×10^{-5}	1.18×10^{-6}	41
10.0	4.84×10^{-5}	1.74×10^{-6}	28
20.0	3.76×10^{-5}	2.28×10^{-6}	21
24.3	3.31×10^{-5}	2.50×10^{-6}	20
49.5	1.99×10^{-5}	4.05×10^{-6}	12
73.5	1.33×10^{-5}	4.39×10^{-6}	11
90.0	1.29×10^{-5}	4.41×10^{-6}	11
100.0	1.29×10^{-5}	4.41×10^{-6}	11

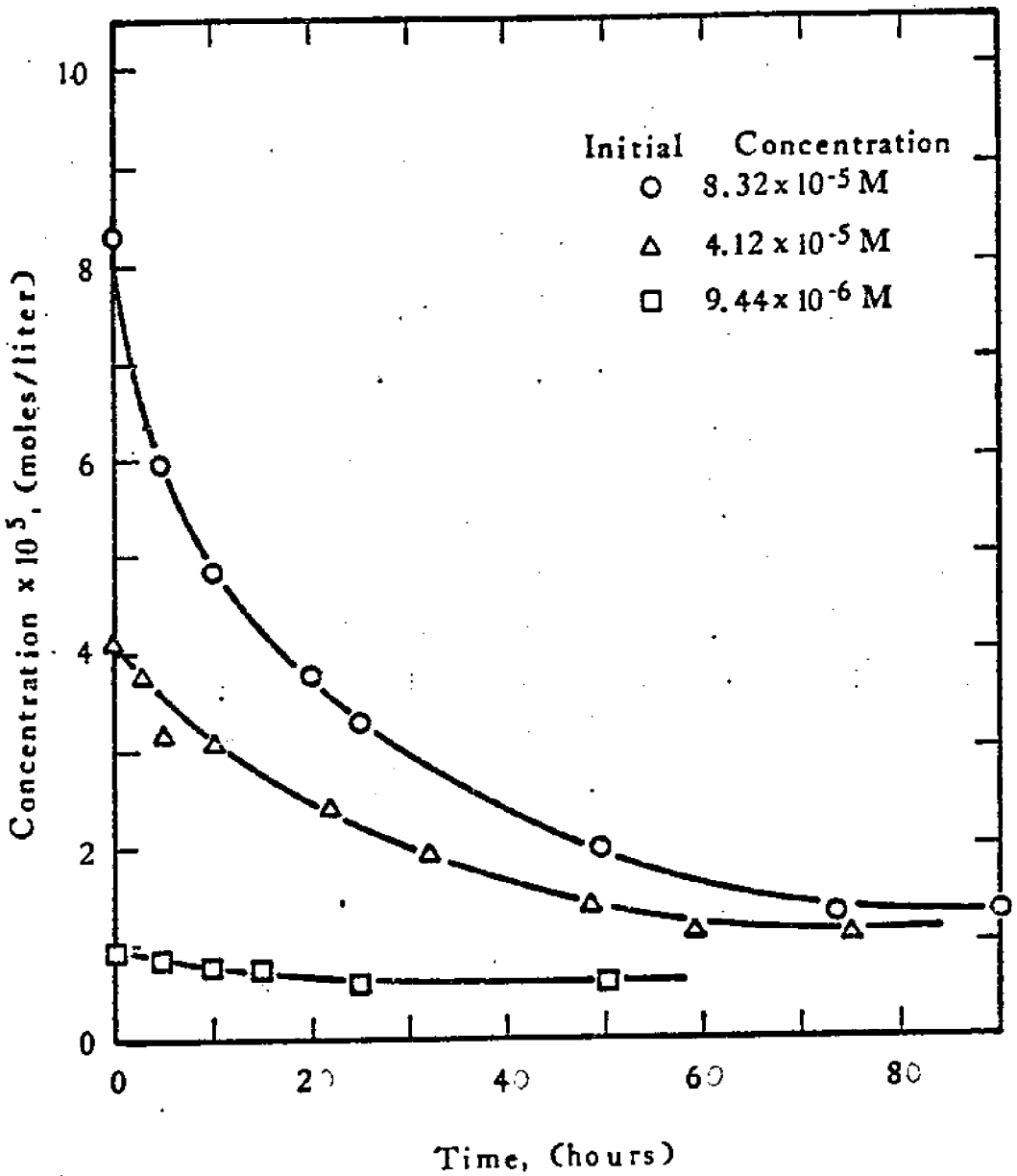

Figure 32: Adsorption Data for Experiments at 92°C

TABLE 9

Adsorption data for 3.89×10^{-5} M surfactant solution at 82°C

Time (hrs)	C(moles/liter)	moles adsorbed	area/molecule ($Å^2$)
0	3.89×10^{-5}		
3.0	3.76×10^{-5}	1.58×10^{-7}	308
4.8	3.76×10^{-5}	1.58×10^{-7}	308
23.0	3.35×10^{-5}	5.26×10^{-7}	93
31.8	2.92×10^{-5}	8.72×10^{-7}	56
50.8	2.82×10^{-5}	9.41×10^{-7}	52
74.3	2.72×10^{-5}	9.98×10^{-7}	49

TABLE 10

Adsorption data for 4.22×10^{-5} M surfactant solution at 87°C

Time (hrs)	C(moles/liter)	moles adsorbed	area/molecule ($Å^2$)
0	4.22×10^{-5}		
3.0	4.10×10^{-5}	1.38×10^{-7}	354
5.0	3.89×10^{-5}	3.81×10^{-7}	132
10.3	3.31×10^{-5}	9.50×10^{-7}	51
23.0	2.71×10^{-5}	1.49×10^{-6}	33
35.8	2.31×10^{-5}	1.81×10^{-6}	27
47.8	2.15×10^{-5}	1.92×10^{-6}	25
71.8	2.15×10^{-5}	1.92×10^{-6}	25

For data on 4.22×10^{-5} M surfactant solution at 92°C refer to Table 7 .

TABLE 11

Adsorption data for 8.32×10^{-5} M surfactant solution at 82°C

Time(hrs)	C(moles/liter)	moles adsorbed	area/molecule ($\AA^2$)
0	8.32×10^{-5}		
3.0	7.94×10^{-5}	4.50×10^{-7}	109
5.0	7.66×10^{-5}	7.66×10^{-7}	64
21.3	5.75×10^{-5}	2.67×10^{-6}	18
28.0	5.41×10^{-5}	2.98×10^{-6}	16
34.3	5.01×10^{-5}	3.30×10^{-6}	15
50.0	4.30×10^{-5}	3.80×10^{-6}	13
103.0	4.10×10^{-5}	3.91×10^{-6}	12

TABLE 12

Adsorption data for 7.94×10^{-5} M surfactant solution at 87°C

Time(hrs)	C(moles/liter)	moles adsorbed	area/molecule ($\AA^2$)
0	7.94×10^{-5}		
3.0	7.69×10^{-5}	2.77×10^{-7}	176
6.0	7.27×10^{-5}	6.97×10^{-7}	70
22.5	5.17×10^{-5}	2.59×10^{-6}	19
30.0	4.45×10^{-5}	3.17×10^{-6}	15
41.0	3.67×10^{-5}	3.71×10^{-6}	13
68.0	2.99×10^{-5}	4.12×10^{-6}	12
85.5	2.99×10^{-5}	4.12×10^{-6}	12

For data on 8.32×10^{-5} M surfactant solution at 92°C refer to Table 8.

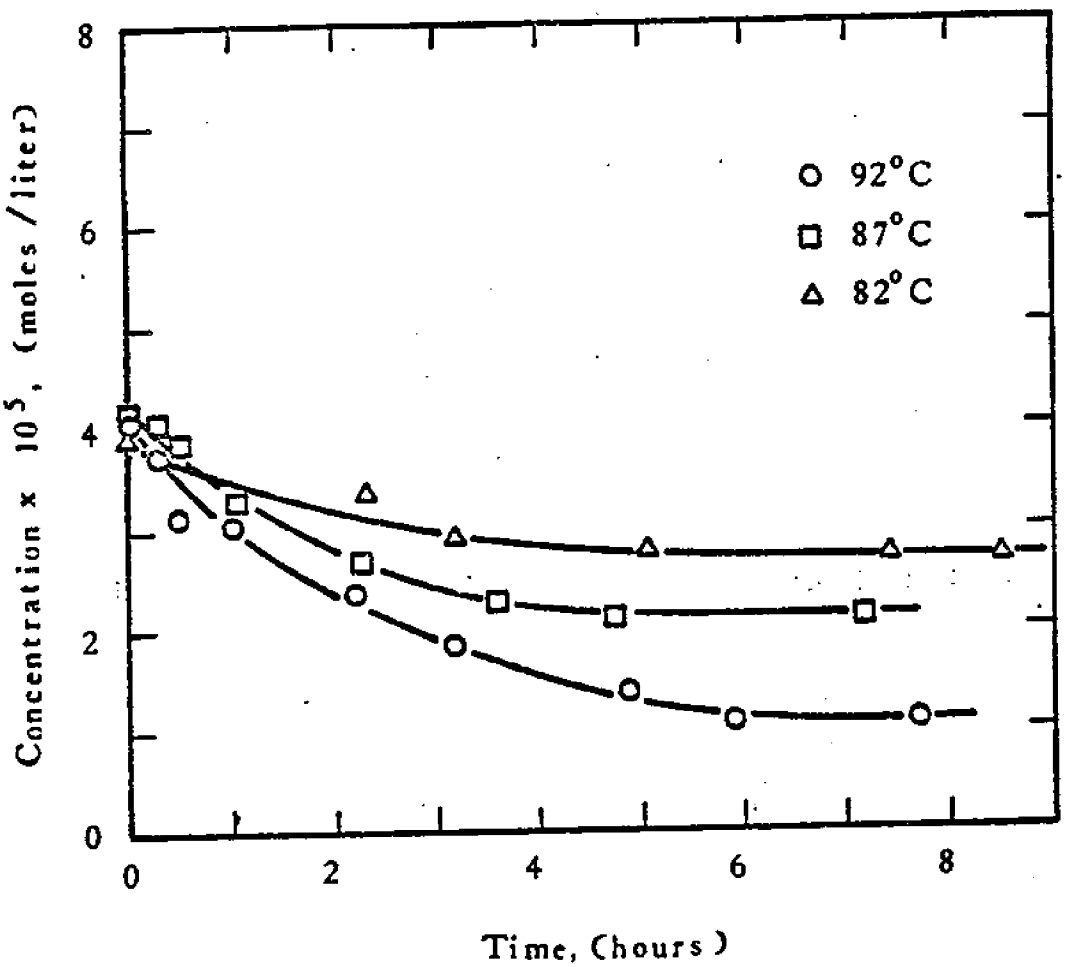

Figure 33: Adsorption Data for Initial Concentrations of 4×10^{-5} M

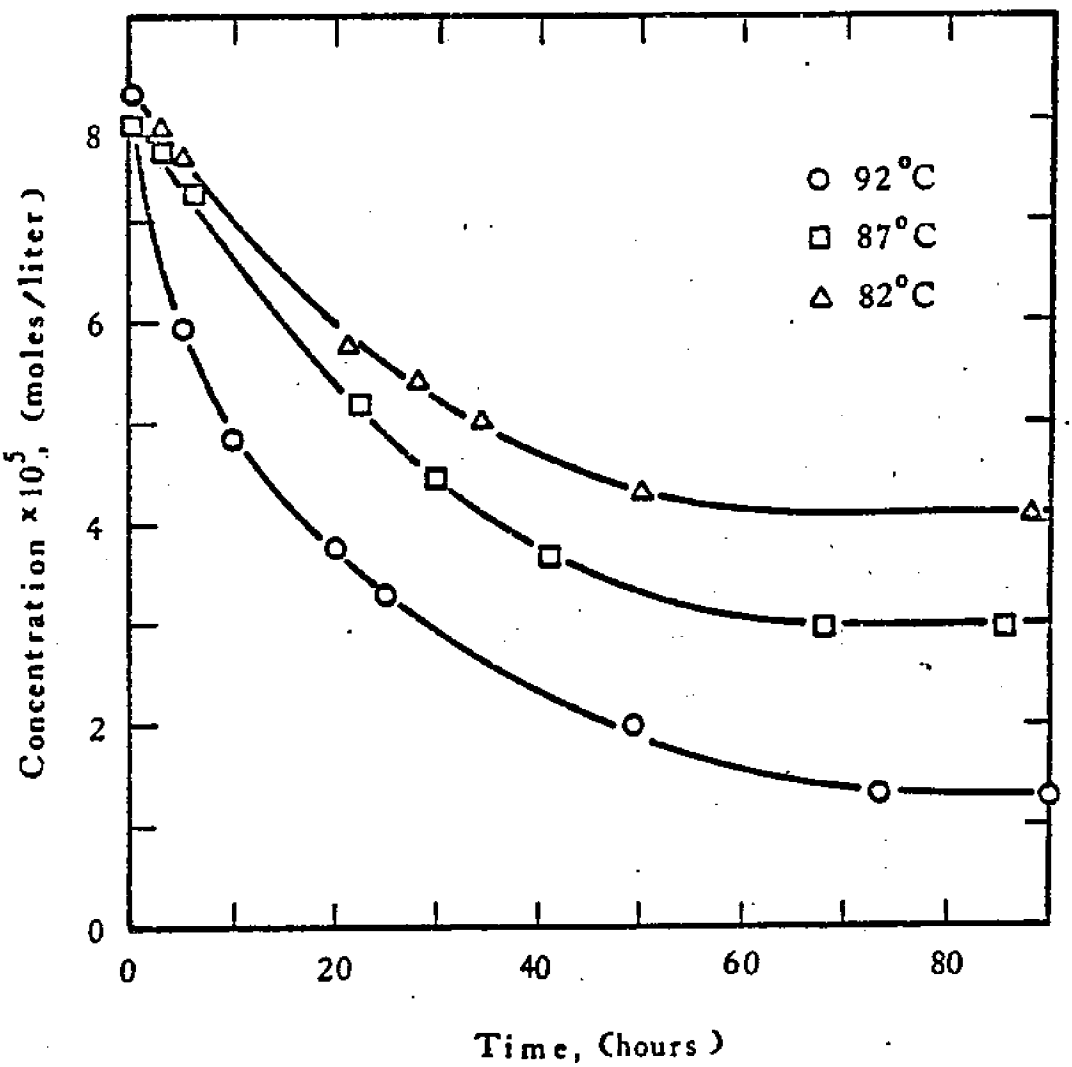

Figure 34: Adsorption Data for Initial Concentrations of 8×10^{-5} M

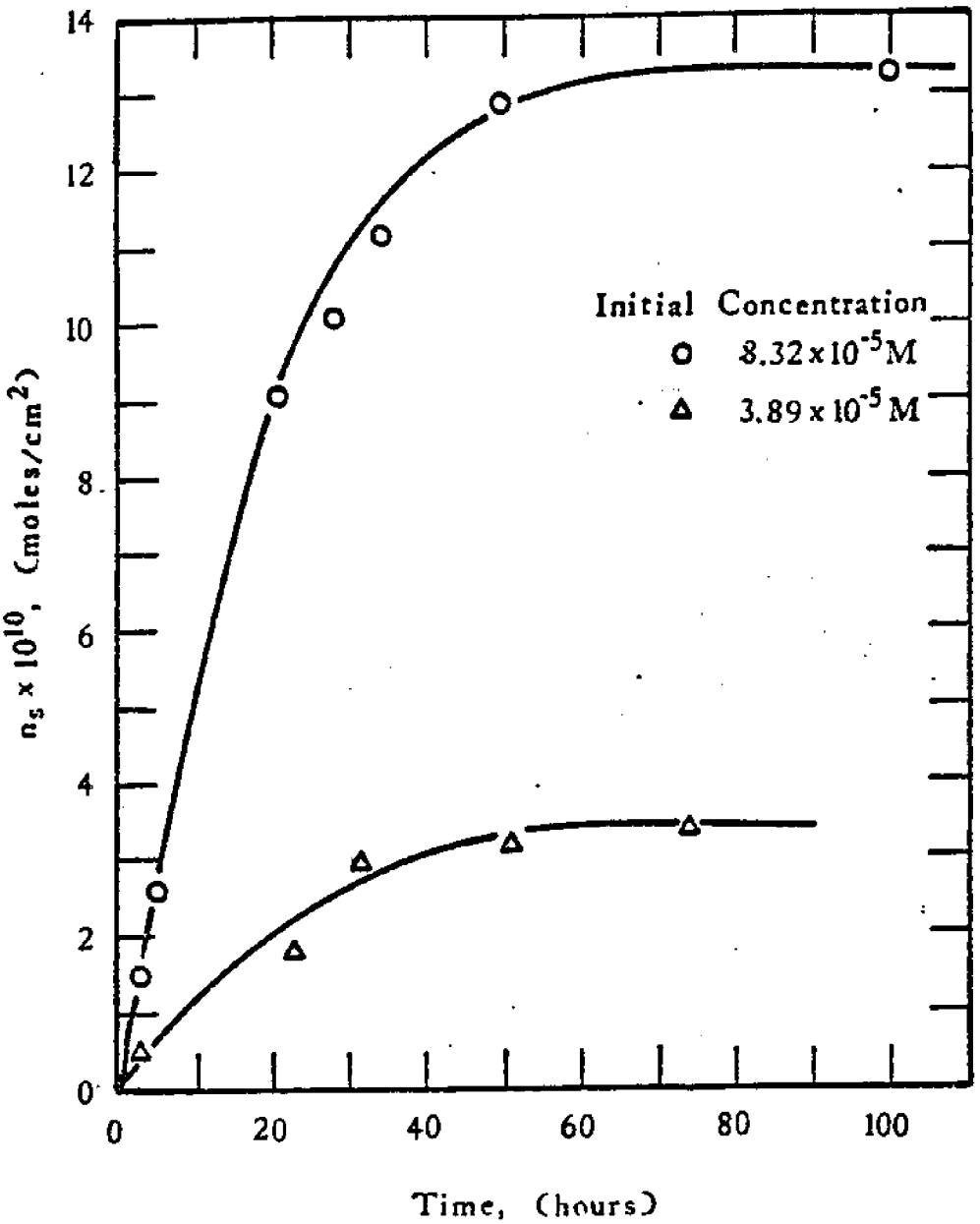

Figure 35: Moles of Surfactant Adsorbed at 82°C as a Function of Time

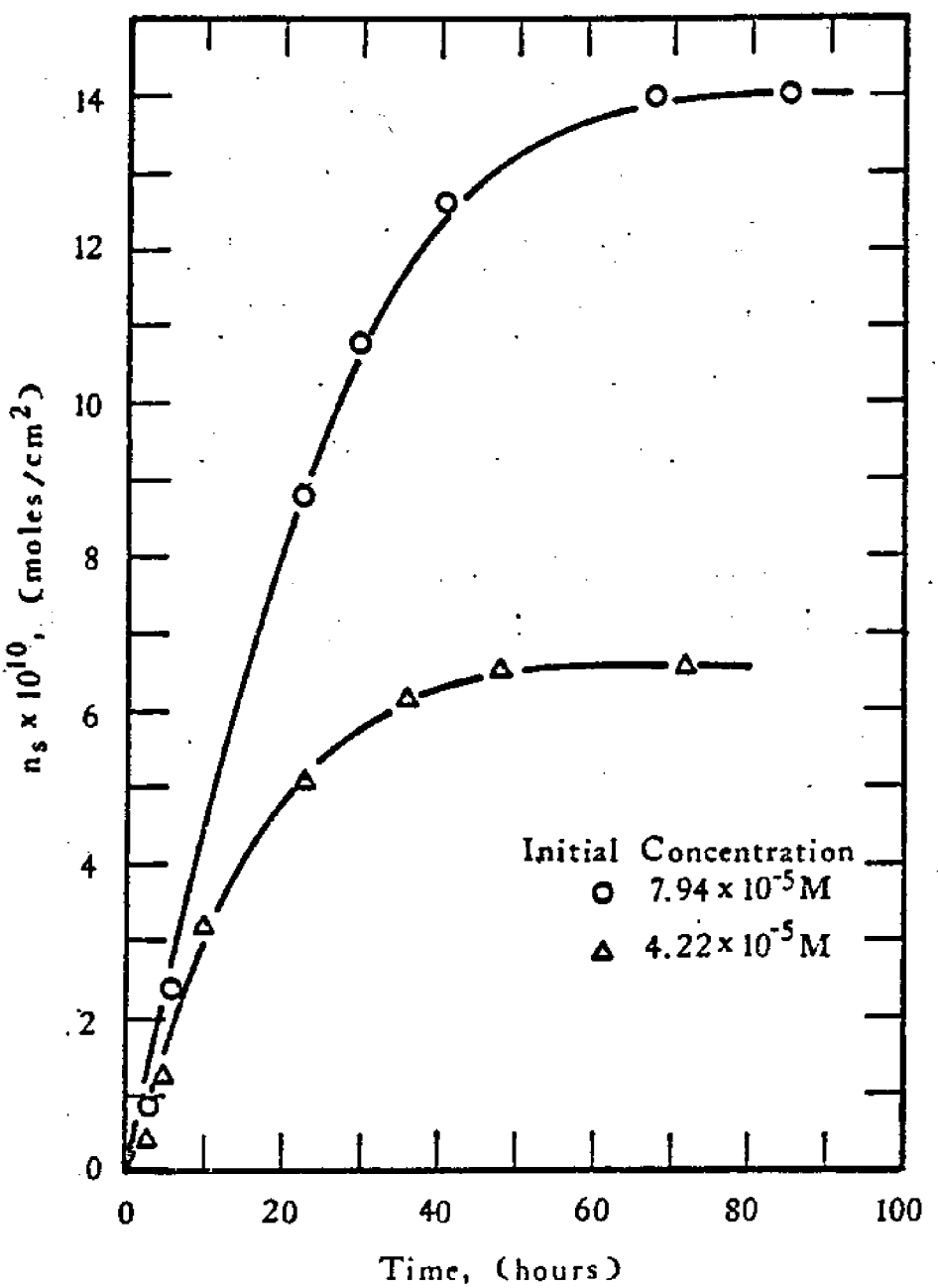

Figure 36: Moles of Surfactant Adsorbed at 87°C as a Function of Time

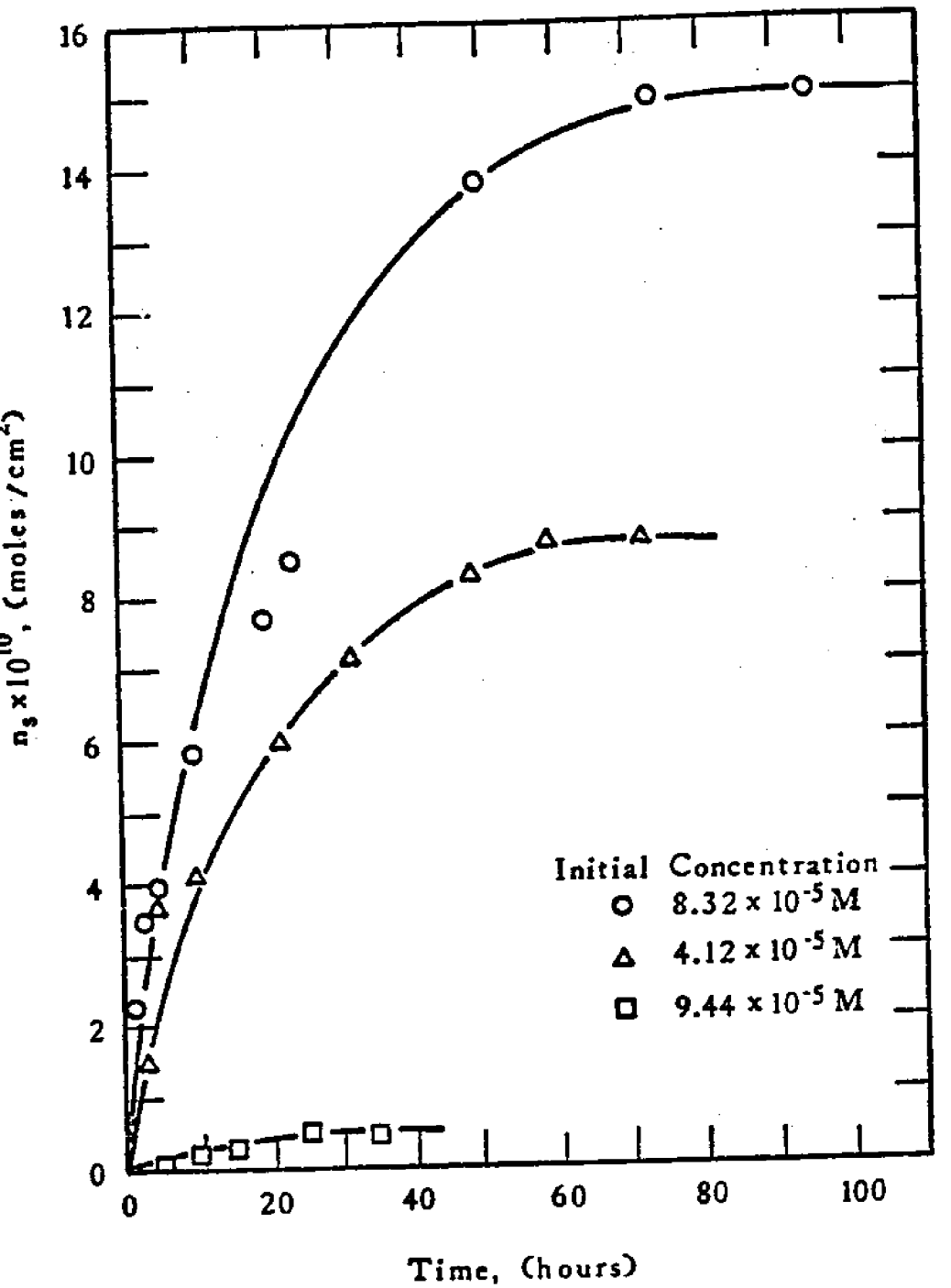

Figure 37: Moles of Surfactant Adsorbed at 92°C as a Function of Time

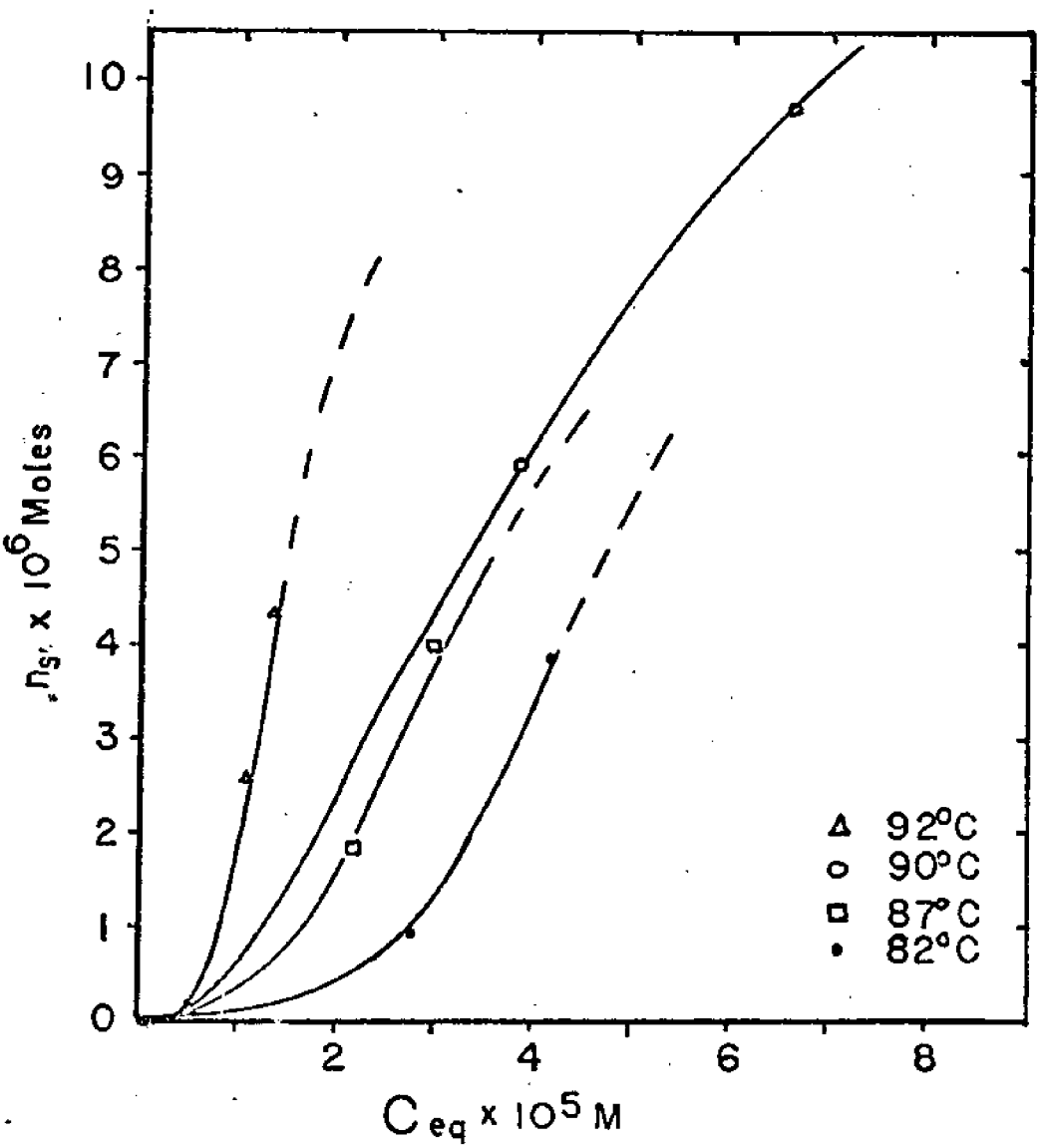

Figure 38: Adsorption Isotherms for LDE on PE at 90° and 82°, 87° and 92° (Garry, 1977).

TABLE 13

Adsorption Rates at 82°C for Initial Surfactant Concentration of 3.89×10^{-5} M

Time (hrs)	dn_s/dt (moles/cm^{2}hr)	kS (cm/hr)
0	1.55×10^{-11}	3.97×10^{-4}
10.0	9.35×10^{-12}	2.71×10^{-4}
30.0	4.30×10^{-12}	1.47×10^{-4}
40.0	2.73×10^{-12}	9.73×10^{-5}
50.0	1.50×10^{-12}	5.40×10^{-5}
60.0	7.50×10^{-12}	2.72×10^{-5}
70.0	6.56×10^{-13}	2.39×10^{-5}
80.0	→ 0	

TABLE 14

Adsorption Rates at 82°C for Initial Surfactant Concentration of 8.32×10^{-5} M

Time (hrs)	dn_s/dt (moles/cm^{2}hr)	kS (cm/hr)
0	6.36×10^{-11}	7.62×10^{-4}
10.0	4.50×10^{-11}	6.45×10^{-4}
20.0	2.87×10^{-11}	4.84×10^{-4}
30.0	1.65×10^{-11}	3.18×10^{-4}
40.0	1.04×10^{-11}	2.22×10^{-4}
50.0	5.51×10^{-12}	1.28×10^{-4}
60.0	2.28×10^{-12}	5.53×10^{-5}
70.0	→ 0	

TABLE 15

Adsorption Rates at 87°C for Initial Surfactant Concentration of 4.22×10^{-5} M

Time (hrs)	dn_s/dt (moles/cm^{2}hr)	kS (cm/hr)
0	2.67×10^{-11}	6.21×10^{-4}
5.0	2.77×10^{-11}	7.19×10^{-4}
20.0	1.52×10^{-11}	5.34×10^{-4}
30.0	9.00×10^{-12}	3.67×10^{-4}
40.0	4.04×10^{-12}	1.84×10^{-4}
45.0	2.50×10^{-12}	1.16×10^{-4}
50.0	$\rightarrow 0$	

TABLE 16

Adsorption Rates at 87°C for Initial Surfactant Concentration of 7.94×10^{-5} M

Time (hrs)	dn_s/dt (moles/cm^{2}hr)	kS (cm/hr)
0	4.17×10^{-11}	5.18×10^{-4}
5.0	4.17×10^{-11}	5.75×10^{-4}
10.0	3.85×10^{-11}	5.92×10^{-4}
30.0	2.00×10^{-11}	4.55×10^{-4}
40.0	1.37×10^{-11}	3.71×10^{-4}
50.0	7.79×10^{-12}	2.41×10^{-4}
60.0	3.07×10^{-12}	1.01×10^{-4}

TABLE 17

Adsorption Rates at 92°C for Initial Surfactant Concentration of 9.44×10^{-6} M

Time (hrs)	$d\eta_s/dt$ (moles/cm^{2}hr)	kS (cm/hr)
0	2.38×10^{-12}	2.52×10^{-4}
10.0	2.08×10^{-12}	2.55×10^{-4}
15.0	1.75×10^{-12}	2.33×10^{-4}
24.0	8.00×10^{-13}	1.34×10^{-4}
35.0	$\rightarrow 0$	

TABLE 18

Adsorption Rates at 92°C for Initial Surfactant Concentration of 4.12×10^{-5} M

Time (hrs)	$d\eta_s/dt$ (moles/cm^{2}hr)	kS (cm/hr)
0	6.25×10^{-11}	1.52×10^{-3}
5.0	3.54×10^{-11}	1.00×10^{-3}
10.0	2.35×10^{-11}	7.61×10^{-4}
20.0	1.43×10^{-11}	5.85×10^{-4}
30.0	8.67×10^{-12}	4.39×10^{-4}
40.0	6.80×10^{-12}	4.21×10^{-4}
50.0	4.81×10^{-12}	3.56×10^{-4}
58.0	2.66×10^{-12}	2.22×10^{-4}
60.0	$\rightarrow 0$	

TABLE 19

Adsorption Rates at 92°C for Initial Surfactant Concentration of 8.32×10^{-5} M

Time (hrs)	dn_s/dt (moles/cm^2hr)	kS (cm/hr)
0	1.78×10^{-10}	2.14×10^{-3}
5.0	4.24×10^{-11}	7.12×10^{-4}
20.0	2.48×10^{-11}	6.66×10^{-4}
30.0	1.89×10^{-11}	6.57×10^{-4}
50.0	1.07×10^{-11}	5.80×10^{-4}
60.0	5.69×10^{-12}	3.67×10^{-4}
70.0	2.92×10^{-12}	2.17×10^{-4}
75.0	$\rightarrow 0$	

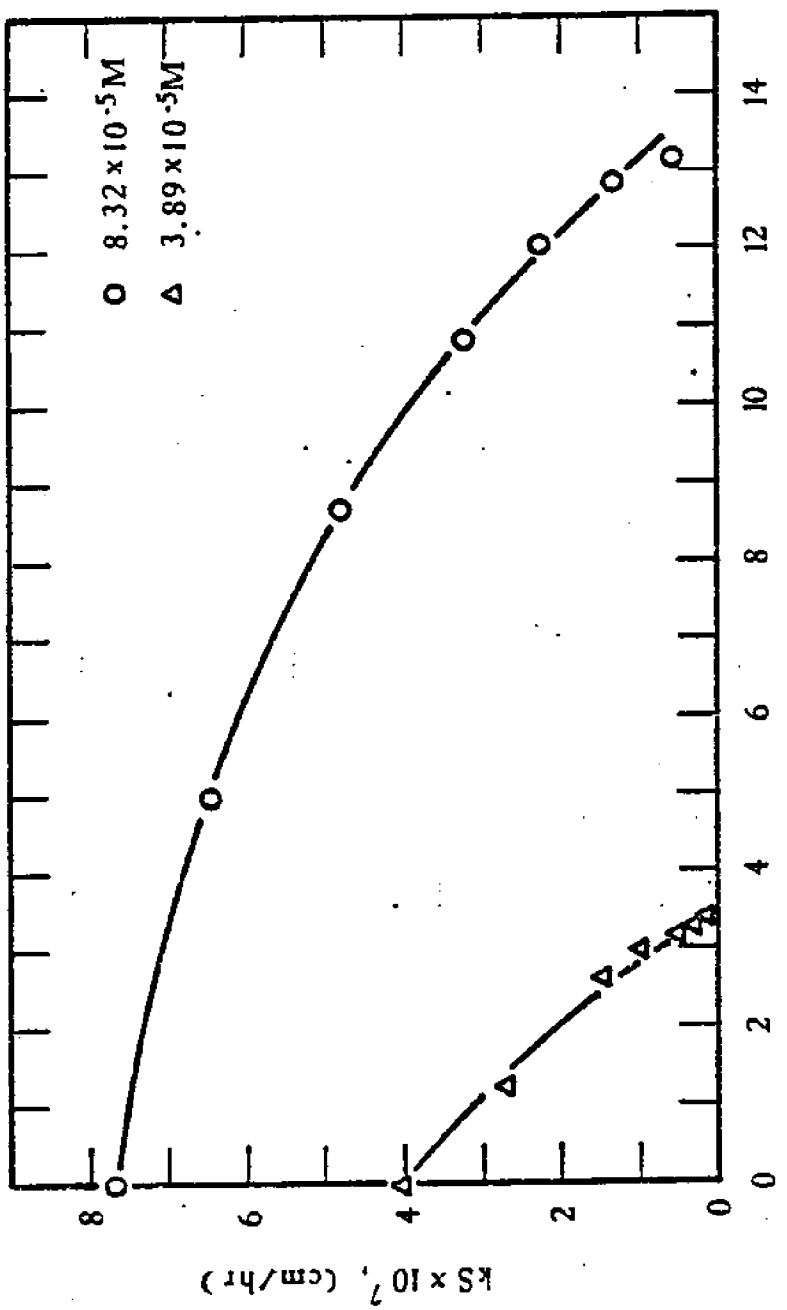

Figure 39: Sticking Coefficient vs Adsorption at 82°C

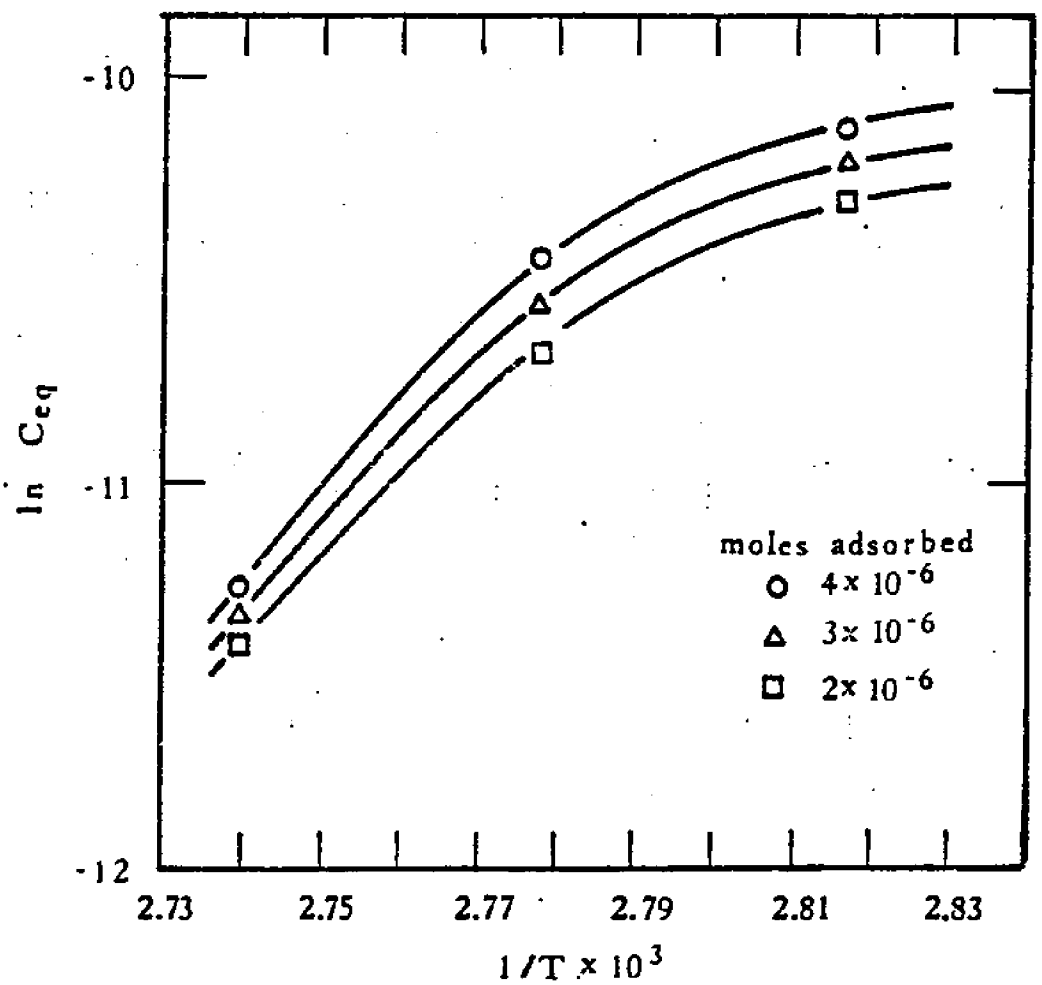

Figure 40: Determination of Heat of Adsorption from C_{eq} at Constant Coverage

Table 20 Tensio-metric Data and Calculated Quantities of Interest for LDE Absorption Runs Done at 90°C and at C_o = 5.44 X 10^{-5}M and C_o = 9.4 X 10^{-5}M.

A. C_o = 5.44 X 10^{-5}M LDE, T = 90°C

t.	CX10^{-5}	n_sX10^{10}	$\frac{dn}{dt}$sX 10^{10}	kS X 10^4	n_s X 10^6	park. area
0	5.44	0	1.00	18	0	-
2.2	5.04	1.99	0.67	13	1.20	83.6
4.8	4.84	2.98	0.53	11	1.80	55.7
12.4	4.01	7.10	0.33	8.2	4.29	23.4
23.4	3.46	9.83	0.04	1.4	5.94	16.9
38	3.74	8.41	→0	→0	5.08	19.8
49	3.77	8.30	→0	→0	5.01	20.0
60	3.77	8.30	→0	→0	5.01	20.0
70	3.82	8.05	→0	→0	4.86	20.6
(hr)	(M)	(mol/cm^2)		(cm/hr)	(mol)	(Å^2/molec)
Error Range:	±0.07	±0.07	±5%	±20%	±0.07	±10%

B. C_o = 9.40 X 10^{-5}M LDE, T=90°C

t	CX10^{-5}	n_sX10^{10}	$\frac{dn}{dt}$s X 10^{10}	kS X10^6	n_s X 10^6	park. area
0.1	9.40	0	3.0	31	0	-
1.5	8.93	2.7	2.7	30	1.6	62.7
3.25	7.86	8.8	2.1	27	5.3	18.9
5.8	7.33	11.8	1.1	15	7.13	14.1
8.0	6.98	13.8	0.60	8.6	8.34	12.0
16.2	6.71	15.5	0.15	2.2	9.36	10.7
24.0	6.58	16.1	→0	→0	9.72	10.3
30.7	6.58	16.1	→0	→0	9.72	10.3
(hr)	(M)	(mol/cm^2)		(cm/hr)	(mol)	(Å^2/molec)
Error Range:	±0.07	±0.07	±5%	±20%	±0.07	±10%

Additional adsorption runs were done at 90°C. Table 20 contains the tensiometric data and several calculated quantities of interest (Appendix XII discusses the processing of tensiometric data and includes original data). Fig. 41 shows LDE solution concentration time behavior for initial concentrations C_o = 5.44 x 10^{-4} M. When converted to plots of specific molar total LDE uptake vs time (Fig. 42), some interesting observations are made. Comparing Fig. 42 to Figs. 32,33, and 34 reveals that at 90°C, equilibrium was reached much faster at either C_o value than at 87°C or 92°C (C_o's used earlier are approximately the same). At C_o = 5.44 x 10^{-5}, equilibrium was reached in 24 hr; it required 60hr to reach it at 92°C for C_o = 4.12 x 10^{-5} M. At C_o = 9.44 x 10^{-5} M, equilibrium again took 24hr; it required 75hr at 92°C for 8.32 x 10^{-5} M. The earlier data at 87°C were 50hr at C_o = 4.22 x 10^{-5} M and >60hr at 7.94 x 10^{-5} M. It is true that the powder used at 90°C was 1208 cm^2/g in area; the earlier batch was only 589 cm^2/g. Perhaps the surface morphologies are different as well, and this could explain the fast adsorption rates at 90°C.

Plotting equilibrium $\underline{n_s}$ (total moles adsorbed for the 5g sample) vs. equilibrium concentration for the 90°C data yields for $\underline{n_s}$ less than about 5 x 10^{-6} moles an isotherm line between the 87° and 90° lines, perhaps closer to the 87° line. (To clarify this a data point below $\underline{n_s}$ = 4 x 10^{-6} moles would be required.) However, the line crosses the <u>extrapolated</u> 87° line at 6 x 10^{-6} moles, and begins to level off between 6 x 10^{-6} moles and 9 x 10^{-6} moles = $\underline{n_s}$. This indicates that possibly the isotherms at other temperatures similarly exhibit such behavior; unfortunately the earlier data does not extend beyond $\underline{n_s}$ = 5 x 10^{-6} moles. Fig. 38 shows adsorption isotherm data for 90°C along with earlier data for 82°, 87° and 92°C.

Initial rates of adsorption at 90°C for both C_o values were each about 1.65 times the rates for similar C_o values at 92°C. The 87°C rates were slower by factors of 4 for the lower concentration and by factors of about 7 for the higher C_o. These values are merely the slopes from the plots in Figure 42.

Calculations of area of PE per adsorbed LDE molecule were also made; the values at 90°C are close to values both above and below this temperature. At C_o = 5.44 x 10^{-4} M, the equilibrium value of 17Å^2/molecule is nearer the 92°C value (17Å/molecule at C_o = 4.22 x 10^{-5} M) than the 87° value (25 Å/molecule). For the higher C_o, all three temperatures showed values of 10-12 Å^2/molecule. Literature from the Stepan Chemical Co. quotes a value for the surface area of the LDE molecule as 25 Å^2. From space-filling models of the hydrophilic head of LDE it appears that a reasonable estimate of the "parking area" it needs on the PE surface, once the aliphatic tail is completely diffused, is about 10-12 Å^2 (see Appendix II). This is precisely the minimum area per molecule seen in both Garry and present data. This suggests a model of a "carpet" of LDE head units, just touching one another, following the porous, irregular contours of the surface region of the PE. In reality, there probably exists "elbow room" around each LDE head, and thus the true condition is perhaps that of a micellar bilayer on the surface with a parking area per molecule closer to 25 Å2 on the PE surface, as suggested by the isotherm data.

Finally, values of kS, the sticking coefficient times rate constant, were calculated for the 90°C data and plotted against $\underline{n_s}$. The resultant curves had a shape intermediate between the corresponding curves for 87°C and 92°C. At C_o = 5.44 x 10^{-5} M, the kS vs n_s plot was identical in shape to the 4.22 x 10-5 plot of 92°C and quite unlike the corresponding 87°C plot (see Fig. 43). However, at C_o = 9.4 x 10^{-5} M, the 90°C plot was in essence an average of the 87°C and 92°C plots, except for the surprisingly high kS values encountered at low n_s. The other kS values also were erratic, but no fluctuations as great as with the 90°C, 9.4 x 10^{-5} M value were reported.

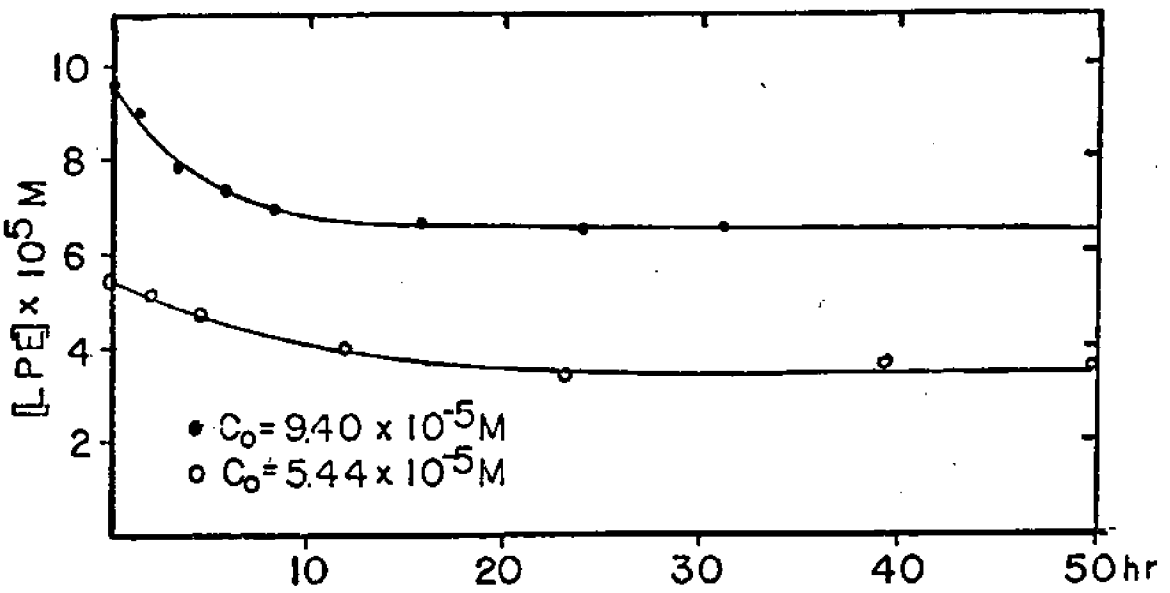

Figure 41 LDE Concentration vs Time for Adsorption on PE at 90°C.

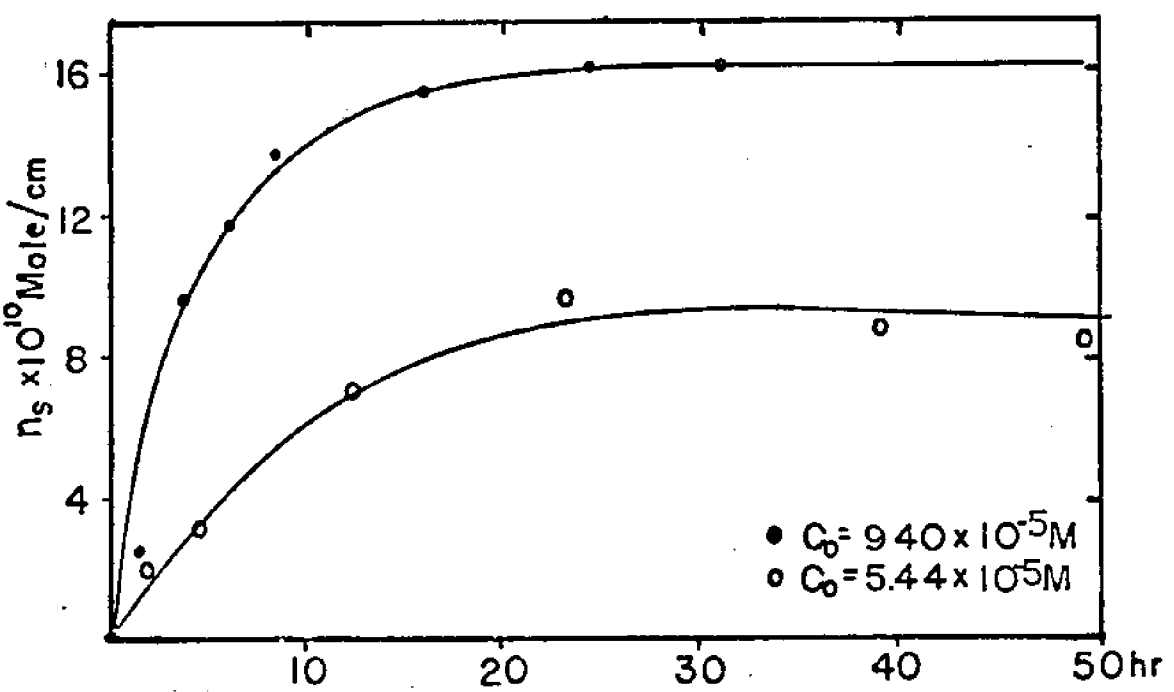

Figure 42 Moles LDE Adsorbed vs Time for PE Powder at 90°C.

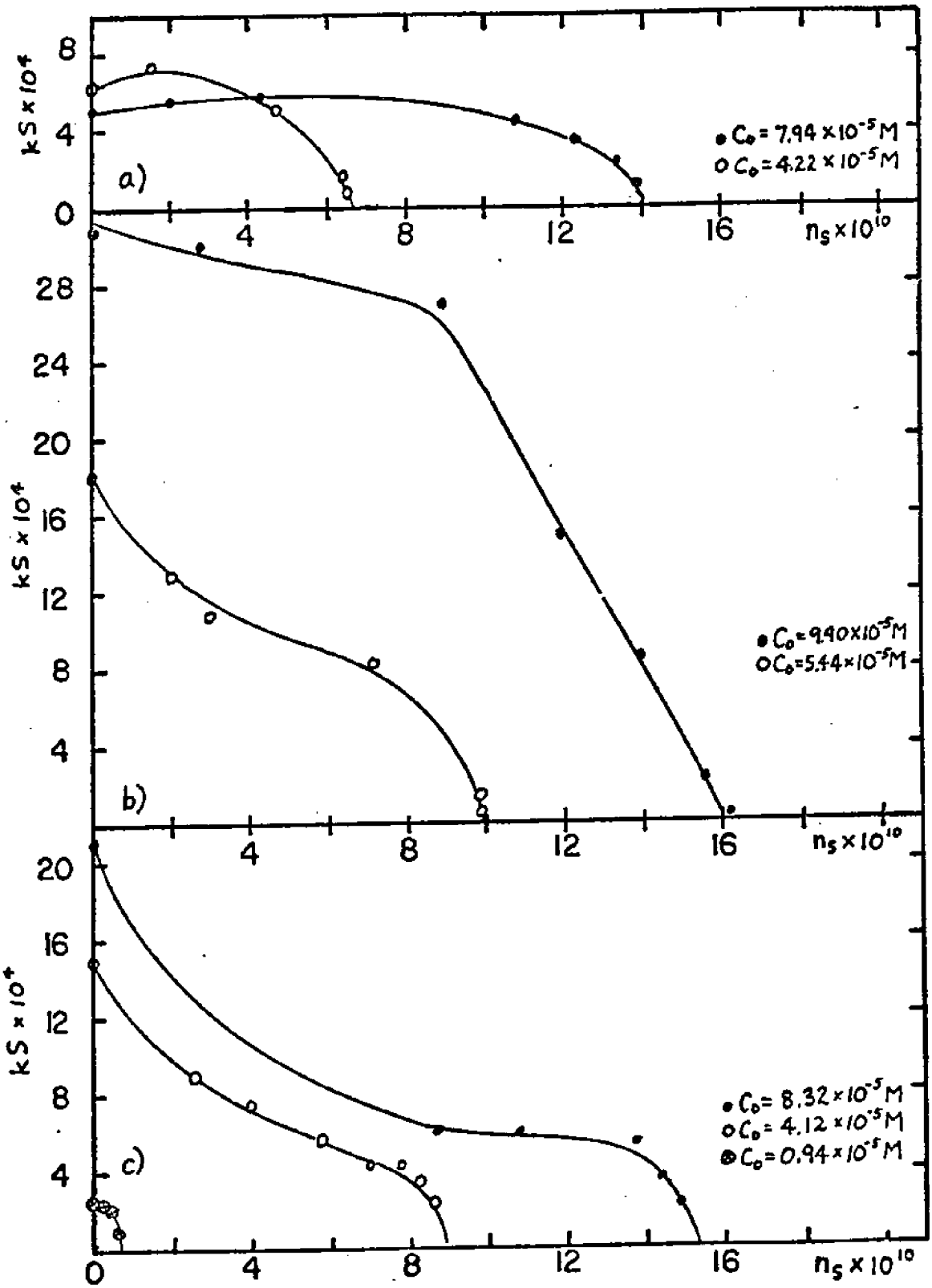

Figure 43: (a) through (c) Plot kS vs Specific Molar Adsorption for LDE on PE at 87°, 90° and 92°, respectively.

Characterization of modified polyethylene surfaces. ATR-IR: As discussed earlier, ATR IR is best for discerning general chemical character, while ESCA reveals more about time-dependent behavior of the surface when subjected to various surface-treatment processes. Figs 44a and 44b compare ATR IR spectrograms for major surface types in the 1800-1300cm^{-1} region, which happens to contain most bands of interest. Figs 44c and 44d actually show time-dependent changes in the 1720cm^{-1} carbonyl peak on plasma-treated samples at two selected gas flowrates. The instrument used was a Perkin-Elmer 283 with Wilks Model 45 ATR module.

Blank PE is characterized in the "carbonyl region" of 1800-1300cm^{-1} by a small CO peak at 1720cm^{-1} and the methylene bending bands at 1470cm^{-1} and 1370cm^{-1}. LDE treatment greatly enhances the csrbonyl and also generates a peak in the 1620 to 1640cm^{-1} area. DM100-treated blank PE shows a modestly enlarged 1720cm^{-1} peak, regardless of period of treatment, and only a shoulder at 1620 to 1640cm^{-1}. Posttreat of LDE strip with DM100 enlarges the CO peak still further, and also enlarges noticeably the small knob at 1625cm^{-1} noted for PE + LDE. Again, varying the length of posttreat causes little change in the ATR IR signal. In other regions of the spectrum, a broad absorption in the 950cm^{-1} to 1150cm^{-1} range appears for all surface types, but is highly variable and not a reliable monitor of chemical moieties on the surface. Another broad band is seen in the OH stretch region above 3000cm^{-1}, but again it is not reliable. The ATR peaks mentioned above appear in Fig. 44a.

Several other surface classes were also amenable to study by ATR, with some help from bands in other regions of the spectrum. These appear in Figure 44b. Blank PE treated with adipic acid (AA) is almost identical to PE + DM100, except for a small shoulder on the carbonyl peak at 1705cm^{-1}. For treatment times greater than 30 minutes, the whole CO peak actually is seen to grow significantly with time. This is probably slow AA adsorption onto PE LDE-treated strips when exposed to AA, show a CO peak significantly larger than

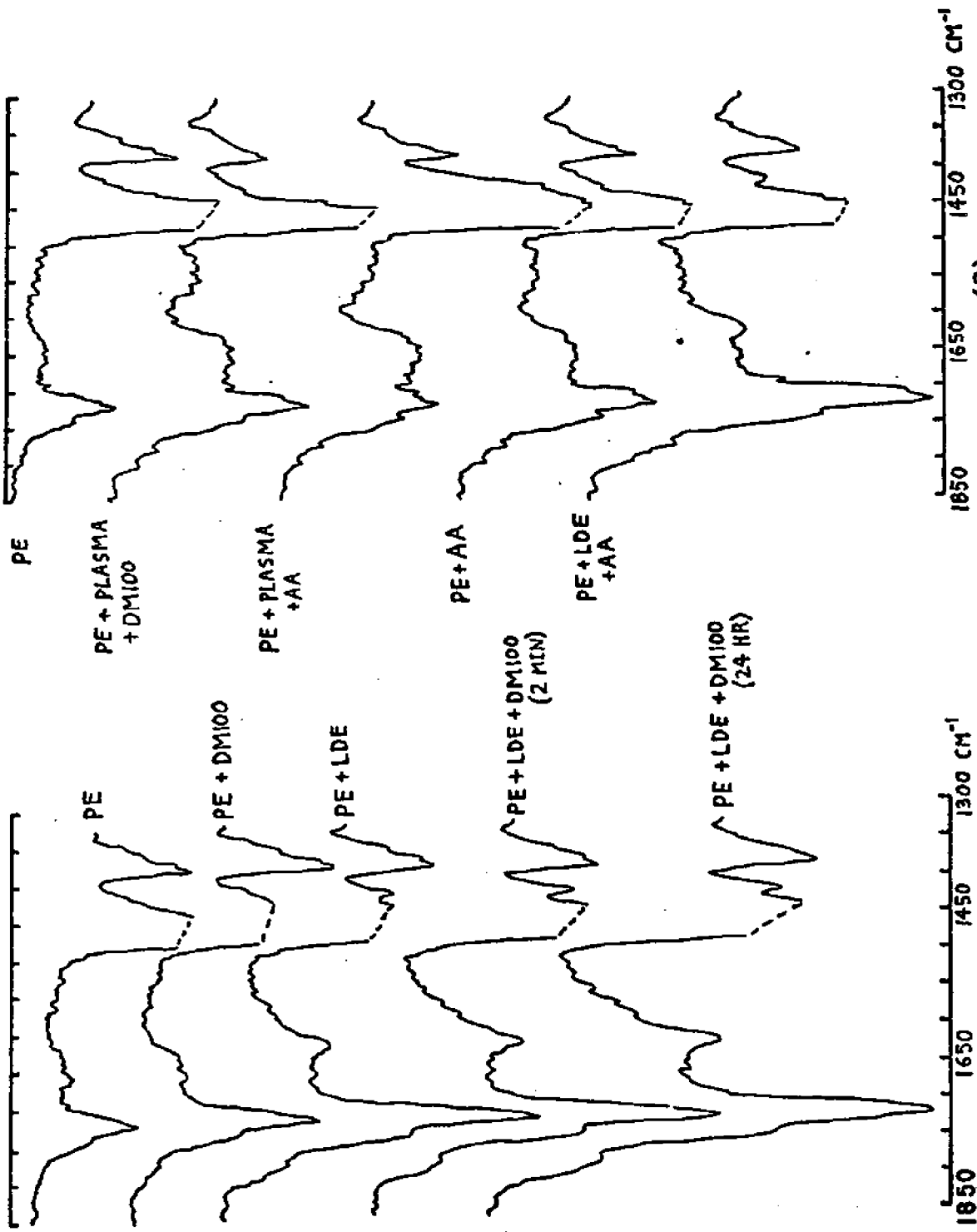

Figure 44 (a) and (b) Representative ATR IR Spectrograms (Carbonyl Region) for Various Surface Modification Methods. Note CO Peaks at 1720 and 1620 cm^{-1}.

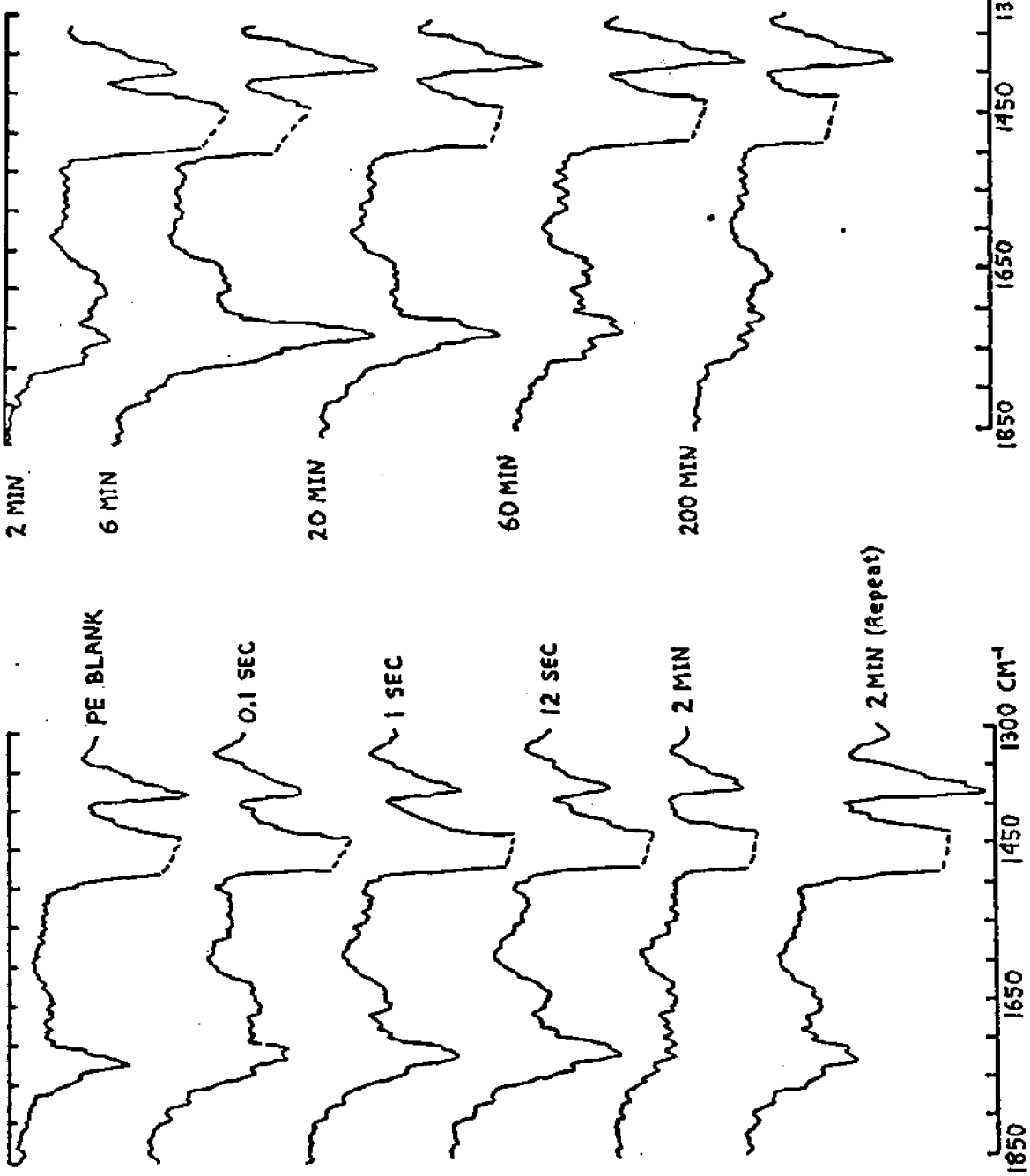

Figure 44 c) ATR IR Spectrograms of the Carbonyl Region for PE + Plasma (2 cm^3/min atm) for Various Exposure Times.

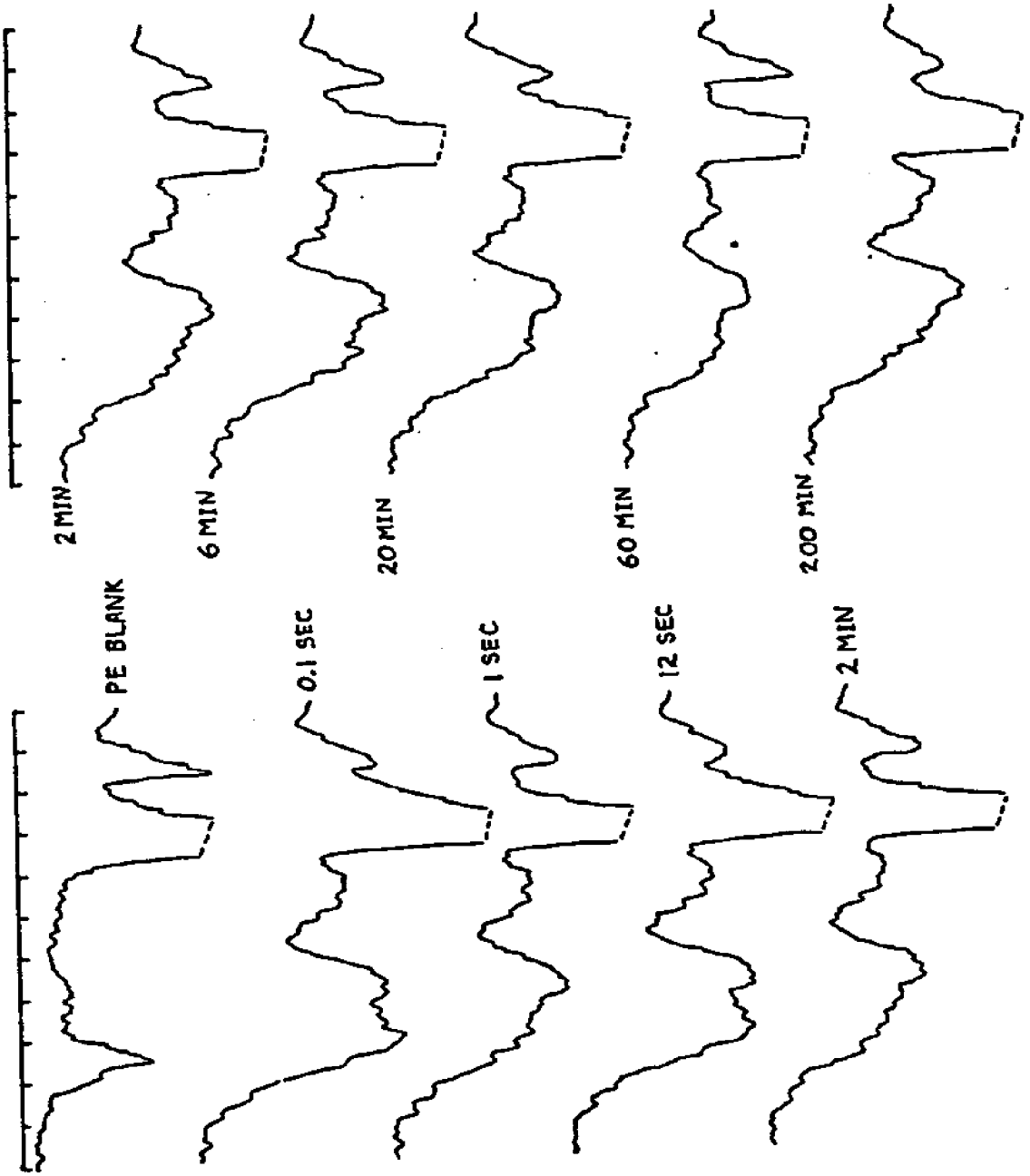

Figure 44 d) ATR IR Spectrograms of the Carbonyl Region for PE + Plasma (25 cm^3/min atm) for Various Exposure Times.

for PE-LDE alone; and the small shoulder at 1705 is still present. No noticeable time-dependence was seen over the 2 min to 24 hr range, however.

Plasma-treated strips (6 min exposure) exposed to DM100 exhibit a peak similar to blank PE, which shows detectable shrinkage at about 6 min DM100 treat, and is almost gone after 200 min to 24 hr. For these samples, a large wide peak at 1105cm^{-1} and a sharp one at 615cm^{-1} are seen at 2 min, and then both show noticeable shrinkage after about 20 min. By 200 min both the 1105cm^{-1} peaks are gone. A shoulder at 1440cm^{-1} exhibits the same time behavior.

Plasma-treated samples posttreated with AA resemble the plasma + DM100 strips in the carbonyl region, except that the 1440cm^{-1} shoulder is invariant with time. The 1105cm^{-1} and 615cm^{-1} show slight shrinkage after 24 hr. Concentration effects were seen to be nil on all of the DM100 and AA-treated samples.

In Figure 44c is seen the plasma treat-time behavior of the 1720cm^{-1} CO peak for plasma-treated samples at the standard air flowrate of 2cm^3/min atm. This peak showed a curious double-maximum behavior over the range of treat time with maxima at about 1 to 12 sec and about 6 to 20 min treat-time, separated by a minimum at 2 min treat-time. The 1720 cm^{-1} peak almost vanished at the 2 min treat time, as was confirmed with a separately prepared sample at 2 min exposure time analysed on a separate occasion. At 0.1 sec the peak is similar in size to that seen in blank PE. This behavior is nicely mirrored by the behavior of the ESCA O/C ratio, and hence seems to reflect actual depletion and replenishment of oxygen occuring in two distinct time regimes.

Even more interesting is the contrast between the above-noted behavior of the 1720cm^{-1} peak and its relatively constant size seen at a higher air flowrate of 25 cm^3/min atm (Figure 44d). Over the entire range of exposure times from 0.1 sec to 200 min, the CO peak remains at a level slightly below that seen for blank PE. Clearly, a different sort of process is dominant in this flow regime. A third set of experiments was attempted at zero flowrate, but leakage problems caused the

chamber pressure to rise beyond the 1.0 torr standard level and to kill the discharge after 2 min. Results resembled the high-flow series above, but probably are rendered invalid by the pressure rise.

Throughout all of these ATR IR investigations, problems existed with atmospheric moisture and carbon dioxide; water absorbs in the carbonyl region and shows up as fine spikes under high resolution. Use of double-beam arrangement in the 283 machine helped reduce the problem to that contributed by adsorbed species (which were unavoidable except by heroic measures). All the work was done at Cryovac; which had available ATR modules for immediate use (none were available at MIT for extended use).

Additional work was done using a single-pass hemicylindrical KRS-5 crystal in place of the flat used above, on a Nicolet 7000 FT IR instrument at Cryovac. Use was made of the data-processing capability to prepare subtraction spectra of the type (PE+LDE+DM100) - (PE+LDE). These subtraction spectra were nearly flat indicating that the chemical changes caused by DM100 posttreat occur in a much smaller volume of surface region than that affected by the LDE pre-treat. ESCA N/C ratios show the expected large increase with DM100 posttreat, however; this rules out the possibility of non-reaction (as do the flexure results).

Transmission IR Studies: In an attempt to better understand the ATR IR spectra of PE + LDE and PE + LDE + DM100, solution-phase LDE + DM100 polymerization reactions were carried out in chloroform (for convenient IR application). These reactions were carried out at room temperature for 24 hr. Each component (LDE and DM100) was dissolved in 50 ml solvent and then the DM100 was poured into the LDE under vigorous stirring. Curing was by H_2O; first in stoichiometric proportion, then in large excess. Transmission IR spectra were obtained on a Perkin-Elmer 513 and compared to the ATR IR spectrograms. LDE showed a carbonyl peak at 1620cm^{-1}, near the feature seen in ATR but nowhere near the 1720 peak always

associated with LDE in ATR. DM100 has a CO peak at 1690cm^{-1}, and an isocyanate band at 2270cm^{-1}. The urethanes obtained from reacting the two show a new shoulder at 1710cm^{-1}, and a second CO peak at 1640cm^{-1}. The size of the 1710cm^{-1} shoulder is a function of stoichiometric ratio of OH to NCO, dwindling to zero as this ratio becomes small. (See Figure 45). Interesting, the NCO peak remained even after stoichiometric addition of water, so long as the ratio of OH to NCO was less than 1.0. Large molar excesses of H_2O finally killed the NCO after long reaction times. These observations are comforting, as they suggest that DM100 preferentially reacts with LDE rather than water, perhaps on the PE surface as well as in solution. Fig. 46 shows the interesting morphological spectrum obtained from preparing polyurethanes of different compositions of LDE and DM100. With $\frac{OH}{NCO}$ greater than 1.0, a taffy-like substance results, very adhesive in nature. This presumably grades into a sticky syrup, then an oily or waxy compound as the composition approaches pure LDE. At the other end, ratios of 1.0 through 0.3 show a tough colorless elastomeric substance which when fully H_2O cured tends to foam (more foamy towards the 0.3 ratio) and become chalky in color. At $\frac{OH}{NCO}$ near 0.1, the uncured polymer is syrupy. Cured, it is a flexible foam. Presumably, beyond 0.1 the foam becomes rigid, as cured DM100 is shellac-like. The tough elastomer found near stoichiometric balance seems ideally suited for abrasion resistance, and its elastivity should assist in tolerating flex-working.

ESCA: All of the surface types studied were examined under ESCA, and it was found that time-dependent behavior could be monitored reasonably well. Despite the weakness of the N1s signal, good data were obtained for N/C and N/O atomic ratios. (All ratios used the relative intensity factors quoted by Berthou and Jorgensen (1975)). Table 21 gives ESCA data.

Looking first at the N/C ratio, a dramatic rise was seen with posttreat time for all DM100-treated samples. This indicates surface adsorption and reaction with whatever reactive species (i.e. OH and NH_2 primarily) lie there. Non-reactive

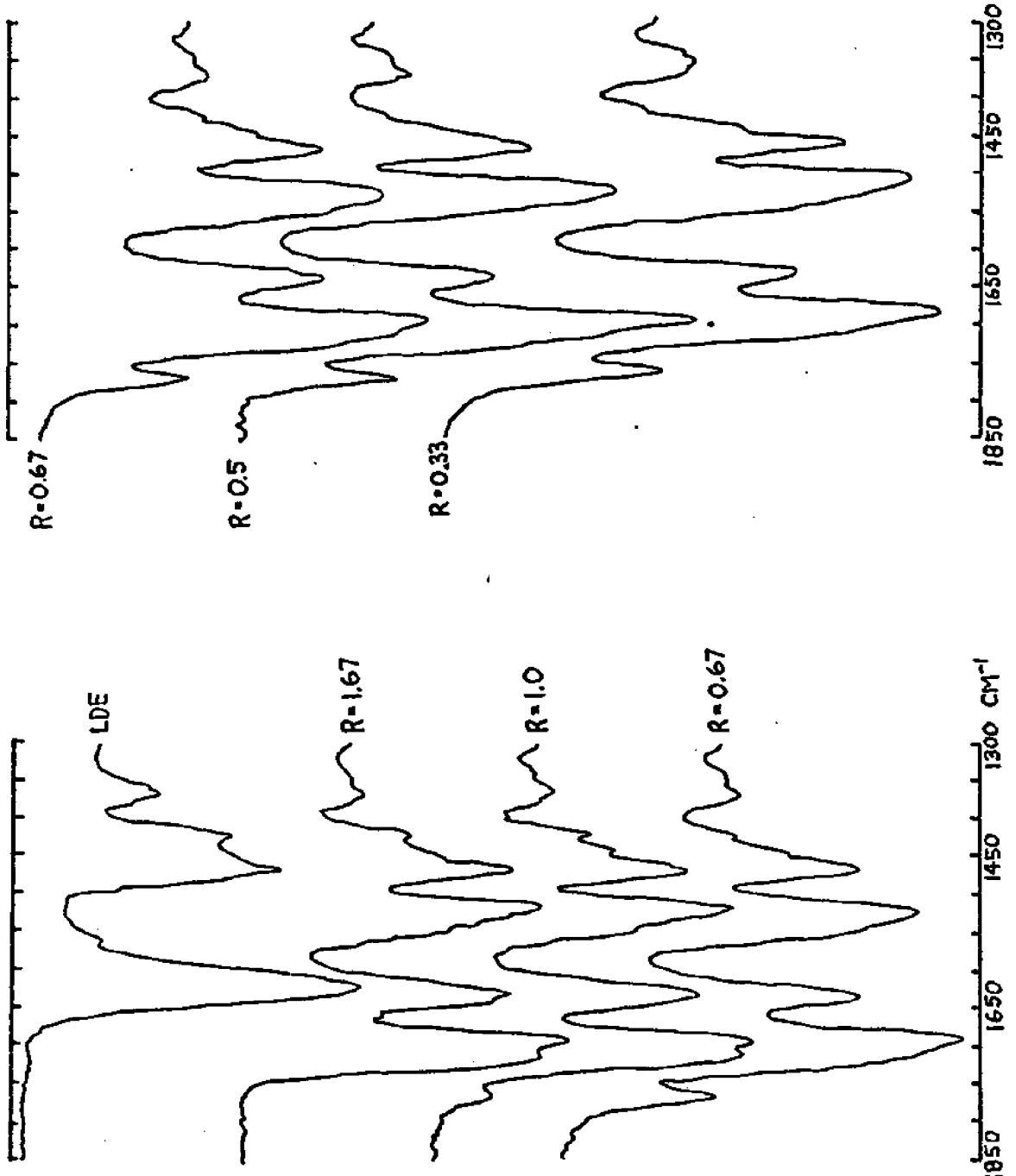

Figure 45: Transmission IR Spectrograms of the Carbonyl Region for Polymers of LDE + DN100 Formulated with Various Stoichiometric Ratios (R) of OH:NCO.

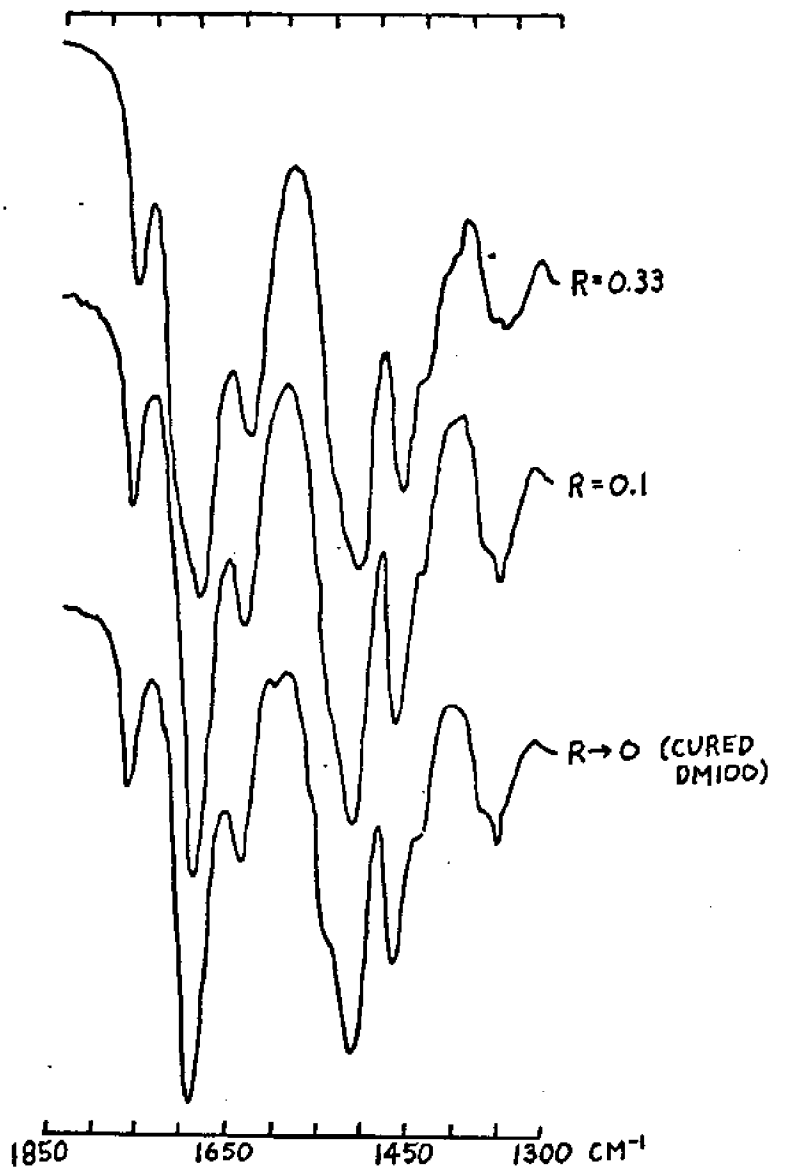

Figure 45: (Continued).

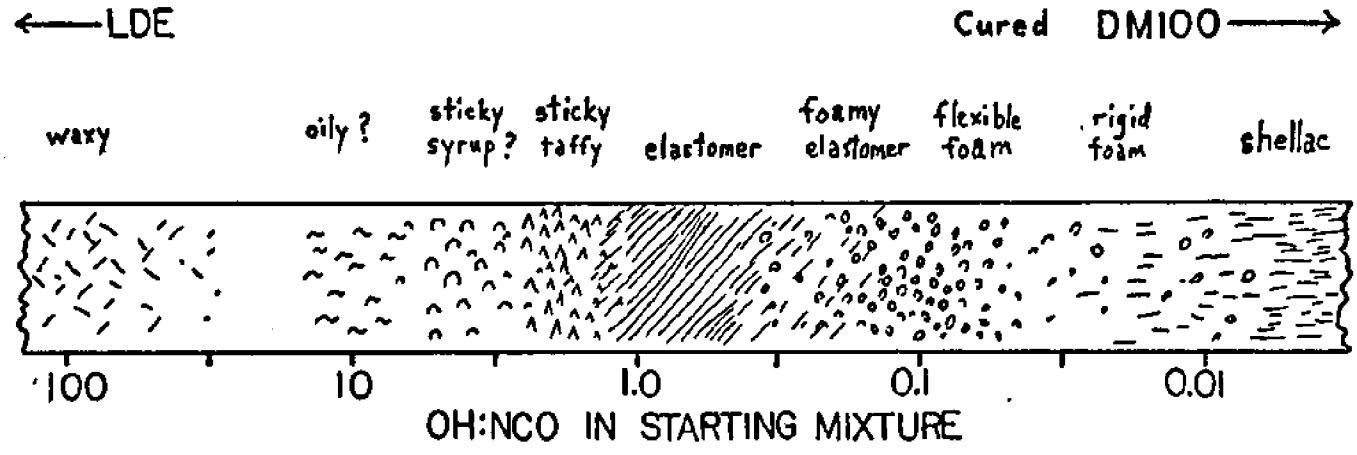

Figure 46: Morphology of LDE + DM100 Polymers of Various Composition.

Table 21. ESCA Atomic-Ratio Surface Data For All Strip Samples Tested, Listed By Series (Nomenclature defined in Appendix VIII).

Series A: PE, PE + LDE, PE + LDE + DM100, PE + DM100 (*)

No.	DM100 Conc.	Time.	O/C	N/O	N/C
1	PE blank		0.12	<0.01	<0.001?
2	PE +LDE		0.15	0.083	0.0046
3	"L"	2 min	0.15	0.094	0.014
4	"H"	2 "	0.12	0.20	0.024
5	"V"	2 "	0.089	0.17	0.015
6	"L"	2 " *	0.14	0.12	0.017
7	"H"	2 " *	0.16	0.30	0.048
8	"V"	2 " *	0.092	0.30	0.028
9	"L"	24 hr	0.11	0.074	0.0081
10	"H"	24 "	0.12	0.080	0.0096
11	"V"	24 "	0.15	0.12	0.018
12	"L"	24 "	0.074	0.10	0.0074
13	"H"	24 "	0.092	0.39	0.036
14	"V"	24 "	0.11	0.34	0.037
15	"V"	20 min	0.16	0.16	0.026
16	"V"	20 min	0.095	0.36	0.034

"L" = 4.44×10^{-7}M DM100
"H" = 4.44×10^{-5}M "
"V" = 4.44×10^{-3}M "

Table 21 (continued)

Series B: PE, PE + LDE, PE + LDE + DM100, PE + DM100 (*)

No.	Conc.	Time	O/C	N/O	N/C
1	"H"	6 min	0.117	0.126	0.0147
2	"H"	20 min	0.101	0.129	0.0130
3	"H"	60 "	0.122	0.152	0.0185
4	"H"	6 " *	0.135	0.156	0.0211
5	"H"	20 " *	0.104	0.287	0.0298
6	"H"	60 " *	0.092	0.192	0.0177
7	PE Blank		0.150	0.0077	0.0014
8	PE + LDE		0.175	0.068	0.0119
9	"L"	24 hr	0.124	0.027	0.0033
10	"H"	24 "	0.151	0.046	0.0069
11	"V"	24 "	0.086	0.152	0.0131
12	"L"	24 " *	0.076	0.070	0.0053
13	"H"	24 " *	0.213	0.115	0.0245
14	"V"	24 " *	0.146	0.276	0.0403

"L" = 4.44×10^{-7}M DM100; "H" - 4.44×10^{-5}M DM100; "V" = 4.44×10^{-3}M DM100.

Table 21. (continued)

Series C: PE + plasma (133 Pa, air, 2 cm^3/min atm flow)

No.	Exposure Time	O/C	N/O	N/C
D-1	0.1 sec	0.287	0.056	0.017
D-2	1 sec	0.263	0.091	0.024
D-3	12 sec	0.241	0.088	0.021
C-1	2 min	0.191	0.060	0.0115
C-2	2 min (opp.side)	0.136	0.056	0.0076
C-3	6 min	0.184	0.069	0.0127
C-4	20 min	0.331	0.057	0.0189
C-7	20 min (repeat)	0.240	0.080	0.0192
C-5	60 min	0.248	0.050	0.0124
C-6	200 min	0.180	0.032	0.0058

Series D: PE + plasma (133 Pa, air, 25 cm^3/min atm flow)

No.	Exposure Time	O/C	N/O	N/C
D-4	1 sec	0.251	0.075	0.019
D-5	2 min	0.333	0.085	0.028
D-6	6 min	0.244	0.076	0.019
D-7	20 min	0.279	0.105	0.029
D-8	200 min	0.289	0.044	0.013

Sample Nomenclature Defined in Appendix VIII.

Table 21. (continued)

Series F: PE + LDE + AA and PE + plasma (6 min, 2 cm^3/min) + AA

No.	Pretreat	Conc.	Time	O/C	N/O	N/C
1	LDE	"H"	24 hr	0.290	0.032	0.0093
2	"	"H"	30 min	0.201	0.038	0.0076
3	"	"H"	2 min	0.246	0.070	0.017
4	"	"V"	24 hr	0.215	0.108	0.023
5	"	"V"	2 min	0.194	0.099	0.019
6	plasma	"H"	24 hr	0.277	0.040	0.011
7	"	"H"	30 min	0.220	0.090	0.020
8	"	"H"	2 min	0.202	0.040	0.0081

"H" = 6.67 X 10^{-5}M AA; "V" = 6.67 X 10^{-3}M AA

adsorption is discounted since all DM100 samples showed retardation of degradation under flexure, and since the H_2O quench would polymerize the DM100 skin to a polyurea. For PE+LDE+DM100, as seen in Figures 47a and 47b, N/C ratios reached equilibrium after about 6 min at "H" concentration of DM100, and after 20 min at the "V" concentration. For PE + plasma + DM100 as seen in Figure 48, equilibrium evidently was not reached at the "H" Concentration; the "V" concentration curve seemed to level off near 24 hr. This behavior is similar to blank PE + DM100, where the N/C ratios leveled off only near 24 hr in each case. The "L" concentration was not monitored by ESCA due to other demands on machine-time. Plotting N/C against concentration (Figures 47c and 47d), one finds an increase from "L" to "V" at 2 min posttreat time for both LDE and blank PE strips; this behavior is also seen at 24 hr. In Figure 49, the N/C vs plasma exposure time relation is given for the low and high flowrates studied. While the high flow series shows a smooth curve peaking near 6 to 20 min, the low-flow trace shows two maxima, the larger at about 1 sec and the smaller near 20 min. A minimum at about 2 min is seen. This exactly parallels the ATR carbonyl behavior mentioned earlier.

The N/O ratio was the best monitor for AA posttreat; since AA contains O but not N, a depletion of N/O could be attributed to a rise in surface AA population (Figures 50a and 50b). This effect was in fact seen for both PE + plasma + AA and for PE + LDE + AA at the "H" concentration of AA (Refer to EXPERIMENTAL section for definition; it is hard to pinpoint the equilibrium owing to paucity of data (again due to machine-time bottlenecks). For the plasma strip it appears to occur after 2 min (the point at 30 min was probably from contaminated sample). For the LDE strip it again seems to be in the 30 to 200 min range. Curiously, at the "V" concentration of AA, the LDE strip actually underwent an increase in N/O, with the ratio levelling off possibly as soon as 2 min. Only two data points were taken, so any interpretation is risky. For both the low- and high-flow plasma exposure series,

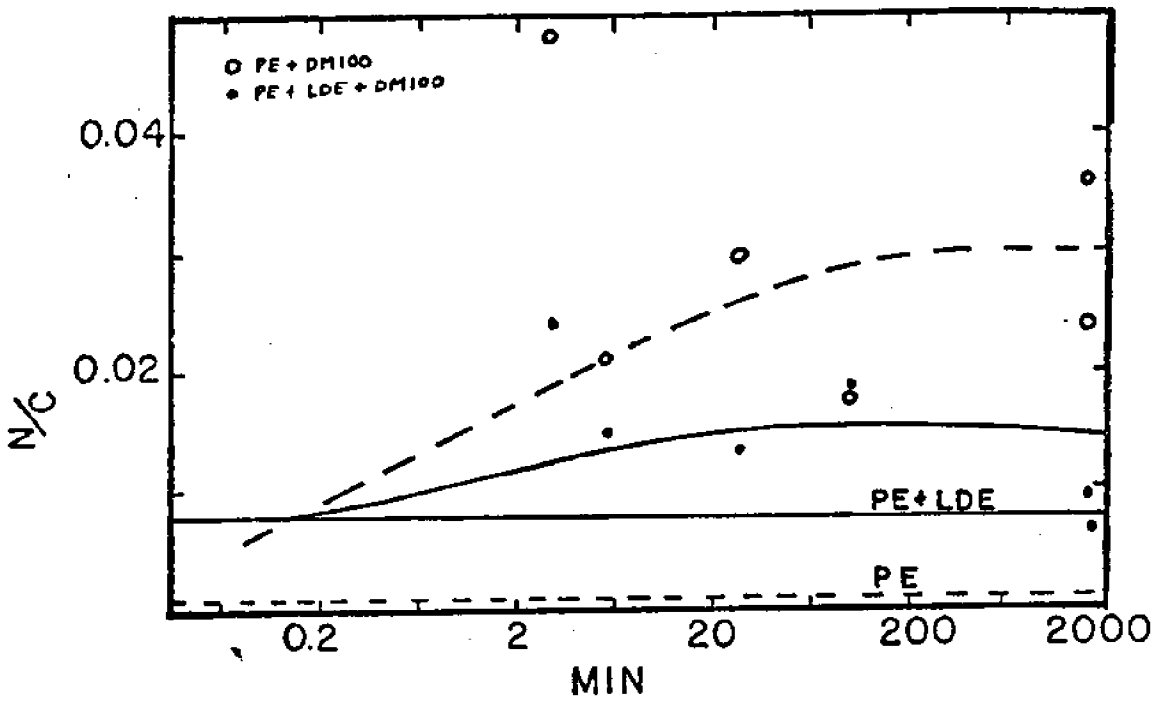

Figure 47. a) ESCA N/C Ratio vs Log Posttreat Time for PE + DM100 and PE + LDE + DM100, at 4.44 x 10^{-5} M DM100.

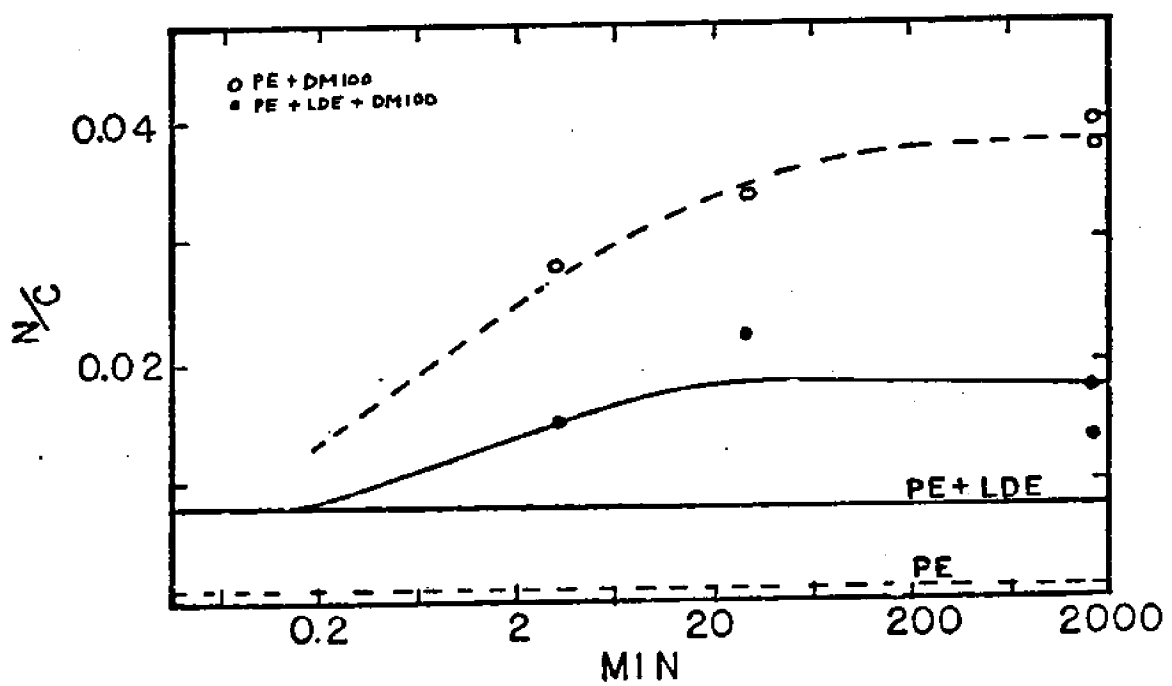

Figure 47. b) N/C Ratio vs Log Posttreat Time for PE + DM100 and PE + LDE + DM100, at 4.44 x 10^{-3} M DM100.

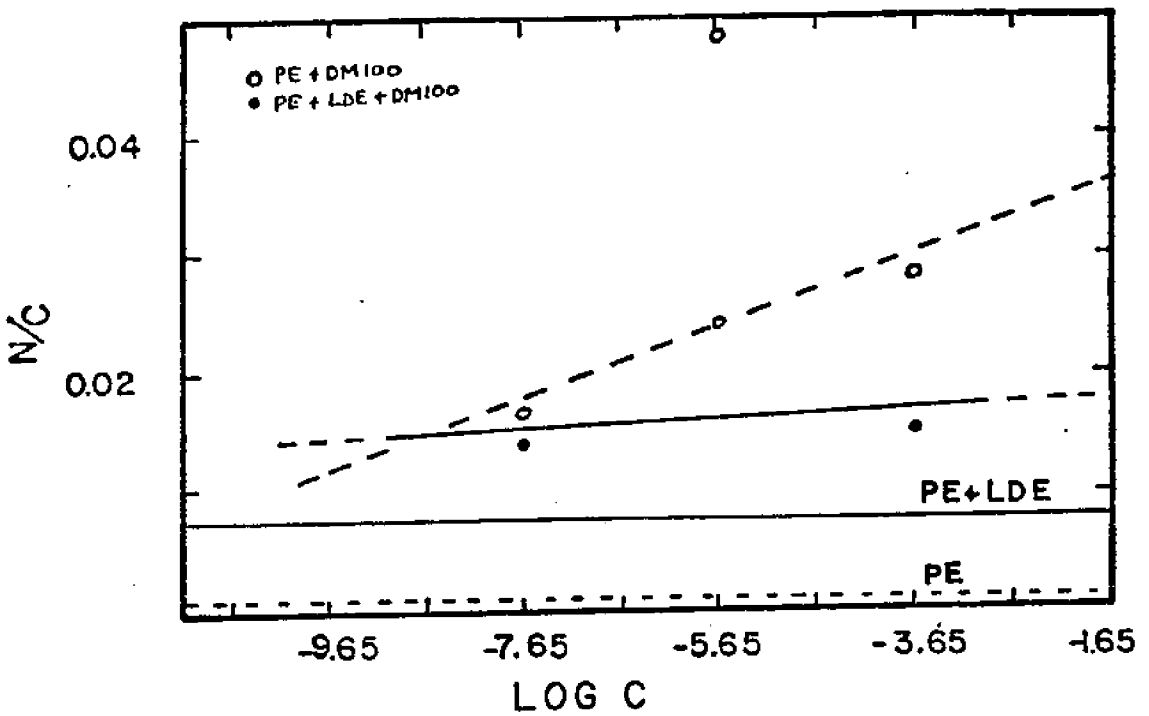

Figure 47. c) ESCA N/C Ratio vs Log Posttreat Concentration for 2-min Posttreats in DM100 of PE and PE + LDE.

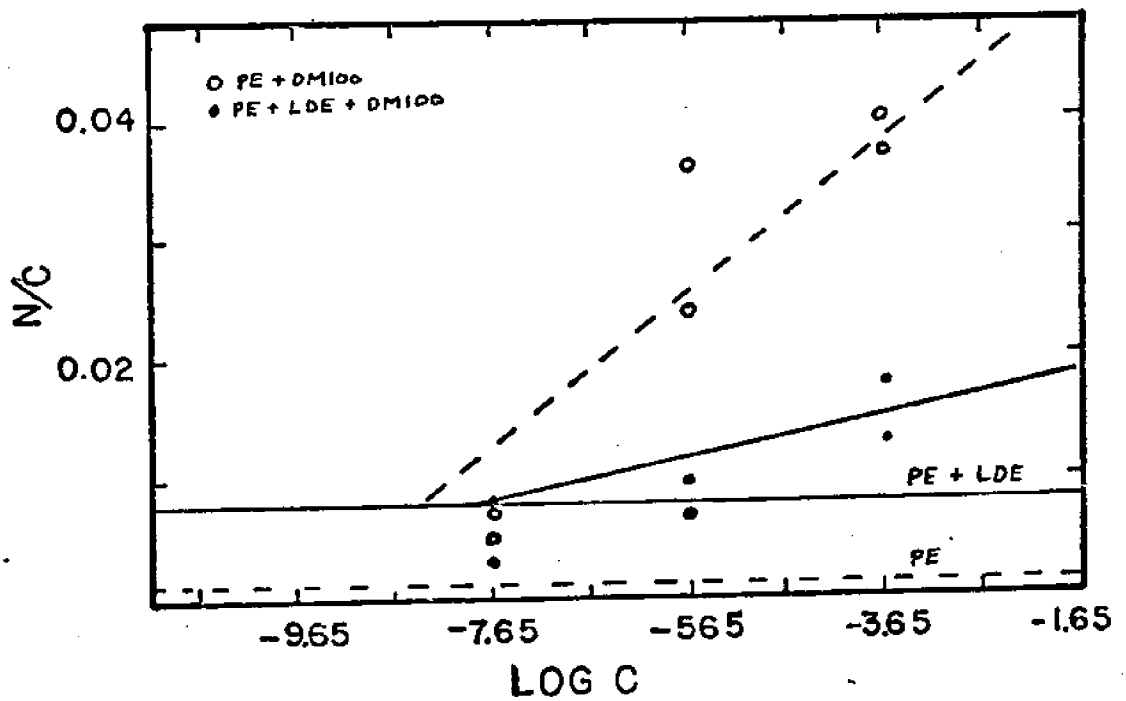

Figure 47. d) N/C Ratios vs Log Posttreat Concentration for 24-hr Posttreats in DM100 of PE and PE + LDE.

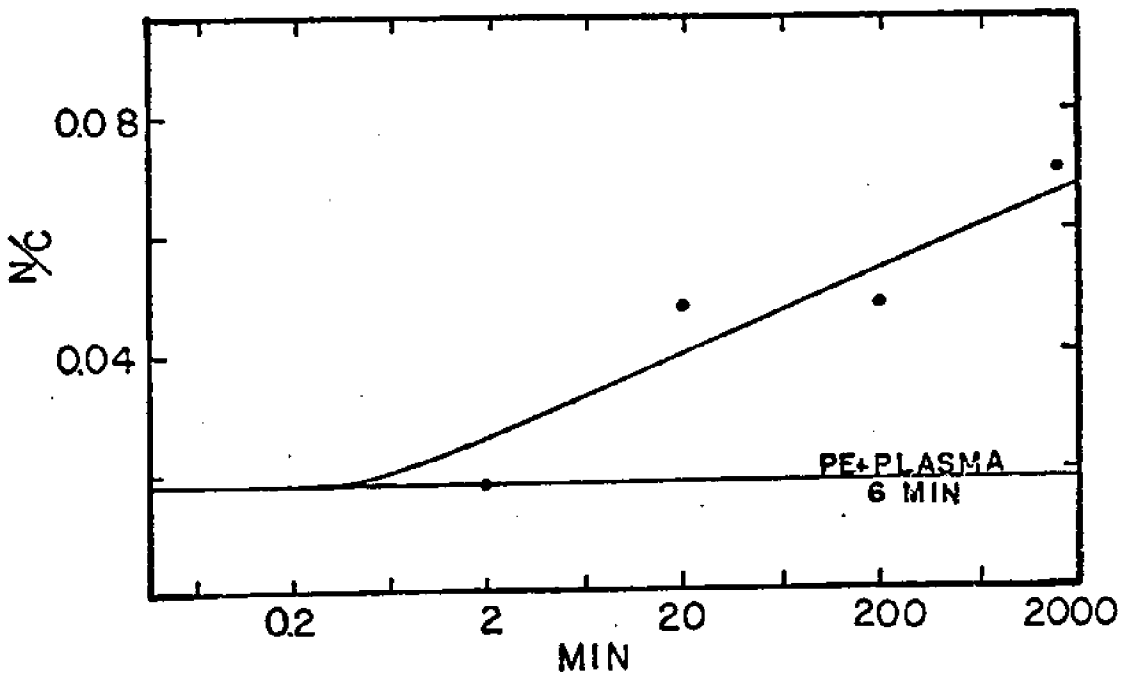

Figure 48. a) ESCA N/C Ratio vs Log Posttreat Time in 4.4×10^{-5} M DM100 for PE Pretreated 6-min in 2 cm^3/min Air Plasma.

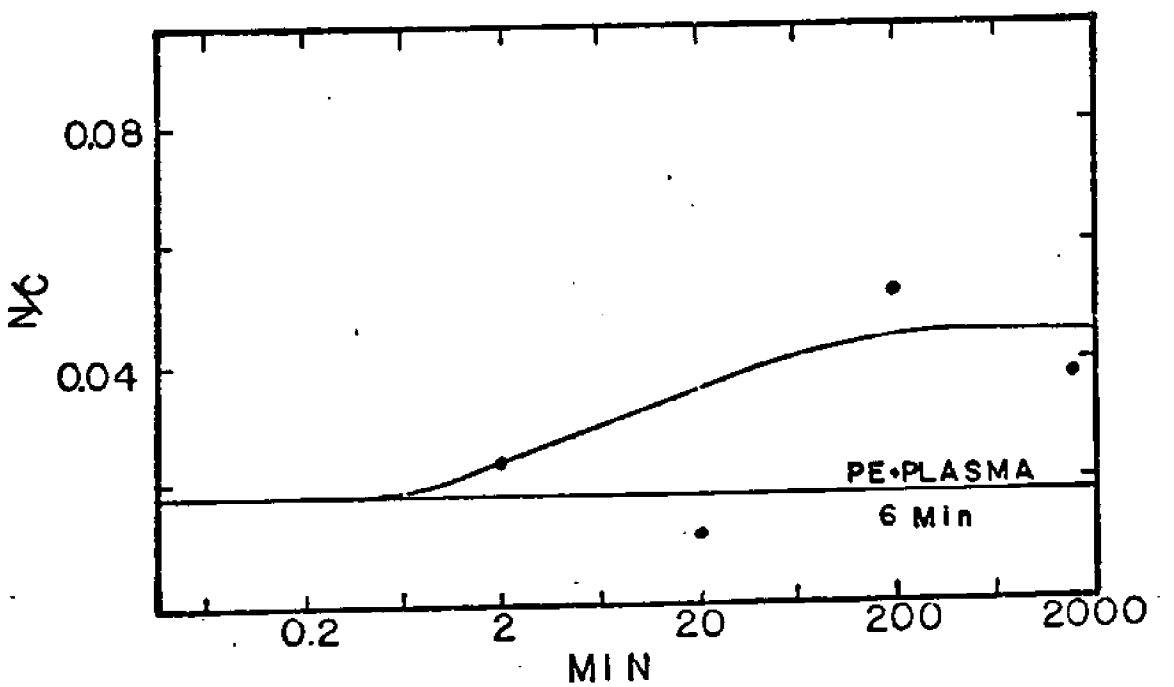

Figure 48. b) N/C Ratio vs Log Posttreat Time for Plasma-Pretreated PE in 4.44×10^{-3} M DM100.

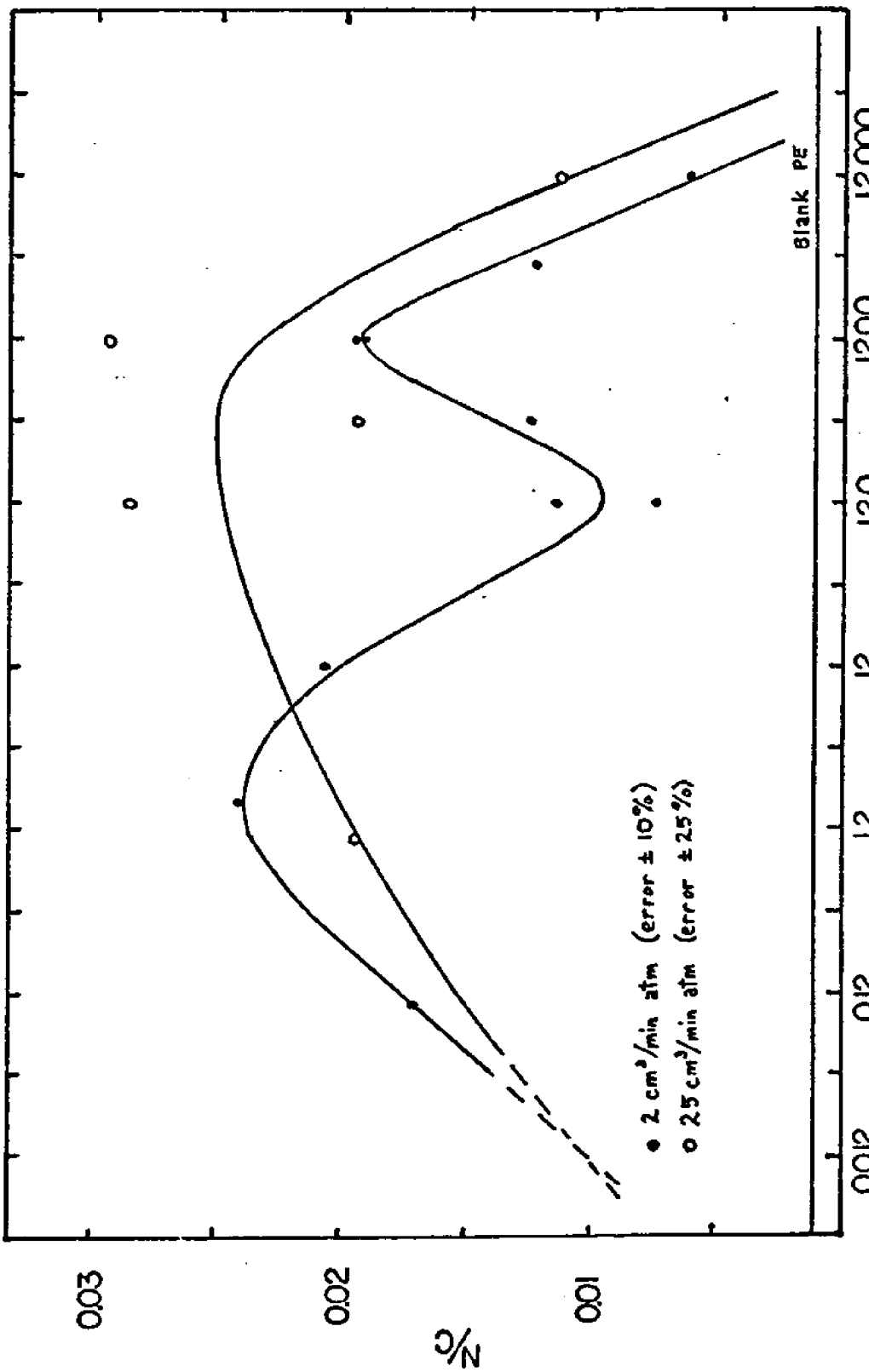

Figure 49. ESCA N/C Ratio vs Log Time of Exposure to Air Plasmas (133 Pa, 50W) at Various Flowrates for Blank PE.

N/O ratios climbed early to peaks somewhere in the 1 sec to 12 sec range, then smoothly decreased through 200 min.

Finally, O/C ratios were monitored for all DM100-posttreated samples, all AA posttreats and the plasma-only series. For AA post-treated samples (Figures 51a, 51b,51c), the expected rise was observed, with no levelling off seen for plasma + AA. For LDE + AA strips, equilibrium seemed to occur roughly between 20 and 200 min, although this interpretation is open to question, again owing to paucity of data. For PE + LDE + DM100, the ratio seemed to drop very slightly; this behavior was noted for PE + DM100. Concentration effects were minimal. For PE + plasma +DM100, an initial rise occurring at or before 2 min was followed by a steady drop through 24 hr; the meaning of this is unclear. It was found that O/C was best used to monitor the AA-posttreated samples, and the plasma series. For low air flowrates (2cc/min atm), the striking bimodal N/C behavior was seen again (Figure 52), as a confirmation of ATR IR carbonyl-peak observations. From 0.1 sec through 2 min, a roughly linear relationship exists (on semilog scales); another roughly linear region of sharper slope extends from 20 to 200 min (both slopes negative). The 2 min to 20 min region, near the later N/C maximum, shows a sharp discontinuity. More data are needed to clarify the nature of this discontinuity. At the high (20 cm^3/min atm) rate of flow, the O/C ratio increases roughly linearly with time over the entire 1 sec to 200 min regime. Clearly, another process dominates at this higher flow regime.

High resolution ESCA studies: These were done for selected surface types; the C, N and O peak energy assignments were made to ± 0.15 eV, and appear in Table 22, along with probable chemical assignments inferred from the literature (as compiled in Wagner, Riggs et. al., 1979). The PE Cls peak at 284.6 eVwas used as an internal standard to correct for sample-charging effects.

Only the slightest hints of shoulders were seen. The C and O peaks were quite smooth and symmetric. N was too faint to attempt deconvolution; only its maximum

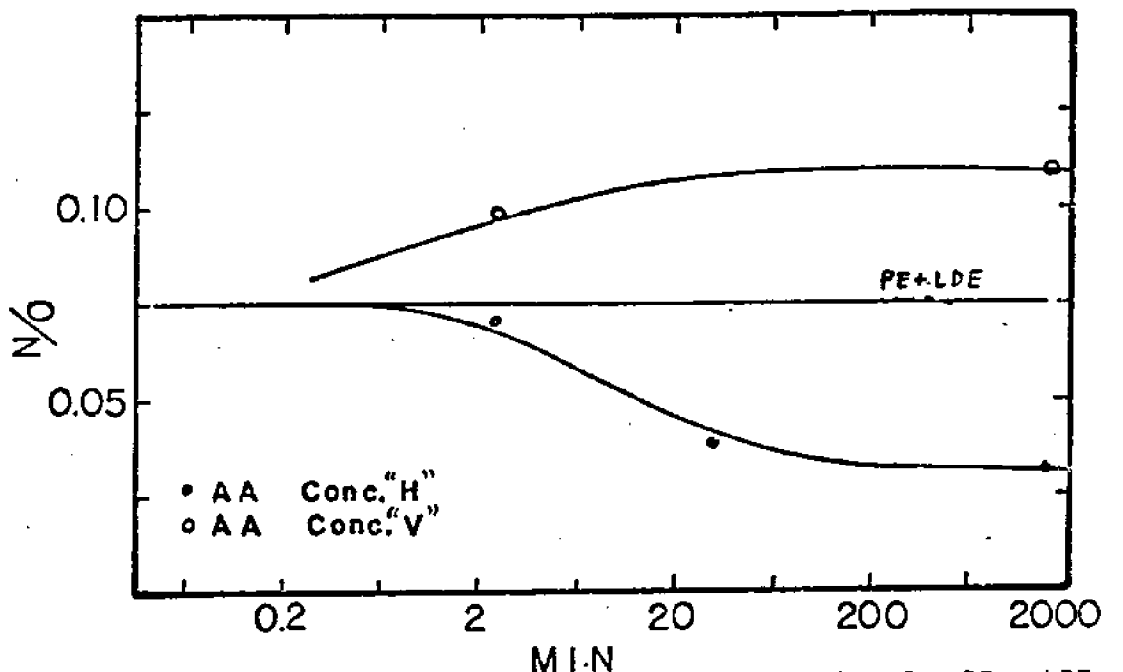

Figure 50. a) ESCA N/O Ratios vs Log Posttreat Time for PE + LDE in AA ("H" = 6.67 X 10^{-5} M; "V" = 6.67 X 10^{-3} M). Curves speculative.

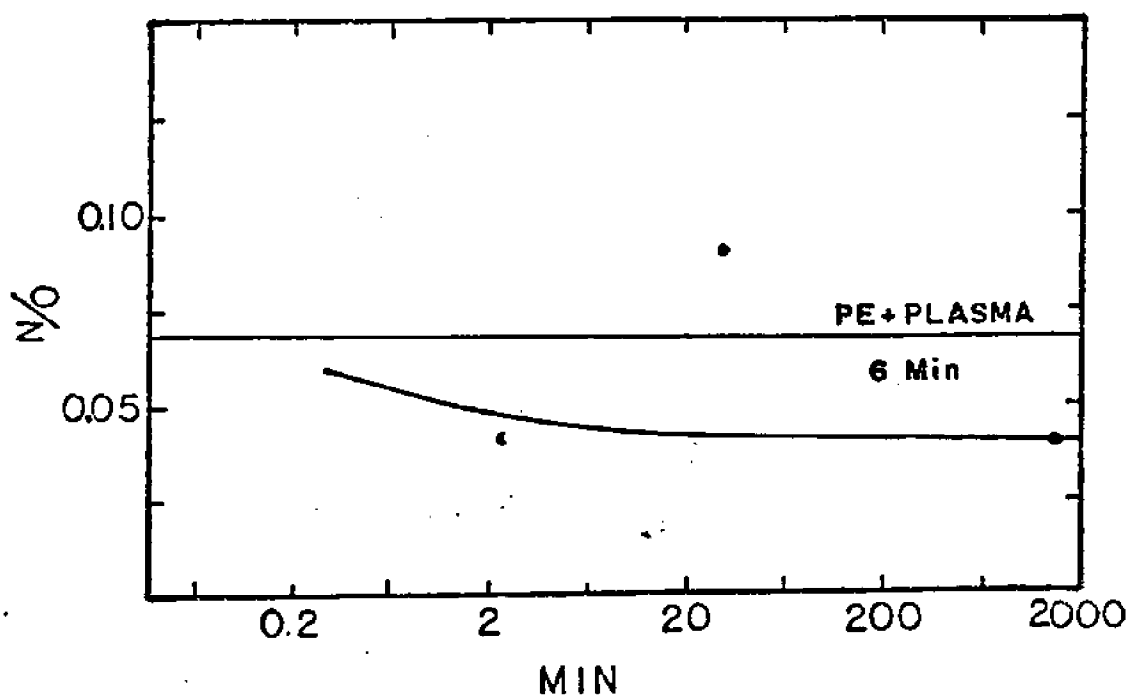

Figure 50. b) N/O Ratios vs Log Posttreat Time for PE + 6-min Plasma Exposure in 6.67 X 10^{-5} M AA. Curve speculative.

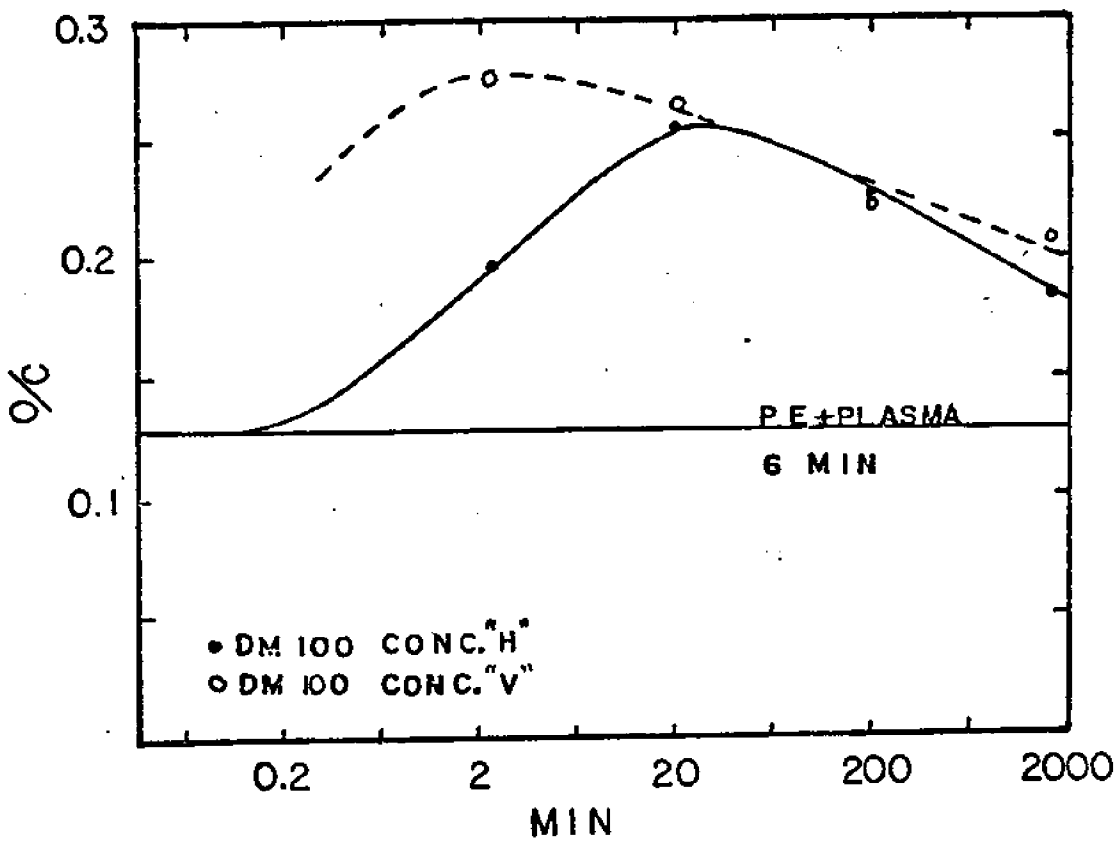

Figure 51. a) ESCA O/C Ratio vs Log Posttreat Time for PE + 6-min Plasma Exposure in DM100 ("H" = 4.44 X 10^{-5}M; "V" = 4.44 X 10^{-3}M).

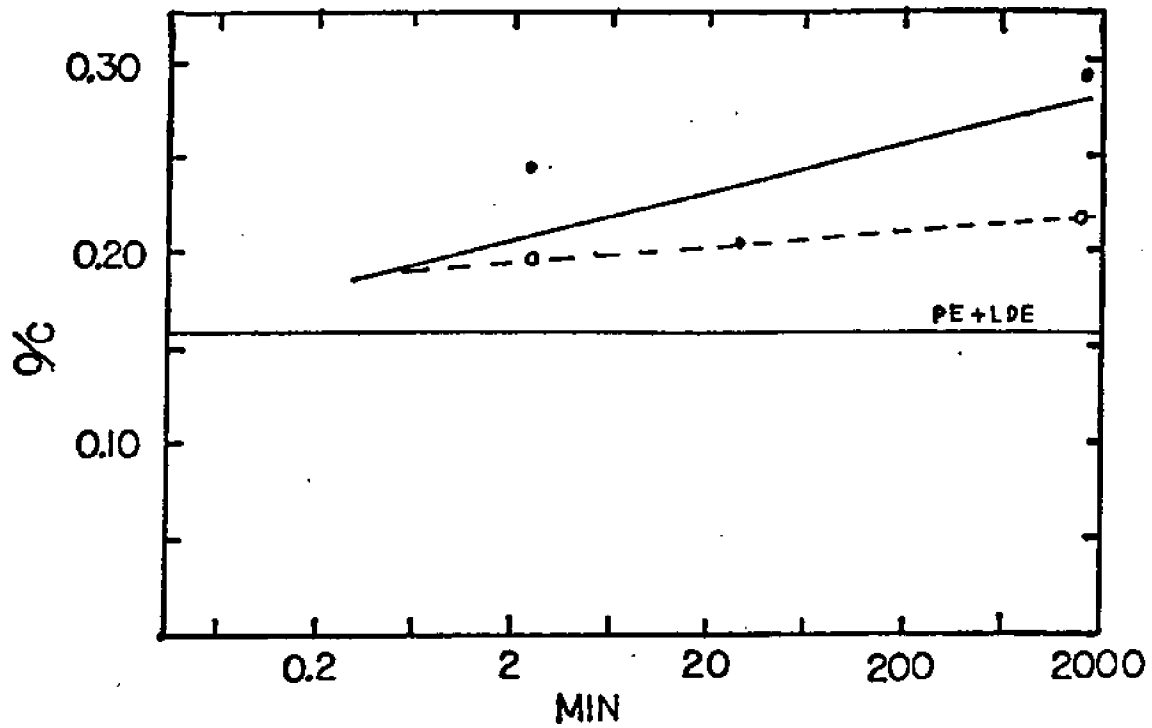

Figure 51 b) ESCA O/C Ratio vs Log Posttreat Time for PE + LDE in AA ("H" = 6.67 X 10^{-5}M; "V" = 6.67 X 10^{-3}M).

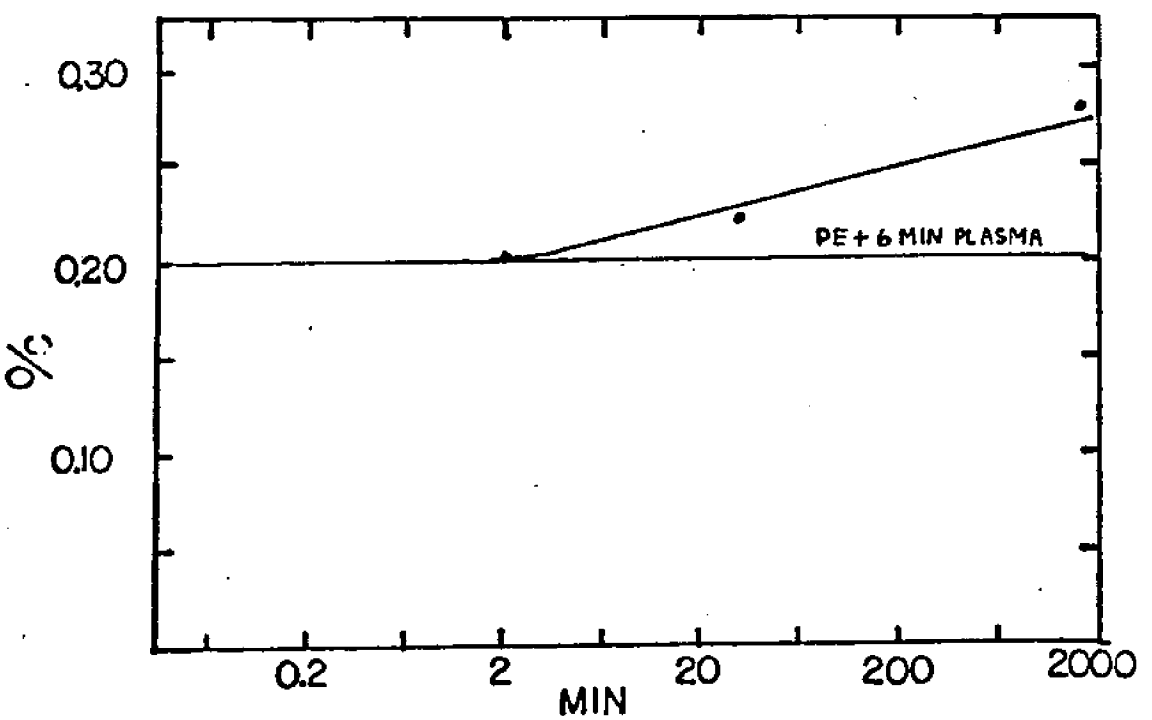

Figure 51 c) O/C Ratios vs Log Posttreat Time for PE + 6-min Plasma Exposure in 6.67 X 10^{-5}M AA.

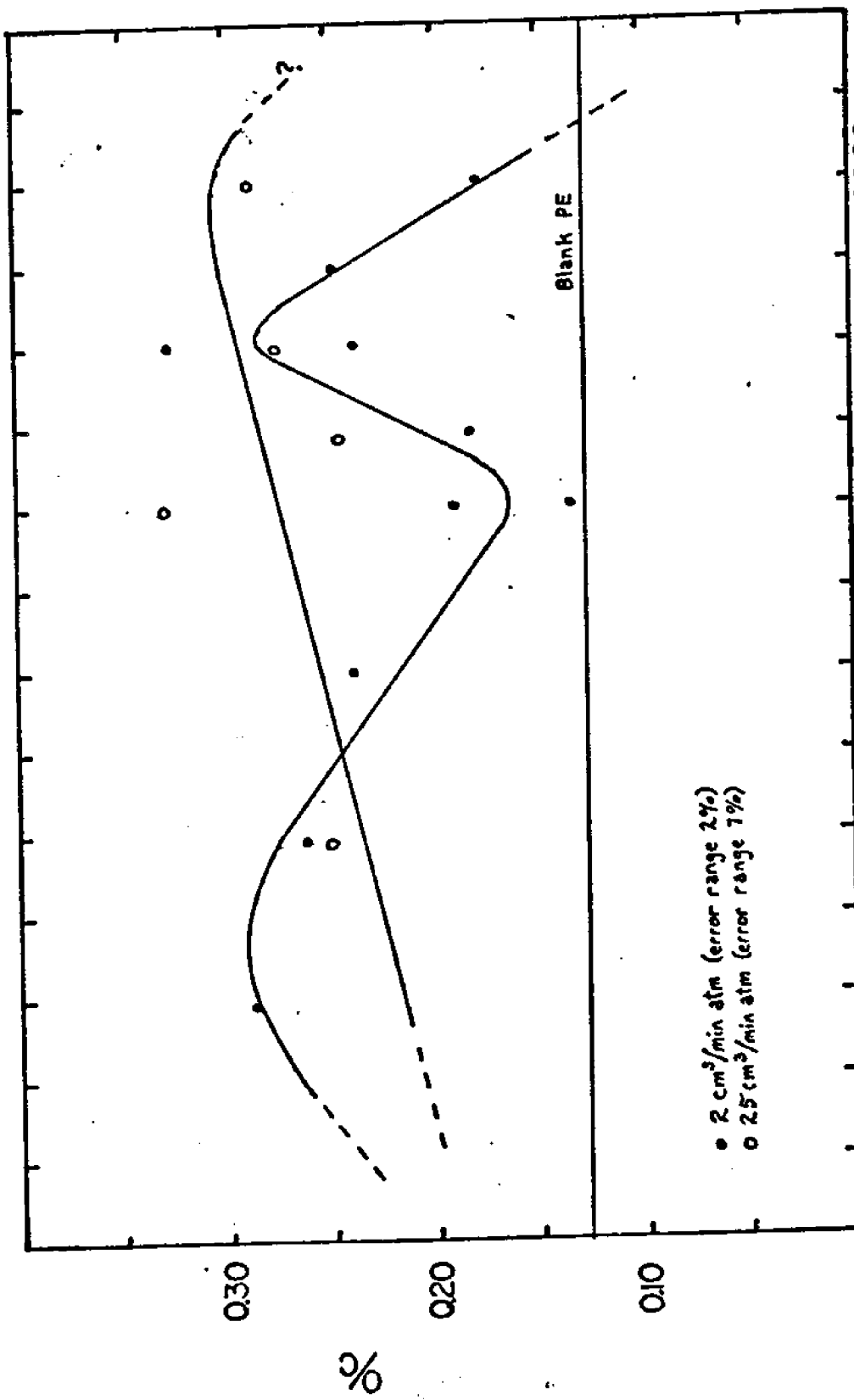

Figure 52. ESCA O/C Ratios vs Log Exposure Time in Air Plasma (133 Pa, 50W) at Various Flow-rates for Blank PE. (For Posttreats, 6-min Specimens were chosen from ATR Data before ESCA Studies could be done).

was given an assignment. For oxygen, PE and PE + LDE had identical values, indicating that the PE oxygen is mostly OH. The PE + plasma samples tested also had similar oxygen energies, again suggesting hydroxyl. For DM100 posttreats, the oxygen peaks were near to that for PE and for PE + LDE. PE + DM100 was at the same value, while PE + LDE + DM100 was slightly shifted down. This suggests that OH and CO show similar shifts in the forms studied (OH, urea, biuret, urethane, amide), and that the oxygen peak is not useful for distinguishing among them.

Nitrogen was more revealing. The DM100 posttreats showed an N1s peak energy value near that inferred from the literature for ureas and biurets (from phenyl-substituted thiourea). PE showed a peak energy near the literature value for guanidine, indicating imine or amine; either as contaminant or as a result of reaction with the atmosphere. Best of all, PE-LDE was different from both of the above, thus indicating once again that the DM100 posttreat has chemically changed the surface character of the PE. And in the plasma-treated samples, N shifts from a value near blank PE at 2 min to a value about 1 eV higher, which cannot be assigned from the literature. Possibly it is due to more π-bonding character. More π character would stabilize a positive charge and thus boost peak-energy levels.

In all cases, carbon lacked any neighbor peaks to the PE peak at 284.6 eV; these were expected for DM100 posttreats but possibly were swamped out by the much greater methylene carbon signal.

Contact angle study: For selected representative samples, contact angles were determined, using distilled water at several drop sizes. Data scatter was high, due in part to serious drop-surface distortion caused by the various scratches, pits and milling grooves found on all sample surfaces. Table 23 summarizes contact angle data. Three readings were taken for each surface, denoted "shiny" and "dull" from reflection specularity, of the selected strips. Included in the survey were PE, PE + LDE, PE + DM100 (2 min and 24 hr posttreat), PE + LDE + DM100 (2 min and 24 hr posttreat), the PE + 2 cc/min plasma from 2 min to 200 min, and a series

of PE + LDE + DM100 and PE + DM100 strips posttreated for a range of periods. Data were not obtained for AA posttreats owing to time pressure, but are expected to be similar to DM100 posttreats since both contain medium-length aliphatic chains linked by carbonyl-rich junctions.

Contact-angle values were similar for blank Garry resin and for PE + LDE; strangely, LDE showed higher (more hydrophobic) angles. This is not consistent with the observation of increased wettability of PE+LDE powder in water. DM100 posttreats were noticeably below PE or PE+LDE. Posttreats at the "L" (4.44×10^{-7} M) concentration had the lowest angles, and samples posttreated 24 hr generally had lower angles than 2 min samples. In all samples, the "shiny" surface, which had greater milling-groove density, usually had higher angles, but there were many exceptions to this. For the two DM100 posttreat series monitored for time behavior, a modest drop in contact angle was seen in the first 6 - 20 min; beyond that the angles seem to level off. This echos faintly the behavior seen in ESCA, and the magnitude of the effect, $\sim 5°$, is just larger than the scatter. The most dramatic data were, as has been the case with ESCA and AIR IR, the plasma-treated series. The angles are already down 20° in 2 min, and from there they continue to drop to a minimum near 6 min to 20 min which is fully 30° below PE at 80°-90°. The angles level off at this value through 200 min. These low angles reflect the high oxidation levels seen by ESCA; once again, no fine structure is discernible. It was concluded after this study that contact angle determination was useful only as a quick screening tool for samples with surfaces as rough as the ones tested.

Table 22. High-Resolution ESCA Photoelectron Peak Energy Assignments (and Probable Chemical Identification) of Cl_s, $O1_s$ and $N1_2$ in Various Modified PE Surfaces

Sample	Element	Corrected Peak Energy	Probable Chemical Type
Blank PE	C	284.6 + 0.15 eV	aliphatic chain
	O	532.0 " "	OH, some CO
	N	400.4 + 0.3 "	NH_2, NH?
PE + LDE	C	284.6 + 0.15 eV	aliphatic chain
	O	532.0 " "	OH, some CO
	N	3.99.9 " "	amide
PE + LDE + DM100 (24 hr at "V" concn.)	C	284.6 ± 0.15 eV	aliphatic chain
	O	531.7 " "	biuret; urethane CO?
	N	399.5 " "	biuret; urethane?
PE + DM100 (24 hr at "V" conc.)	C	284.6 ± 0.15 eV	aliphatic chain
	O	532.1 " "	biuret; urea CO?
	N	3.99.5 " "	biuret; urea
PE + Plasma (2 min. at 2 cm^3/min atm)	C	284.6 ± 0.15 eV	aliphatic chain
	O	532.2 " "	OH, CO: COOH?
	N	400.7 " "	NH_2,NH?
PE + Plasma (60 min. at 2 cm^3/min atm)	C	284.6 ± 0.15 eV	aliphatic chain
	O	531.9 " "	OH,CO;COOH?
	N	401.6 ± 0.3 "	NH_2,NH?(-C=N-C-)?

Chemical assignments made by using model-compound data in Wagner et.al. (1979).
"V" = 4.44 x 10^{-3}M DM100.

Table 23. Data from Contact-Angle Determinations on Selected Surface Types. (Each Datum an Average of 3 Raw Readings).

Sample	"Shiny" surface	"Dull" surface
PE blank	90°	81°
PE+LDE	91°	87°
PE+LDE+DM100 ("V"; 24 hr)	86°	84°
" ("H"; 24 hr)	84°	94°
" ("L"; 24 hr)	85°	72°
" ("H"; 2 min)	85°	82°
" ("L"; 2 min)	83°	86°
PE+DM100 ("V"; 24 hr)	85°	87°
" ("H"; 24 hr)	81°	85°
" ("L"; 24 hr)	86°	83°
" ("H"; 2 min)	84°	79°
" ("L"; 2 min)	88°	82°
PE+LDE+DM100 ("V"; 60min)	80°	87°
" ("V"; 20 min)	85°	88°
" ("V"; 6 min)	77°	82°
" ("V"; 2 min)	86°	90°
PE+DM100 ("V"; 60 min)	86°	89°
" ("V"; 20 min)	91°	89°
" ("V"; 6 min)	82°	90°
" ("V"; 2 min)	92°	90°
PE+plasma (2 min, 2 cm^3/min)	70°	59°
" (6 min, ")	63°	63°
" (20 min, ")	66°	51°
" (60 min, ")	58°	58°
" (200 min, ")	60°	63°

Error Range $\pm$5° in absence of scratches
$\pm$15° in presence of scratches

Flexure performance of surface-modified PE samples. One criterion of the practical worth of the various surface modification methods is the actual extent of retardation of degradation achieved. In this respect there was considerable variation, but all methods tested showed at least modest success.

PE + LDE: Both the plasma- exposure and the LDE initial treatments showed retardation; LDE seemed more effective.At 70 rpm (Fig 53a, Table 24) blank PE suffered a crystallinity drop from about 51.5% down to 45% after 6.0 log cycles flex. Extrapolation of the PE - LDE data obtained under identical flexure conditions shows that 45% crystallinity is not reached until 8.4 log cycles flex. Assuming a reasonable model of 1 rpm flex in real-life marine installations, this means that the blank polymer required about 1.65 years to degrade to 45% crystallinity from 51.5%, The PE - LDE samples, meanwhile, would not reach this level until after several centuries! A more realistic measure is perhaps the log cycles flex required to drop noticeably, e.g. 1%, below unflexed specifications, or from 51.5% down to 50.5% . For blank PE, about 4.7 log cycles were required; for PE - LDE, it took about 5.4 log cycles. In "real" terms, the derived lifetimes are 30 days and 150 days. Thus, LDE extends the lifetime of blank PE by a full factor of 5.0 by this measure.

At 400 rpm (Figure 53b), similar dramatic improvement over blank PE is seen for PE + LDE strip. The crystallinity-loss slopes are shallower for both PE and LDE for two reasons. First, the 400 rpm apparatus operated at a lower flex amplitude (0.6mm vs. 1.0mm for the 70 rpm rig), and second, the onset of degradation occurs earlier at 400 rpm and thus an inherently gentler slope is seen between 3.5 and 5.5 log cycles. Beyond 5.5 log cycles flex, this effect is negligible. For blank PE after 6,3 log cycles flex, the crystallinity was down from 51% to 47,5%; for PE + LDE it was still near 49,5%. To reach 50% crystallinity required 4.3 log cycles for PE and about 5.2 to 5,3 log cycles for PE + LDE. This means that the "lifetime" has been enhanced by a factor of 8 to 10 (in terms of the 1

Table 24. X-Ray Data for PE Refluxed 75 hr at 90°C in 8.33 X 10^{-5}M LDE and Flexed for Various Log Cycles at 70 rpm and 400 rpm. (Sample Nomenclature From Appendix VII.) Some Samples Reacted 24 hr in Dilute DM100 Solution

No.	Log Cycles	rpm	X_c(100)	Treat
F-1	Standard #1	-	51.3	None
2	4.11	70	51.3	LDE
3	4.60	"	51.5	"
4	5.02	"	51.0	"
5	5.32	"	51.1	"
6	5.48	"	50.2	"
7	5.78	"	49.5	"
8	6.23	"	49.1	"
9	0	"	52.8	"
G-1	Standard #1	-	51.0	None
2	Standard #2	-	51.0	"
3	6.28	400	47.7	"
4	"	"	48.1	"
5	"	"	49.4	"
6	"	"	50.2	"
7	"	"	49.5	"
8	"	"	49.5	LDE+"L"
9	"	"	50.6	LDE+"H"
10	"	"	49.8	LDE+"V"

"L" = 4.44 X 10^{-7}M; "H" = 4.44 X 10^{-5}M; "V" = 4.44 X 10^{-3}M DM100

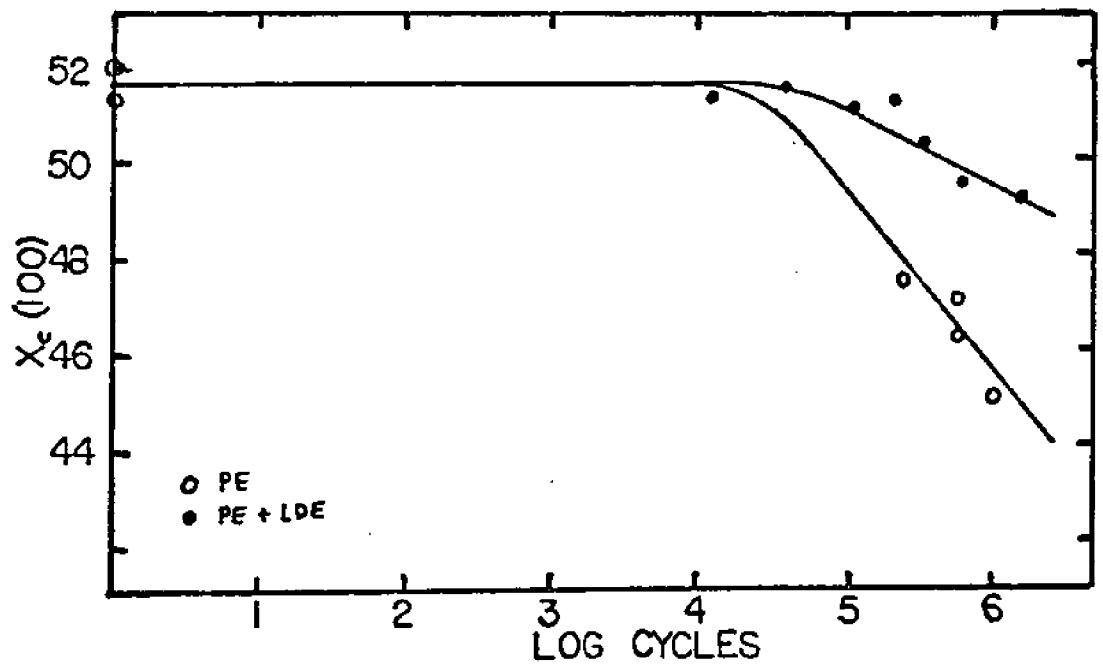

Figure 53. a) Crystallinity vs Log Cycles Flex for PE and PE + LDE at 70 rpm. (75 hr at 8.33 X 10^{-5}M LDE).

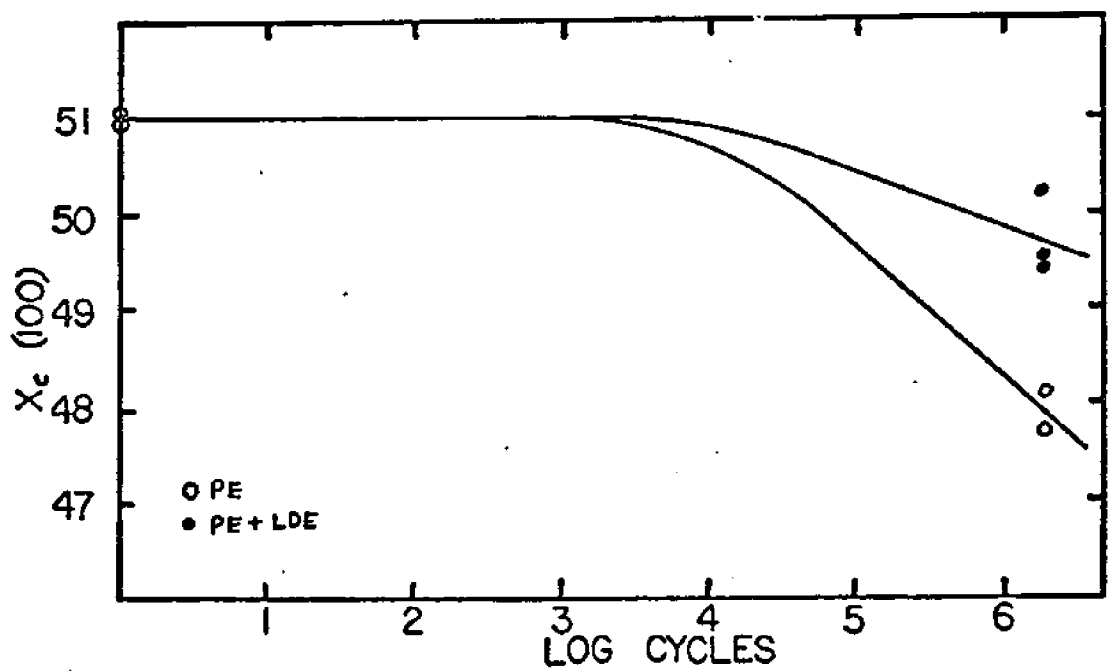

Figure 53. b) Crystallinity vs Log Cycles Flex for PE and PE + LDE at 400 rpm.

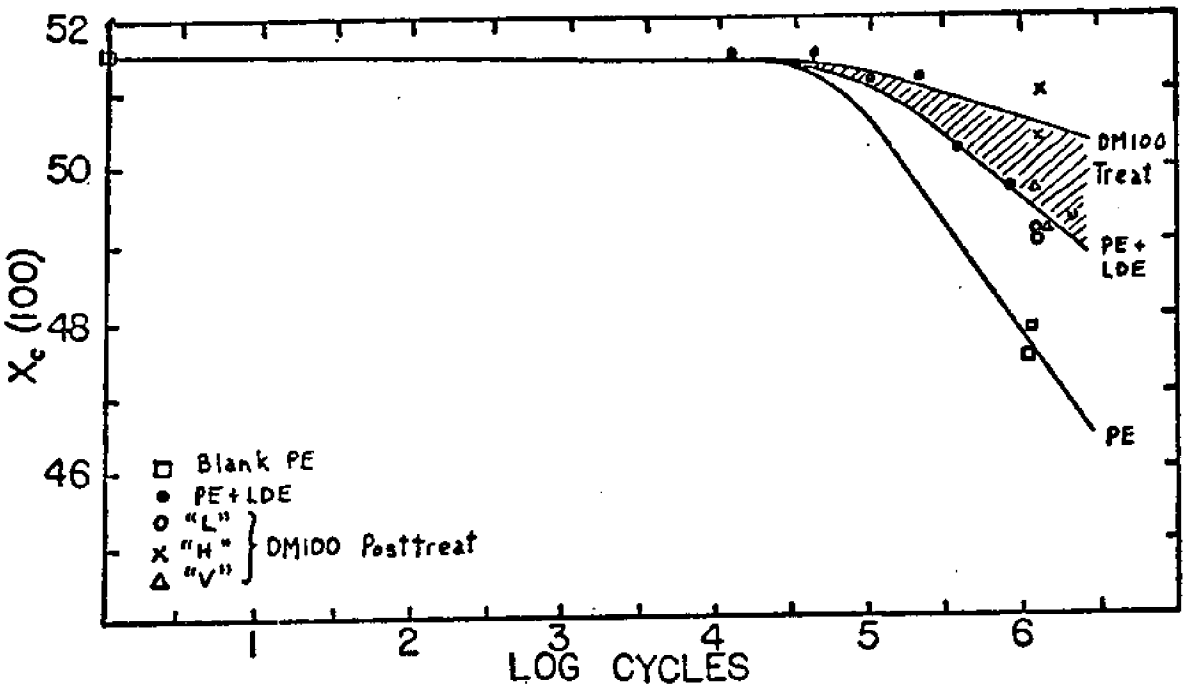

Figure 54. a) Crystallinity vs Log Cycles Flex for PE + LDE and PE + LDE + DM100 at 70 cycles.

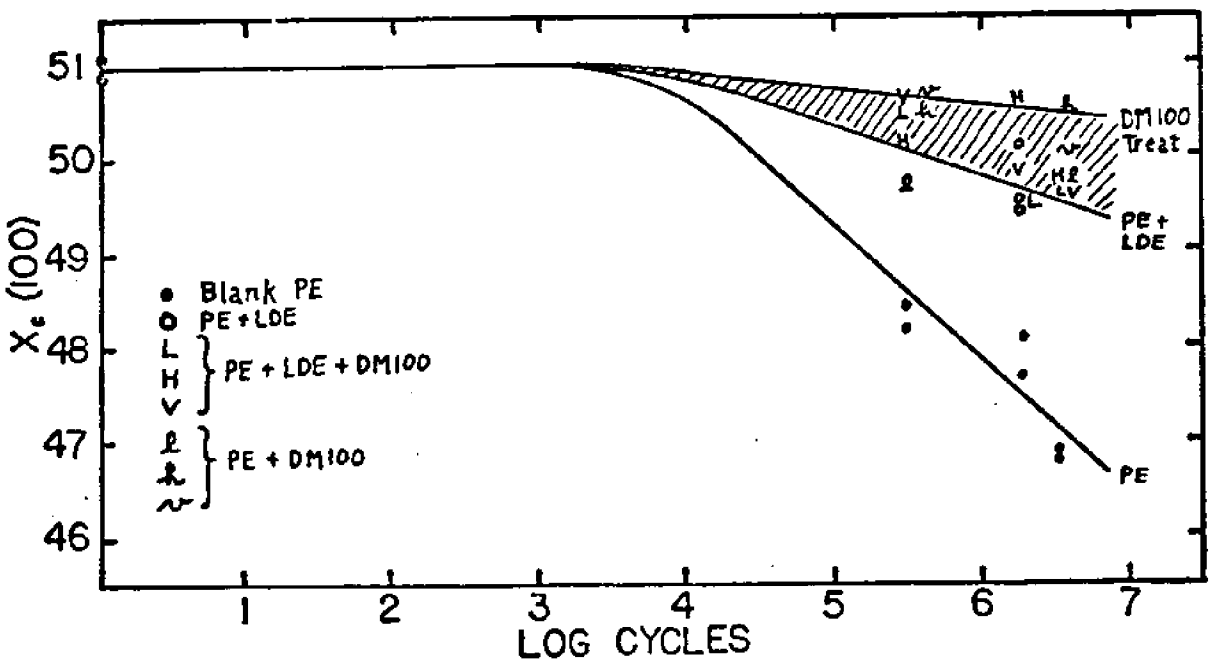

Figure 54. b) Crystallinity vs Log Cycles Flex for PE + LDE, PE + DM100 and PE + LDE + DM100 at 400 rpm. "L" and "ℓ" = 4.44 X 10^{-7}M; "H" and "h" = 4.44 X 10^{-5}M; "V" and "∿" = 4.44 X 10^{-3}M.

Table 25. X-Ray Data for PE+LDE+DM100 Strip and PE+DM100 Strip, Posttreated and Flexed as Noted. Sample Nomenclature From Appendix VII.

No.	Pretreat	Posttreat Time	Posttreat Conc.	Flex rpm	Flex Log Cycles	X_c(100)
H-1		Standard #1		-	0	51.1
2		Standard #2		-	0	52.0
3	LDE	100 min	"L"	70	6.05	48.6
4	"	"	"L"	"	"	48.8
5	"	"	"H"	"	"	50.0
6	"	"	"H"	"	"	50.8
7	"	"	"V"	"	"	49.5
8	"	"	"V"	"	"	48.8
9	"	"	neat	"	"	49.1
10	"	"	neat	"	"	47.7
I-1		Standard #1		-	0	50.9
2		Standard #2		-	0	50.7
3		Standard #3		-	0	51.2
4		Blank #1		400	5.49	48.2
5		Blank #2		"	"	48.4
6	LDE	24 hr	"L"	"	"	50.4
7	none	"	"L"	"	"	49.7
8	LDE	"	"H"	"	"	50.2
9	none	"	"H"	"	"	50.5
10	LDE	"	"V"	"	"	50.6
11	none	"	"V"	"	"	50.6
12		Blank #3		"	6.48	46.8
13		Blank #4		"	"	46.7
14	LDE	24 hr	"L"	"	"	49.6
15	none	"	"L"	"	"	49.7
16	LDE	"	"H"	"	"	49.7
17	none	"	"H"	"	"	50.5
18	LDE	"	"V"	"	"	49.6
19	none	"	"V"	"	"	50.0

"L" = 4.44×10^{-7}M; "H" = 4.44×10^{-5}M; "V" = 4.44×10^{-3}M

rpm model, from about 12 days to about 95 to 120 days).

The difference in extrapolated "real-life" time frames is interesting to note; it is perhaps a measure of the nonlinearity of the accelerated-test approach. The lower figures for "lifetimes" derived from 400 rpm data indicate that the 400 rpm flex cycle regimen is more damaging to the sample than is a slower cycling rate, e.g. 70 rpm. This effect was noted also in PMMA in going from 30 to 60 rpm. It is possible that 1 rpm is less damaging still, for the same number of flex cycles, than either 70 or 400 rpm.

DM100 Posttreat: Posttreatment with DM100 was found to enhance retardation of degradation even above PE + LDE alone. This added enhancement was noted both at 70 rpm and 400 rpm (Figures 54a and 54b, respectively; data in Table 25). Posttreats prepared from "L", "V", and "H" concentrations of DM100 were all tested. It seemed that "L" (4.44×10^{-7} M) did little to improve performance over PE + LDE baseline at either cycle frequency. "V" (4.44×10^{-3} M) showed marginal improvement after 6.0 to 6.5 log cycles (perhaps of order 0.5% crystallinity, not much above the scatter) at each cycle frequency. The "H" concentration (4.44×10^{-5} M) posttreat did best; it retarded crystallinity loss by about 1.0 to 1.5% at 70 rpm and by perhaps 0.5% at 400 rpm (the lower flex amplitude and more demanding cycling regimen). For the sake of comparison, PE + DM100 strips were also prepared at the "L", "H", and "V" DM100 concentrations, and flexed for 6.5 log cycles at 400 rpm. Surprisingly, they did as well as the PE + LDE + DM100 strips, being comparable to the "H" and "V" PE + LDE + DM100 strips at 6.5 log cycles. The "L" PE + DM100 strip was comparable to PE + LDE. Taking an average over all DM100-treated strips, an enhancement of about 0.5% over PE + LDE loss retardation is seen after 6.5 log cycles at 400 rpm. In other words, to reach 50% crystallinity required about 6.4 log cycles, vs. 5.3 log cycles for PE + LDE. Thus the "lifetime" of DM100 treated PE is perhaps 12 times greater than at 400 rpm. For a typical 1 rpm situation, this is equivalent to ~120 days for PE + LDE vs. 1400 days (4 yr) for PE + LDE + DM100 and PE + DM100. PE lasts only 12 days under these conditions. This dramatic

Table 26. X-Ray Data for PE + plasma (air, 133 Pa, 2.0 cm^3/min atm) and PE + plasma + DM100 (posttreat for 24 hr). Samples Flexed at 400 rpm. Nomenclature from Appendix VII.

No.	Pretreat Time	Posttreat Conc.	$X_c(100)$	Log Cycles
J-1		Standard #1	50.9	-
2		Standard #2	51.1	-
3		Blank #1	49.3	5.41
4		Blank #2	48.1	"
5	2 min	-	49.4	"
6	6 "	-	49.4	"
7	20 "	-	49.9	"
8	20 "	-	48.6	"
9	60 "	-	51.0	"
10	200 "	-	49.7	"
11		Blank #3	47.2	6.15
12		Blank #4	47.7	"
13	2 min	-	48.4	"
14	6 "	-	49.0	"
15	6 "	-	49.0	"
16	20 "	-	48.8	"
17	60 "	-	49.0	"
18	200 "	-	49.0	"
K-1		Standard #1	51.0	-
2		Standard #2	51.1	-
3		Blank #1	47.9	6.50
4		Blank #2	48.5	"
5	6 min	-	49.4	"
6	"	-	49.5	"
7	"	4.44×10^{-5}M	49.5	"
8	"	4.44×10^{-5}M	50.2	"
9	"	4.44×10^{-3}M	50.1	"
10	"	4.44×10^{-3}M	49.8	"

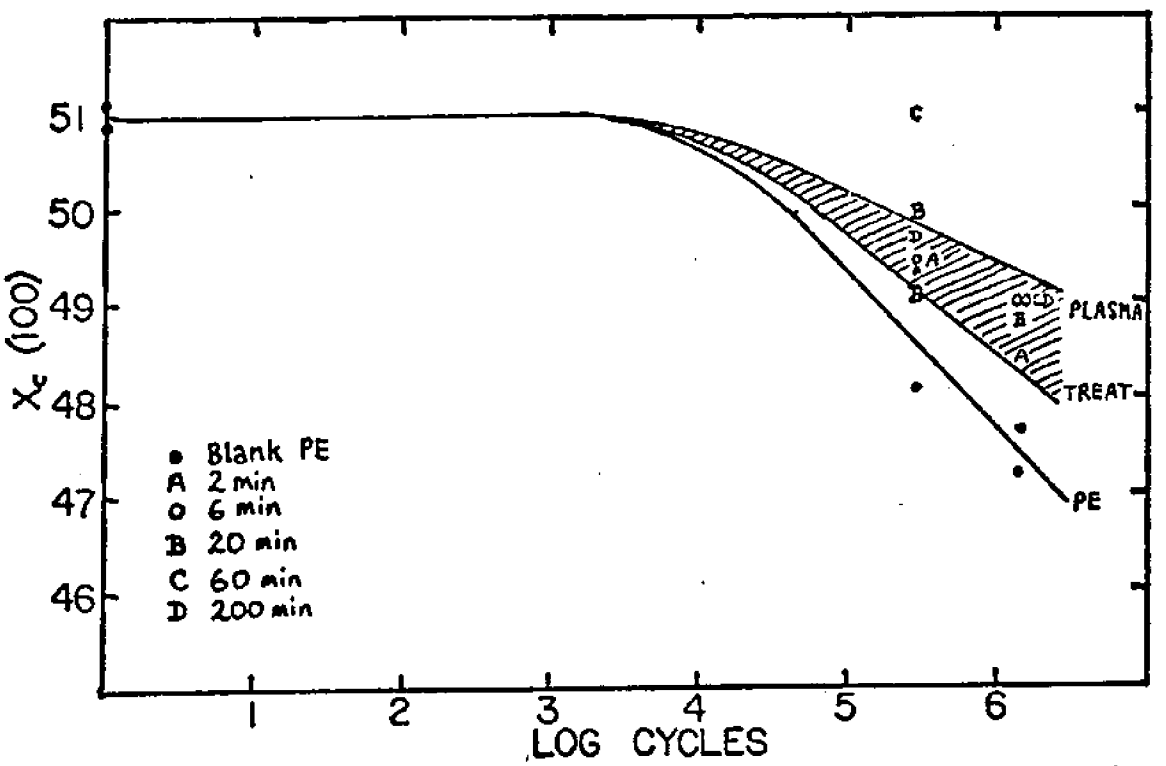

Figure 55. a) Crystallinity vs Log Cycles Flex for PE + Plasma (2 cm^3/min atm) for Various Exposure Times.

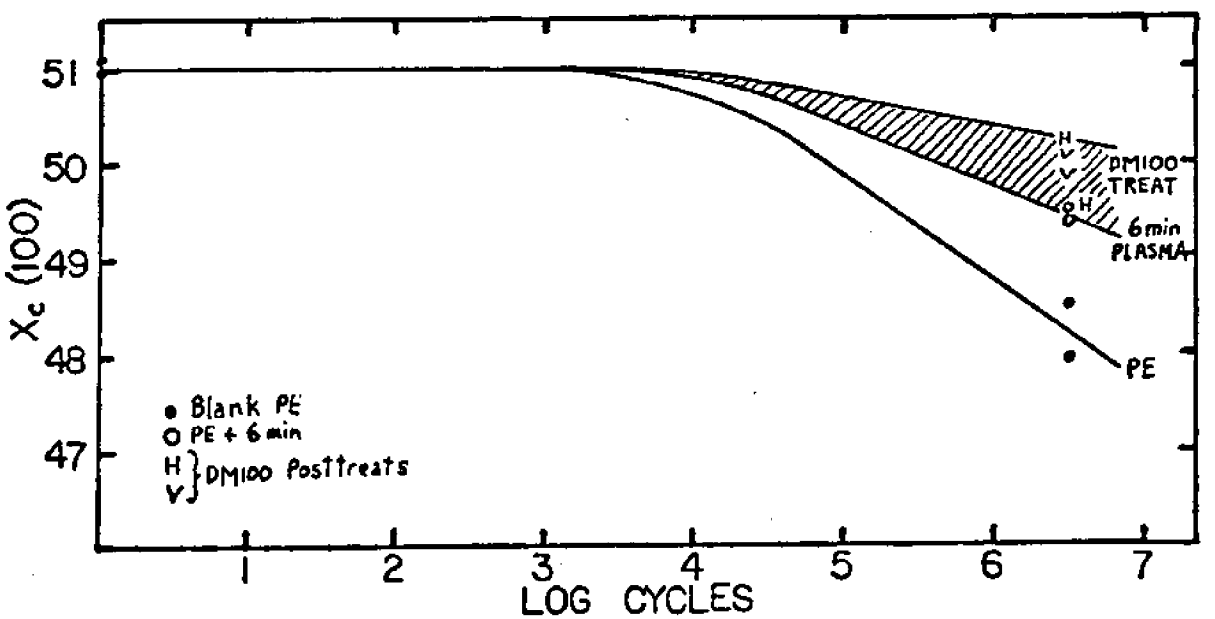

Figure 55. b) Crystallinity vs Log Cycles Flex for PE + Plasma (6-min exposure) + DM100 ("H" = 4.44 X 10-5M; "V" = 4.44 X 10^{-3}M).

enhancement recalls the Lagergren-Olsson-Swedenborg 1974 result in which thrombogenesis was reduced by a factor of about 50 to 100 through use of polymer + surfactant + bonded heparin shunts as compared to untreated shunts. Here, the lifetime-enhancement factor was perhaps 100 to 150.

Plasma Treatment: With plasma treatment at 1.0 torr (10^2 Pa) and 2.0 cm^3/min atm flowrate in air, less spectacular results were achieved than with PE + LDE (see Fig 55a and Table 26). Treatment time of 2, 6, 20, 60, and 200 min were all tested; 2 min seemed marginally less effective (0.3% crystallinity) at 6.2 log cycles than the other times, which were very nearly equal in performance. On average, to reach 50% crystallinity from an initial value of 51% required 5.1 log cycles vs. 4.6 for blank PE. A later run with lower flex amplitude due to shaft fatigue in the flexor showed 5.5 log cycles to 50% for 6-min plasma-treated strip vs. 4.85 log cycles for blank PE. In each case, the "lifetime" enhancement is by a factor of about 3 to 5, vs. 5 to 10 for PE + LDE. This result was not expected initially, but in retrospect is perhaps due to several mechanisms described later. Using the 1 rpm model, this means lifetime extension from 12 to 45 days in the initial run and from 50 to 200 days at the lower amplitude.

DM100 posttreats applied to 6-min plasma-exposed strip at the "H" and "V" concentrations ("V" = 4.44 x 10^{-3} M;"H"= 4.44 x 10^{-5} M) again caused enhancement over plasma-only strip. After 6.5 log cycles the posttreats were all about 0.5% higher in crystallinity than plasma-only controls (see Fig. 55b). To reach 50% crystallinity required 6.3 log cycles vs. 5.5 for plasma-only, for an enhancement factor near 6.0. This factor is noticeably less than the DM100 posttreatment enhancement factor over PE + LDE. The cumulative enhancement factor of PE + plasma + DM100 over blank PE is thus near 25; less than the factor for PE + LDE + DM100 but nevertheless quite promising. PE samples that last 50 days before degrading to 50% crystallinity at 1 rpm would still be intact after ~1200 days with the plasma + DM100 treatment, at a similar flex amplitude.

AA Posttreats: Adipic acid was also tested as a posttreat on both PE + LDE and PE + plasma strip. The philosophy behind the choice of AA was that it contains a medium-length aliphatic chain and at least two acid moieties (triacids were not easily available in the desired configuration); this would lend the resultant polyester coating a flexibility similar to LDE-DM100. Enhancement over blank PE was seen, but on a more modest scale than for DM100 posttreats. PE + LDE + AA dropped to 50% crystallinity from 51% after 5.6 log cycles flex vs. 5.15 log cycles for blank PE (the shaft was damaged even more on this run, and repairs were not feasible at the time; flex amplitudes were again lower than for most runs). This implies an enhancement factor of only about 3 for the LDE + AA treatment, less than the 5-10 for LDE only and far less than the 100 to 150 seen for LDE + DM100. However, it does show significant improvement over blank PE.

Plasma + AA treatment proved to be more effective; crystallinity was still just above 50% after 6.5 log cycles vs. 48.7% for blank PE (see Fig 56 and Table 27). To reach 50% probably required about 6.9 log cycles flex vs. 5.k5 log cycles for PE, for an enhancement factor of about 50 to 60. The figure is based on only two data points at the "H" concentration of AA (6.67×10^{-5} M), and could be as low as 15-20 or as high as 100 due to the ± 0.3% error in crystallinity measurement. In any event, however, plasma + AA seems to be more effective than LDE + AA treatment. Interestingly, the LDE + AA data were the same at both "H" and "V" concentrations for AA posttreat ("V" = 6.67×10^{-3} M of AA).

Irradiated Strip: Finally, strips exposed to 500 eV electrons both on the surface only and isotropically were flex-tested. Both dosages tested (2.9 MR and 11.5 MR) showed virtually no degradation at 70 rpm after 6.15 log cycles(see Fig 57a and Table 28). The consequent "lifetime-enhancement" factor is very high, probably at least 100 or more, for isotropically irradiated strip. While blank PE dropped to 50.5% from 51.5% crystallinity after about 5.1 log cycles, irradiated PE showed essentially zero drop after 6.15 log cycles, and it seems that such behavior could extend out as far as 7.5 or 8.0 log cycles. For surface-irradiated

Table 27. X-Ray Data for PE+LDE+AA (24 hr posttreat) and PE+plasma (6 min at 2 cm^3/min atm) + AA (24 hr posttreat) at Various AA Concentrations. Flexed 400 rpm.

No.	Pretreat	Posttreat Conc.	X_c(100)
1		Standard #1	50.8
2		Standard #2	50.7
3		Standard #3	51.5
4		Blank #1	48.8
5		Blank #2	48.8
6	LDE	6.67×10^{-5}M	49.3
7	LDE	6.67×10^{-5}M	49.7
8	LDE	6.67×10^{-3}M	49.3
9	LDE	6.67×10^{-3}M	50.1
10	plasma	6.67×10^{-5}M	50.2
11	plasma	6.67×10^{-5}M	50.3

Table 28. X-Ray Data for Blank PE Irradiated Isotropically or on the Surface (Half-Thickness 75μm) with 500 keV Electrons, Then Flexed at 70 rpm for Various Log Cycles.

No.	Irradiation Mode	Dosage	Log Cycles	$X_c(100)$
M-1	Standard #1		-	51.2
2	Isotropic	11.5 MR	0	51.0
3	"	"	4.16	50.6
4	"	"	5.36	49.8
5	"	"	5.70	51.0
6	"	"	6.00	49.9, 50.8
7	Unirradiated	0 MR	4.16	51.4
8	"	"	5.36	47.4
9	"	"	5.70	46.4, 47.0
10	"	"	6.00	45.0
11	Standard #1		-	52.0
12	Isotropic	2.9 MR	4.30	51.5
13	"	"	4.87	51.9
14	"	"	5.14	50.5
15	"	"	5.47	50.9
16	"	"	5.60	52.2
17	"	"	5.77	51.1
18	"	"	5.90	50.7
19	"	"	6.11	50.4
N-1	Standard #1		-	51.3
2	Standard #2		-	50.6
3	Surface Dose	0 MR	6.17	48.2
4	"	"	"	48.2
5	"	0.6 MR	"	48.2
6	"	"	"	50.2
7	"	"	"	49.0
8	"	2.0 MR	"	51.3
9	"	"	"	51.5
10	"	"	"	52.4

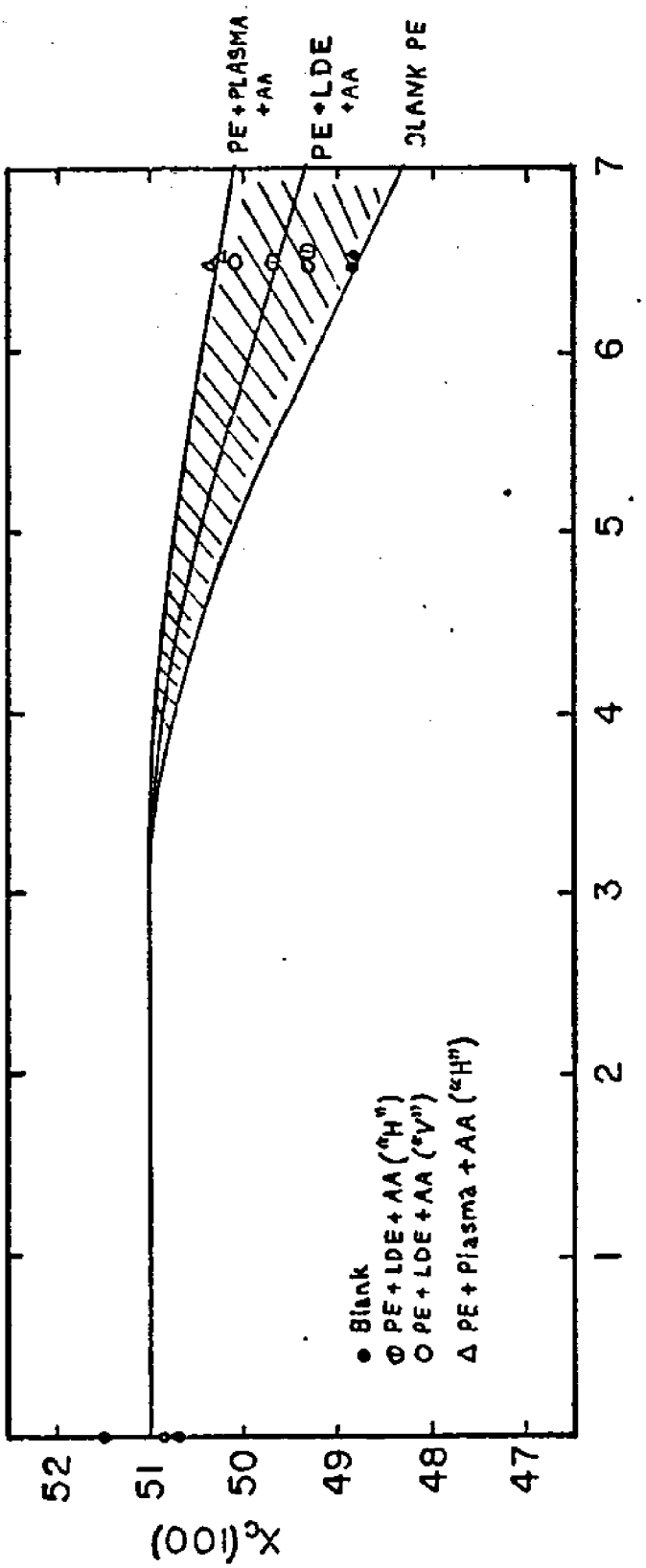

Figure 56 Crystallinity vs Log Cycles Flex at 400 rpm for PE + LDE + AA and PE + Plasma + AA. "H" = 6.67×10^{-5}M; "V" = 6.67×10^{-3}M AA.

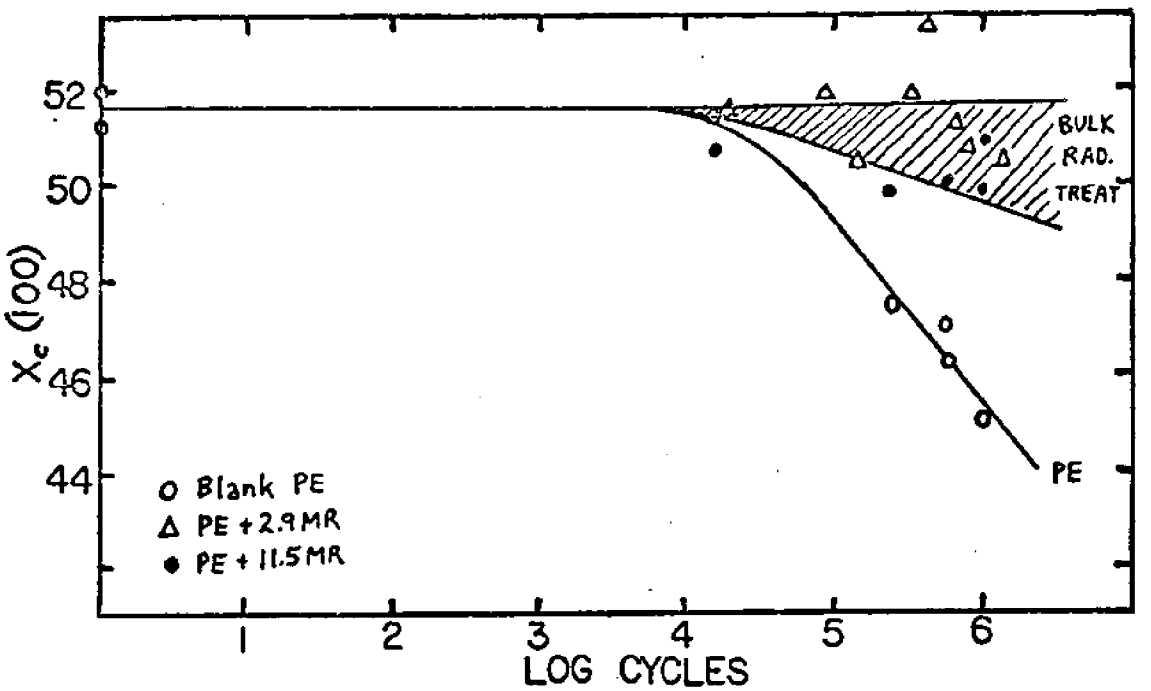

Figure 57. a) Crystallinity vs Log Cycles Flex for Isotropically Irradiated PE Blank (500 keV) at Various Dosages. (70 rpm).

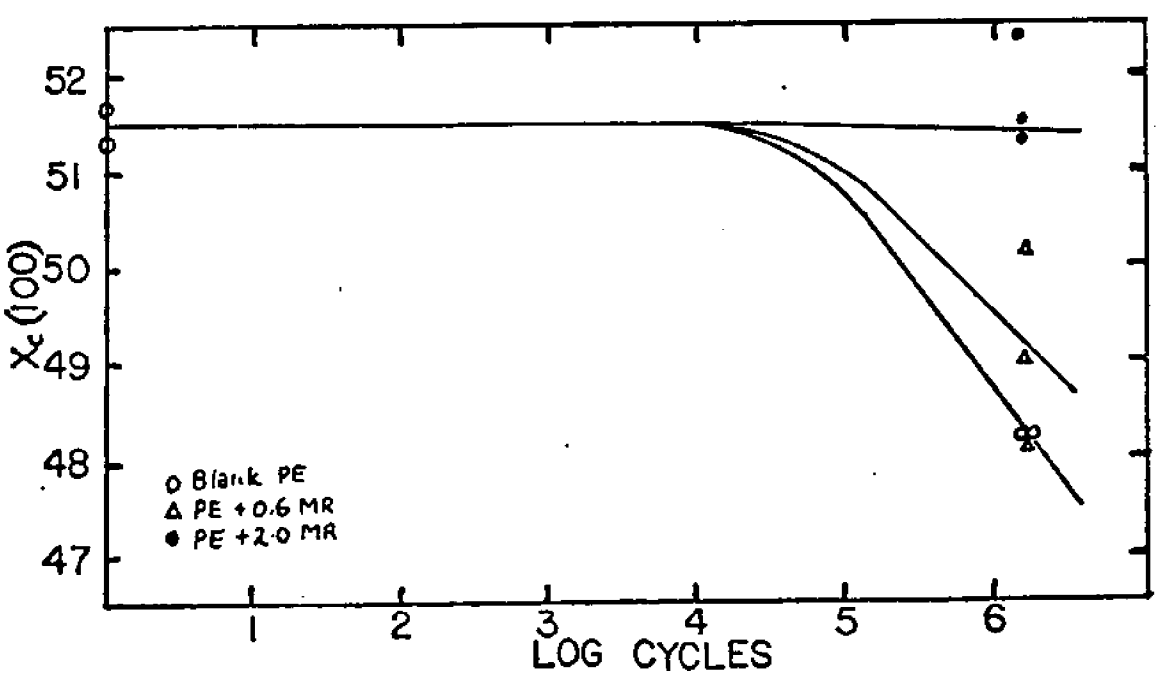

Figure 57. b) Crystallinity vs Log Cycles Flex at 70 rpm for PE Surface Irradiated with 500 keV Electrons.

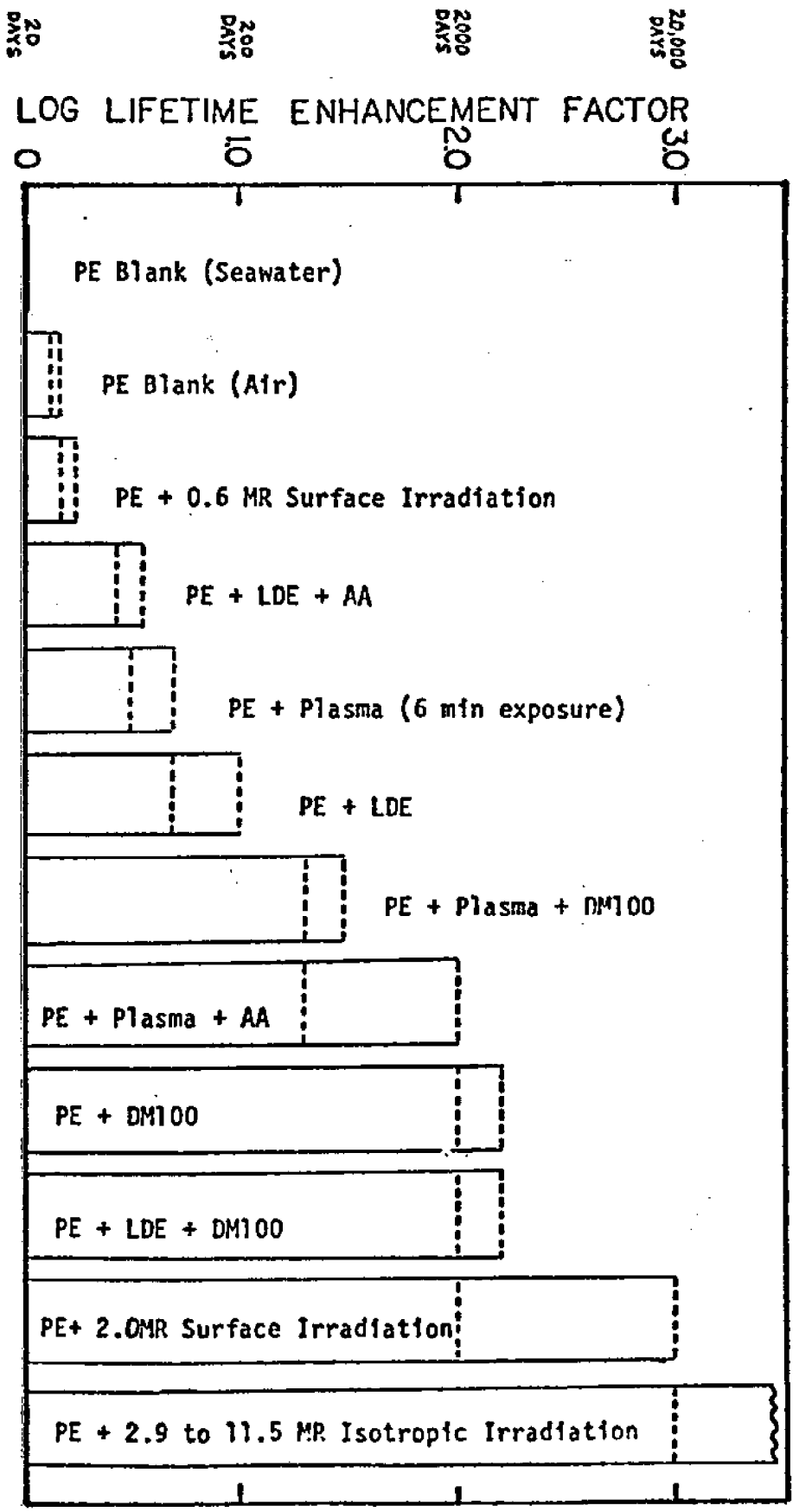

Figure 58. Log Enhancement Factors for the Surface Modification Methods Studied. Area between Broken Lines on Each Bar Denotes Uncertainity. (Enhancement Factor = (time required for treated sample to lose 1% crystallinity) ÷ (time required for PE crystallinity in seawater to drop 1%)).

PE, similar zero-loss behavior was seen out as far as 6.2 log cycles at 70 rpm (Figure 28B). To drop to 50.5% from an initial 51.5% probably would have required 7.5 to 8.0 log cycles , while blank PE required only about 5.15 log cycles. The enhancement factor is thus well over 100, maybe near 1000, which is probably better than the best purely chemical treatment, LDE + DM100. For a dosage of 0.6 MR, the enhancement effect was much more modest. To drop to 50.5% crystallinity only required 5.35 log cycles vs. 5.15 for blank PE, for an enhancement factor of about 1.6, the lowest encountered for any treatment protocol. This probably indicates the lower limit of dosage required to show measurable effect on crystallinity degradation at 70 rpm, for the type surface skin (~5% of bulk thickness) tested.

All of the flexure-performance results, in terms of lifetime-enhancement factors, are summarized in Figure 58, along with equivalent lifetimes for treated strip in a 1 rpm environment. This chart illustrates the broad range of surface modification processes studied which produce results reflecting an equally wide range of effectiveness.

DISCUSSION

The results just presented as a body illustrate the variety of forms that seawater-promoted polymer degradation can assume. For semicrystalline resins such as PP and low-density PE (LDPE), the primary degradation mode seems to be crystallinity loss, with little or no molecular-weight loss occurring in the flex regime studied. For amorphous resins, such as PMMA and atactic PS, molecular-weight loss is the dominant failure mode. Research done by du Pont of Canada (Szpak) indicates that highly crystalline resins (high-density PE in this case) actually become even more crystalline, hence more brittle and more subject to stress-crack failure.

The degradation-retarding effects of various surface-modification processes on LDPE are similarly diverse, and suggest several different retardation modes, including steric blockage of diffusion, as well as ionic barriers.

Initial flex experiments, in the vertical machine, on PE and PMMA established the exponential character of the degradation process beyond an initial onset region. PMMA seems to be sensitive to flex frequency (Appendix IX), even in the 30 to 60 rpm range, indicating a relatively long relaxation time. Both resins degrade faster in seawater than in air; this is consistent with the oxidant and ion-diffusion models discussed below. Stress-strain testing of PE and PMMA revealed an earlier onset of degradation for PMMA at 60 rpm; this method was found to be the best monitor of occurrence of onset. This finding supports the idea that the semicrystalline PE resin should have a higher internal strength (due to ΔH_{cryst}) than the amorphous PMMA.

General Considerations: In searching for a degradation mechanism for each polymer studied, there are a number of possibilities ranging from simple chain breakage to more subtle changes in polymer morphology. A summary of some of the currently accepted mechanisms is given in this section. Unfortunately, some of these theories are based on experiments in which the polymers have undergone much more violent processing (e.g. grinding) than the present work and therefore may not be applicable.

The mechanochemical degradation of molecular weight has been studied extensively for various modes of polymer processing and fabrication. The accepted mechanism explains that the entangled nature of the polymer chains allows those devices producing shear action in these material to impart sufficient energy to individual molecular bonds to cause them to break as shown in figure 59, (Watson, p. 1086). Electron Spin Resonance Spectroscopy has verified the presence of these free radicals which can result from the grinding or mastication of raw polymers (Sohma and Sakaguchi, p. 157-180).

Given the presence of free electrons at the new polymer chain ends formed by chain scission, it has been found that oxygen and other radical scavengers expedite the molecular degradation process. The marine environment provides a whole range of radical scavengers from chlorine ions and other radicals to dissolved oxygen, thereby making it a likely location for this type of degradation.

It has been found that chain scission is further accelerated by the propagation of end radicals to neighboring polymer molecules leaving two stable terminal ends where the radicals were and two new radicals on the adjacent molecules. This submicro crack as it is termed, propagates in this way leaving a trail of stabilized end groups behind it (Figure 60). The ratio of the number of stable ends formed to the number of these cracks in one polyethylene sample was found to be about 1000 (Sohma and Sakaguchi, p. 160-162). This mechanism is known as Zhurkov's model (Zhurkov et. al., p. 1509).

Approaching the degradation from a different angle, we find that physical properties like stiffness and yield point are dependent on crystallinity for many

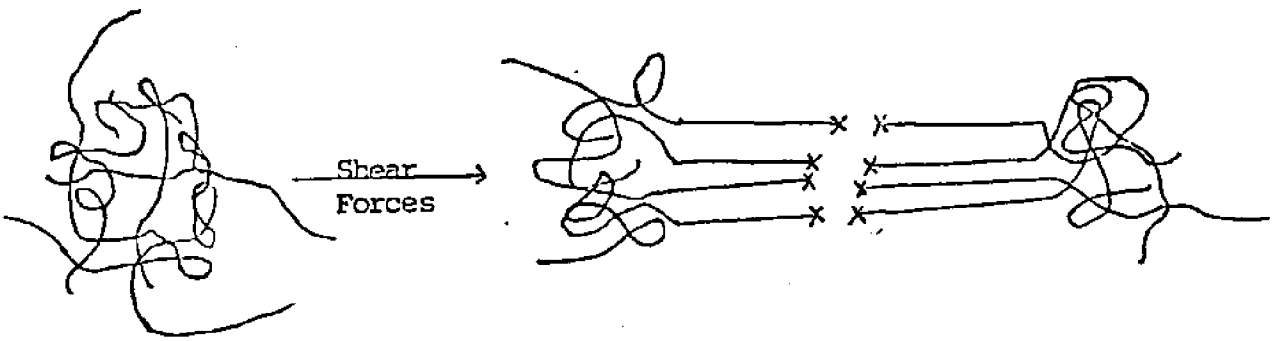

x = Point of Chain Scission

Figure 59. Mechanochemical Degradation

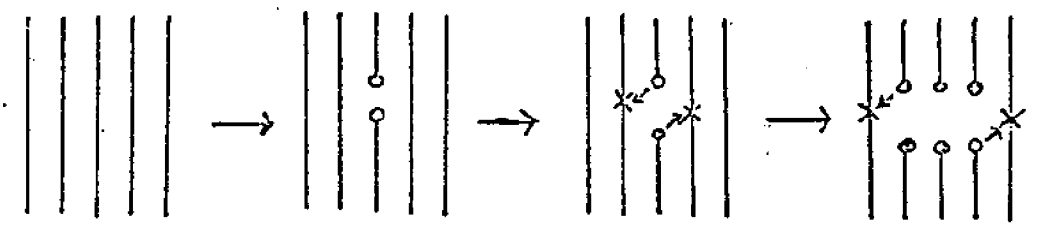

o = Unpaired Electron

o = Terminal Double Bond

x = Point of Hydrogen Abstraction

Figure 60. Submicrocrack Propagation (After: Sohma and Sakaguchi, p. 159).

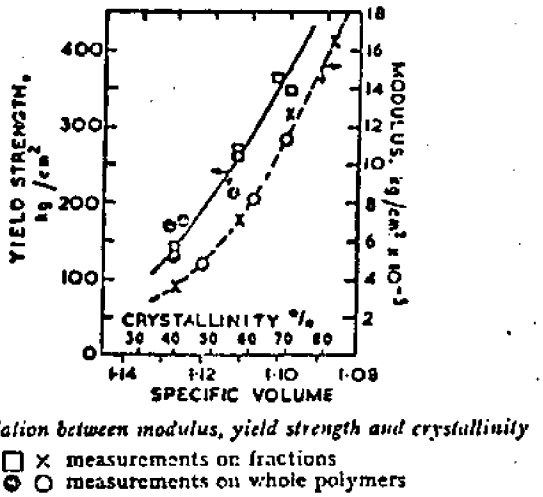

Figure 61. Crystallinity Affect on Modulus and Yield Strength For Polypropylene.

(From: Wijga, p. 26)

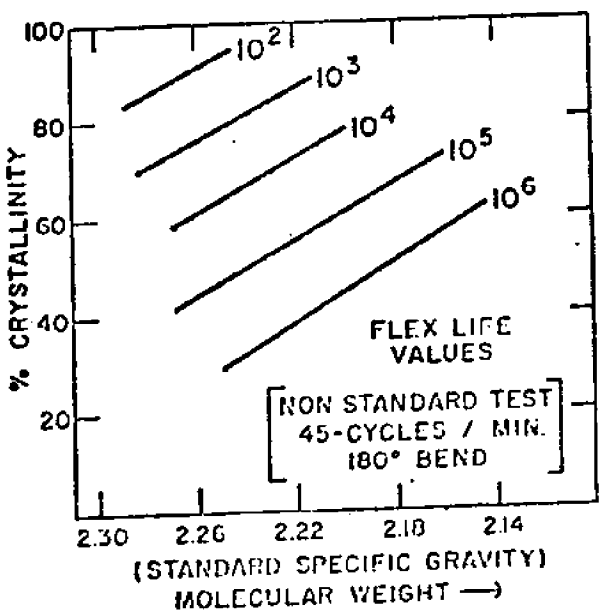

Figure 62. Flex Life Dependence on Crystallinity and Molecular Weight.

(From: Thomas, et.al., p. 93)

polymers. As crystallinity decreases, both stiffness and yield stress also decrease and with these changes, the chance of brittle failure is also decreased (Figure 61) (Sperati et.al, 1953; Starkweather, et.al., 1956; Wijga, 1959). A combination of crystallinity and molecular weight has been shown to affect hardness, flexural fatigue resistance or flex life, softening temperature and elongation at tensile break (Billmeyer, 1965). Figure 62 shows the affect of crystallinity and molecular weight on flex life in a teflon resin. Flex life increases with increasing molecular weight and decreasing crystallinity (Thomas, et.al, 1956). Although the flexure in this experiment was much more drastic than the present case (a full 180 degrees), the implications are still quite clear.

A process of crystalline degradation has been proposed by Flory as a simple migration of polymer chains from the crystalline to the amorphous regions, thereby decreasing the bulk crystalline fraction.

Finally, a degradation mechanism has been proposed as a combination of the two preceeding cases and has been confirmed by Electron Spin Spectroscopy (Peterlin, 1970; Sohma and Sakaguchi, p. 158). In a semicrystalline polymer where islands of crystallinity are connected by individual polymer chains, a mechanical stress applied to the bulk polymer will cause chain scission in those molecules connecting the crystalline regions but not in the crystalline regions themselves (Figure 63).

Figure 63. Peterlin Model for Semicrystalline Degradation

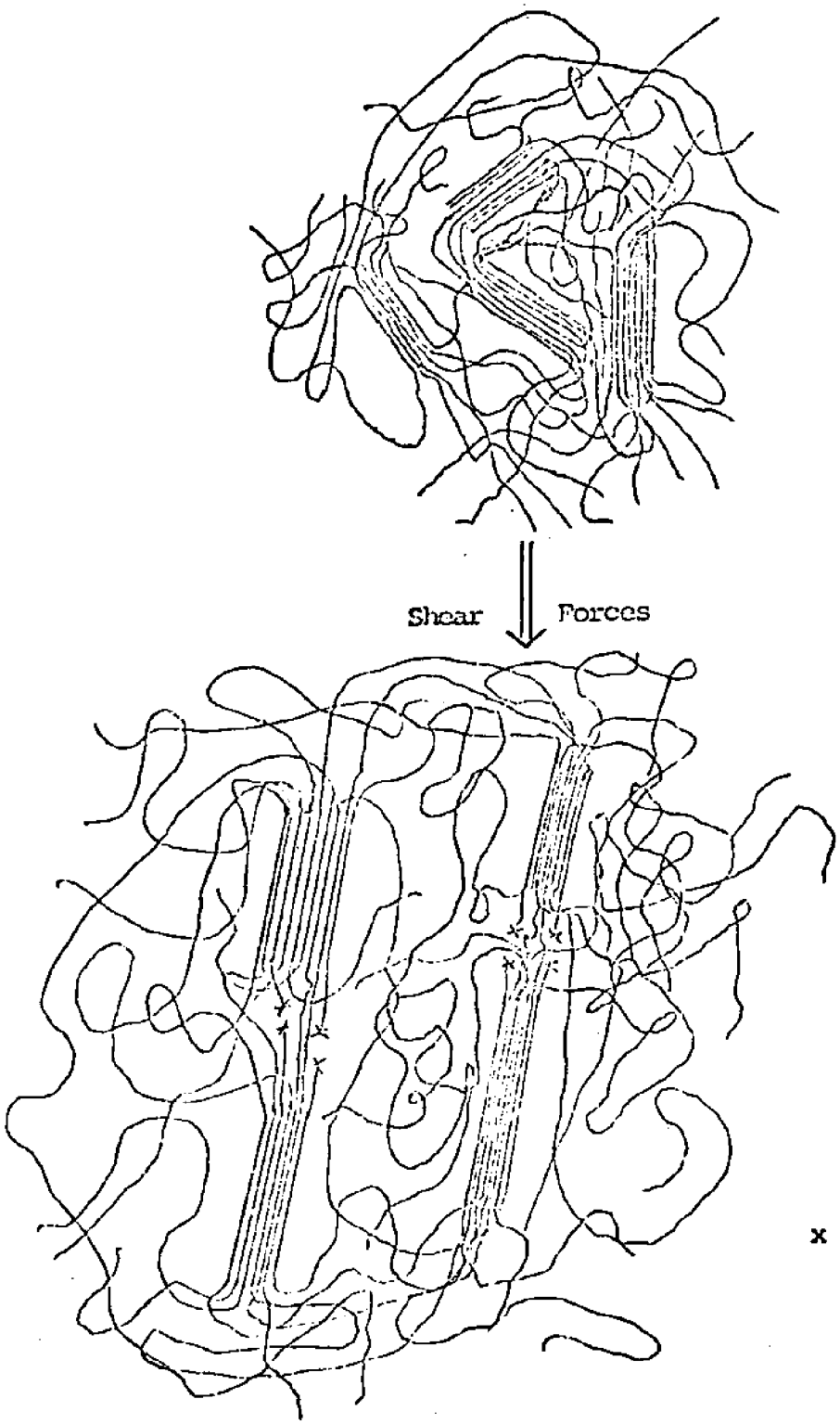

Melt Viscosity Studies: PE: While decreasing crystallinity with respect to flexure was reproduced from the previous work, both the starting point and rate at which the decreases occurred differed. There are two possible explanations for this. First, it is not certain that the deflection height was the same for both sets of experiments. No work was done on deflection distance dependence of degradation so no conclusions can be made at this point. The second possible cause lies with the X-ray diffraction measurement technique. This technique required hand approximations directly on the X-ray scan data and it is not clear that these were done in the same way as in the previous work or even from sample to sample. (Later X-ray measurements used a fairly reproducible standard baseline algorithm)

Viscosity was not found to vary with flexure and the only difficulty in the analysis came in the estimated region of experimental error. For individual samples, the variations may appear significant but no overall reproducible effect was found. At any rate, in view of the fact that any effect that may or may not be present is measurable only at the extreme limit of accuracy of the mechanical spectrometer, it was concluded that melt viscosity was of little utility as a monitor of polyethylene degradation.

PP: Crystallinity data for polypropylene were erratic, with no trend detectable in the resulting values. This can be attributable to two possible causes. First, the samples were much older than any of the others tested and although all samples were stored in a freezer to prevent changes in morphology after the experiments had been completed, we do know what the long term (approx 7 months) effect of this storage might be. A second problem area was again with the interpretation of X-ray scans. A base line curve for each sample had to be hand fitted to the diffraction response and it was even more difficult to do this reproducibly on polypropylene than on polyethylene.

Briefly, the same arguments for the viscosity results for polyethylene apply here. Even if there were a change in molecular weight, it is only measurable at

the limits of accuracy of the mechanical spectrometer and therefore not very useful for comparison purposes.

PS: In contrast to polyethylene and polypropylene, the molecular weight measurements made with the mechanical spectrometer showed significant and reproducible decreases with respect to flexure. The mechanical spectrometer, was thus found to be useful as a tool for monitoring polystyrene degradation. Best data spread between flexed and unflexed PS samples was encountered in a higher shear-rate regime; the differences due to flexure decreased considerably at lower shear-rates; this is consistent with a fundamental model of molecular weight loss as the dominant degradation mode for PS.

Possible polyethylene degradation modes: The test PE resin, according to characterization by the methods described earlier, was a low-density PE with a rather low softening range (Table 1) near 110°C and a recrystallization peak near 90°C. Other DSC data indicated it to be a single resin and not compounded.

Since the test PE resin was LDPE, it was expected to lose crystallinity upon degradation under flexure; a HDPE (high-density) resin might actually have become more crystalline, as discussed earlier. LDPE's are of lower molecular weight but of higher branch density, and hence are more likely to possess a higher entanglement density than the more linear HDPE resins. When an LDPE is mechanically worked, crystallites are pulled apart and disoriented, thus increasing the amorphous fraction of the bulk polymer. Loss of crystallite structure also is probably associated with loss of strength as the yield-stress vs. crystallinity data suggest. This is reasonable, since from DSC, crystallization in the test PE resin adds about 118.9 kJ/kg to the energy content of the polymeric bond structure of a crystallite, relative to the amorphous phase. A loss of crystallinity therefore is equivalent to a loss in average bond-energy density, hence a more weakly bonded structure which has lower yield strength.

For a HDPE resin, the degree of entanglement is lower; mechanical working pulls apart some crystallites, but allows the less-entangled amorphous phase to crystallize onto the remaining crystallite fragments, and the effect is a net increase in crystalline fraction. Recrystallization probably occurs also in LDPE upon working, but it is hindered by the greater degree of entanglement in the amorphous region, so that the net effect is crystallinity loss.

The effect of seawater upon this process, in the case of the test LDPE, was to accelerate this crystallinity loss, probably by accelerating processes which increase the density of such deformities as chain ends; these along with chain entanglements help hinder recrystallization to a greater degree than if no saline-induced chain cleavage occured. The net result is a greater extent of

degradation; an "enhancement"factor of about 0.7 relative to air. Even though the molecular weight is lower, crystallinity does not rise because the entanglement density originating from the initially high molecular weight is "frozen in" at temperatures below about 100°C, and the only effect of lower molecular weight (as caused by carbon-chain cleavage) is to increase chain-end density and to actually impede recrystallization; meanwhile, mechanical working continues to break down crystallites and lower overall crystalline fraction.

In the air environment, the degradation probably is a consequence mainly of carbon-carbon bond breaking mechanically induced (i.e. the chain is actually pulled apart due to steric hindrance when overstressed). An important additional mechanism perhaps involves diffusion of oxygen through the polymer; mechanically stressed sites would be energetically susceptible to oxidation and subsequent chain cleavage at those sites. LDPE similar to the test resin is slightly permeable to oxygen; various free-radical oxidation mechanisms are thought to be important (See Ref. 12).

In distilled water, hydronium ion exists in dilute ($\sim 10^{-6}$ M) solution along with bicarbonate and hydroxide; dissolved oxygen is also present. Isolated from contact with air, such water would have an ion concentration of about 10^{-7} M. It is conceivable that mechanically stressed carbon bonds, especially on tertiary carbon, are energetically susceptible to oxidation or carbonium ion formation followed by some process resulting in carbon-carbon bond breakage. A typical sequence would perhaps be oxidation of a susceptible carbon followed by acid-catalyzed carbonium formation, then further reaction with an oxidant to cleave the carbon-carbon bond, leaving behind terminal carbonyls or COOH groups. The precise mechanism is open to question and could easily be the topic of more research; in any event, these reactions are extremely slow under normal conditions, and produce noticeable effects here only because of the large stress-loading of the target carbon chains. Dissolved oxygen is a prime candidate for the oxidant involved; in air it forms OH and carbonyl on the surface, as seen by ATR and ESCA. In addition, mechanically-induced cleavage would continue as in air.

With a marine flexure environment, the electrolytic properties such as conductivity and total ion concentration are enhanced by perhaps 10^4 or so; the ion-promoted oxidation and cleavage steps should proceed more rapidly. Higher carbon-carbon cleavage rates, of course, imply faster degradation. Cleavages occuring within crystallites would disrupt their internal order, thus assisting in their break-up by the flex cycling process. In seawater, the crystallite-disruption process would proceed more rapidly; this was observed in fact. The actual cleavage mechanism should be different in seawater because of its mild alkalinity; base-catalyzed cleavage should predominate over the acid mechanism suggested for distilled water. The purely mechanical cleavage mechanism is probably minor relative to the seawater-promoted pathways, even though it is not expected to be impeded. Additionally, trace-metal-catalyzed cleavage routes should probably be regarded as at least minor contributors.

From the observation that onset of degradation in all three environments occurs much sooner at 400 rpm than at 70 rpm, it can be inferred that the mechanical breakdown of crystallites occurs more efficiently at the higher speed. This is perhaps due to the high acceleration of flex, which results in faster energy input to the sample, and possible resulting in a somewhat higher equilibrium energy content, at least until significant breakdown has occurred. Thereafter, breakdown seems to proceed at a rate similar to the rate encountered at 70 rpm with similar flex amplitude. In this later log-cycle regime, relaxation of the sample seems to be sufficiently fast to overcome the higher energy input rate at 400 rpm.

Effects of surface modification on polyethylene degradation. The primary goal of a surface-modification technique, in view of the discussion above, would be to impede transport of ions and of dissolved oxygen into the bulk phase of the polymer. A barrier would then probably possess some heteroatom content, perhaps even ionic character, and in addition would be both flexible and abrasion-resistant. In this research a variety of surface treatments which generally satisfied these requirements were characterized and tested, and it was found that each provided at least a minimal impediment to degradation.

Untreated test PE resin was found by ESCA to be surprisingly well oxidized in the upper 10 nm; the C/O ratio was about 7-8 and the C/N ratio about 700. The oxygen appears to be predominantly carbonyl and hydroxyl; relative abundances of the two were not clearly discernible. Nitrogen is probably mostly amine. As mentioned earlier, the actual surface zone is perhaps 10 to 100 nm thick (probably closer to 10 nm), and probably consists of a hilly, furrowed "terrain" with an occasional pore.

The conclusion is inferred from the weakness of the ATR-IR carbonyl signal from the control samples used in the LDE- and plasma- posttreat experiments. These samples were treated with DM100 or AA only, and while they show only a modest increase in the 1720 cm^{-1} ATR carbonyl band, on ESCA the DM100-treated controls show dramatic nitrogen uptake expected of a sample with a thin DM100 layer (blank PE contains nearly no surface nitrogen). These observations were made in spite of the fact that the controls were swelled slightly by the toluene solvent (DM100 is not expected to diffuse any more easily into cold unswelled PE than is LDE). They indicate that the DM100 is isolated in a surface region more comparable to the ESCA sampling depth than that of ATR, and this in turn puts a sort of upper limit to the depth of the "fuzzy" region of the PE surface.

On the molecular level, the amorphous nature of the surface zone suggest that it is riddled with "ultra-pores" on a scale of 1-5 Angstroms; the "surface" seen

by BET probably does not include such fine structure. Most oxygen probably is in this porous zone; smaller quantities lie deeper, on a scale of microns into the bulk, where they are detected by ATR IR. Oxygen molecules and various ions diffuse relatively unhindered through the "ultra-pores", and then do their damage.

Treatment with annealing seems to do little to impede ionic and O_2 diffusion; this supports the idea that it is mainly interstitial and not through larger-scale pores that would be obliterated by softening during the annealing process.

Surfactant Adsorption on PE. LDE treatment seems to create a dense carpet of surfactant molecules on the surface zone of the PE, probably a micellar bilayer. A combination of steric hindrance and electronic forces centered on the hetero-atoms in the LDE head moieties apparently markedly retard ionic transport to the interior, and at least partly retard oxygen transport, as inferred from the slower degradation of LDE-treated PE in seawater than for untreated PE in air.

The mechanism of LDE adsorption, as elucidated by the research seems to be a two-step precursor mechanism up to about 90°C (the location of the DSC re-crystallization peak, and probably the point at which the tail-diffusion thermal barrier is overcome). Entire LDE molecules physisorb onto the surface very rapidly, then slowly diffuse tail-first into the PE "ultrapores" until hindered by the hydrophilicity of the head moieties. At 90°C, the precursor mechanism seems to compete roughly equally with direct adsorption-diffusion; above this temperature the rapid diffusion is dominant. Since the chief impediment to tail diffusion is steric in nature, the transition at 90°C to a direct adsorption-diffusion mechanism probably means that the activation barrier to diffusion has been over-come thermally; i.e. $E_{act} \sim 3/2$ RT, where T = 363°K. Thus, $E_{act} \sim 4.5$ kJ/mole. This value is typical of the purely physical mechanism theorized.

In any event, the result is an LDE layer which occupies virtually the entire "parking area" available on the PE surface, as determined by tensiometric studies. Two potential cross-polymerization sites exist on each molecule, namely the

hydroxyls. The probable bilayer nature of the LDE layer possibly causes a complex structure to form upon cross-polymerization, especially with a trifunctional species.

DM100 Posttreats: Treatments with DM100 in large stoichiometric excess seems to cause a high degree of urethane formation, as indicated by ESCA data which show about the theoretically expected enhancement in N/C ratio relative to LDE-treated surface. Exposure of blank PE to DM100 showed a much larger pickup of nitrogen; final N/C ratios were about twice those seen for PE + LDE + DM100. Low volatility ($<10^{-8}$ torr) and surprisingly large enhancement factors seen for PE + DM100 indicate that a polyurea coating of form [R-NH-CO-NH-R']n, where R and R' denote aliphatic chains, has formed at the surface region, probably anchored to polyethylene by an occasional urethane link to a polyethylenic OH group. Polyurea is the expected product of adsorbed DM100 quenched with water; free amine should also be in abundance. In addition, the polyurea contains biuret groups from the original DM100. ESCA data suggest that amine nitrogen is minor relative to urethane, biuret and urea forms, but the certainty of this is limited by the weakness of the observed N_{1s} signal.

In either case, the DM100-cross-polymerized surface coating retards transport, presumably of ions, into the interior to a greater degree than LDE alone. The DM100 polyurea coating is probably chemically bonded (grafted) directly to the PE skeleton; the total strength of this bonding, while probably less than the sterically-anchored, more numerous "pilings" anchoring LDE-DM100, appears adequate for the job. The LDE-DM100, however, would have the added advantage of chemical stability against hydrolysis (important in alkaline environments and in seawater) and demonstrated flexibilty in the demanding 400 rpm flex-cycle regime.

Adsorption of DM100 onto PE and PE + LDE occurs rapidly at room temperature and low concentration, indicating little problem with steric hindrance at the adsorption/reaction sites, and that the activation barrier is low. This result is in accordance with what is know about polyurethane reactions in solution.

Plasma Treatment: Exposure of model blank PE to plasma causes a complex oxidation and nitrification scheme to occur over the observed interval of 0.1 sec to 200 min (about 6 orders of magnitude in time). Further, these phenomena are seen to be flow-rate dependent. At low flowrates (i.e. long residence times for activated species in the vicinity of the PE surface), surface oxygen content rises very rapidly (<0.1 sec) initially, and then declines slowly. Beyond about 20 min, some new surface oxidation process apparently becomes dominant, as surface oxygen content rises again and then again slowly declines (although faster, vs log time, than the initial decline). At the high flowrate, a slow increase in surface oxygen content dominates over the entire time range studied. The low-flow results may suggest that some sort of chemical etching or leachout or oxidized sites continually occurs, and that two different oxidation mechanisms become favorably promoted after specific amounts of exposure to the activated environment. While the initial process occurs very rapidly, the second process seems to require a 6 to 20 min latency period, while the PE surface is "readied", presumably by the same process that is slowly etching off oxygen laid down by the first process. Very little chemical-shift data could be gleaned from high-resolution ESCA. ATR IR data shows peak carbonyl activity coincident with onset of the "slow" oxidation process; however, the "fast" process does not show such a peak until the 1 to 10 sec range, well after the slow etch has begun. The actual mechanism is expected to be a complex system of parallel reactions, which is the usual situation encountered for plasma and flame environments containing a "shotgun" variety of free radicals, molecular fragments, and other activated species.

Nitrification also undergoes a double maximum process; the maxima also seem to agree well with maximum ATR IR carbonyl levels ($\sim$1 sec and $\sim$20 min). Etching occurs after 1 sec and a second nitrification process starts in the 2 to 6 min range, only to be etched in turn after peaking at 20 min. The second etching regime possibly is associated with a modest degree of crosslinking, similar to what occurs during CASING. In this time regime, considerable surface opacity also appears,

perhaps due to large-scale oxidation and subsequent volatilization of oxidized surface fragments. What is left behind is a modestly oxidized and crosslinked surface.

Fast flowrates seem to sweep the chamber sufficiently to drastically reduce activated species residence time near PE surface. Oxidation and etching may then be closely balanced; the net result being a slow gain in surface O content. Frosting occurs as at low flow; hence both oxidation and etching are important. Carbonyl formation shows no peaks as seen at low flowrates; evidently some necessary intermediate is swept away before it can react to and thus contribute to carbonyl formation. Nitrification is seen to follow a smooth rise toward about 2 to 20 min, and then a decline similar to that seen at low flowrates. The pattern seems to be roughly an envelope encompassing the two low-flow N peaks. The effect of high flow on nitrification seems to be a smearing of the two dominant low-flow processes into one broad process of nitrification which is cut back only by the long-time etching which acts as a sort of final cleanout of all oxidation and nitrification.

The result is, after about 6 min, a shallow crosslinked surface layer (see Schonhorn and Hansen, 1967) probably containing large numbers of OH and CO moieties, and significant numbers of amine or imine as well. An appreciable ion-transport barrier has evidently been constructed despite possible increase of surface area from etching, although it is not as effective as the dence LDE bilayer seen before.

Plasma + DM100: Posttreat with DM100 presumably causes polyurea and polyurethane networks to become anchored to the plasma-generated OH and NH_2 sites, and the enhancement factor is boosted to levels just above that of LDE alone. Ion transport is hindered further due to charge effects (see below); the thin crosslinked skin is not expected to pose an effective barrier any more than a window screen bars rain, but it does serve to strengthen the carbon-skeletal base of the polymerized DM100 layer. It is interesting to note that both plasma and plasma + DM100 enhance seawater performance beyond air-environment levels; this suggest some sort of barrier, probably electronic, to oxygen diffusion as well as ion transport.

AA Posttreats: Adipic acid posttreats generate a polyester coating anchored by LDE tails or by ester and amide links to polyethylene OH and NH_2. This result is indicated by observation of expected O/C enhancement under ESCA. The process is slower than for DM100 polyurethane formation; equilibrium probably was not achieved with PE + LDE+ AA. This is probably due to a competing hydrolysis reaction, catalyzed by the modest ion content of the distilled-water reaction environment. The LDE-AA polyester presented a poor ion barrier relative to LDE alone; this can perhaps be explained by the idea that AA actually promotes ion diffusion into the interior, when cross polymerized onto LDE. The quality of the coating could also be responsible; it is not a network but a series of long LDE-AA-LDE-AA..,chains. Such a surface region might contain large gaps which expose naked PE surface, and which, being relatively free of charge effects, allow significant passage of ions. On PE + LDE, such gaps would be, on average, closed most of the time due to kinetic motion of the freely rotating ethanol groups on LDE. A test of this last hypothesis would be to test either LDE + triacid or LDE + disocyanate on PE strip.

An alternate test of the "gap" theory is PE + plasma + AA, which seems to perform almost as well as PE + LDE + DM100, and at least as well as PE + plasma + DM100. Here, the AA would bond with the plentiful OH and NH_2 species for an intimately-bound polyester coating similar to plasma + DM100. Despite the linear nature of this coating, it seems to retard ion and O_2 diffusion effectively; this suggests a more complex explanation for the relative failure of LDE + AA.

In each of the chemical treatments discussed above, the presumed oxygen- and ion-barring mechanism is the forming of a population of charged species from the environment which cluster in the vicinity of heteroatom groups with small charges of opposite sign on the surface coat, e.g. amide, OH, biuret, urethane, urea, ester, etc. These ions repel any newcomers and also sterically clog the molecular gaps through which still other ions and neutral species such as O_2 could pass into the interior. This model at once explains the ion-barrier and O_2-barrier effect.

Substitution of cluster members and subsequent diffusion into the interior of displaced cluster ions could, and probably does, occur, the extent of this contributing to the observed enhancement factor as much as the initial barrier-forming ability. Such substitution seems to be slow relative to barrier formation, if it occurs at all, since the barrier does in fact work in every case.

Electron Irradiation: Surface bombardment with 500 KeV electrons tends to be a sort of extreme case of the plasma-exposure method. Considerable cross link density is generated above about 0.6 MR surface dose, and the literature (e.g. Lanza in Crystalline Olefin Polymers) contains much work on radiation-induced surface chemistry. Dissolved O_2 has been reported to suppress crosslinking; this effect is probably minor in the current work due to sufficiently high doses used. Surface oxidation, pre-existent and radiation-generated, probably suppresses immediate surface (<<1μm) crosslink levels, but deeper levels (to the 75 μm treat depth) are probably unaffected. Radiation-induced oxidation increases ink-adhesion, hence is equivalent to at least 0.1 sec of air-plasma exposure. The stupendous enhancement factor seen at 2.0MR is probably chiefly due to steric hindrance of ion and oxygen diffusion caused by crosslinking, but this comes about in a peculiar way.

As PE is subjected to high-energy electrons, amorphous targets are immediately crosslinked after the hydrogens are spalled off. In crystallites, a broad 4.25 Å gap separates the rigidly-locked polyethylene chains; the only recourse for the energized carbon is to transmit its energy to its two nearest neighbors; this process is repeated, in a traveling wave, until the 500KeV is dissipated; this takes tens or hundreds of transfer steps. The process almost always runs out of crystallite, and once into the bordering amorphous region, the energy wave will encounter carbons which are in greater relative motion; the first carbon close enough to a neighbor chain gets crosslinked to that chain. The result after 2.0 MR of such impacts is very low crystalline crosslink density, with "shells" of highly-crosslinked amorphous region encasing each crystallite, and causing it to be far more resistent to breakdown

than when unirradiated. The intervening amorphous region has lower crosslink density. Evidently a 75 μm layer of such material is sufficient to greatly reduce degradation of unshielded internal material. The threshold for this effect is near 0.6 MR, as determined by flex results. Surface chemical barriers probably exist, similar to those encountered in the plasma-treated samples; however, they alone cannot account for the observed hindrance of degradation. Interestingly, the 0.6 MR strips performed not as well as the 6-min plasma strip; this suggests that the chemical contribution is at best very minor (2.0 MR and 0.6 MR probably have comparable surface-oxidation levels).

POSSIBLE EXTENSIONS OF WORK

The scope of this work was limited by time considerations only; the potential avenues for future research are virtually endless. One could begin by confirming the baseline degradation behavior of the resins studied, and extending such baseline to other environments (as already done for LDPE). New resins could be studied, e.g. HDPE, ethylene-vinyl acetate (used in food packaging), Teflon, PVC (polyvinyl chloride), nylons, various elastomers as isoprene and polybutylene rubbers, etc. All are known to degrade, and can potentially be surface-treated to retard such degradation.

A later phase could be more quantitative mechanistic studies of the degradation process in various chemical environments (e.g. air, distilled water, seawater). Such tools as ESR, ESCA, gas chromatograph, mass spectrometry, SEM and permeability measurements should reveal considerable detail. For example, ESCA depth-profiling of a surface layer can, in principle, be done to 10 nm resolution. ESR studies should reveal what intermediates and free-radical species form during the oxidative chain-schission process.

A particularly interesting chemical system to explore is the polymer surface exposed to glow-discharge plasmas of various compositions. The cursory studies discussed for LDPE are indicative of the complexity and great potential for optimization for a broad range of surface types.

The surface modification studies done on LDPE should be repeated for the other major resin classes. The nature of the this retardation gives hope of successful application to other major polymers.

APPENDICES

I Structural Configurations of LDE, DM100 and Adipic Acid

II Physical Property Data for LDE, DM100 and Adipic Acid

III Preliminary Calculations for Expected Surfactant Adsorption by Polyethylene

IV LDE Tensiometric Calibration Curve: Surface Tension vs. Concentration

V Basis for Establishing Posttreat Solution Concentration Tested on PE Strip

VI Dilute Solution Viscosity Measurements - Theory and Data

VII A. Preliminary DE Flexure Runs in Air and Seawater at 60 rpm
B. Instron Stress-Strain Measurements

VIII Deconvolution of Wide-Angle X-ray Diffractograms: Two Algorithms Used in this Work

IX Study of Effect of Flexure Frequency on Degradation of PMMA

X Data for Melt Viscosity Studies on PE, PP, and PS.

XI Calculation of Surfactant Adsorption Rate if Mass Transfer Limited

XII Data from LDE Adsorption Experiments on PE Powder

APPENDIX I

Structural Configurations of LDE, DM100 and Adipic Acid

1) (lauric diethanolamide, $C_{11}H_{23}CON(C_2H_4OH)_2$, Stepan Ninol AA-62)

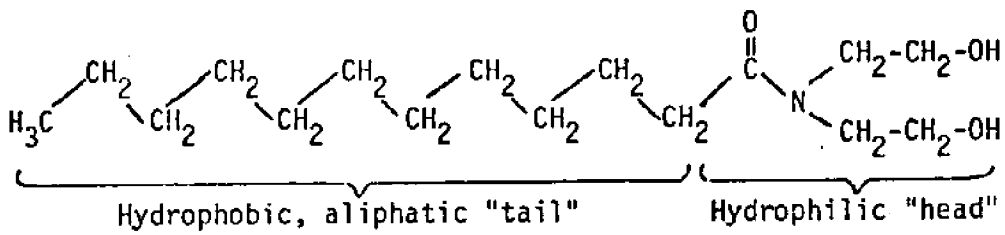

2) DM100 (tris [N,N',N'' -hexamethylene - isocyanato] biuret, $(OCNC_6H_{12})_3C_2H_2N_3O_2$, Mobay Desmodur N-100)

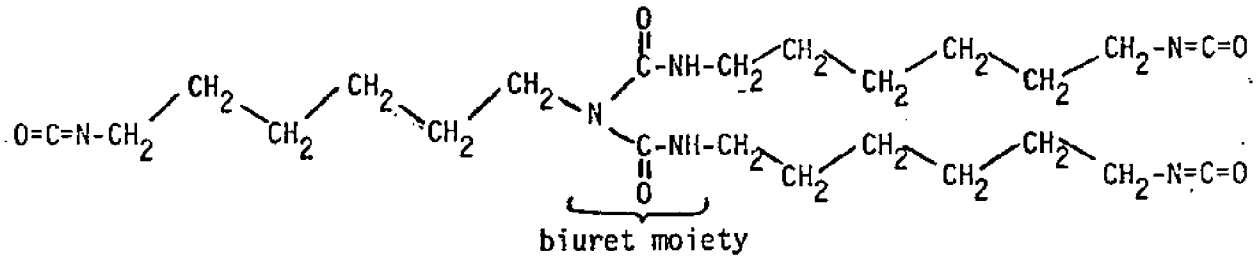

3) Adipic Acid (AA, HOOC C_4H_8COOH[1])

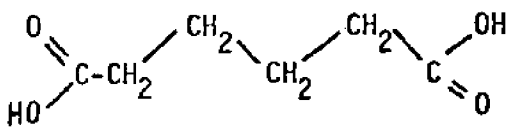

APPENDIX II

Physical Data for LDE, DM100, and Adipic Acid

1) LDE: A superamide formed from the corresponding ester in order to suppress byproduct formation. Supplied in solid (wax) form from Stepan Chemical Co.

Composition (Pugh, 1977)	90% LDE 7% lauryl amine 3% other surfactants
m.p. (D'Alelio and Reid, 1937)	38.7°C
b.p. (" ")	190°C
Solubility in water (Kritchevsky)	1 g/100 cm^3 = 3.5 x 10^{-2}M
Molecular Weight	287.43 g/mol
Density (estimated from C.R.C. data)	0.85 g/cm^3
Critical micelle concentration (Garry)	26.5 dyne/cm = 2.65 x 10^{-2}nt/m
Surface area of molecule (Stepan Chemical)	25 $Å^2$
Surface area of head region (space-filling model estimate)	12 $Å^2$
Transmission IR Absorbances: (Hummel)	ν_{OH} = 3333 cm^{-1} ν_{CO} = 1613 cm^{-1} $\nu_{OH\ BEND}$ = 1053 cm^{-1}
(Present work)	ν_{OH} = 3375 cm^{-1} ν_{CO} = 1720 cm^{-1} $\nu_{OH\ BEND}$ = 1060 cm^{-1}
ATR IR Absorbances:	ν_{CO} = 1715cm^{-1}; shoulder at 1615-20 cm^{-1}
Impurity Absorbances:	ester, 1740cm^{-1}; ether, 1111 cm^{-1}; n-alkyl residue, 720 cm^{-1} (none actually observed for LDE batch used)
ESCA Atomic Ratios on Garry PE:	O/C= 0.16 N/C= 0.007 N/O= 0.075

2) DM100: A biuret condensation product of 3 moles of hexamethylene-1,6-diisocyanate (HDI) and 1 mole water. Supplied neat from Mobay Chemical Co.

Composition (Mobay Chemical)	98% DM100 2% HDI, dimers, oligomers, etc.
Viscous, pale yellow liquid, similar in appearance but heavier than refined honey	
Solubility in dry toluene	>2 g/100 ml
Molecular weight	478.65 g/mol
Density (model-compound estimate)	0.93 g/cm^3
Mean Span between NCO moieties	18-19 Å
Molecular Volume	200 $Å^3$
Transmission IR Absorbances:	ν_{NCO}= 2270 cm^{-1} ν_{CO}= 1764 cm^{-1} (from NCO?) ν_{CO}= 1694, 1637 cm^{-1} (biuret)

ATR IR Absorbances (adsorbed 24 hr and quenched on PE blank): Weak 1720 cm-1 peak, slightly above surface-oxidation background level.

ESCA Atomic Ratios on Garry PE (24-hr adsorption and quench):

DM100 Concn. in soln.=	4.44 x 10^{-5}M:
	O/C= 0.08
	N/C= 0.03
	N/O= 0.30
DM100 Concn. in soln.=	4.44 x 10^{-3}M:
	O/C= 0.12
	N/C= 0.04
	N/O= 0.35

3) AA: Supplied in crystal form by major houses.

Composition	99.99% adipic acid
Melting Range	151-153°C
Solubility in distilled water	~2 g/100 ml
Molecular Weight	146.15 g/mol
Density	1.360 g/cm^3
Mean Span between acid protons	9-10 Å
Molecular Volume	50 Å^3
Molecular Parking Area on PE	30 Å^2
Acidity:	$K_1 = 3.9 \times 10^{-5}$
	$K_2 = 5.24 \times 10^{-6}$

ATR IR Absorbances: $\nu_{CO} = 1720\ cm^{-1}$; shoulder at $1705\ cm^{-1}$

ESCA Atomic Ratios on PE + LDE after 24 hr reaction:

AA Concn. in soln.= 6.67×10^{-5}M:
O/C= 0.26
N/C= 0.009
N/O= 0.03

AA Concn. in soln.= 6.67×10^{-3}M:
O/C= 0.22
N/C= 0.023?
N/O= 0.11?

APPENDIX III

Preliminary Calculations for Expected Surfactant Adsorption by Polyethylene

As referred to in the experimental portion of the thesis, some preliminary calculations were done in an effort to predict the quantity of surfactant which could be adsorbed by sheet polyethylene as well as polyethylene particles of 100 micrometers in diameter.

3" × 1" × 1/6" sheet polyethylene

surface area of polymer	$6.50\ in^2 = 41.935\ cm^2$
density of polymer	$.940\ g/cm^3$
surface area of surfactant molecule (Stepan Chemical Co.)	$2.5 \times 10^{-15}\ cm^2$
specific surface area of polymer	$14.502\ cm^2/g$

adsorption –

$$\frac{14.502\ cm^2/g}{2.5 \times 10^{-15} cm^2/molecule \times 6.023 \times 10^{23}\ molecules/mole}$$

$$= 9.631 \times 10^{-9}\ moles/g\ polymer$$

Assuming 1/3 of amorphous areas (45%) undergo successful adsorption results in adsorption of $1.445 \times 10^{-9}\ \frac{moles}{g\ polymer}$

For 100 mμ particles

specific surface area of polymer $= 6/d_p p_p$ $637.6\ cm^2/g$

adsorption -

$$\frac{637.6\ cm^2/g}{2.5 \times 10^{-15}\ cm^2/molecule \times 6.023 \times 10^{23}\ molecules/mole}$$

$= 4.234 \times 10^{-7}$ moles/g polymer

Assuming 1/3 of amorphous areas (45%) undergo successful adsorption results in adsorption of

6.352×10^{-8} moles/g polymer

Assuming one has mixture of 10 g polyethylene in 100 cm^3 of 10^{-5} M surfactant solution:

initial moles of surfactant	1×10^{-6} moles
10 g polyethylene adsorbs	6.352×10^{-7} moles
moles of surfactant remaining in solution	3.658×10^{-7} moles
change in solution concentration	63.5%

Conclusion: With an assumption of minimum surfactant adsorption (15% of total available polymer area), polyethylene particles with diameter of 100 micrometers appear to cause a significant concentration change of the bulk surfactant solution upon adsorption (63.5%) whereas sheet polyethylene does not (1.45%).

APPENDIX IV

LDE Tensiometric Calibration Curve: Surface Tension vs. Concentration

An empirical calibration curve was developed for converting raw surface-tension data to solution concentration data for dilute LDE solutions in distilled water. Raw measurements were made by the du Nuoy Ring technique which measures the torsional force required to pull a previously-measured ring free of the fluid interface being studied (see Adamson, 1967).

The raw readout, P_T, is a sum of surface-tension forces and the dry weight of the ring P_D. The apparent surface tension γ_a is obtained from

$$P_N = P_T - P_D = 4\pi R\gamma_a$$

where R is the radius of the ring. From this the true surface tension γ is obtained from the observation that $\gamma = \gamma_a F$, where F is an empirically-determined correction factor arising from meniscus effects and ring wetting effects. Zuidema and Waters (1941) have compiled empirical data for F as a function of R and wire radius r, and as a function of the γ_a reading. Typical values encountered in the present work were in the range of 0.904 to 0.936 = F, for R/r = 52.8.

The true surface tension γ is related to concentration C by the empirical curve shown below. Between the critical micelle concentration at 3.55×10^{-4}M and about 3.35×10^{-6}M there lies a linear zone where

$$\log C = -4.47 - 0.043(\gamma - 50.0)$$

and γ is in dynes/cm. Above and below this linear zone, surface tension is insensitive to concentration, and tensiometric data cannot be obtained.

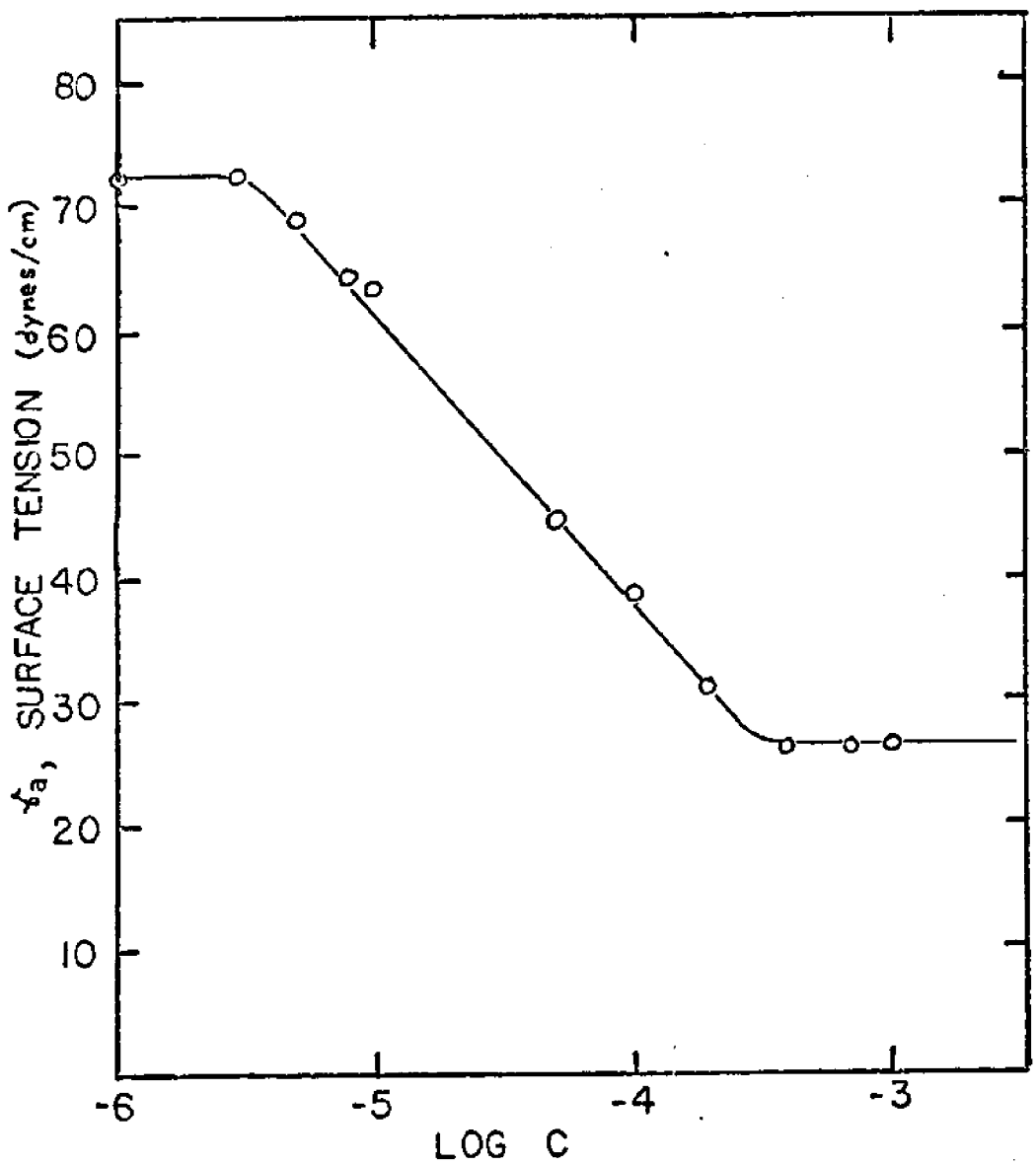

Surface Tension vs. Log LDE Concentration (Garry, 1977).

APPENDIX V

Basis for Establishing Posttreat Solution Concentrations Tested on PE Strips

Deciding the most informative DM100 and AA postrreat solution concentrations to employ in order to evaluate concentration effects on cross-polymerization was a special problem. The system is heterogeneous; it was not clear that a given stoichiometric ratio of NCO or COOH to OH in homogeneous phase would correlate to any degree to that ratio when defined as (total moles of NCO or COOH in solution): (total moles OH bound to the PE surface), which shall be called α.

It was finally decided to try three values of α:$\alpha = 1.2$, $\alpha = 120$ and $\alpha = 12{,}000$ (the 20% surplus was added to overcome probable error in surface-area modeling of the strip, and to correct for degradation from undessicated moisture still in solution).

To determine what actual molarities are implied by these α values, a solution volume of 100 ml per 1" x 3" strip was assumed, and the strip was assumed to be a perfect parallepiped of dimensions 1.00" x 3.00" x 0.062". This yields a surface area/strip value of $\underline{A_s} = 41.92\ cm^2$/strip. Given the density $\rho = 0.918\ g/cm^3$, A_s then equals 14.99 cm^2/g of strip.

Using a reasonable parking-area/molecule figure (obtained from tensiometric adsorption studies on powder) of 25 $\mathring{A}^2$/molecule, this then yields the molarity/strip of adsorbed LDE $\underline{M_s}$. Since strip mass $m_s = 2.80$ g;

$$M_s = \frac{\underline{M_s}}{m_s} = \frac{A_s}{A_{mol}\, N_{avog}} = 9.95 \times 10^{-9} \text{mol LDE/g of PE strip}$$

and finally $\underline{M_s} = 2.78 \times 10^{-8}$ mol LDE/strip.

Then the molarity of the posttreat solution solution is given by

$$\text{molarity} = \alpha\beta M_s (1000\ \text{ml/l}) \div (50\ \text{ml})$$

where α = 1.2, 120 or 12,000 and β is 1.0 for AA and 0.667 for DM100 (equivalence ratio). For α = 1.2, the resultant molarity of 4.44×10^{-7}M DM100 or 6.67×10^{-7}M AA is labeled "L" for "Low Concentration", and similarly for α = 120 ("H" for "High Concentration") and α = 12,000 ("V" or "Very High Concentration").

The true value for A_s could be as much as 10% to 20% low, and probably is, because of the furrowing of the surface discussed in the text. From Garry calculations of mass transfer of LDE to the PE surface, it was found that the mass-transfer LDE flux limit is about 6.7 to 7.7 orders of magnitude higher than observed adsorption rates, it is thought that the cross-polymerization reactions are similarly unaffected by mass-transfer limitations even though the rates were perhaps 2-3 orders of magnitude faster than for LDE adsorption ($\leq 2 \times 10^{-10}$ moles/in for LDE, perhaps $\sim 10^{-9}$ mole/m for AA and as high as $\sim 10^{-7}$ to 10^{-8} mole/hr for DM100, vs. 1.2×10^{-2} to 1.3×10^{-4} mole/hr for mass-transfer limited LDE transport).

APPENDIX VI

Dilute Solution Viscosity Measurements - Theory and Data

High polymer molecules possess the capacity to greatly increase the viscosity of the liquid in which they are dissolved, even when present at concentrations which are quite low. As shown by Flory (1953), the viscosity can be approximated by the time required for a solution to pass between two fiducial marks of an Ostwald viscometer. The viscosity of the solution divided by the viscosity of the solvent results in the relative viscosity, η_r. Billmeyer (1971) notes that the specific viscosity, $\eta_{sp} = \eta_r - 1$, then represents the incremental viscosity attributable to the polymer solute. The ratio η_{sp}/C (for C being solution concentration) is a measure of the specific capacity of the polymer to increase the relative viscosity. The value of this ratio at infinite dilution ($C = 0$) is the intrinsic viscosity, $[\eta]$. Plots of η_{sp}/C vs. C are very nearly linear for $\eta_r < 2$ and thus can be extrapolated to $C = 0$ with a fair degree of accuracy.

Alternatively, the intrinsic viscosity may be defined as $[\eta] = [(\ln \eta_r)/C]_{C \to 0}$. Both methods should arrive at the same values for $[\eta]$. The intrinsic viscosity is related to molecular weight by the equation (Billmeyer, 1971)

$$[\eta] = KM^a$$

for M being the molecular weight and K and a constants. For the chloroform polymethylmethacrylate system at 25°C values for K and a are 3.4×10^{-5} dL/g and 0.83 respectively (Braudrup and Immerqut, 1966).

A sample calculation is given below:

Sample E - 10 hours flexure time

Concentration of PMMA in $CHCl_3$	.2123 g/dL ± .13%
Viscosity of $CHCl_3$ ≈ time	28.155s ± .28%
Viscosity of Solution ≈ time	62.14s ± .14%

$$\eta_r = \frac{62.14 \pm .14\%}{28.15 \pm .28\%} = 2.21 \pm .31\% = 2.21 \pm .01$$

$$\eta_{sp} = 1.21 \pm .01 = 1.21 \pm .82\%$$

$$\eta_{red} = \frac{1.21 \pm .82\%}{.2123 \pm .13\%} = 5.70 \text{ dL/g} \pm .84\% = 5.70 \text{ dL/g} \pm .05 \text{ dL/g}$$

$$1/c \ln \eta_r = 3.74 \text{ dL/g} \pm 1.14\% = 3.74 \text{ dL/g} \pm .04 \text{ dL/g}$$

For solutions of concentrations below, similar values are obtained:

concentration	η_r	η_{sp}	η_{red}	$1/c \ln \eta_r$
.2123 ± .13%	2.21 ± .31%	1.21 ± .57%	5.70 ± .59%	3.74 ± 1.14%
.1061 ± .20%	1.52 ± .47%	.52 ±1.34%	4.93 ±1.35%	3.96 ± 2.19%
.0530 ± .32%	1.24 ± .40%	.24 ±2.08%	4.54 ±2.11%	4.11 ± 2.86%

Plotting η_{red} versus concentration defines a straight line with intercept [η]. Similarly, a plot of $1/c \ln \eta_r$ versus concentration is linear with intercept [η], as shown in Figure 23. With [η] = 4.25 dL/g, the molecular weight of this sample is 1,527,000 grams. Listed below are the hours of flexure for each sample as well as the concentrations, η_r, η_{red}, [η], and molecular weight.

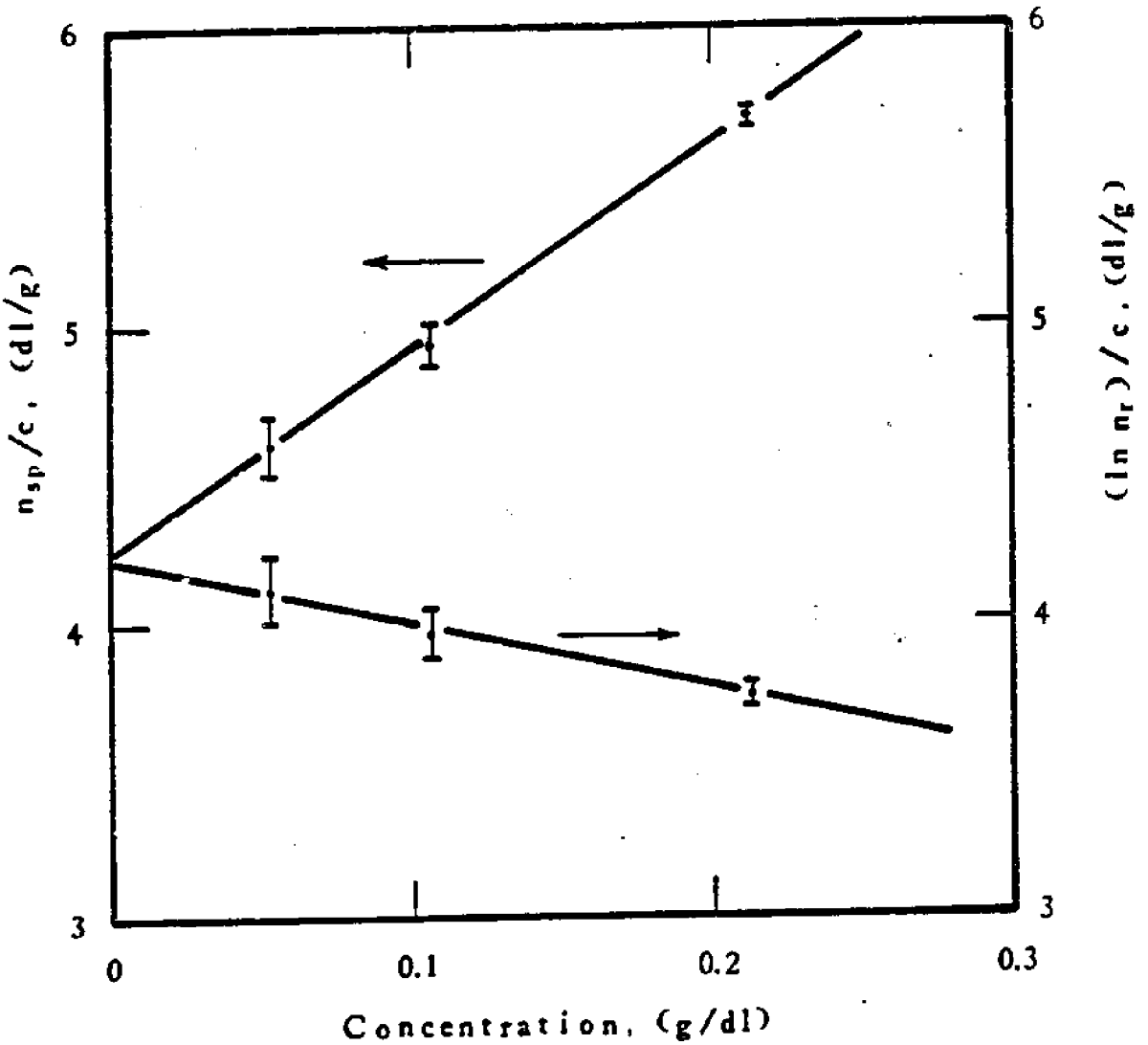

Figure 23: Determination of [η] for Sample PMMA Solution

TABLE A

PMMA samples flexed in air at 60 cycles per minute

sample	hrs	concentration (g/dL)	η_r	η_{red}	$[\eta]$ (dL/g)	M.W.
Blank	0	.2112	2.31	6.18		
		.1056	1.57	5.37	4.600	1521000
		.0528	1.26	4.99		
A'	24	.2037	2.11	5.43		
		.1018	1.51	4.99	3.800	1211000
		.0509	1.21	4.19		
G'	52.5	.2414	2.41	5.83		
		.1207	1.57	4.72	3.650	1153000
		.0603	1.25	4.08		
B'	72	.2075	2.16	5.59		
		.1037	1.48	4.64	3.615	1140000
		.0518	1.21	4.08		
F'	148	.2038	2.13	5.53		
		.1019	1.46	4.55	3.620	1142000
		.0509	1.21	3.87		
C'	168	.2116	2.14	5.41		
		.1058	1.47	4.45	3.475	1087000
		.0529	1.21	3.94		
E'	196	.2120	2.17	5.52		
		.1060	1.47	4.47	3.425	1069000
		.0530	1.21	3.92		
D'	220	.2213	2.25	5.63		
		.1106	1.50	4.50	3.400	1059000
		.0553	1.22	3.95		

TABLE B

Flexure of PMMA Samples in Simulated Seawater at 30 cycles per minute.

sample	hrs	concentration (g/dL)	η_r	η_{red}	[η] (dL/g)	M.W.
A	1	.2185	2.31	6.00	4.560	1509000
		.1093	1.57	5.22		
		.0546	1.27	5.02		
		.0273	1.13	4.75		
B	1	.2211	2.31	5.92	4.540	1501000
		.1105	1.58	5.28		
		.0552	1.27	4.83		
C	5	.2151	2.28	5.95	4.425	1455000
		.1075	1.57	5.24		
		.0537	1.25	4.73		
D	5	.2162	2.29	5.97	4.400	1445000
		.1081	1.56	5.21		
		.0540	1.25	4.68		
E	10	.2123	2.21	5.70	4.250	1386000
		.1061	1.52	4.93		
		.0530	1.24	4.59		
F	10	.2172	2.24	5.71	4.300	1406000
		.1086	1.56	5.13		
		.0543	1.26	4.72		
		.0271	1.12	4.20		
G	25	.2141	2.24	5.74	4.025	1298000
		.1071	1.54	5.04		
		.0530	1.24	4.46		
		.0268	1.11	4.18		
I	25	.2155	2.22	5.66	4.075	1317000
		.1085	1.54	4.94		
		.0542	1.24	4.47		
		.0271	1.11	4.18		
H	35	.2112	2.19	5.63	4.125	1337000
		.1056	1.52	4.91		
		.0528	1.24	4.47		
		.0264	1.11	4.24		

Table B - continued

sample	hrs	concentration (g/dL)	η_r	η_{red}	$[\eta]$ (dL/g)	M.W.
J	35	.2170	2.29	5.94		
		.1077	1.54	5.03	4.125	1337000
		.0539	1.24	4.45		
		.0269	1.12	4.33		
P	120	.2320	2.30	5.60		
		.1160	1.52	4.49	3.650	1154000
		.0580	1.23	3.95		
		.0290	1.11	3.74		
Q	120	.2257	2.27	5.63		
		.1128	1.52	4.61	3.700	1173000
		.0564	1.23	4.06		
		.0282	1.09	3.09		
K	204	.2157	2.20	5.56		
		.1078	1.49	4.53	3.630	1146000
		.0539	1.22	4.05		
		.0269	1.10	3.90		
L	204	.2169	2.20	5.51		
		.1085	1.49	4.51	3.625	1144000
		.0542	1.22	4.03		
		.0271	1.10	3.82		
M	391	.2321	2.32	5.70		
		.1085	1.54	4.62	3.550	1113000
		.0542	1.24	4.13		
		.0271	1.11	3.86		
R	522	.2424	2.38	5.71		
		.1212	1.55	4.53	3.425	1069000
		.0606	1.24	4.02		
		.0303	1.11	3.58		
S	522	.2237	2.23	5.52		
		.1118	1.50	4.46	3.450	1078000
		.0559	1.22	3.97		
		.0279	1.10	3.63		
N	644	.2342	2.33	5.68		
		.1171	1.50	4.57	3.400	1059000
		.0585	1.22	3.98		
		.0293	1.10	3.58		

TABLE B - Continued

sample	hrs	concentration (g/dL)	η_r	η_{red}	[η] (dL/g)	M.W.
O	644	.2576	2.53	5.95	3.370	1048000
		.1288	1.61	4.76		
		.0644	1.27	4.17		
		.0322	1.12	3.70		
T	724	.2332	2.31	5.61	3.350	1040000
		.1166	1.53	4.52		
		.0583	1.23	3.93		
		.0292	1.10	3.47		
U	765	.2450	2.36	5.53	3.350	1040000
		.1225	1.54	4.42		
		.0612	1.24	3.86		
		.0306	1.11	3.54		

APPENDIX VII

A. Data for Preliminary PE Flexure Runs in Air and Seawater at 60rpm.

TABLE 1

Crystallinity Data for PE flexed in air at 60 c.p.m.

hours flexure	total area	crystalline area	% crystallinity
0	527	273	52
24.0	504	262	52
52.5	575	263	51
72.0	552	274	50
148.0	545	247	45
168.0	514	239	46
220.0	505	224	44

TABLE 2

Crystallinity Data for PE flexed in Synthetic Seawater at 60 c.p.m.

hours flexure	total area	crystalline area	% crystallinity
48.0	553	275	50
89.0	533	258	48
151.0	570	255	45
185.0	547	244	45
310.0	532	226	43
319.0	552	239	43
408.0	475	195	41

APPENDIX VII

B. Instron Stress-Strain Measurements

As a further proof of polyethylene degradation due to flexure, stress-strain measurements were made on the samples. The output from the recorder must be converted from (x,y) measurements (for y proportional to the applied force and x proportional to time) to stress-strain data. The correlation of strain (ε) to x is

$$\varepsilon = \frac{x \times \text{crosshead speed}}{l_o \times \text{chart speed}}$$

for x in inches, l_o being the sample length at time zero in inches, the crosshead speed and chart speed in inches per minute. For the experiments involved, the crosshead speed was 2 inches per minute and the chart speed was 50 inches per minute resulting in

$$\varepsilon = \frac{0.04\ x}{l_o}$$

Similarly, the stress (σ) is related to y as follows:

$$\sigma = \frac{y \times \text{force for recorder deflection of 1"}}{w \times h}$$

for y in inches, the force in pounds per inch, w being the sample width and h being the thickness, both in inches. The force required for a recorder deflection of one inch

was 5 pounds such that

$$\sigma = \frac{5\,y}{w \times h}$$

The (x,y) values as well as the proper conversion to stress-strain measurements are tabulated in Table 27 for samples undergoing varied flexure times up to 310 hours.

TABLE 1

Stress-Strain Data for Polyethylene Flexed in Seawater at 60 cycles per minute.

Hours of Flexure	(x,y)	Stress	Strain	Yield Stress	Initial Slope of Stress-Strain Curves
0	(0.40,2.0)	394	0.014	1221	28000
	(1.0,4.0)	788	0.039		
	(3.3,6.0)	1182	0.126		
	(4.3,6.2)	1221	0.162		
0	(0.25,1.0)	213	0.006	1237	28000
	(0.52,2.0)	427	0.014		
	(0.88,3.0)	640	0.025		
	(1.4,4.0)	853	0.041		
	(2.3,5.0)	1067	0.069		
	(3.7,5.6)	1195	0.111		
0	(0.20,1.0)	213	0.007	1216	28000
	(0.45,2.0)	427	0.016		
	(0.78,3.0)	640	0.029		
	(1.3,4.0)	853	0.046		
	(2.2,5.0)	1067	0.081		
	(3.4,5.5)	1173	0.127		
48	(0.8,2.1)	489	0.021	1164	26667
	(1.8,3.5)	815	0.046		
	(3.0,4.3)	1001	0.077		
	(6.0,5.0)	1164	0.154		

Table 1 - Continued

Hours of Flexure	(x,y)	Stress	Strain	Yield Stress	Initial Slope of Stress-Strain Curves
48	(0.5,1.6)	341	0.012	1131	26667
	(1.2,2.9)	619	0.028		
	(3.5,4.2)	896	0.083		
	(5.0,4.9)	1045	0.119		
	(7.2,5.3)	1131	0.171		
48	(0.5,1.4)	326	0.013	1140	26667
	(1.1,2.6)	605	0.029		
	(2.0,3.6)	838	0.052		
	(3.9,4.5)	1047	0.102		
	(7.0,4.9)	1140	0.183		
89	(0.5,1.6)	410	0.013	1229	25455
	(1.2,2.8)	717	0.032		
	(2.6,4.0)	1024	0.069		
	(5.3,4.7)	1203	0.141		
89	(0.7,2.1)	448	0.018	1131	25455
	(1.6,3.5)	747	0.041		
	(2.9,4.5)	960	0.074		
	(4.0,4.9)	1045	0.102		
	(7.0,5.3)	1131	0.179		
89	(0.6,1.8)	384	0.014	1024	25455
	(1.2,2.7)	576	0.028		
	(2.8,4.0)	853	0.065		
	(4.3,4.5)	960	0.100		
	(7.0,4.8)	1024	0.163		

Table 1 - Continued

Hours of Flexure	(x,y)	Stress	Strain	Yield Stress	Initial Slope of Stress-Strain Curves
185	(0.5,1.5)	320	0.013	1109	25000
	(1.6,3.4)	725	0.042		
	(3.4,4.6)	981	0.089		
	(5.0,5.0)	1067	0.131		
185	(0.4,1.2)	279	0.010	1147	25000
	(1.3,2.8)	652	0.031		
	(3.1,4.2)	977	0.075		
	(5.5,4.8)	1117	0.133		
310	(0.5,1.3)	277	0.012	1045	24000
	(1.5,3.0)	640	0.036		
	(2.7,4.0)	853	0.064		
	(5.5,4.8)	1024	0.130		
310	(0.5,1.6)	341	0.012	1103	24000
	(1.1,2.8)	597	0.027		
	(2.6,4.3)	917	0.064		
	(4.5,5.0)	1067	0.111		
310	(0.3,1.2)	256	0.008	1045	24000
	(0.9,2.5)	533	0.024		
	(2.3,4.0)	853	0.060		
	(1.8,4.8)	1024	0.125		

APPENDIX VIII

Deconvolution of Wide-Angle X-ray Diffractograms: Two Algorithms Used In This Work

Crystallinity of all flex samples was monitored by wide-angle X-ray diffraction; Garry found that using the region between 2θ= 30° and 2θ= 12° generated reliable crystallinity data.

The problem is to deconvolute accurately the superimposed 110 and 200 crystalline lines from the amorphous background, and this background in turn from the air-scatter baseline. The Garry technique (a) was to sketch carefully the missing baselines by visual judgment. This method yields an error bar of about ± 1.0% crystallinity, which was adequate for most of the work done at 70 rpm. The areas thus defined are then traced by compensating polar planimeter, and from them the crystalline fraction X_c is found by

$$X_c = \frac{A_c}{A_c + A_a}$$

(Matthews, Peiser, and Richards, 1949), where A_c and A_a are the deconvoluted diffractogram areas of the crystalline and amorphous peaks. In practice, such X_c values are low, probably since the 12° to 30° range does exclude significant minor diffraction maxima. To correct for this and possible detector error, a strip of Garry PE of well-known X_c was scanned alongside each batch of test samples X-rayed, and a correction factor F=(true X_c/measured X_c) was derived empirically. New standard calibration strips were cut from the same well-characterized PE sheet for each third or fourth machine session, to minimize any degradation effects of the 10-min scan.

Scan rates were 2°/min, source voltage 35 kV, time constant in the

2 sec range, and ordinate expansion settings were 2000 to 10,000 cycles per sec. The machine used was a General Electric wide-angle diffractometer.

All 400 rpm work was done with a different deconvolution algorithm which generated an error closer to natural data scatter under optimal conditions (about $\pm$ 0.3% crystallinity). The 110 peak angle at 2θ = 21.2° was found on the chart, and points placed 1.5° below and 3.7° above this angle. A straight line connecting these points became the arbitrary baseline of the crystalline region of the diffractogram. Another line was ruled between points lying 7.5° below and 5.7° above the 110 peak angle; this became the amorphous-region baseline (see (b)). Performing this algorithm on the standard gave the correction factor F to convert measured X_c to true X_c.

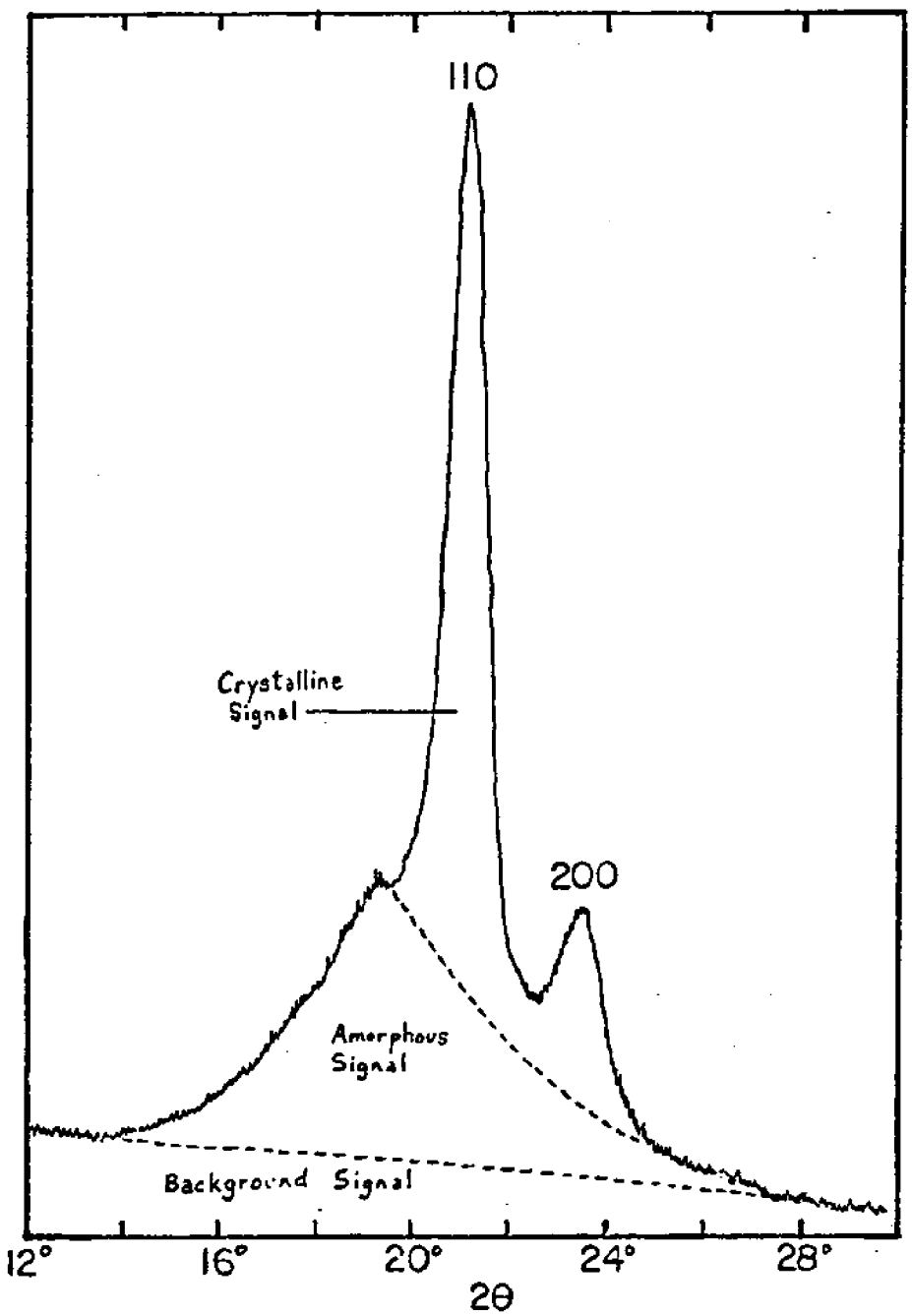

a) X-Ray Diffractogram Deconvolution by Garry Method (Sketching of Baselines by Eye).

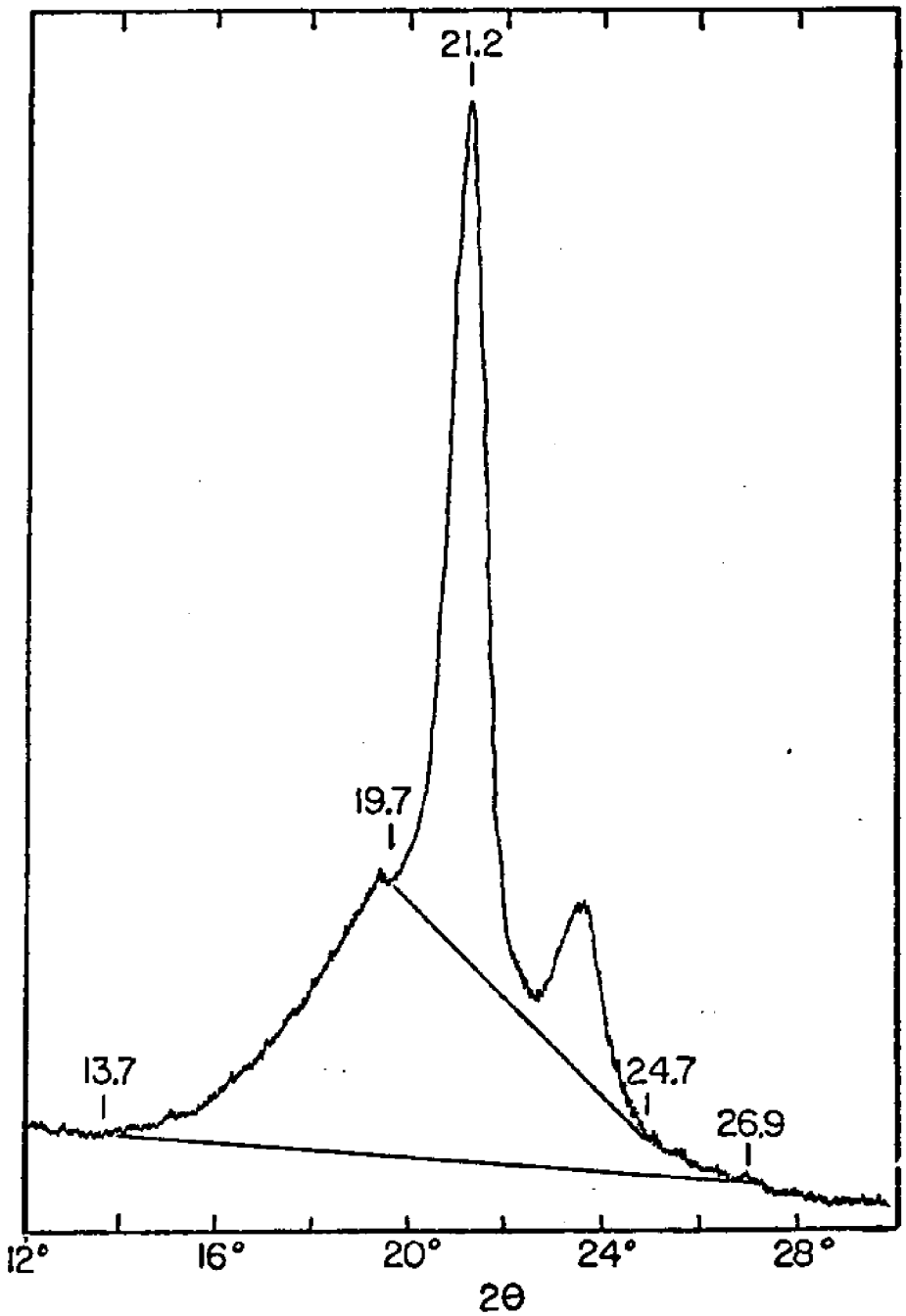

b) X-Ray Diffractogram Deconvolution by Method used for 400 rpm Flex Data.

APPENDIX IX

Study of Effect of Flexure Frequency on Degradation of PMMA

Skibo, Hertzberg, and Manson (1976) found that polymethyl methacrylate undergoing mechanical stress was sensitive to the frequency of the stress whereas crystalline polymers (polyethylene, polypropylene) were not. Because the flexure of PMMA in air was at 60 cycles per minute (c.p.m.) and that in synthetic seawater was at 30 c.p.m., it was necessary to investigate the effect of flexure frequency on PMMA degradation.

Flexure of polymethyl methacrylate in air at 30 c.p.m. and 60 c.p.m. gave the results found in Tables 22 and 23 (see Appendix VII), respectively.

TABLE 22

Flexure of PMMA in air at 30 cycles per minute

sample	hours	concentration (g/dL)	η_r	η_{red}	$[\eta]$ (dL/g)	MW
A"	24	.2050	2.12	5.47		
		.1025	1.49	4.76	3.985	1,280,000
		.0513	1.22	4.33		
B"	52	.2134	2.18	5.52		
		.1067	1.50	4.69	3.860	1,232,000
		.0532	1.22	4.21		
C"	72	.2067	2.14	5.49		
		.1034	1.48	4.63	3.800	1,209,000
		.0517	1.22	4.17		
D"	150	.2024	2.16	5.51		
		.1012	1.46	4.55	3.665	1,158,000
		.0506	1.21	4.11		

Figure 22 plots molecular weight of polymethylmethacrylate in grams per g-mole as a function of log flexures for frequencies of flexure of 30 c.p.m. and 60 c.p.m. The slopes of the curves are nearly equal indicating that the rate of degradation is independent of frequency within the range investigated. However the molecular weight at any time (i.e. number of cycles) is less for flexure at the higher frequency. For the straight line portion of the graph, the equation of the line can be found for each frequency; at 60 c.p.m. $y = 1.560 \times 10^5 X + 1.975 \times 10^6$ and at 30 c.p.m. $y = 1.560 \times 10^5 X + 2.006 \times 10^6$ for y being the molecular weight in grams for g-mole and X being log flexures. The data for polymethylmethacrylate flexure at 30 c.p.m. in air can then be compared with that for flexure at 30 c.p.m. in synthetic seawater (see Tables 22 and 24, respectively). For the linear portion of the graph of PMMA flexure in synthetic seawater (Figure 8), the equation of the line is $y = 1.874 \times 10^5 X + 2.192 \times 10^6$ for y being the molecular weight and X being log flexures. Thus, from the slopes, it is obvious that the rate of degradation is much greater in seawater (-1.874×10^5 g/g-mole) than in air (-1.560×10^5 g/g-mole); however the actual molecular weights for flexure in seawater are greater than in air up to 5.6×10^5 flexures at which point the curves cross and the molecular weight of samples flexed in air is greater than that of samples flexed in synthetic seawater.

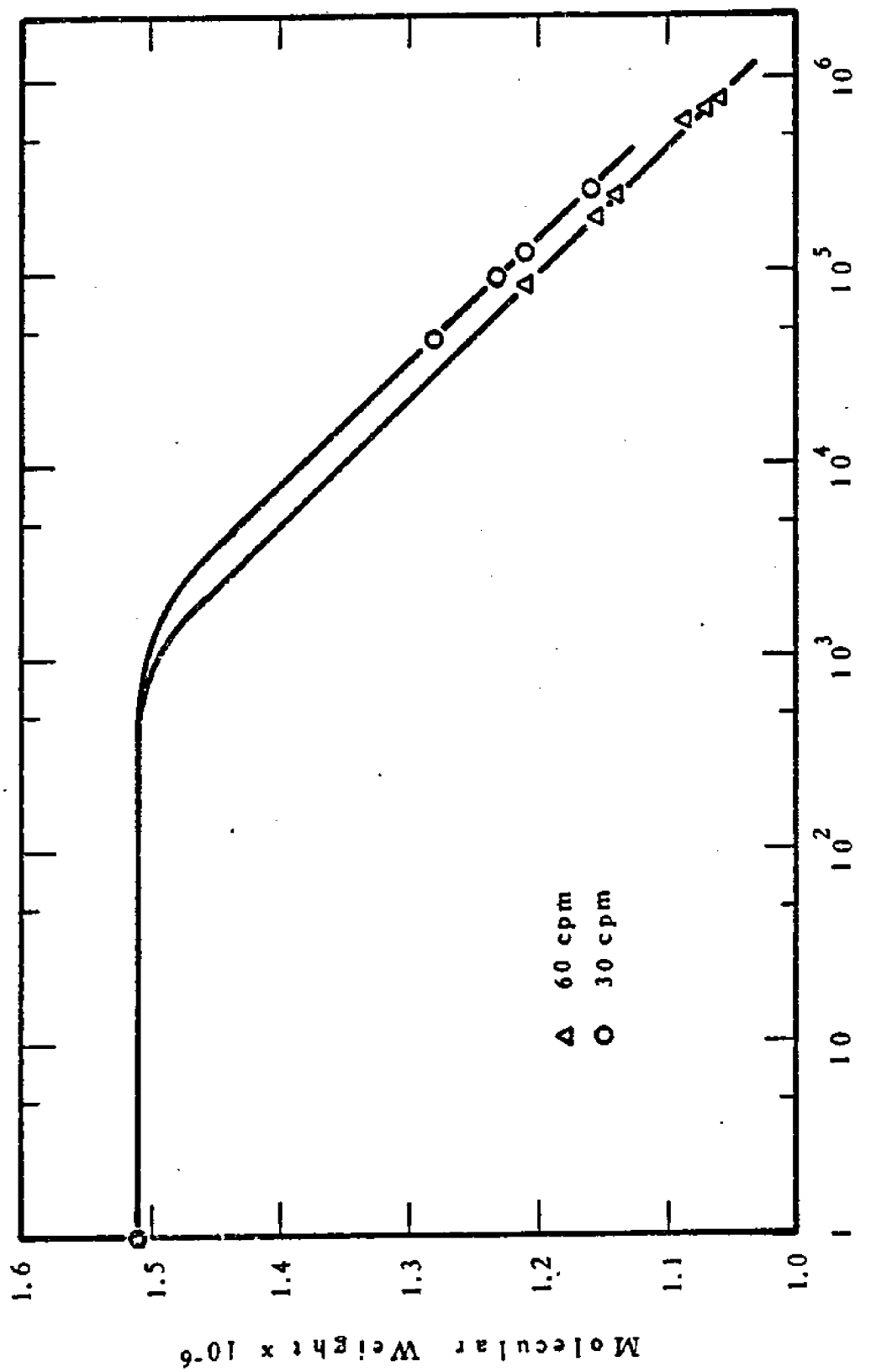

Figure 22: Effect of Flexure Frequency on PMMA Degradation in Air

APPENDIX X

Data for Melt Viscosity Studies on PE, PP and PS.

Fig. 19 Data:

Repeat Run

Cycles Flexed	% Crystall.
Unflexed	52.8
1.45×10^4	51.4
2.29×10^5	47.4
5.01×10^5	46.7*
1.00×10^6	45.0

* Average of 2 values

MJGarry Thesis

Cycles Flexed	% Crystall.
Unflexed	52
1.73×10^5	50
3.20×10^5	48
5.44×10^5	45
6.66×10^5	45
1.12×10^6	43
1.15×10^6	43
1.47×10^6	41

Fig. 20 Data:

Angular Velocity (Rad/Sec)	Blank Viscosity (Poise)	Flexed Viscosity (Poise)
.001	1.13×10^5	9.6×10^4
.0016	9.9×10^4	9.9×10^4
.0025	9.6×10^4	9.98×10^4
.004	9.12×10^4	9.36×10^4
.0063	8.53×10^4	8.69×10^4
.01	7.68×10^4	8.02×10^4
.016	6.75×10^4	6.9×10^4
.025	5.76×10^4	6.05×10^4
.04	4.68×10^4	4.44×10^4
.063	3.73×10^4	3.72×10^4
.1	2.98×10^4	2.93×10^4
.16	2.4×10^4	2.28×10^4
.25	1.8×10^4	1.69×10^4

Fig. 22 Data:

Angular Velocity (rad/Sec)	Blank Viscosity (Poise)	Flexed Viscosity (Poise)
.001	1.65×10^5	1.73×10^5
.0016	1.61×10^5	1.74×10^5
.0025	1.58×10^5	1.73×10^5
.004	1.48×10^5	1.56×10^5
.0063	1.32×10^5	1.39×10^5
.01	1.16×10^5	1.2×10^5
.016	1.00×10^5	9.9×10^4
.025	8.32×10^4	7.87×10^4
.04	6.99×10^4	6.12×10^4
.063	5.09×10^4	5.03×10^4
.1	3.99×10^4	4.18×10^4
.16	2.96×10^4	3.3×10^4
.25	2.24×10^4	2.38×10^4

Fig. 24 Data:

Cycles Flexed	% Crystall.
Unflexed	49.1
7.2×10^4	49.3
1.42×10^5	53.1
4.01×10^5	55.5
7.34×10^5	50.5
9.88×10^5	48.9
1.16×10^6	50.0

Fig. 25 Data:

Angular Velocity (Rad/Sec)	Blank Viscosity (Poise)	Flexed Viscosity (Poise)
.001	3.08×10^5	2.98×10^5
.0016	2.99×10^5	2.79×10^5
.0025	2.87×10^5	2.61×10^5
.004	2.58×10^5	2.36×10^5
.0063	2.29×10^5	2.15×10^5
.01	1.97×10^5	1.87×10^5
.016	1.65×10^5	1.61×10^5
.025	1.24×10^5	1.30×10^5
.04	9.18×10^4	9.72×10^4
.063	5.21×10^4	6.10×10^4
.1	3.03×10^4	3.65×10^4
.16	1.32×10^4	1.68×10^4
.25	3.46×10^3	5.18×10^4

Fig. 28 Data:

Angular Velocity (Rad/Sec)	Blank Viscosity (Poise)	Flexed Viscosity (Poise)
.001	1.63×10^5	1.34×10^5
.0016	1.44×10^5	1.29×10^5
.0025	1.42×10^5	1.19×10^5
.004	1.30×10^5	1.06×10^5
.0063	1.22×10^5	9.75×10^4
.01	1.10×10^5	8.35×10^4
.016	9.53×10^4	7.28×10^4
.025	8.35×10^4	6.34×10^4
.04	7.26×10^4	4.92×10^4
.063	5.87×10^4	3.58×10^4

Fig. 30 Data:

Angular Velocity (Rad/Sec)	Blank Viscosity (Poise)	Flexed Viscosity (Poise)
.001	6.56×10^4	5.28×10^4
.0016	6.0×10^4	5.4×10^4
.0025	5.95×10^4	5.38×10^4
.004	5.72×10^4	5.04×10^4
.0063	5.43×10^4	4.88×10^4
.01	5.04×10^4	4.61×10^4
.016	4.78×10^4	4.08×10^4
.025	4.48×10^4	3.74×10^4
.04	3.79×10^4	3.21×10^4
.063	3.18×10^4	2.67×10^4
.1	2.68×10^4	2.26×10^4
.16	2.21×10^4	1.83×10^4

APPENDIX XI

Calculation of Surfactant Adsorption Rat if Mass Transfer Limited

1) Calculation of diffusion coefficient for lauric diethanolamide in water (Satterfield, 1975).

$$D = \frac{1.05 \times 10^{-9} T}{\mu V_b^{1/3}} = 1.658 \times 10^{-5} \text{ cm}^2/\text{s}$$

D - diffusion coefficient (cm^2/s)

T - temperature (363°K)

μ - viscosity of solution (3.147×10^{-3} poise)

V_b - molar volume of surfactant (392.10 cm^3/g)

2) Knowing D, the Peclet number, N_{Pe}^*, for an agitated system can be found (Satterfield, 1975).

$$N_{Pe}^* = \frac{g d_p^3 \Delta\rho}{18 \mu D}$$

g - acceleration of gravity (981 cm/s^2)

d_p - particle diameter (10^{-2} cm)

$\Delta\rho$ - density difference of polymer and solution (.025 g/cm^3)

N_{Pe}^* - 26.11

$$N_{Sh} = \frac{k_c^* d_p}{D} = 4.0 \qquad \text{(Satterfield, 1975)}$$

N_{Sh} - Sherwood number

k_c^* - mass transfer coefficient for agitated system (cm/s)

$k_c^* \approx .5\ k_c = .0066$ cm/s

$k_c = .0133$ cm/s

3) Calculation of rate

$$N_v = k_c A_p (C_L - C_S)$$

A_p - surface area of polymer per volume solution ($58.8\ cm^2/cm^3$)

C_L - bulk solution concentration (moles/cm^3)

C_S - surface concentration (approaches 0 if adsorption is mass transfer limited

For C_L ranging from 9.44×10^{-9} moles/cm^3 to 8.32×10^{-8} moles/cm^3, the rate ranges from 1.33×10^{-3} moles/hr to 1.17×10^{-2} moles/hr. Because the maximum apparent rate is 1.78×10^{-10} moles/hr, mass transfer from the bulk solution to solid surface is negligible.

APPENDIX XII

Data from LDE Adsorption Experiments on PE Powder

A) $T = 90 \pm 0.5°C$, $C_o = 5.44 \times 10^{-5}$ M LDE

t,hr	P_T	γ_a	γ, dyne/cm	C, mol/l x 10^5
0	55.6	48.8	44.4	5.44
2.2	57.6	50,5	46.0	5.04
4.8	57.9	50.8	46.4	4.84
12.4	60.1	52.7	48.3	4.01
23.4	61.7	54.1	49.8	3.46
38	60.8	53.3	49.0	3.74
49	60.9	53.4	49.1	3.77
60	60.9	53,4	49.1	3.77
70	60.7	53.2	48.8	3.82

B) $T = 90 \pm 0.5°C$, $C_o = 9.40 \times 10^{-5}$ M LDE

t,hr	P_T	γ_a	γ, dyne/cm	C, mol/l x 10^5
0.1	49.1	43.9	39.7	9.40
1.5	49.7	44.4	40.2	8.93
3.25	51.3	45.9	41.5	7.86
5.8	52.1	46.6	42.2	7.33
8.0	52.6	47.0	42.7	6.98
16.2	53.2	47.6	43.1	6.71
24.0	53.4	47.7	43.3	6.58
30.7	53.4	47.7	43.3	6.58

See APPENDIX III for calculations which generated the quantities above from raw P_T data.

LITERATURE CITATIONS

1. Adamson, A.W., (1967) Physical Chemistry of Surfaces, New York: Interscience Publishers.

2. Anand, M., (1979) Personal communication.

3. Baird, R.W. and Baird W.G., (1975) "Cold Plasma Treatment of Materials", U.S. Pat. No. 3,870,610.

4. Baird, W.G., (1978,1979) Personal communication.

5. Battelle Columbus Laboratories, (1970) "Plasma Modification of Polymers", Management Summary, Oct. 14.

6. Battelle Columbus Laboratories, (1971) "Plasma Modification of Polymers", Proposal Supplement, May 15.

7. Berthou, H. and Jorgensen, C.K., (1975) "Relative Photoelectron Signal Intensities Obtained with a Magnesium X-ray Source", Analytical Chemistry, 47, 3.

8. Billmeyer, F.W., Jr., Textbook of Polymer Science, Interscience Publishers (John Wiley and Sons), New York, 1965, p. 221.

9. Ceresa, R.J., (1965) "Block Graft Copolymers", Encyclopedia of Polymer Science and Technology, II. New York: Interscience Publishers.

10. D'Adelio, G.F. and Reid, E.E., (1937) "Three Series of N-Substituted Aliphatic Amides", Journal of the American Chemical Soc., 59, 111.

11. Demchik, R.P., Mandell, J.F., McGarry, F.J., (1973) "Marine Environment Effects on Fatigue Crack Propagation in GRP Laminates for Hull Construction", M.I.T. Civil Engineering Report R74-2.

12. Dolphin and Wick, (1977) Tabulation of Infrared Spectra, New York: Interscience Publishers.

13. "Ethylene Polymers", Encyclopedia of Polymer Science and Technology, Vol. 6, pp. 275-315.

14. Hall, J.R., Westerdahl, C.A.L., Bodnar, M.J., "Activated Gas Surface Treatment of Polymers for Adhesive Bonding", Picatinny Arsenal Technical Report 4001.

15. Hall, J.R., Westerdahl, C.A.L., Devine, A.T., Bodmar, M.J., (1969) "Activated Gas Surface Treatment of Polymers for Adhesive Bonding", Journal of Applied Polymer Science, 13, pp. 2085-96.

16. Hammer, N.E., (1966) Marine Coatings - A Symposium, Oct. 5-7.

17. Harmer, N.E. and Ballentine, D.S., (1971) "Radiation Processing", Chemical Engineering, April 18, May 3.

18. Harick, N.J., Internal Reflection Spectroscopy, New York: Interscience Publishers.

19. Helmuth and Wunderlich, (1965) Journal of Applied Physics, 36, 3039.

20. Hermans, P.H. and Weidinger, A., (1960) "On the Determination of the Crystalline Fraction of Polyethylenes from X-ray Diffraction", Die Makromoleckulare Chemie, 44, pp. 24-35.

21. Hollahan, J.R. (1969) "Radiofrequency Plasma Reactor for Polymer Surface Treatment", Journal of Scientific Instruments, Series 2, pp. 203-5.

22. Hummel, D., (1962) Identification and Analysis of Surface Active Agents. New York: Interscience Publishers.

23. Jacobs, B.L., (1968) Proceedings of First Joint Aero and Marine Corrosion Technology Seminar, July 10-12.

24. Kipling, J.J., (1965) Adsorption from Solutions of Non-Electrolytes, New York: Academic Press.

25. Kritchevsky, J., (1957) "The Alkolamides", Journal of the American Oil Chemists Society, 34, 178.

26. Lagergren, H.R. and Ericsson, J.C., (1971) "Plastics with a Stable Surface Monolayer of Crosslinked Heparin: Preparation and Evaluation", Transactions of the American Society of Artificial Internal Organs, 17, 10.

27. Lagergren, H.R., Olsson, P., Swedenborg, J., (1974) "Inhibited Platelet Adhesion: A Non-Thromogenic Characteristic of a Heparin-Coated Surface", Surgery, 75, 643.

28. Lagow, R. and Margrave, J.L. (1974) "The Controlled Reaction of Hydrocarbon Polymers with Elemental Fluorine", Polymer Letters, 12, 177.

29. Lanza, V.L., (1964) "Irradiation-Properties Changes", Crystalline Olefin Polymers, Vol. 20, Part II, Ch. 7 of High Polymers, New York: Interscience Publishers.

30. Mandelkern, L., Gopalan, M.R., and Jackson, J.F., (1967) Journal of Polymer Science, Part B: Polymer Letters, 5, 1.

31. Matthews, J.L., Peiser, H.S., Richards, R.B., (1949) "The X-ray Measurement of the Amorphous Content of Polyethene Samples", Acta Crystallographica, 2, 85.

32. The Merck Index, 9th ed., (1976) Martha Windholz, ed., New Jersey: Merck Co.

33. Mitchell, S., (1976,1978) Technical measurements made.

34. Perry, R.H. and Chilton, C.H., Chemical Engineers' Handbook, McGraw Hill Book Company, New York, Fifth Edition, p. 23.

35. Peterlin, A., Polymer Science Symposium, (1970), No. 32, p. 297.

36. Pike, L., (1975) "Irradiation Dosimetry Within Cryovac" presented to Cryovac World Irradiation Conference, Sept.

37. Pike, L., Ashcraft, C. and Stone, R., (1978-1979) Personal communication and technical measurements made.

38. Pugh, A.T., (1957) Manufacturing Chemist, 28, 557.

39. Rasmussen, J.R., Bergbreiter, D.E., Whitesides, G.M., (1977) "Location and Mobility of Functional Groups at the Surface of Oxidized Low-density Polyethylene Film", Journal of the American Chemical Soc., 99, 14.

40. Rasmussen, J.R., Stedronsky, E.R., and Whitesides, G.M., (1977) "Introduction, Modification, and Characterization of Functional Groups on the Surface of Low-density Polyethylene Film", Journal of the American Chemical Soc., 99, 14.

41. Saunders, J.H. and Frisch, K.C., (1962) Polyurethanes: Chemistry and Technology, New York: Interscience Publishers.

42. Schonhorn, H. and Hansen, R.H., (1966) "A New Technique for Preparing Low-Surface-Energy Polymers for Adhesive Bonding", Polymer Letters, 4, 203.

43. Schonhorn, H. and Hensen, R.H., (1967) "Surface Treatment of Polymers for Adhesive Bonding", Journal of Applied Polymer Science, 11, 1461.

44. Schonhorn, H., (1977) Personal communication to M.J. Garry.

45. Schonhorn, H., Ryan, F.W. Hansen, R.H., (1969) "Surface Treatment of Polypropylene for Adhesive Bonding", Journal of Adhesion, 2, 93.

46. Sohma, J. and Sakaguchi, M., "ESR Studies on Mechanical Degradation of Polymers and Reactivity of Radicals Produced by Scission", Degradation and Stabilization of Polymers, Halstead Press, p. 157-180.

47. Sperati, C.A., Franta, W.A., Starkweather, H.W., (1953) "The Molecular Structure of Polyethylene V. The Effect of Chain Branching and Molecular Weight on Physical Properties", American Chemical Society Journal, 75, 6127.

48. Starkweather, H.W., Jr., More, G.E., Hansen, J.E. et al., Journal of Polymer Science, 21, 189 (1956).

49. Szpak, E., (1978) Personal communication, (RGD).

50. Thomas, P.E., Lontz, J.F., Sperati, C.A., McPherson, J.L., Society of Polymer Engineers Journal, 12, 5, (June, 1956), p. 89.

51. Trump, J.G., Van de Graaff, R.J., Cloud, R.W., (1940) "Cathode Rays for Radiation Theory", American Journal of Roentgenology and Radium Therapy, 48, 5.

52. Wagner, C.D., Riggs, W.M., David, L.E., Moulder, J.F., Muilenberg, G.E. (ed), (1979), Handbook of X-Ray Photoelectron Spectroscopy, Perkin Elmer and Physical Electronics Corp.

53. Watson, W.F., "Mechanochemical Reactions", Chemical Reactions on Polymers, Ed. Fettes, Vol. XIX, p. 1086.

54. Weidinger, A. and Herman, P.H., (1961) "On the Determination of the Crystalline Fraction of Isotactic Polypropylene from X-Ray Diffraction", Die Makromolekulare Chemie, 50, pp. 98-115

55. Wijga, P.W.O., "Structure and Properties of Polypropylene", Physical Properties of Polymers, SCI Monograph No. 5, The Macmillan Company, New York, 1959, p. 35-45.

56. Zhurkov, S.N., Zakrevskii, V.A., Korgukov, V.E., Journal of Polymer Science, A-2, 10, 1509

57. Zuidema, H.H. and Waters, G.W., (1941) "Ring Method for the Determination of Interfacial Tension", Industrial Engineering Chemistry, 13, 312.